The clustering and X-ray properties of faint galaxies

Roche, Nathan

The Clustering and X-Ray Properties of Faint Galaxies

Nathan Roche

Thesis submitted to the University of Durham
for the degree of Doctor of Philosophy

May 1994

ABSTRACT

The clustering properties of faint ($23 \leq B \leq 27$) galaxies were investigated, with the aim of obtaining information about their redshift distribution, $N(z)$, and therefore about the processes of galaxy evolution causing the steep rise in the galaxy number counts at $B > 23$. We calculated the angular correlation function, $\omega(\theta)$, for galaxies detected on a CCD survey reaching a blue magnitude of $B_{ccd} = 25.0$ and a red magnitude of $R_{ccd} = 23.5$, and on a smaller area reaching a very faint limit of $B_{ccd} = 27.0$.

The $\omega(\theta)$ amplitude of galaxies was found to decrease much more steeply between magnitude limits of $B_{ccd} = 23$ and $B_{ccd} = 25$ than predicted by models in which galaxy clustering is stable in proper co-ordinates and the galaxy redshift distribution possesses a no-evolution form. At a $B = 24.5$ limit the $\omega(\theta)$ amplitude was found to be only $\sim \frac{1}{4}$ that expected from a non-evolving model, enabling us to reject such a model at the 4σ level. The red-limited sample, $R_{ccd} = 23.5$, also gave a $\omega(\theta)$ amplitude lower than the non-evolving prediction, although the difference was less significant ($\sim 2\sigma$). A pure luminosity evolution model, which accounts for the excess in the galaxy number counts by enabling galaxies undergoing rapid star-formation at $1 \leq z \leq 4$ to become visible at $B > 23.5$, gave a good fit to the $\omega(\theta)$ results without requiring any departure from stable clustering.

The $B_{ccd} \leq 24.5$ galaxies with redder ($B - R \geq 1.5$) colours gave a significantly higher $\omega(\theta)$ amplitude than the bluer galaxies at the same limit, consistent with a stable clustering model with no luminosity evolution. As these red galaxies would lie at $z < 1$, within an approximately non-evolving $N(z)$, this result suggests that galaxy clustering is indeed stable out to at least $z \sim 0.5$. The low $\omega(\theta)$ amplitude of the $B_{ccd} \leq 24.5$ sample was found to be associated only with the bluer galaxies, supporting the PLE model interpretation of the drop in $\omega(\theta)$ amplitude at $B > 23.5$ as being caused by the appearance of blue star-forming galaxies at high redshifts. If all the blue galaxies seen at $B \sim 24.5$ are instead at $z < 1$, they must belong to a separate population of dwarf starburst galaxies, which must be intrinsically clustered extremely weakly compared to normal galaxies.

The combination of our $\omega(\theta)$ results at $B_{ccd} = 25.0$ and $B_{ccd} = 27.0$ limits with those obtained by Efstathiou et al. (1991) at $B = 26$ gave some indication that the steep drop in $\omega(\theta)$ amplitude at $23 \leq B \leq 25$ levels out at $25 \leq B \leq 27$. This would be expected if galaxies with L^* luminosities are seen out to some maximum redshift at $B \sim 25$, so that $N(z)$ becomes no more extended at fainter magnitudes. The amplitude of $\omega(\theta)$ at this limit would depend only on the value of the maximum redshift, on q_0, and on the rate of evolution of clustering. The observed amplitude of $\omega(\theta) \simeq 4 \times 10^{-4}(\mathrm{deg})^{-0.8}$ would be consistent with $3 \leq z_{max} \leq 4$, stable clustering and any value of Ω from 0 to 1.

If galaxies are seen out to their maximum redshifts at $B \sim 25$, the gradient of the differential galaxy number counts at even fainter magnitudes would follow the faint end slope of the galaxy luminosity function. The galaxy number counts from our deep CCD survey are much higher at $B > 24.5$ than the predictions of $q_0 = 0.5$ PLE models, and appear to rise more steeply at $25 \leq B \leq 27.5$, with $\frac{d(logN)}{dm} \sim 0.3$, than even our $q_0 = 0.05$ PLE model would predict. The observed number count gradient at $B > 25$, in combination with the levelling out of the $\omega(\theta)$ scaling, would then suggest that the luminosity function steepens to $\alpha \simeq -1.75$ at high redshifts, in addition to undergoing the strong brightening of the L^* luminosity predicted by PLE models.

We also investigated the X-ray properties of faint ($18 \leq B \leq 23$) galaxies, by cross-correlating their positions with those of X-ray sources (without identifications as either

QSOs or stars) detected on deep ROSAT images. The results indicated that $\sim 1\%$ of all $B \leq 21$ galaxies were detected above a 4σ threshold on the ROSAT X-ray images, with the cross-correlation between sources and galaxies being of 3σ significance. As the detected galaxies would possess L_X/L_B ratios higher than those typical of local galaxies by factors of ~ 100, these results suggest a wide dispersion of $\sigma \sim 0.8$ in the distribution of $\log(L_X/L_B)$ for galaxies.

Spectroscopic investigation of the galaxies identified as probable X-ray sources indicated that they included both star-forming and early-type galaxies, with a mean redshift of $z \simeq 0.22$, and were mainly of $L \sim L^*$ luminosity in the blue band, but possessed very high X-ray luminosities of $L_X \sim 10^{42}$ ergs s^{-1}. On one ROSAT image we also detected a rich galaxy cluster at a high redshift of $z = 0.561$, and estimated its X-ray luminosity as $L_X \simeq 5.4 \times 10^{43}$ ergs s^{-1}, which is only about $\sim 30\%$ of that expected for a cluster of the same richness seen locally.

The number counts of galaxies in the 0.5–2.0 keV band were estimated as 27.18 ± 10.35 deg^{-2} at a flux limit of $10^{-14.4}$ ergs cm^{-2}s^{-1}. The number counts of detected QSOs appear to level out at $\sim 10^{-14}$ ergs cm^{-2}s^{-1}, suggesting that QSOs faintward of our detection limits would produce only $\sim 30\%$ of the unresolved X-ray background (XRB).

The autocorrelation function (ACF) of the unresolved 0.5–2.0 keV XRB was measured on 3 ROSAT images (totalling 1.05 deg^2), and was found to show no significant signal – we obtained a 2σ upper limit of $\omega(\theta) \leq 1.4 \times 10^{-3}(\mathrm{deg})^{-0.8}$ on its amplitude. This would be consistent with normally clustered galaxies as the origin of most of the XRB, if their X-ray luminosity increases with redshift sufficiently that a large proportion of the X-ray flux is produced by galaxies at $z > 1$.

A very significant ($> 5\sigma$) cross-correlation was detected between $18 \leq B \leq 23$ galaxies on AAT photographic plates and the fluctuations in the unresolved XRB on the same 3 ROSAT images. The cross-correlation amplitude, after applying corrections for the effects of galaxy clustering, indicated that these $18 \leq B \leq 23$ galaxies produced $16.8 \pm 2.1\%$ of the unresolved 0.5–2.0 keV background, corresponding to a volume X-ray emissivity of $\rho(0.5\text{–}2.0 \text{ keV}) = (5.27 \pm 0.65) \times 10^{38}$ ergs s^{-1}Mpc^{-3}. This is about an order of magnitude higher than the emissivity expected from the L_X/L_B ratio typical of normal galaxies, but a $\sigma \sim 0.8$ dispersion in $\log L_X/L_B$ ratios could account for this. The number counts of X-ray detected galaxies and the galaxy/XRB cross-correlation amplitude are both consistent with a slightly smaller dispersion in $\log(L_X/L_B)$ of $\sigma = 0.7$, if combined with an exponential increase with look-back time of the X-ray luminosity of galaxies, with a timescale of $\tau = 0.4H_0^{-1}$.

Extrapolation of our estimate of the galaxy X-ray emissivity to higher redshifts, predicts that non-evolving galaxies would account for $\sim 35\%$ of the unresolved 0.5–2.0 keV background, with most of the galaxy contribution produced at $z < 1$. However, with a $\tau = 0.4H_0^{-1}$ rate of X-ray luminosity evolution, the predicted contribution of high-redshift ($1 \leq z \leq 4$) galaxies to the XRB is greatly increased, accounting for the lack of signal in the ACF. Galaxies out to $z \sim 4$ would then produce in total $\sim 70\%$ of the unresolved XRB, accounting for the entire non-QSO component.

No part of this work has previously been submitted for a degree in any University.

Some of the results described in this thesis have been published elsewhere in the following papers:

Roche, N., Shanks, T., Metcalfe, N. and Fong, R., 'The angular correlation function of galaxies with $B \sim 25$ mag', 1993. *Mon. Not. R. astr. Soc.*, **263**, 360.

Metcalfe, N., Shanks, T., Roche, N., and Fong, R., 'Galaxy Number Counts to $B = 28^m$', 1993. 16th Texas/PASCOS Symposium, Ann. NY Acad. Sci. 688, eds. C.W. Akerlof and M.A. Sredniki, pp 534–538.

Roche, N., Shanks, T., Metcalfe, N. and Fong, R., 'Galaxy Clustering to $B = 27^m$', 1994. *'Astronomy from Wide-Field Imaging'*, IAU Symp. 161, eds. MacGillivray, H.T. et al., Kluwer:Dordrecht, pp 635–643.

Metcalfe, N., Shanks, T., Fong, R. and Roche, N., 'Galaxy Number Counts to $B = 28^m$', 1994. *'Astronomy from Wide-Field Imaging'*, IAU Symp. 161,
eds. MacGillivray, H.T. et al., Kluwer:Dordrecht, pp 645–648.

Metcalfe, N., Shanks, T., Fong, R. and Roche, N., 'Galaxy Number Counts – III: Deep CCD Observations to $B = 27.5$ mag', 1994. Submitted to *Mon. Not. R. astr. Soc.*.

Acknowledgements

First of all I would like to thank my supervisors – Tom Shanks for providing most of the initial ideas for both the $\omega(\theta)$ and X-ray sections of this work, and for encouraging me to persist with investigations which took some time to bear fruit – and Richard Fong for many interesting discussions about galaxy clustering and evolution.

I would also like to thank Nigel Metcalfe for the very major contribution he made to the work described in this thesis in carrying out the reduction of the deep CCD images into faint galaxy catalogues, and for helping me with the use of photographic plate data – and also Palmira Arenaz and others at the Isaac Newton Telescope who helped Nigel and myself to look almost to the Edge of the Universe, and see galaxies where no one has seen galaxies before.

I would like also to thank my parents, my sister Hadassah, and my penfriends Melissa Mansberger and Suzanne Richer for their encouragement and interest, and all others who have made this period of my life more enjoyable – including David Austin of the National Anti-Vivisection Society for organising the Animals Defenders Half Marathon, and everyone at the Skye Environmental Centre – where my visit last autumn did much to provide the revitalization I needed for the completion of this work, and helped to further enhance my interest in Nature, whether seen as seals in Loch Coruisk or as galaxies billions of light years distant.

I acknowledge the support of an SERC research studentship.

Nathan Roche,

Easter 1994.

'I have seen the *Gronks* swarming in the star-spawned outer reaches of space – a sure sign of inter-galactic disaster!'

Starlord magazine, May 1978.

'Nought may endure but Mutability'

Percy Shelley.

Contents

Chapter 1

Introduction

1.1 Aim

In this thesis, we first present an investigation of galaxy evolution through studies of the clustering properties, in addition to the number counts, of very faint and distant galaxies. This may provide information about the evolutionary processes causing the large excess observed in their numbers compared to the predictions of non-evolving models. Our dataset includes very deep CCD images, on which we detected several thousand galaxies in total, to blue magnitudes as faint as $B = 27.5$ on one field and to $B = 25.0$ over a larger area.

Secondly, we present an investigation of the X-ray properties of faint galaxies, using high-resolution X-ray images recently obtained using the ROSAT satellite, and photographic plates of the same areas of sky. Our dataset includes lists of X-ray sources to a flux limit of $S \sim 5 \times 10^{-15}$ ergs s^{-1}, the X-ray background intensity imaged with ~ 25 arcsec resolution, and the positions of all galaxies brighter than a magnitude limit of $B = 23$, over a total area ~ 1 deg^2.

The principal techniques employed are the calculation of autocorrelation functions of both optical and X-ray data, and cross-correlations between the two. This will enable us to measure the scaling with depth of galaxy clustering to the faintest and remotest limits currently reached by CCD surveys – possibly to the epoch of galaxy formation – and to estimate the contribution of faint galaxies to the X-ray background (XRB).

In the remainder of this Chapter we briefly review the current evidence for galaxy evolution, as given by the number counts and colours of galaxies as functions of apparent magnitude in many previous surveys. We describe in some detail the ingredients of various galaxy evolution models which have been used to interpret these observations. We then discuss how the clustering of galaxies can also provide information about the extent and nature of their evolution, briefly reviewing past investigations of the clustering of galaxies and describing the methods by which we aim to distinguish between the previously described evolutionary models through measuring the clustering of the galaxies on our deep CCD frames.

In this Chapter we shall further review the current status of research into the origins of the XRB. We describe briefly the nature of the individual X-ray sources which have been resolved out of the background, and the constraints which may be set on the surface density and clustering properties of the fainter unresolved sources, through measurements of the small-scale fluctuations in the XRB intensity. As our investigations will address in particular the question of whether a large fraction of the XRB is produced by faint galaxies rather than QSOs, we describe briefly the known mechanisms of X-ray emission from galaxies, and the predictions of the galaxy contribution to the XRB given by various models. We then describe the methods by which we aim to estimate the clustering of the sources of the XRB, to compare with the known clustering of faint galaxies, and the methods by which we aim to estimate the galaxy contribution directly by cross-correlating the positions of several thousand faint galaxies with both individual X-ray sources and the fluctuations in the unresolved XRB.

1.2 The Faint Blue Galaxy Excess

Number counts of galaxies as a function of magnitude, as obtained from a number of CCD and photographic surveys, are *significantly higher* faintward of a blue magnitude of $B \sim 22$ than would be expected if a galaxy population identical to that observed locally is simply seen out to greater distances.

In a Universe with a low deceleration parameter (ie. $q_0 \sim 0$), look-back time $T(z)$ relates to redshift z approximately as

$$T(z) = H_0^{-1}(1 - (1+z)^{-1}) \text{ Gyr}$$

where the Hubble time H_0^{-1} (the approximate age of the Universe), is equal to 19.56 Gyr for the value of the Hubble Constant assumed hereafter in this thesis of $H_0 = 50$ km s^{-1}Mpc^{-1}.

If galaxies typically formed at $z \sim 4$ or $z \sim 5$, then from the above equation, the local galaxy population is observed at an age of ~ 16 Gyr. Galaxies at $B \sim 22$, with a mean redshift $z \sim 0.25$, are typically observed at epochs approximately 4 Gyr earlier than local galaxies. An excess in the numbers of $B \geq 22$ galaxies would therefore indicate that galaxies at epochs ~ 4 Gyr ago and earlier were typically more luminous than present-day galaxies and/or existed with a higher comoving number density than galaxies seen locally.

At $22 \leq B \leq 26$ the galaxy counts in successive magnitude intervals rise more steeply, with $\frac{d(logN)}{dm} \simeq 0.45$ (where N is galaxies counted per square degree per unit magnitude interval and m is magnitude), than non-evolving model predictions for this magnitude range ($\frac{d(logN)}{dm} \simeq 0.34$). Hence the ratio between the observed galaxy counts and non-evolving predictions becomes larger for even fainter galaxies, increasing by $\sim 30\%$ with each successive magnitude interval faintward of $B \sim 22$.

Tyson (1988) found from a deep CCD survey reaching $B = 27$ and comparable depths in R and I passbands that the excess in the galaxy counts exceeded a factor of 5 at $25 < B < 27$ – and also that the increasingly large excess in the galaxy number count on going to fainter magnitudes was accompanied by a strong trend towards *blueness* in the mean colours of the galaxies. The effect of this *colour evolution* on the number counts is to produce a steeper increase in galaxy counts with magnitude for shorter wavelengths of observation. Tyson found the differential count gradients of faint galaxies to steepen from $\frac{d(logN)}{dm} = 0.34$ at $\lambda \sim 9000$Å (the I band) to $\frac{d(logN)}{dm} = 0.45$ at $\lambda \sim 4500$Å (the B band). Similar counts of galaxies, and a very similar variation in $\frac{d(logN)}{dm}$ with the wavelength of observation, were seen in the deep CCD surveys of Metcalfe et al. (1991, hereafter MSFJ); Lilly, Cowie and Gardner (1991, hereafter LCG); Neuschaefer (1992) and Driver et al. (1994). Galaxy counts in the near ultraviolet U-band rise even more steeply than in the blue band at comparable depths (Guhathakurta 1989). In contrast, galaxy counts in the infra-red K-band, centered on 2.2μm, show the least evolution (LCG, Glazebrook 1991).

One of the principal aims of this thesis is to obtain information about the redshift distribution, $N(z)$, of galaxies as faint as $24 \leq B \leq 27$. Although the form of the $N(z)$ faintward of $B \simeq 22.5$ remains uncertain at present, it is probable that many of the the galaxies detected at $24 \leq B \leq 27$ are at high redshifts of $z > 1$. Galaxies with $z > 1$ would be observed at look-back times exceeding 10 Gyr, and would therefore be seen less than 6 Gyr after their formation. Hence if galaxies evolve rapidly during their first few Gyr, the $B \geq 24$ galaxies may differ greatly in their typical properties from those seen locally, or even those at $B \sim 22$. The high number counts and blue colours of $B \geq 24$

galaxies suggest that changes in the observable properties of galaxies with time/redshift are indeed very significant, and we now consider the nature and cause of this evolution.

1.3 Star-Formation Histories of Galaxies

The steep number count gradient of faint galaxies observed in blue and ultraviolet passbands, and the trend towards blueness in 0.3–2.2μm colours at fainter magnitudes, both indicate a higher mean star-formation rate for galaxies at earlier cosmological epochs. Galaxies undergoing very rapid star-formation activity will contain a large component of newly formed stars. The distribution of stellar masses within this 'instantaneous-burst population' has been found in local galaxies to approximately follow the power-law

$$\psi(M) \propto M^{-2.35}$$

known as the Saltpeter Initial Mass Function, over a very wide range of stellar masses, from $M \sim 0.1 M_{\odot}$ to $M \sim 100\ M_{\odot}$ (see e.g. Bruzual 1981). A star-forming galaxy will therefore contain significant numbers of massive, blue giant stars which, on account of their high temperatures ($T_{effective} \geq 20000K$), are very luminous at blue and near-ultraviolet wavelengths, dominating the spectral energy distribution (SED) of the entire galaxy at $\lambda \leq 4000$Å.

The relation between the main sequence lifetime of a star $\tau_{MS}(M)$ in Gyr and its mass in units of the solar mass ($M_{\odot}$) is approximately (Guhathakurta 1989)

$$\log(\tau_{MS}(M)) = 1.0 - 3.6\log(M) + 1.0(\log(M))^2$$

Stars of one solar mass will shine for 10 Gyr, but a star of mass $M = 5\ M_{\odot}$, which on the main sequence would have spectral type B6 and $T_{eff} = 14000K$, has a much shorter lifetime of 0.1 Gyr. For an even more massive $M = 20\ M_{\odot}$ star, with main sequence spectral type B0 and $T_{eff} = 27000K$, the lifetime is only 0.01 Gyr.

The important point is that the lifetimes of massive, hot blue stars are very short in comparison to H_0^{-1} and the present ages of galaxies, whereas yellow or red dwarf stars, with lower masses ($M \leq M_{\odot}$), survive for H_0^{-1} timescales or longer. Consequently, if a galaxy ceases to form new stars, its blue/UV luminosity will decrease and its 0.3–2.2μm colours redden, over timescales much shorter than H_0^{-1}, as all the massive blue stars in the galaxy 'die off' in supernova explosions and the turn-off point in the main sequence gradually moves downwards to the longer-lived, less massive stars, with lower luminosities and redder colours. After several Gyr without forming new stars, most of the energy output of the galaxy will be as red/IR light from the remaining red dwarf and post-main-sequence red giant stars (see Bruzual and Charlot 1993, for graphs showing the evolution of galaxy spectra over the whole 1000Å to K-band range).

The spectral evolution of galaxies is essentially a convolution of the evolution of an instantaneous-burst population of stars and the change with time of the star-formation rate (SFR). The decline in SFR results from the gas available to form new stars being used up in the star-formation process itself, being only partially replaced by supernovae and other forms of mass loss from 'dying' stars. If the SFR at any time, $\Psi(t)$, is approximately proportional to the amount of gas remaining in the galaxy, it must then decrease as $\Psi(t) \propto \exp(-\mathrm{t}/\tau_{\mathrm{SFR}})$.

If the flux at any wavelength λ emitted by an instantaneous-burst stellar population evolves after star-formation as $f_{\lambda}(t)$, a galaxy with a SFR evolving as $\Psi(t)$ will emit a

total flux $F_\lambda(t)$ where

$$F_\lambda(t) = \int_0^t \Psi(t-\tau) f_\lambda(\tau) d\tau$$

The convolution of $\Psi(t)$ with $f_\lambda(t)$ spreads out its decline, initially very rapid at blue/UV wavelengths, into a more gradual luminosity and colour evolution ($F_\lambda(t)$) for the galaxy as a whole. Hence galaxies with longer SFR evolution timescales retain relatively blue colours and high blue-band luminosities for a longer period after galaxy formation. Galaxies for which the exponential timescale τ_{SFR} is a large proportion of their age will still contain some massive blue stars at the present epoch, although with numbers lower than the proportion in the initial starburst population. The wide range in present-day galaxy colours can therefore be explained as resulting from a wide range of τ_{SFR} timescales (see eg. Bruzual 1981, Koo and Szalay 1984, Charlot and Bruzual 1993).

We now consider the evolution of two representative types of galaxy at opposite extremes of the Hubble sequence of morphological types, which runs from elliptical galaxies (type E) through lenticulars (S0), bulge-dominated spiral galaxies (Sa), intermediate spirals (Sb), 'loose' disk-dominated spirals (Sc and Sd) to Magellanic-type (Sm) and irregular (Irr) galaxies.

The galaxies with the reddest colours ($B-R \sim 1.5$) at the present day are elliptical or lenticular in morphology. For these galaxies (E/S0/Sab), described as 'early-type', τ_{SFR} is very short in comparison to the age of the galaxies. A model with $\tau_{SFR} = 1.44$ Gyr, for example, (the $\mu = 0.5$ model investigated further in this thesis), gives a reasonably good fit to present-day E/S0 galaxy spectra at an age after galaxy formation of 16 Gyr. Such a galaxy forming at $z \sim 4.5$ ($\sim$ 16 Gyr ago) would have undergone very rapid star-formation in its first $\sim$ 3 Gyr (the epochs corresponding to $z \geq 2$) but very little since then, the supply of gas for star-formation having been used up. This accounts for the very low gas content of early-type galaxies at the present day – the ratio of gaseous to stellar mass is typically less than 0.02. However, the gas content of ellipticals is of great importance, on account of its very high temperature ($T \sim 10^7 K$), when we observe these galaxies at X-ray rather than optical wavelengths (see Section 1.8).

When the age of the galaxy reaches several τ_{SFR} timescales, star formation will have effectively ceased and further spectral evolution is described as 'passive', as it results simply from the ageing of an existing stellar population. After a few Gyr of passive evolution, only low-mass ($M < M_\odot$) stars remain and the subsequent luminosity and colour evolution are very slow. Hence early-type galaxies at $0.5 \leq z \leq 1$ appear only slightly bluer and more luminous than those at $z \sim 0$, their observed colour and luminosity evolution being consistent with essentially passive evolution since the epoch corresponding to $z \sim 2$ (see e.g. Aragón-Salamanca et al. 1993).

However, early-type galaxies observed at $z \sim 2$ or even higher redshifts would be seen during their initial period of very rapid star-formation. Hence, high-redshift ellipticals are expected to be very blue in colour, and visible at much brighter apparent magnitudes than if no evolution had occurred. Although direct spectroscopic observations have yet to confirm this, high-redshift early-type galaxies are obviously very plausible candidates for explaining a large proportion of the 'excess' of very blue galaxies at $B > 23$.

Galaxies at higher redshifts will be observed in shorter wavelength regions of their spectra, as well as at earlier cosmological epochs. A change in apparent magnitude, known as the 'k-correction', results from the shift between rest-frame and observed wavelength. At $\lambda \sim 2000$Å the flux f_ν will be lower by about an order of magnitude than the 4500Å flux for a galaxy containing only old, low-mass stars. The only stars of low mass which produce significant amounts of flux at $\lambda \sim 2000$Å are the central stars of

planetary nebulae, a very small proportion of the total at any one time due to the short duration of this phase of stellar evolution. Consequently, a red E/S0 galaxy observed in the blue band will be dimmed greatly at $z \sim 1$ if little evolution has occurred at $0 \leq z \leq 1$.

Figure 1.1 shows the k-corrections for non-evolving E/S0 and Sab galaxies observed in the blue passband, in magnitudes as a function of redshift. The k-correction 'dimming' evidently increases rapidly with redshift to $\sim 2.5^m$ at $z = 1$. A '(k+e)-correction' appropriate for early-type galaxies is also shown, where an 'e-correction' – the effect of the evolution of the star-formation rate with time, converted into an evolution with redshift – is combined with the k-correction produced by redshifting of the spectrum. The k-corrections and (k+e)-corrections used in this thesis are as given by MSFJ, and the evolutionary models are as originally computed by Bruzual (1981), with a galaxy formation redshift $z_{formation} = 4.7$, galaxy ages of 16 Gyr ($H_0 = 50$ km s^{-1}Mpc^{-1} is assumed), and the time-redshift relation for $q_0 = 0$. The k-corrections for all galaxy types, given by MSFJ only to a redshift of $z = 1.5$, are assumed to remain constant at the $z = 1.5$ value at higher redshifts.

The (k+e)-correction shown here for early-type galaxies is given by the Bruzual (1981) model with the exponential star-formation rate decrease parameterized as $\mu = 0.5$, equivalent to $\tau_{SFR} = 1.44$ Gyr. This evolution model predicts only a moderate brightening of $\sim 0.5^m$ at $z = 0.8$. However, at $z \sim 2$, corresponding to the epoch of active star-formation, the enhancement of the UV ($\lambda \sim 1500$Å) luminosity by the presence of massive stars is expected to brighten the apparent blue magnitude by as much as $\sim 5^m$ relative to a present-day early-type galaxy placed at the same redshift.

In contrast, galaxies with the bluest present-day colours ($B - R \sim 0.7$) possess loose spiral or irregular morphologies (type Sd/Sm/Irr) and still contain large quantities of gas – the ratio of gaseous to stellar mass is typically ~ 0.5, and exceeds unity in some cases. For these galaxies, described as 'late-type', $\tau_{SFR} \sim H_0^{-1}$ or longer, and therefore star-formation continues at the present day at a rate not much less than at early epochs. The long τ_{SFR} exponential timescale means that the increase in SFR with look-back time will be approximately linear, and quite slow – if the $\lambda \sim 2000$Å luminosity is roughly proportional to the SFR, the evolutionary brightening at high redshifts will amount to no more than $\sim 1^m$ (i.e. exp(~ 1)) relative to the blue apparent magnitude of a present-day late-type galaxy placed at the same redshift.

The k-correction will be zero if a galaxy emits equal amounts of energy in successive logarithmic intervals of wavelength λ, or equivalently, successive logarithmic intervals of frequency ν, i.e. the SED is described by the power-law $f_\lambda \propto \lambda^{-1}$. This can also be expressed as $f_\nu \propto \nu^{-1}$, where f_ν is flux per unit frequency/energy interval. The SEDs of actively star-forming galaxies, containing stars of a very wide range of masses and temperatures, are reasonably well approximated by $f_\nu \propto \nu^{-1}$ over a very wide range of wavelengths. For galaxies undergoing very rapid 'starbursting', so that the total energy output is dominated by an initial burst stellar population, the power-law index may be closer to $f_\nu \propto \nu^0$ – hence the bluest faint blue galaxies have been described as 'flat-spectrum objects' (see e.g. LCG).

In the SED of a black-body with effective temperature T_{eff}, f_ν has its maximum value at an energy $E = 2.44 \times 10^{-4} T_{eff}$ eV, corresponding to a wavelength $\lambda = (5.1 \times 10^7 / T_{eff})$Å. Hence the observed range of a factor of ~ 20 in wavelength of the flat or power-law regions of these spectra, from $\lambda \sim 1000$Å to the K-band at $\lambda \sim 22000$Å, corresponds to the range of a factor of ~ 20 in the effective temperatures of the stars found in star-forming galaxies ($T_{eff} \simeq 2800K$ to $T_{eff} \sim 60000K$). We can see from

this that the flat or power-law SED of starburst galaxies reflects the fact that the stellar initial mass function also follows a power-law, from the most massive and hottest stars to the least massive and coolest stars.

Figure 1.2 shows the blue-band k-correction for an Sdm type galaxy, and the (k+e)-correction given by the Bruzual (1981) 'Irr' model, which incorporates an almost constant star-formation rate ($\tau_{SFR} \sim 100$ Gyr). As a result of the relatively flat SED, the k-correction 'dimming' with redshift is much less than for an early-type galaxy.

The evolutionary brightening in the 'Irr' model is approximately linear with redshift to $z \sim 1$, where it amounts to $\sim 0.8^m$. Although the luminosity evolution of late-type galaxies is expected to be moderate in comparison to that in early-types at high redshifts, it may still play a part in explaining the blue galaxy excess. The more 'linear' late-type evolution means that much of the brightening occurs at moderate redshifts where such galaxies will tend to dominate the redshift distribution in a blue-limited sample, on account of their small k-corrections.

Furthermore, the high present-day gas content of late-type galaxies would enable bursts of very rapid star-formation to occur even at very recent epochs, perhaps triggered by interactions between galaxies. Therefore a certain proportion of these galaxies may be much brighter at low or moderate redshifts than the gradual evolution of the Bruzual model would predict, and some of the faint blue galaxy excess could then consist of these 'late starburst' galaxies at $z < 1$. However, the importance of low redshift, late starbursts in comparison to initial starbursts at higher redshifts in explaining the high number counts remains very uncertain in the absence of spectroscopic data at $B \geq 24$.

The majority of galaxies, including our own, are spirals with morphological types Sb, Sbc or Sc and lie between the above extremes in colour ($B - R \sim 1$) and gas content (ratio of gaseous to stellar mass 0.05–0.5). These galaxies possess a relatively blue spiral or disk component and a redder bulge component, but the spectral evolution of the galaxy as a whole can be reasonably well represented by intermediate SFR timescales of 2 Gyr $\leq \tau_{SFR} \leq$ 7 Gyr (Charlot and Bruzual 1993), and the k-corrections and (k+e)-corrections will also lie between those of E/S0 and Sdm types. Figure 1.3 shows k-corrections for Sbc and Scd spiral galaxies together with a Bruzual (1981) 'Scd model' (k+e)-correction appropriate for the these approximate types.

In this thesis we shall be attempting to study the clustering and the X-ray properties of star-forming and passive galaxies separately, and one way to do this would be to divide our galaxy sample by $B - R$ colours.

Figure 1.4 shows $B - R$ colour as a function of redshift, ie. the difference between the blue and red k-corrections added to the local $B - R$,

$$(B - R)_z = (B - R)_{z=0} + k_B(z) - k_R(z)$$

for non-evolving galaxies over the range of spectral types from E/S0 to Sdm. For early-type galaxies, the k-correction is much smaller in the red passband than in the blue passband out to $z \sim 0.5$ (where the observed red band corresponds to 'blue' in the rest-frame). As these galaxies undergo little evolution at moderate redshifts, the $B - R$ colour of a red galaxy will become even redder with distance, from $B - R \sim 1.5$ at $z = 0$ to $B - R \sim 2.5$ at $z = 0.5$ (as has been observed by, e.g. Couch et al. 1985). The Sdm galaxies, with very small k-corrections in either passband, will remain relatively blue ($B - R < 1$) in the observed $B - R$ colour out to $z \sim 3$.

Dividing a sample of galaxies at $B - R = 1.5$ would clearly be effective in separating rapidly star-forming galaxies from passive galaxies at all $0 \leq z \leq 3$ redshifts, but the

separation of redshift from SFR effects may be less accurate for galaxies of intermediate Hubble type. For example, a non-evolving Sbc spiral would, on account of the $\lambda \simeq 4000$Å break in its spectrum, appear as red at $z \sim 0.5$ as an elliptical at lower redshift. The selection of a subsample of 'passive' galaxies as those with $B - R \geq 1.5$ would then effectively set an upper limit on the SFR of the galaxies included – approximately that of a present-day Sbc type – but may exclude some galaxies with even lower SFRs (e.g. Sab type) at low redshifts. However, the fact that the excess in the number counts at $23 \leq B \leq 24$ above no-evolution predictions is made up entirely of galaxies blueward of this colour (MSFJ) suggests that such a division is still useful, and that the onset of significant SFR evolution would shift the $B - R$ colour to $B - R < 1.5$ in most or all galaxies.

In addition to very blue colours, star-forming galaxies possess strong emission lines in their spectra, in particular from OII at 3727Å and OIII at 5007Å, although the lines are not broadened as in QSO spectra. Rapid star formation results in OII(3727Å) equivalent widths as large as W[OII] $\sim$ 20–100 Å, whereas passive galaxies (i.e. those with no ongoing star-formation) will have much weaker (W[OII] $<$ 5Å) emission lines. It may also be useful to divide a galaxy sample by OII(3727Å) equivalent width, e.g. at W[OII] = 20Å, which is approximately the median value observed at depths of $B \geq 21$ where a sample becomes much more dominated by star-forming galaxies than at brighter magnitudes.

Classification of galaxy types by W[OII] rather than $B - R$ would avoid the redshift dependence of the $B - R$ colour caused by the difference in blue-band and red-band k-corrections, but may suffer other problems. For example, OII observations of brighter galaxies may be affected by selection effects if the spectroscopic slits only cover part of the galaxy (as OII emission may be concentrated in the spiral arms and/or HII regions), and for fainter galaxies W[OII] estimates would suffer larger statistical errors than measurements of the colours, due to the small number of photons detected in a single emission line compared to a broad colour passband. Indeed, with presently available instruments it is very difficult to detect even a very strong emission line in the spectrum of any galaxy as faint as $B \sim 24$, and if the galaxy lies at $z > 1$ the 3727Å line will be shifted into the near-infrared, where the much higher sky background imposes somewhat brighter limits on spectroscopy. Consequently, for all galaxies at $B > 24$, and any $23 \leq B \leq 24$ galaxies which may be at $z > 1$, neither W[OII] nor the redshift can be directly measured at present, and we are limited to the use of broad-band colours to classify individual very faint galaxies.

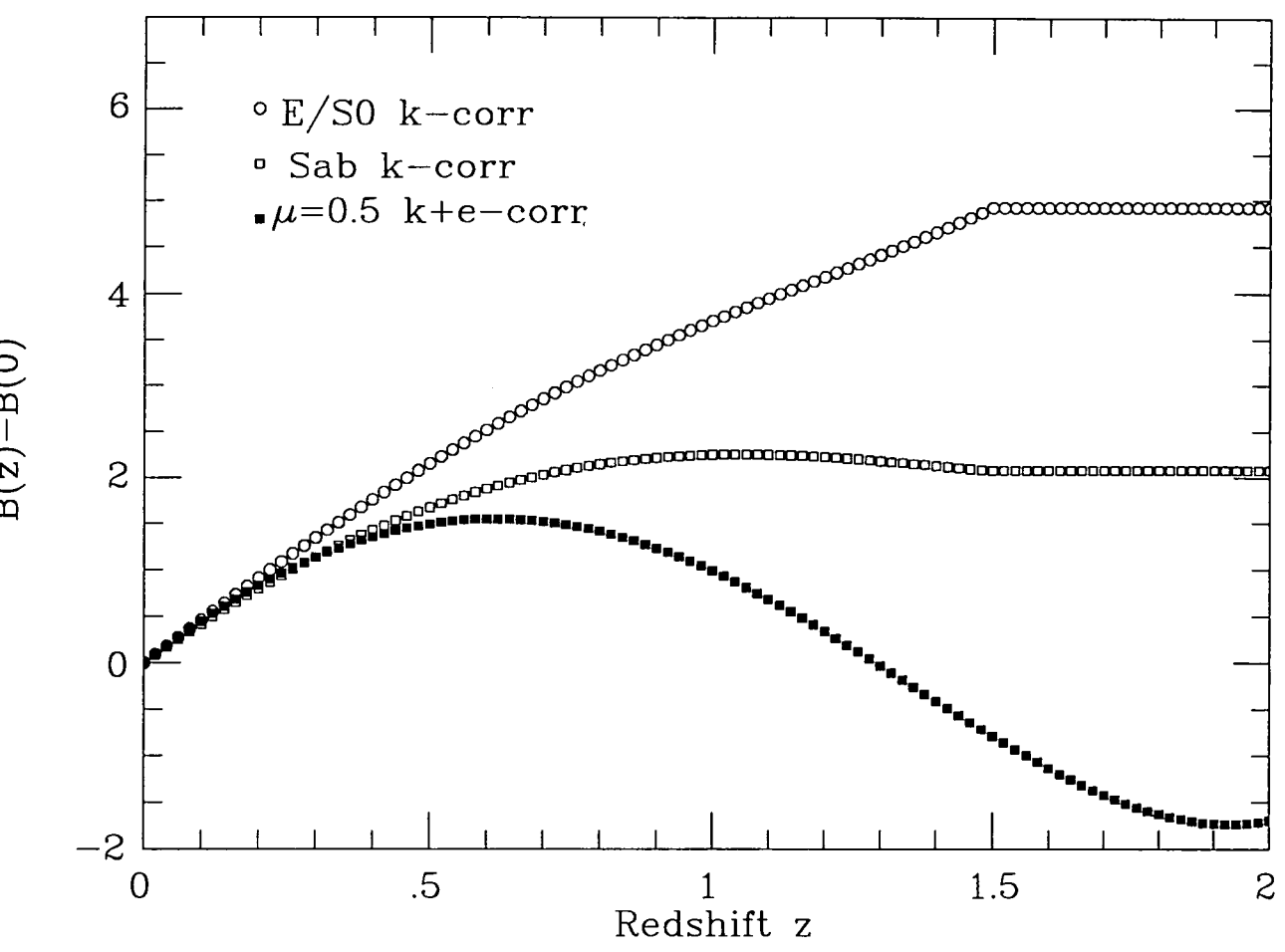

Figure 1.1 The blue-band k-corrections for early-type (E/S0 and Sab) galaxies, and the Bruzual (1981) $\mu = 0.5$ model (k+e)-correction for the evolution of early type galaxies, in magnitudes as a function of redshift.

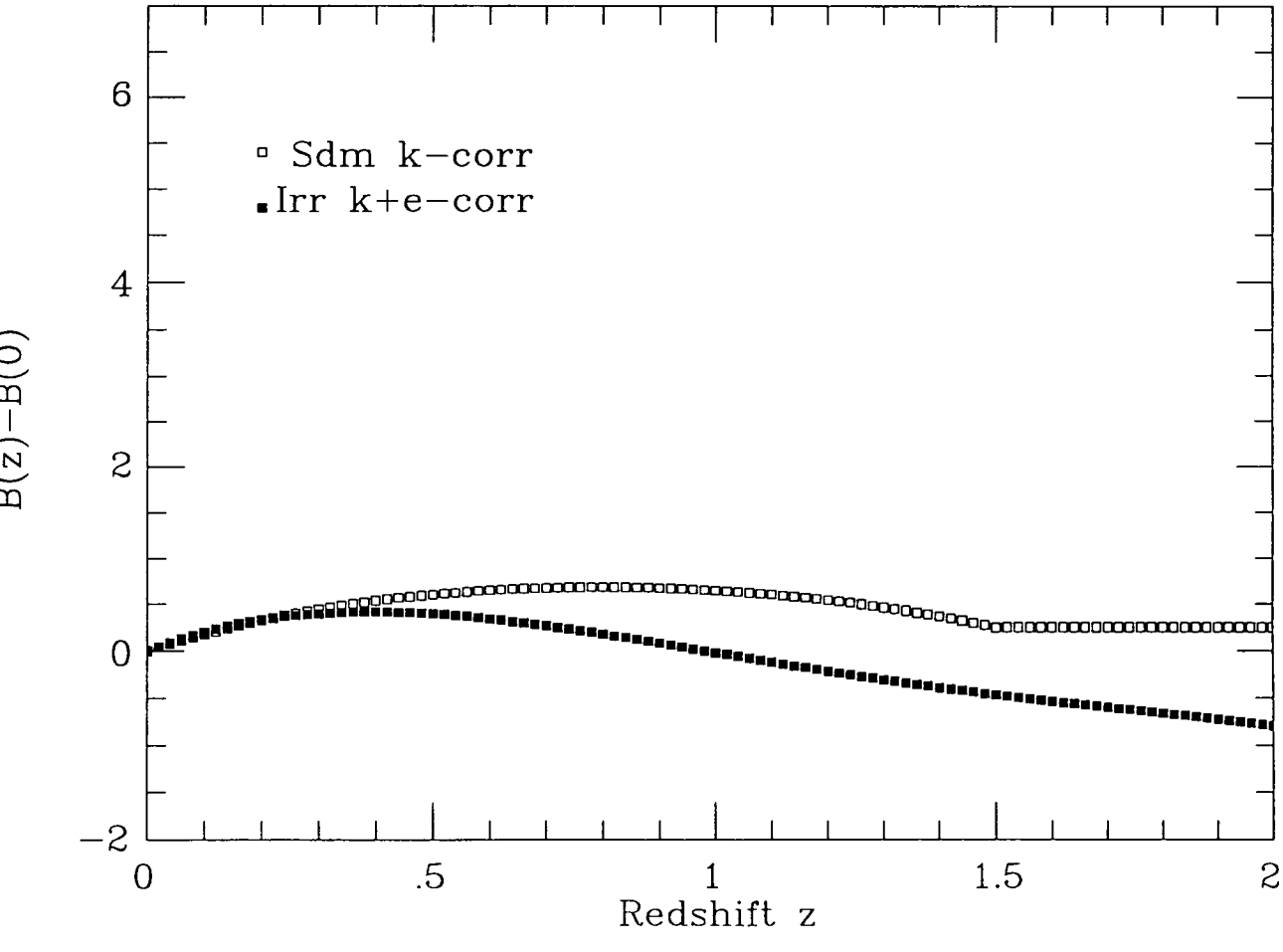

Figure 1.2 The blue-band k-correction for late-type (Sdm) galaxies, and the Bruzual (1981) 'Irr' model (k+e)-correction for the evolution of late-type galaxies, in magnitudes as a function of redshift.

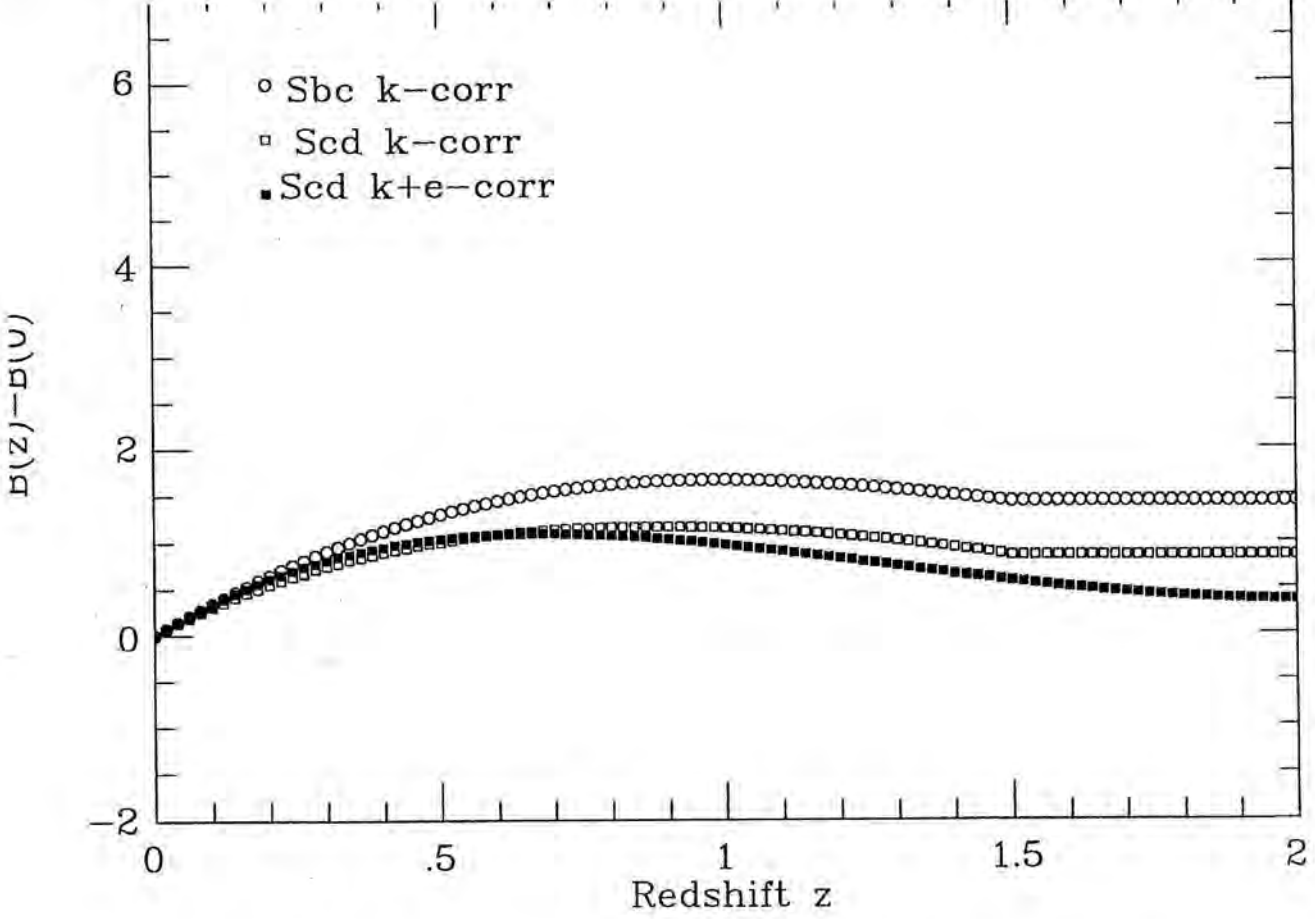

Figure 1.3 The blue-band k-corrections, for 'intermediate' spiral (Sbc and Scd) galaxies, and the Bruzual (1981) 'Scd' model (k+e)-correction for the evolution of spiral galaxies, in magnitudes as a function of redshift.

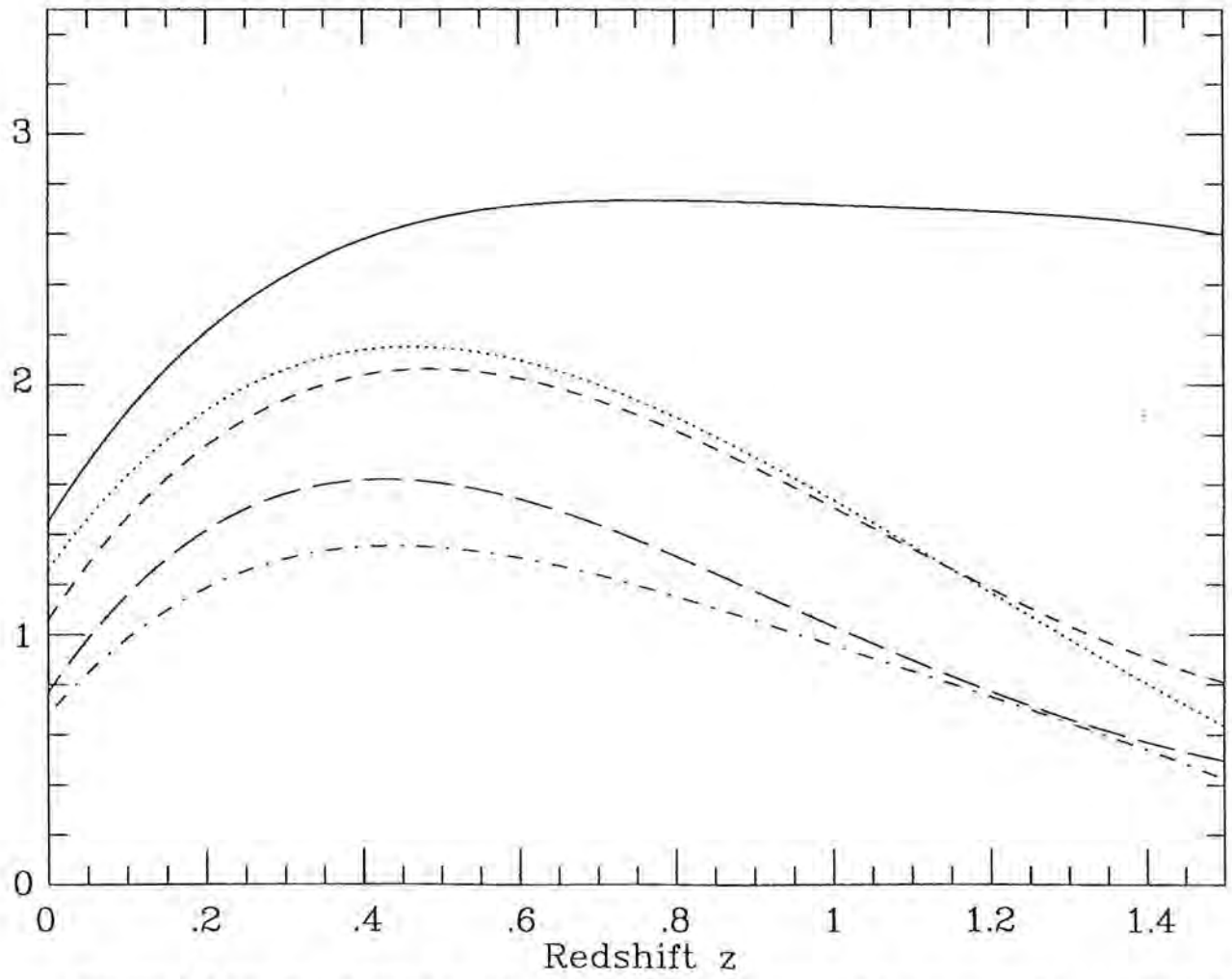

Figure 1.4 The $B - R$ colour as a function of redshift, of non-evolving galaxies of type E/S0 (solid line, top), Sab (dotted), Sbc (short dashes), Scd (long dashes) and Sdm (dot-dash, bottom).

1.4 The Luminosity Function of Galaxies

In this thesis a number of models of galaxy evolution will be compared with various types of observations. In order to compare with observations in which the apparent magnitudes, but not the redshifts, of the faint galaxies are measured, we must convert the evolution of the properties of galaxies (i.e. luminosity, colour, number density), given by each model as a function of time/redshift, into a prediction of the distribution of galaxy redshifts $N(z)$ – and the total numbers of galaxies (i.e. the number counts) – at any given apparent magnitude. To do this we need to incorporate in our models not merely the evolution with redshift of galaxies with an 'average' luminosity, but also the distribution of galaxy luminosities at each redshift.

Galaxies vary greatly in their luminosities, over a range exceeding a factor of ~ 1000. The relation between the number of galaxies of a given luminosity found per unit volume of space, and the galaxy luminosity – the *galaxy luminosity function* (LF) – is usually represented as the Schechter function

$$\phi(L) = \phi^*(L/L^*)^{\alpha}\exp(-L/L^*)$$

which is parameterized by a characteristic luminosity L^*, a faint-end slope α and a density normalization ϕ^*. In terms of absolute magnitude M this can be expressed as

$$\phi(M) = 0.92\phi^*\exp[\exp(0.92(M - M^*)) + 0.92(1 + \alpha)(M - M^*)]$$

the factors of 0.92 in this expression being 0.4 ln (10).

The parameters of the *zero-redshift* LF for the models used in this thesis are listed in Table 1.1, with separate normalizations (ϕ^*), faint-end slopes (α), and characteristic absolute magnitudes (M^*_B in the blue-band, M^*_K in the infra-red K band) for each morphological type.

The B-band LFs are as given by MSFJ, with small ($\leq 0.1^m$), but colour-dependent, corrections applied to convert b_J magnitudes into the B_{ccd} system used here (see MSFJ). These B-band LFs were converted to equivalent K-band LFs by adding mean $B_J - K$ colours for each morphological type (from Glazebrook 1991) to the respective blue absolute magnitudes M^*_B to give the M^*_K magnitudes listed in Table 1.1, while assuming the same values of α and ϕ^* to apply in the two passbands.

With these luminosity functions, half the blue light emitted within a large volume of space at the present day will be produced by the galaxies more luminous than $M_B = -20.6$ ($L \simeq 0.6L^*$), which possess a number density of 1.0×10^{-3} Mpc^{-3}. For each one of these 'giant' galaxies there will be, on average, 24 'dwarfs' with $-20.6 < M_B \leq -14.6$ (ie. on the faint-end slope of the luminosity function), producing about the same total luminosity. We initially assume the LFs to cut-off seven magnitudes faintward of M^*, but this is only a lower limit on the range of luminosities over which the power-law faint-end slope extends. If, for example, the faint-end slope extends a further $\sim 7^m$ faintward (to globular cluster sizes), there would be even larger numbers of galaxies at $M_B > -14.6$ than at all brighter luminosities, but the contribution of these very small dwarf galaxies to the total luminosity density will be less than 5% if $\alpha \geq -1.5$.

Hence, although the great majority of galaxies are dwarfs ($L < 0.25L^*$), the total luminosity density is dominated by the less numerous $L \sim L^*$ galaxies. As the more luminous galaxies are seen out to greater distances than dwarfs at a given magnitude limit, the galaxies in the peak of the redshift distribution $N(z)$ of a magnitude limited sample will also be those with $L \sim L^*$ luminosities (unless the faint-end slope is extremely steep, i.e. $\alpha \leq -1.8$). This will be true for $N(z)$ at all magnitude limits until

galaxies can be seen out to their maximum redshifts, at very faint magnitudes of $B \sim 25$ or fainter, where $N(z)$ and the number counts may then become dominated by dwarf galaxies. (see Chapter 4).

1.5 Pure Luminosity Evolution Models

In this and the following Section we review a number of evolutionary models which have been proposed to explain the excess of faint blue galaxies. In all these models, a significant enhancement of star-formation processes at earlier epochs produces an increase in the total luminosity density of galaxies, given by the summation $\int L\phi(L)dL$ over the luminosity function, with redshift. However, as the shape of the LF is described by three parameters (L^*,ϕ^*,α), models of galaxy evolution can differ greatly in their assumptions about which parameters (or combinations of any two or of all three parameters), evolve to accomodate the increase in the total $\int L\phi(L)dL$. We discuss the effects of the different possible forms of galaxy evolution on the number counts and the redshift distribution, $N(z)$, of galaxies at a given apparent magnitude, briefly describe the effect of q_0 on the number counts, and show how $N(z)$ may provide much more information about the processes of galaxy evolution than number counts alone.

If we assume for now that the distribution of stellar mass into galaxies remains constant with time, so that the increased star-formation rate at earlier epochs simply brightens each individual galaxy, the effect on the LF is that L^* increases with redshift while ϕ^* and α remain constant. This is described as *pure luminosity evolution* (PLE). In other words, PLE models of galaxy evolution are defined by the assumptions that:

(i) The number of galaxies per unit of comoving volume is conserved.

(ii) The star-formation histories of galaxies, and therefore their luminosity and colour evolution, are independent of galaxy mass or present-day galaxy luminosity and relate only to morphological type. Giant and dwarf galaxies of the same morphological type would therefore have evolved, relative to their present-day luminosities, by the same number of magnitudes when seen at a given redshift.

A brightening of L^* with redshift would increase z_{mean} and the maximum redshift at which any galaxies are visible at a given apparent magnitude. PLE models therefore predict that high redshift ($z > 1$) galaxies will be seen at significantly brighter apparent magnitudes (and with bluer colours) than would be the case if galaxies did not evolve, with the effects of increased star-formation in high-redshift galaxies being enhanced by the redshifting of the UV wavelengths most sensitive to the SFR into the B-band.

Figure 1.5 illustrates this by showing the apparent magnitude as a function of redshift for evolving and non-evolving Sab and Irr galaxies of absolute magnitude $M_B = -21.0$ (for $H_0 = 50$ km s^{-1}Mpc^{-1}), ie. $L \sim L^*$ luminosity, with the distance modulus–redshift relation of a $q_0 = 0.05$ Universe. With the Bruzual evolution, high redshift galaxies will appear in the sample quite suddenly on going to fainter limits, over a narrow range of magnitudes centred on $B \simeq 24$, whereas if L^* does not brighten with redshift they will appear more gradually at $B \sim 25$. Furthermore, if L^* evolves as strongly as this model predicts, it should be possible to see galaxies out to $3 < z < 4$, where they may be first forming, within the limits of the deepest CCD surveys ($B \simeq 27.5$), whereas this would not be the case without luminosity evolution. In this thesis we shall be investigating both these consequences of L^* evolution for the redshift distribution of faint galaxies, by means of an analysis of faint galaxy clustering.

We now compute the galaxy counts expected in the absence of any form of evolution, using the luminosity functions and k-corrections for the five galaxy types, as described

above. A pure luminosity evolution model was also computed using the same luminosity functions, with the three Bruzual (1981) model (k+e)-corrections described above – the $\mu = 0.5$ ($\tau_{SFR} = 1.44$ Gyr) model used for E/S0/Sab types, the spiral evolution model for Sbc and Scd types and the 'Irr' model for Sdm galaxies. As the (k+e)-corrections were only tabulated by Bruzual (1981) to to $z = 2.0$, we here assume them constant from $z = 2.0$ to $z = 4.0$, the redshift corresponding to the Lyman limit 'cutting off' the blue band and the maximum galaxy redshift included in the models plotted here. The non-evolving model and this 'simplified' Bruzual PLE model are essentially the same as those used by MSFJ in interpreting their number counts.

In our non-evolving K-band model, the k-correction assumed for all galaxy types was the Bruzual (1981) no-evolution K-band model. Our K-band PLE model used the Bruzual (1981) $\mu = 0.5$ model (k+e)-corrections, as computed for the K band, for the E/S0/Sab galaxies, but assumed the non-evolving k-correction for all later types.

Figure 1.6 shows the blue-band galaxy number counts from a number of photographic and CCD surveys, compared with the no-evolution and PLE models, for both $q_0 = 0.5$ and $q_0 = 0.05$ cosmological geometries. Figure 1.7 shows the same comparison, again for both $q_0 = 0.5$ and $q_0 = 0.05$, for the infra-red K band, using our non-evolving and PLE models and the most recent K-band number counts as tabulated by Gardner, Cowie and Wainscoat (1993).

The comparison of observations in these two passbands will be particularly informative due to the very different stellar populations producing most of the flux in each case; the K-band emission being dominated by the redder stars, which comprise most of the luminous mass, and being increased very little by star-forming activity. The K-band emission from a hot body will be increased little by raising its temperature above that of a 'cool' M star ($T \sim 3000K$), whereas the corresponding temperature for blue-band emission is $T \sim 15000K$, that of a massive B-type star. Hence the K-band luminosity of a galaxy will approximately be proportional to the total mass existing as stars of any type, whereas the B-band luminosity is very sensitive to the relative proportions of hotter and cooler stars.

At the fainter magnitude ranges shown here, the Bruzual model L^* evolution raises the predicted count in the blue band to a much greater extent than in the K band, as would be expected for a model in which the 'extra' luminosity added to high redshift galaxies is mainly in the form of very hot blue stars. The observed counts appear to confirm this – Bruzual's PLE models giving a good fit to the counts in both passbands over a very wide range of magnitudes. Indeed, in a low q_0 Universe, PLE models fit the number counts well from the shallowest large-area surveys to at least $B \simeq 26$ and $K \simeq 23$. We can conclude from this that the same star formation history appears to produce the required amount of evolution in both of these widely separated passbands.

Early type galaxies would be expected to redden from $B - K \sim 4.0$ at $z = 0$ to $B - K \sim 6.5$ when they are seen at $z \sim 0.5$ because of k-correction effects, but the $\mu = 0.5$ model predicts that this reddening would be reversed at higher redshifts by the increase in SFR, giving $B - K \sim 4.0$ again at $z \sim 2$. This is exactly the trend in median $B - K$ with K magnitude that is observed, the turn-over from reddening to bluening, accompanied by a flattening in the count slope from $\frac{d(logN)}{dm} \simeq 0.67$ to $\frac{d(logN)}{dm} \simeq 0.26$ occurring at $K \simeq 17 - 18$ (Gardner, Cowie and Wainscoat 1993). This K magnitude corresponds to blue magnitudes of $B > 22$, where the appearence of excess galaxies with blue colours keeps the blue-band count gradient relatively steep to much fainter limits.

The separation of star-formation from other effects achieved by observing in the K-band allows us to check our local normalization ϕ^*, for which a relatively high value

has been assumed in these models (see MSFJ). The blue-band counts might be well-fitted by a model with a significantly lower (by as much as 50%) local ϕ^*, but stronger luminosity evolution, especially at $z < 0.5$ (where the L^* evolution is quite weak in the Bruzual models used here), which would raise the counts as $B \sim 18$ and fainter magnitudes sufficiently to compensate for the lower ϕ^*. However, in the K-band this extra luminosity evolution, being associated with star-formation, would be much weaker than in the B-band. Hence the extra evolution needed to fit the blue-band counts with a low ϕ^* would not increase the number counts in the K-band sufficiently to compensate for the lowering of the normalization, and if the local ϕ^* was reduced by as much as 50% the observed K-band counts would be significantly underpredicted.

The fact that the very moderate K-band luminosity evolution expected from the Bruzual models is sufficient to fit the K-band counts at faint ($17 \leq K \leq 23$) magnitudes therefore appears to favour the high normalization used by, for example, MSFJ. This would suggest that the lower normalization derived from some surveys at $14 \leq B \leq 17$ may be an underestimate of the true large-scale local normalization – resulting from, for example, large-scale structures and/or selection effects due to low surface brightness galaxies being under-represented in brighter photographic surveys. We would not then require any rapid evolution of galaxies between the shallower $14 \leq B \leq 17$ surveys and the low redshifts ($z \sim 0.1$) of $B \sim 18$ galaxies to fit the higher normalization at $B \sim 18$ (see MSFJ).

The PLE models with $q_0 = 0.5$ fit the counts just as well as in a low-q_0 Universe at $B < 24.5$ and $K < 20$, where the q_0-dependence is small, but significantly underpredict the counts faintwards of these magnitudes. As shown by, e.g. Guiderdoni and Rocca-Volmerange (1990), the high galaxy counts at $B > 24.5$ strongly favour a very open Universe ($q_0 \leq 0.15$), for *any* form of PLE model – adding even larger amounts of L^* evolution would overpredict the counts at brighter magnitudes instead of improving the fit at $B \geq 24.5$. The sensitivity of the modelled counts of very faint galaxies to q_0 results from the effect of the cosmological geometry on the comoving volume available for galaxies. Figure 1.8 illustrates this by showing the differential comoving volume element $\frac{dV_{com}}{dz}$ as a function of redshift for $q_0 = 0.5$ and $q_0 = 0.05$. At $z = 0.4$, $\frac{dV_{com}}{dz}$ in a $q_0 = 0.05$ Universe is larger than that in a $q_0 = 0.5$ Universe by a factor of only 1.39, but this increases to a factor of 3.45 at $z = 1.8$, so the effect of q_0 on the galaxy number counts will obviously become much greater at the magnitudes at which high redshift ($z > 1$) galaxies become visible.

However, we cannot immediately rule out a $\Omega = 1$ Universe on the basis of faint galaxy number counts alone. The possibility remains that additional (non-PLE) forms of galaxy evolution may be contributing to the high number counts, as we now discuss in the next section.

Type	ϕ^*	α	M_B^*	M_K^*
E/S0	7.61×10^{-4}	-0.7	-21.0	-24.93
Sab	4.35×10^{-4}	-0.7	-21.02	-24.80
Sbc	5.43×10^{-4}	-1.1	-21.33	-24.84
Scd	2.83×10^{-4}	-1.5	-21.45	-24.35
Sdm	1.52×10^{-4}	-1.5	-21.45	-23.71

Table 1.1 The luminosity function parameters, at zero redshift, assumed in all our evolving and non-evolving models. The density normalization (ϕ^*) in galaxies per cubic Mpc, the faint-end slope (α), and the characteristic absolute magnitudes in the blue-band (M_B^*) and in the K-band (M_K^*) are listed separately for the luminosity functions of galaxies in each of five morphological types (into which the galaxies in these models are divided). A Hubble constant of $H_0 = 50$ km s^{-1}Mpc^{-1} is assumed.

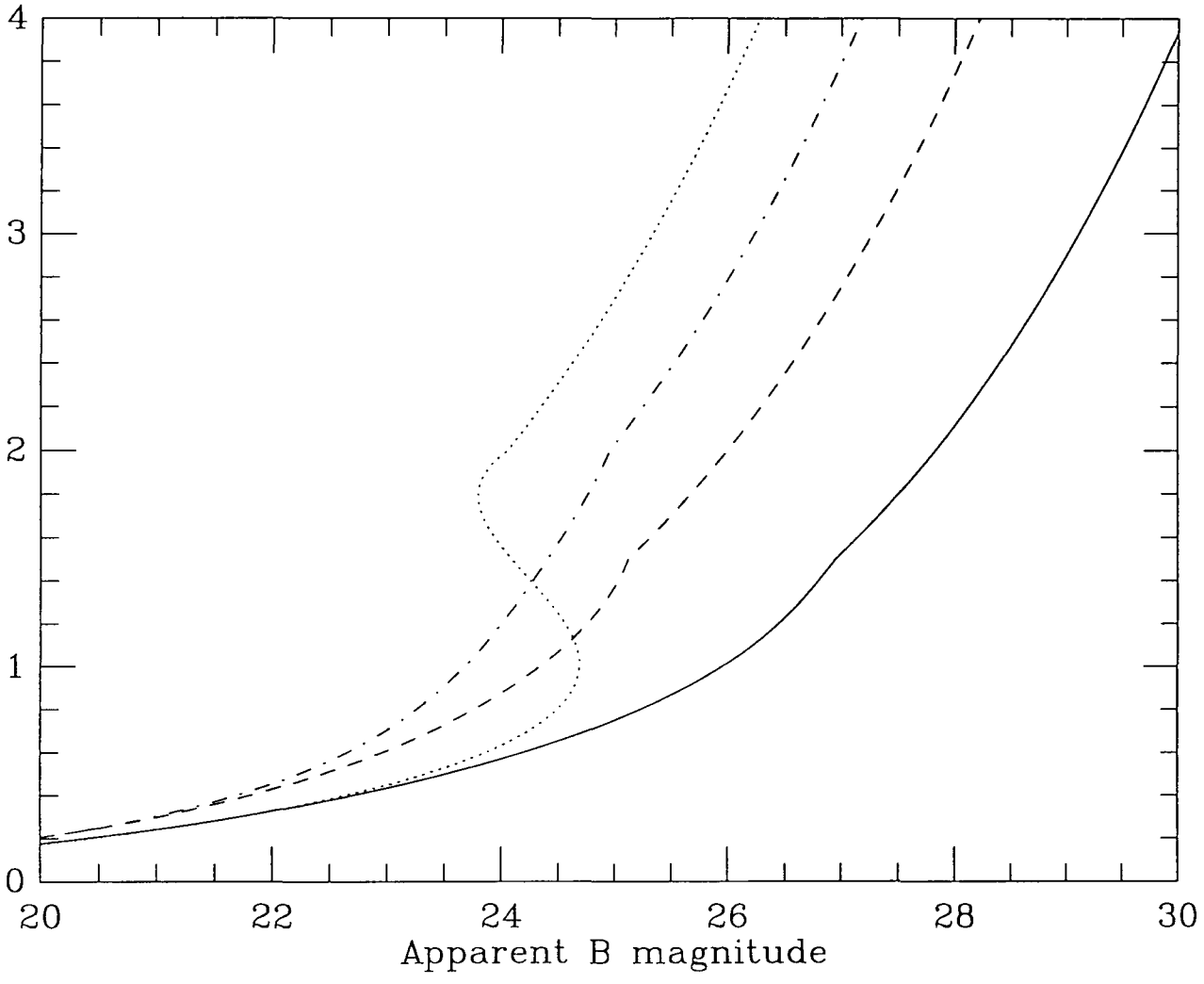

Figure 1.5 Apparent magnitude as a function of redshift, in a $q_0 = 0.05$ Universe, for galaxies with absolute magnitude $M_B = -21.0$ at $z = 0$. This relation is shown here for Sab galaxies with no evolution (solid line) and with Bruzual $\mu = 0.5$ model evolution (dotted line); and for Sdm galaxies with no evolution (dashed line) and with Bruzual 'Irr' model evolution (dot-dash line).

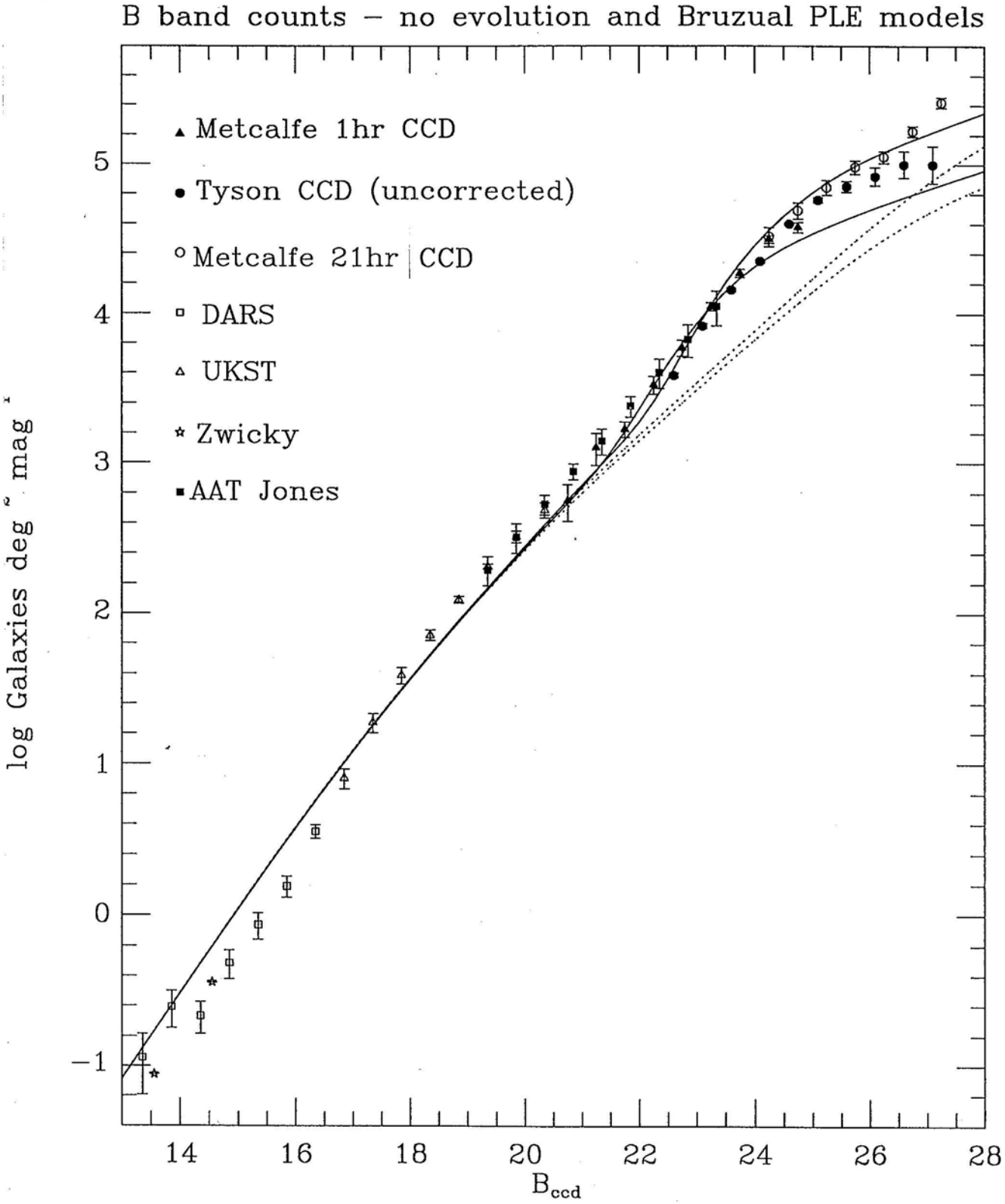

Figure 1.6 Observed galaxy number counts in the blue band, including the 1 hr CCD data of MSFJ and photographic counts as given by MSFJ and JSF, the Tyson (1988) survey and the 21 hr CCD counts of Metcalfe et al. (1994). These are compared with a non-evolving model (dotted lines) and our Bruzual pure luminosity evolution model (solid lines), both models being shown for both $q_0 = 0.5$ (lower) and $q_0 = 0.05$ (upper) geometries.

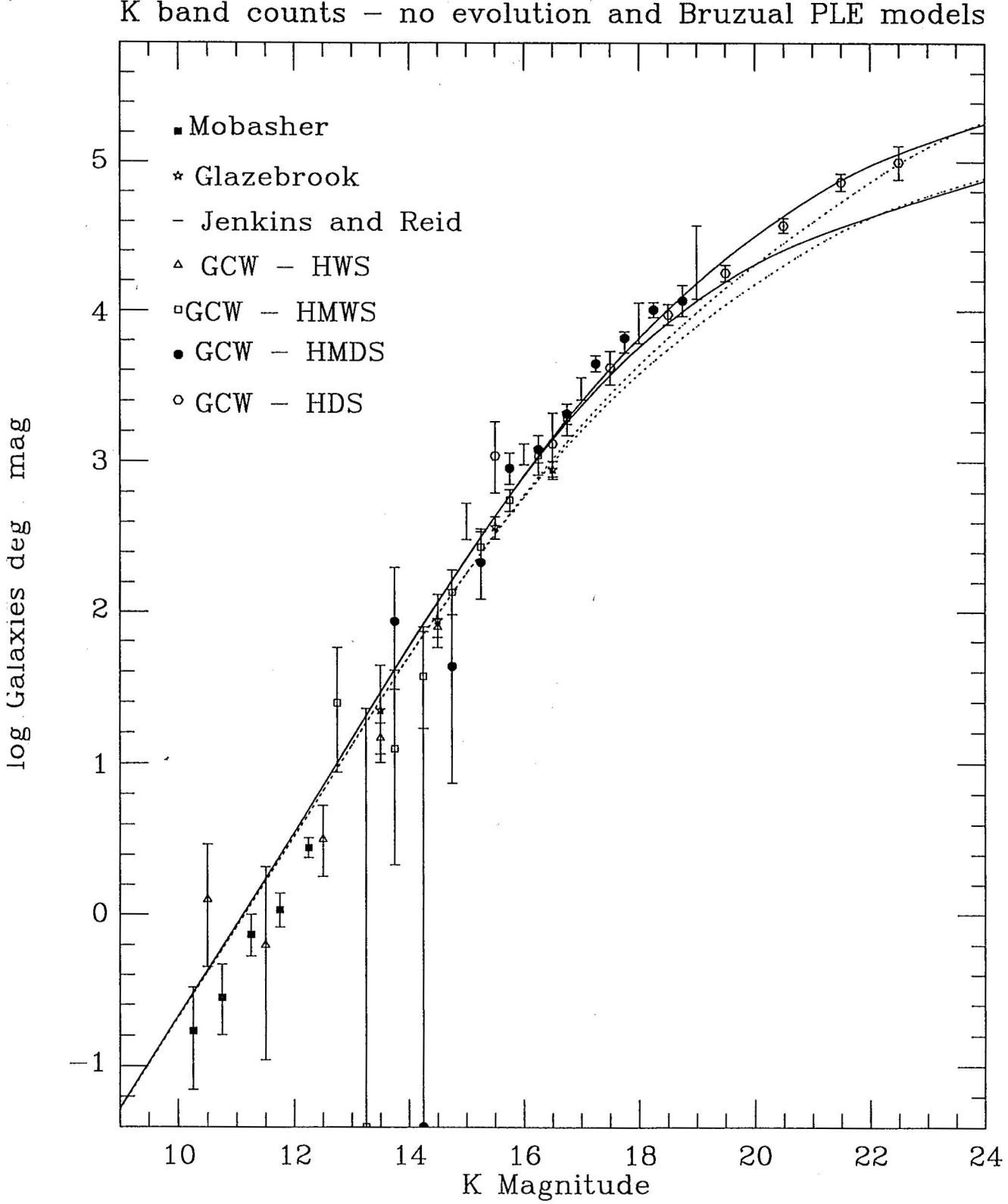

Figure 1.7 Observed galaxy number counts in the K band, from Gardner, Cowie and Wainscoat (1993, GCW), Glazebrook (1991) and Mobasher et al. (1986). These are compared with a non-evolving model (dotted lines) and our Bruzual pure luminosity evolution model (solid lines), both models being shown for both $q_0 = 0.5$ (lower) and $q_0 = 0.05$ (upper) geometries.

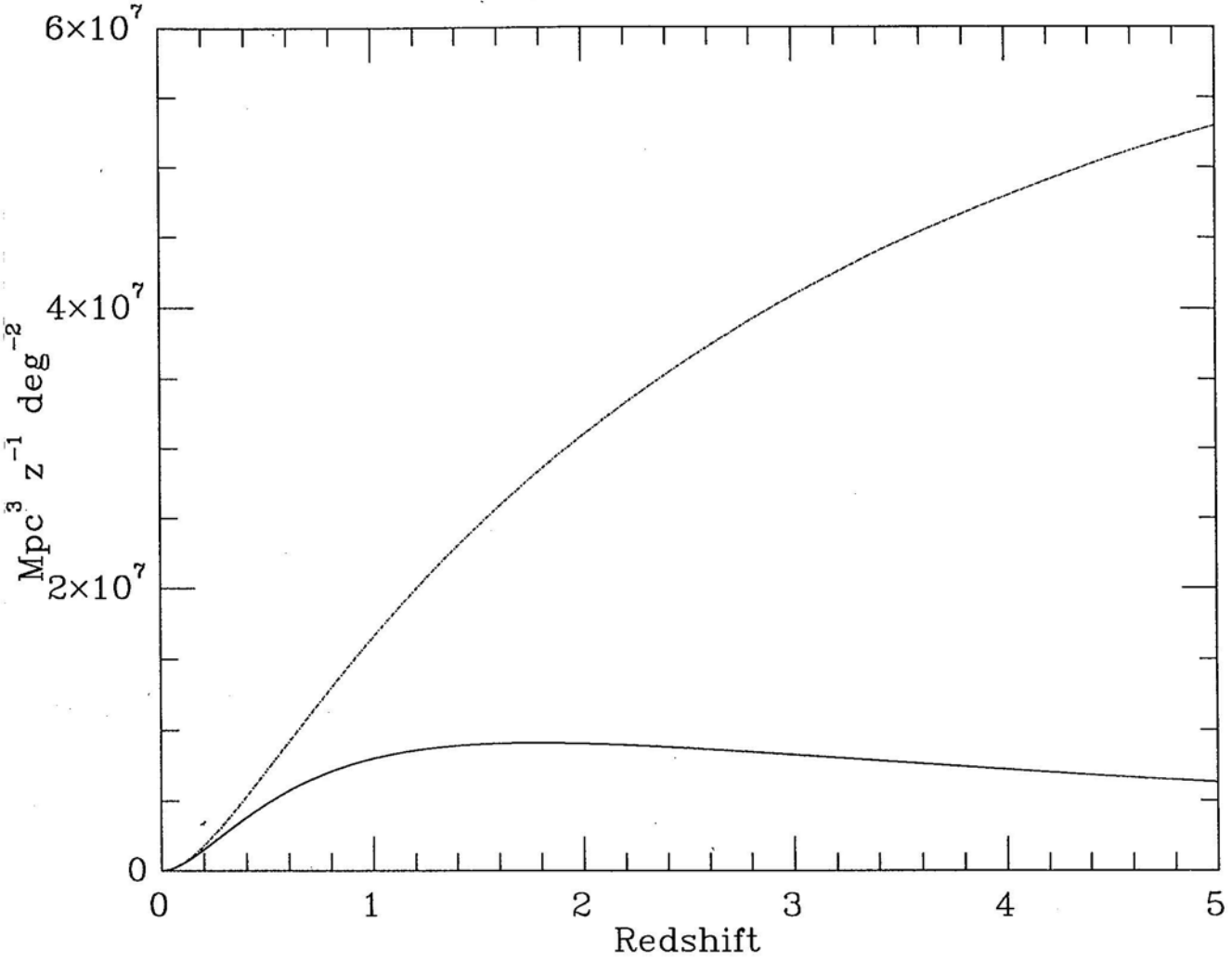

Figure 1.8 Differential comoving volume element ($\frac{dV_{com}}{dz}$) as a function of redshift for $q_0 = 0.5$ (solid line, lower) and $q_0 = 0.05$ (dotted line, upper).

1.6 Merging and Luminosity-Dependent Evolution Models

The first indication that the galaxy luminosity function may have evolved in a more complicated way than a simple brightening of L^* with redshift came from the spectroscopic survey of Broadhurst, Ellis and Shanks (1988, hereafter BES). To $b_J = 21.5$ it was found that the mean redshift (0.216) and the form of the redshift distribution $N(z)$ were as given by a no-evolution model, with no $z > 0.5$ galaxies detected. However, relative to the non-evolving model used for comparison, the observations showed an excess in both the number and the proportion of blue galaxies with a strong 3727Å OII emission line – i.e. galaxies undergoing rapid star-formation activity. In a deeper spectroscopic survey reaching $b_J = 22.5$, Colless et al. (1990) also found a no-evolution $N(z)$ with $z_{mean} = 0.31$, and a similar excess of high-SFR galaxies.

The fact that these star-forming galaxies were found within the no-evolution $N(z)$ rather than, as PLE models would predict, as an extended 'tail' at higher redshifts, appeared to suggest that present-day low-luminosity galaxies brighten to a greater extent out to $z \sim 0.7$ than do $L \sim L^*$ galaxies – a *luminosity-dependent luminosity evolution.*

As a possible physical mechanism for this type of evolution, BES hypothesised that short (duration $\sim$ 0.1 Gyr) bursts of star-formation in gas-rich late-type galaxies occurred much more frequently in the past, even at relatively recent epochs ($z \sim 0.2$), with the important additional assumption that all these bursts involve approximately the same fixed mass of gas. A 'BES' starburst would greatly increase the blue-band luminosity of a dwarf galaxy, for a period of $\sim$ 0.1–1 Gyr, but would produce much less effect on the total luminosity if it occurred in a giant galaxy. These starbursts would cause the absolute magnitude of $L < L^*$ galaxies to brighten by a greater number of magnitudes than that of $L \sim L^*$ galaxies, resulting in a steepening of the faint-end slope of the luminosity function (α) with increasing redshift, with somewhat less evolution of L^* than in a PLE model.

However, the $B < 22.5$ spectroscopic results may still be consistent with Bruzual-type PLE models if the luminosity function of blue galaxies possesses a significantly steeper faint-end slope than that of redder galaxies, for which there is observational evidence (Shanks 1989), and a high local normalization of the counts is assumed. Much more serious problems are posed for PLE models by claims, on the basis of smaller and less complete surveys, that a no-evolution $N(z)$, with $z_{median} \sim 0.4$, is seen even at $22.5 \leq B \leq 24$ (Lilly, Cowie and Gardner 1991; Cowie, Songaila and Hu 1991; Glazebrook et al. 1993). In this range of magnitudes the excess in the counts is much greater, a factor of $\sim$ 2.5 above non-evolving predictions even with our high normalization, and a PLE model can only explain these counts by adding a large high-redshift component to the redshift distribution, which would increase the median redshift to $z_{median} \sim 1.0$.

These results led to suggestions that the physical merging of galaxies, in addition to the enhancement of star-formation at earlier epochs, is a major process in galaxy evolution. The galaxies seen today would then have existed at earlier epochs as several sub-components – at higher redshifts the comoving number density would be greater and the mean galaxy mass correspondingly less. However, the increased SFR needed to explain the blue colours would raise the luminosity per unit mass, as observed in the blue band, so tending to compensate for the smaller masses of the sub-components. In the blue band there might then be little change in L_B^* with redshift, and a merging model could resemble a pure density evolution model. The 'excess' galaxies could then be accomodated in the smaller comoving volume elements existing at lower redshifts, giving $N(z)$ close to a no-evolution form, but with a raised normalization. Similarly, an increase in ϕ^* with redshift could also enable an $\Omega = 1$ Universe to accomodate the high

galaxy counts at $B > 24.5$.

A low median redshift at faint magnitudes could also result from the existence at moderate redshifts of a large population of starbursting dwarf galaxies, which has somehow 'disappeared' between $z \sim 0.4$ and the present day (Babul and Rees 1992). When the total galaxy LF is considered, the effect of a *luminosity-dependent density evolution* of this type would be a steepening of the faint-end slope with redshift, similar to that produced by the luminosity-dependent luminosity evolution of the BES model. As the faint-end of the total galaxy LF is a power-law extending over a very wide range of magnitudes (to at least 7^m faintward of M^*), luminosity and density evolution of the dwarf galaxies only will be essentially equivalent in their effects on $N(z)$.

For $L << L^*$ dwarf galaxies,

$$\phi(L) \simeq \phi^*(\frac{L}{L^*})^\alpha$$

so that increasing L^* to βL^* has the same effect on $\phi(L)$, and therefore on $N(z)$, as increasing ϕ^* to $\beta^{-\alpha}\phi^*$. In contrast, L^* and ϕ^* evolution would produce very different effects on $N(z)$ when applied to $L \sim L^*$ galaxies, at the 'knee' of the LF. As the peak of $N(z)$ at a given magnitude normally consists of $L \sim L^*$ galaxies, the former would increase the redshift at which the peak is seen, the latter would increase the height of the peak with little change in its position.

However, the true form of $N(z)$ at $B \sim 24$ remains very uncertain. Lilly, Cowie and Gardner (1991) did conclude that two of the $B \simeq 24$ flat spectrum objects they examined spectroscopically, for many hours without detecting emission lines, were probably at $z > 1.25$, and the Glazebrook et al. (1993) survey contained a proportion $\sim 30\%$ of mainly very blue unidentified objects, which could also have been high-redshift star-forming galaxies. As we shall discuss in more detail in Section 2.5, the constraints from spectroscopic surveys on the relative numbers of high and low redshift galaxies at $B \sim 24$, and therefore the relative importance of L^* and ϕ^* evolution in explaining the high number counts, are very limited with present data.

Obtaining a spectroscopic redshift obviously requires many more photons, by a factor of ~ 100 even when strong emission lines are present, than does simply measuring the position and broad-band magnitude of a galaxy. Although measuring the spectroscopic redshift of any galaxy as faint as $B \sim 24$ is very difficult and time-consuming, imaging of the galaxies in broad colour passbands is possible for galaxies several magnitudes fainter than this. The presently observable properties of faint ($24 \leq B \leq 27$) galaxies therefore consist of magnitudes, colours, and – through analysis of their positions on the CCD images – their clustering.

Because actively star-forming galaxies possess flat or power-law SEDs in the range of wavelengths accessible to ground-based observers (ie. U-band to K-band), their observable colours would be approximately independent of redshift out to $z \sim 3$. Therefore high redshift and low redshift faint blue galaxies cannot be distinguished by their colours alone, and spectral lines *must* be detected to provide a redshift for an individual galaxy. In this thesis we resort to statistical methods which are less direct, but deeper-reaching, than spectroscopy – as described in Section 1.7 following, analysis of the *clustering* of very faint ($24 \leq B \leq 27$) galaxies does provide some information about their redshift distribution.

1.7 Correlation Functions of Faint Galaxies

We can obtain images containing large numbers ($> 10^3$) of galaxies as faint as $23 \leq B \leq 27$, and from these calculate correlation functions for galaxies at the magnitude limits where $N(z)$ becomes very sensitive to the form of galaxy evolution (in particular the degree of brightening of the L^* luminosity at high redshifts), but spectroscopy becomes difficult or impossible. In this section we describe how the angular two-point correlation function, $\omega(\theta)$, can be used as a probe of the redshift distribution $N(z)$ of galaxies, with sufficient sensitivity to distinguish between different evolutionary models, and therefore how the scaling of $\omega(\theta)$ with magnitude limit proves to be a very useful diagnostic of the processes involved in galaxy evolution.

The clustering of galaxies in three dimensions is described by the two-point correlation function $\xi(r)$, in which the intrinsic strength of this clustering (i.e. the $\xi(r)$ amplitude) is parameterized as the correlation radius r_0, the distance at which the probability of finding another galaxy is twice that expected from a random distribution. The value of r_0 was estimated by Groth and Peebles (1977), from the Zwicky catalogue limited at $B \simeq 15$, to be approximately 4.3 h^{-1} Mpc, where $h = (H_0/100$ km s^{-1}Mpc$^{-1})$.

We discuss the form and possible evolution of $\xi(r)$ in Section 3.2, but galaxy redshifts are required to determine r_0 and the form of $\xi(r)$ directly. In this thesis we are primarily concerned with the projection of the three-dimensional clustering described by $\xi(r)$ onto the two-dimensional sky, producing a two-dimensional clustering of the projected galaxy distribution, which is described by the angular correlation function function $\omega(\theta)$ and is measurable without any redshift data. Observations have indicated that $\omega(\theta)$ follows a $\theta^{-0.8}$ power-law (Peebles 1980), out to angular separations corresponding to physical separations of the clustered galaxies of $r \sim 10$ h^{-1} Mpc, i.e. to at least $\theta \sim 20$ arcmin even on the very deepest ($z_{mean} \sim 1$) images, and that the index of the power-law remains approximately constant to the faintest limits of photographic surveys (Jones, Shanks and Fong 1987, hereafter JSF).

The amplitude of the $\omega(\theta)$ power-law is related to the amplitude of the 3-dimensional two-point correlation function $\xi(r)$ by means of an integration over $N(z)$ using Limber's formula. The derivation of Limber's formula is described by, for example, Phillipps et al. (1978) and Peebles (1990), and is also given in Appendix 1 of this thesis. Essentially, Limber's formula incorporates an integration over $[N(z)]^2$ weighted by a term which decreases with increasing angular diameter distance $d_A(z)$. The result of the Limber's formula integration is therefore lowered if either

(i) The variance of the redshifts of galaxies in the sample is increased, and/or

(ii) The typical angular diameter distance of the galaxies is increased.

The angular diameter distance as a function of redshift for both $q_0 = 0.5$ and $q_0 = 0.05$ geometries is shown on Figure 1.9. At low redshifts $d_A(z) \propto z$ approximately, with little q_0-dependence. Beyond $z \sim 1$ $d_A(z)$ increases little with redshift, but at these depths shows a significant dependence on q_0, $d_A(z)$ at a given redshift being greater for lower q_0 geometries. At such depths that $z_{mean} \geq 1$, the angular diameter distances may not increase significantly on going to even fainter limits, but the $\omega(\theta)$ amplitude will still be affected by any increase in the variance of the redshifts. For a lower q_0, a given $N(z)$ will produce a lower $\omega(\theta)$ amplitude, on account of the greater angular diameter distances of the galaxies, but the dependence of $\omega(\theta)$ on q_0 will only be significant at such depths that $z_{mean} > 1$.

On going to fainter limits the variance and mean of the redshifts of galaxies in the sample would both be expected to increase, giving through Limber's formula a lower

$\omega(\theta)$ for a constant r_0. Essentially, the wider the range of redshifts over which galaxies are distributed the more the observable clustering will be diluted by projection, and the clustering of more distant galaxies will contribute less to $\omega(\theta)$ as their r_0 will be projected to a smaller angle on the sky. Hence the scaling of the $\omega(\theta)$ amplitude of the galaxies with survey depth, from large-area shallow surveys such as the Zwicky catalogue to the depest CCD images ever obtained, will relate primarily to the change of $N(z)$ with the magnitude limit.

The interpretation of $\omega(\theta)$ results in terms of the $N(z)$ of faint galaxies will depend on a number of assumptions made in the models – in particular any evolution in the intrinsic clustering of galaxies over the range of redshifts in the survey would influence the scaling of $\omega(\theta)$ (see Chapter 3) in addition to the effect of luminosity evolution. Despite this, the great sensitivity of $\omega(\theta)$ to $N(z)$ enables the analysis of faint galaxy clustering to provide more information about galaxy evolution than number counts alone.

Previously a number of authors have attempted to measure the clustering at increasingly faint limits. Shanks et al. (1980) determined the $\omega(\theta)$ amplitudes for five UK Schmidt Telescope plates, reaching limits of $b_J \sim 21$. The amplitudes were found to scale from the (15^m limited) Zwicky amplitude as predicted by Limber's formula, providing an important test of its validity over a wide range of magnitudes. However, such depths as are attainable with UK Schmidt plates are insufficient to effectively probe luminosity evolution.

Koo and Szalay (1984) determined the scaling of $\omega(\theta)$ for two 0.2 deg^2 fields in the range of $22 \leq J \leq 24$. Comparisons were made with the predictions of a non-evolving model and several PLE models. These authors concluded that the fall-off of clustering amplitude with magnitude limit was greater than predicted by models which included neither luminosity nor clustering evolution. The results were well-fitted by a model with 'mild' luminosity evolution (a mixture of Bruzual PLE models with low q_0 and a high galaxy formation redshift), with no need to invoke any evolution of the clustering.

Stevenson et al. (1985) obtained $\omega(\theta)$ amplitudes from larger AAT plates to a similar depth, in the red band as well as in the blue. When plotted against galaxy number density the amplitudes for the two passbands were found to be very similar and unexpectedly low, a little lower than those of Koo and Szalay (1984), but the slope of the scaling is about the same. JSF (1987) and Infante (1990) obtained similar amplitudes and scaling from even larger areas of sky ($\geq$2 deg^2).

At fainter limits ($B > 24$, $R > 23$), where the effects of luminosity evolution on the $\omega(\theta)$ amplitude are likely to be greatest, surveys can only be carried out using CCDs. At present, these unfortunately cover much smaller areas than photographic plates. Efstathiou et al. (1991) analysed the clustering of the $24 \leq B \leq 26$ galaxies on the 12 deep CCD fields of the Tyson (1988) survey, covering a total of 107 arcmin^2. Couch, Jercevic and Boyle (1993), and Neuschaefer (1992) then published $\omega(\theta)$ results from CCD surveys covering larger areas than Tyson, but to slightly less deep limits. In this thesis we present results from a CCD survey covering 284 arcmin^2 to $B_{ccd} = 25.0$, 331 arcmin^2 to $R_{ccd} = 23.5$, and 20 arcmin^2 to $B_{ccd} = 27.0$.

At the magnitude limits considered here, the dominant effect on the correlation amplitudes is likely to be luminosity evolution – in particular the evolution of $L \sim L^*$ galaxies – which as discussed above may greatly modify the redshift distribution faintward of $B \sim 23$. If L^* evolution is the main cause of the excess in the number counts of $B > 23$ galaxies, these faint galaxies will have a much higher mean redshift, and therefore a much *lower* $\omega(\theta)$ amplitude, than predicted by non-evolving models. In contrast, as discussed in Section 1.5 above, the effect of merging-dominated evolution

on $N(z)$ is to increase its normalization (relative to the no-evolution prediction) without greatly changing its form (ie. both z_{mean} and the variance of the redshifts). This would give a $\omega(\theta)$ amplitude much closer to the no-evolution prediction, if we assume that the merging process itself does not greatly alter the intrinsic clustering of the galaxies. Hence we initially (in Chapter 2) represent merging-dominated evolution simply by a non-evolving model.

The difference between the $\omega(\theta)$ amplitudes predicted by our PLE and no-evolution models is greatest (a factor of ~ 4) at $24 \leq B \leq 25$, the magnitude range best covered (in terms of numbers of galaxies) by our CCD surveys. It is therefore hoped that correlation analysis of our CCD dataset will enable us to exclude at a high level of statistical significance at least one of these two models of $N(z)$ at $24 \leq B \leq 25$, and therefore determine whether merging or L^* evolution is the main cause of the high galaxy count at these magnitudes.

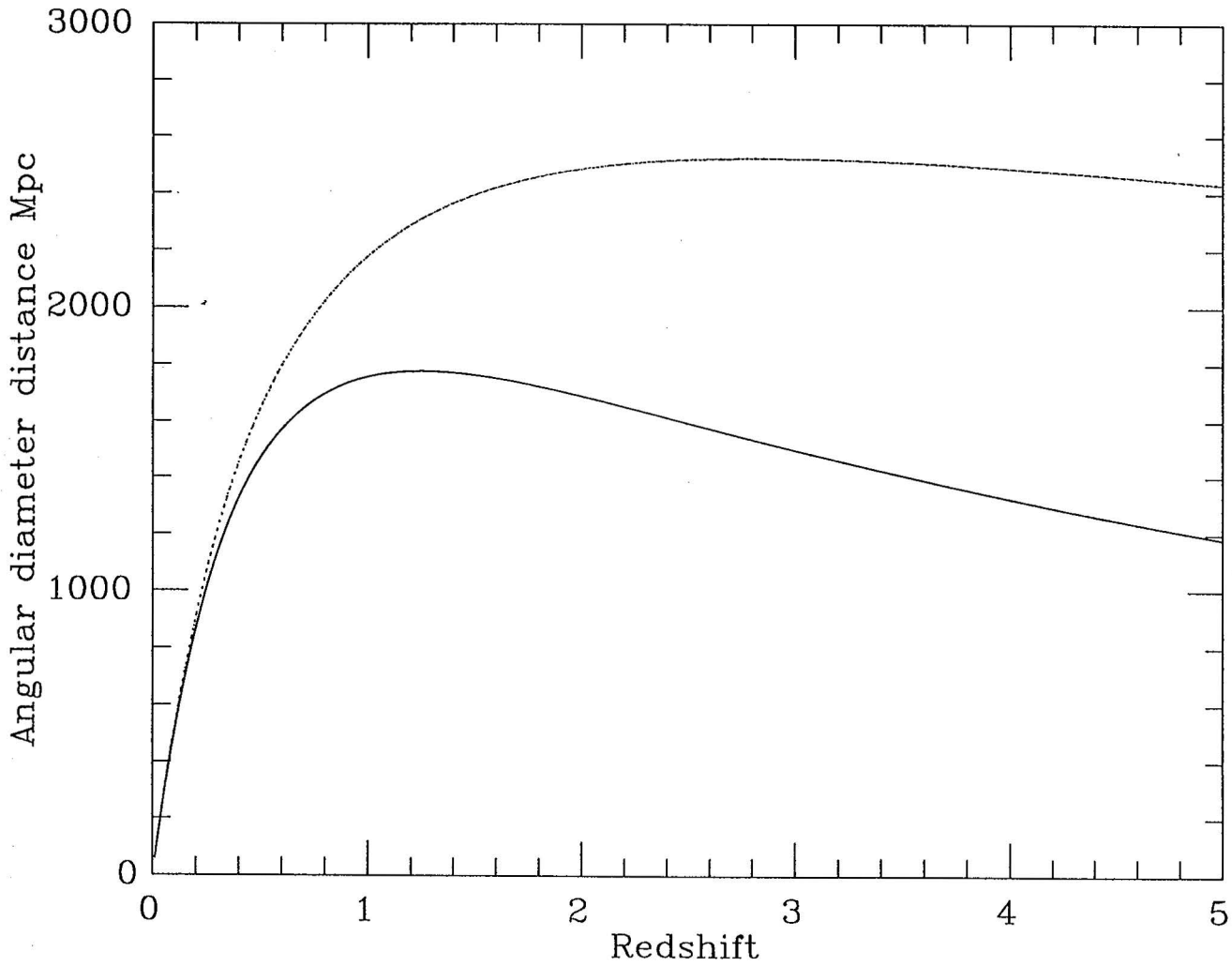

Figure 1.9 Angular diameter distance (d_A) as a function of redshift for $q_0 = 0.5$ (solid line, lower) and $q_0 = 0.05$ (dotted line, upper).

1.8 X-ray Studies of Faint Galaxies

In this thesis we shall also be using correlation techniques to investigate the X-ray background (XRB), as observed in the 0.5–2.0 keV energy range with the ROSAT satellite, and in doing so obtain information about the X-ray properties of faint galaxies. The aim is both to identify individual galaxies as X-ray sources, and to study the bulk X-ray properties of large samples of faint galaxies by estimating their total emission in the range of energies considered.

The high resolution imaging capabilities of orbiting X-ray telescopes such as *Einstein* and more recently ROSAT have enabled the origin of the XRB to be investigated by resolving as much of the flux as possible, on very deep images, into discrete sources. The source positions are then matched with objects visible on photographic plates, with the aim of identifying the optical counterparts to the X-ray sources which can then be examined spectroscopically using ground-based telescopes.

In this way, deep imaging of the Pavo field with the *Einstein* Observatory found most of the detected X-ray sources to be QSOs at $z_{mean} \sim 1$, with these QSOs accounting for 15% of the total X-ray flux (Griffiths et al. 1992). The superior resolution and lower background noise of the ROSAT PSPC in comparison to the *Einstein* IRC has enabled larger numbers of sources to be resolved out of the background. Shanks et al. (1991) found that, in a long 30 ksec ROSAT exposure of a 0.35 deg^2 field, used previously for an optical/UV QSO survey (Boyle et al. 1990) and known as QSF3, about 35% of the 0.5–2.0 keV flux could be resolved into individual sources. Follow-up spectroscopy with the AAT identified 24 out of a total of 39 X-ray sources as being QSOs with $z_{median} \simeq 1.5$, a QSO surface density more than twice that found on the earlier deep *Einstein* images, and similar results were obtained from the QSF1 field. Evidently, QSOs dominate the component of the XRB resolvable at present into individual sources, and the Shanks et al. (1991) results give a lower limit of 30% on their contribution to the total 0.5–2.0 keV background intensity.

However, three of the Pavo field X-ray sources, and a total of seven of the X-ray sources on QSF1 and QSF3, appeared to be associated instead with either early-type or star-forming galaxies with $19 < B < 21$ and typical redshifts of $z \sim 0.3$ (Griffiths et al. 1993). In this thesis it is this probable non-QSO component of the XRB we shall be investigating, in particular that which may be produced by $B \leq 23$ galaxies i.e. those visible on photographic plates and within the reach of faint-object spectrographs.

We shall be cross-correlating new lists of X-ray sources with galaxies on photographic plates, with the aim of finding more X-ray emitting galaxies. Our dataset includes a new ROSAT image almost twice as deep as the QSF field images used previously, enabling very faint (X-ray flux $S \sim 3 \times 10^{-15}$ erg cm^{-2}s^{-1}) sources to be detected. The deeper limit will obviously improve the probability of detecting some galaxies together with what would be expected to be an even higher surface density of QSOs. On the basis of earlier results most of these QSOs should be bright enough in the optical bands to be identified by spectroscopy, and hence excluded from the lists of X-ray sources to be cross-correlated with galaxies, thus improving the statistics of our analysis.

Normal galaxies will have a much higher density in the sky than QSOs, and faintward of $B \sim 21$ it will become increasingly difficult to match individual galaxies with the sources as their mean angular separation falls to less than the width of the ROSAT point-spread function ($\sim$ 25 arcsec). Even so, it may still be possible to detect an overall correlation, by comparing the total number of galaxies seen within the point-spread function radius of any of the unidentified sources with that expected by chance. In most cases, follow-up spectroscopy will be carried out on the optical galaxy or stellar image

closest to the source position, and our cross-correlation would provide an indication of how many of these source 'identifications' are genuine as opposed to chance co-incidences.

Galaxies in general, including our own, are much weaker sources of X-rays than QSOs. A typical $L \sim L^*$ spiral or elliptical galaxy produces an X-ray luminosity in the ROSAT band of $L_X \sim 10^{39-41}$ ergs s^{-1}, compared to $L_X \sim 10^{44-45}$ ergs s^{-1} typical of high-redshift QSOs. Stars of all types emit some X-rays from their coronae, but normal stars such as the Sun possess relatively low X-ray luminosities of $L_X \sim 10^{27-28}$ ergs s^{-1}, and a larger proportion of the X-ray emission of most galaxies is produced by smaller numbers of much more luminous sources.

These include O-type blue giant stars ($L_X \sim 10^{32-33}$ ergs s^{-1}), supernova remnants ($L_X \sim 10^{34-37}$ ergs s^{-1}), and various accreting binaries. Low-mass X-ray binaries are typically composed of a star of mass $M \sim M_\odot$ accreting onto a neutron star, producing an X-ray luminosity $L_X \sim 10^{34-37}$ ergs s^{-1}. Massive X-ray binaries (MXRBs), in which a giant star of mass $M \sim 10M_\odot$ or greater accretes onto a black hole, can produce very high X-ray luminosities of $L_X \sim 10^{38-39}$ ergs s^{-1}.

Diffuse thermal bremsstrahlung emission, from very hot ($T \sim 10^7$–$10^8 K$) gas, may also be an important source of X-rays, particularly for giant ellipticals (gas temperature $kT \sim 1.5$ keV) and galaxy clusters ($kT \sim 7$ keV). In general, the X-ray emission of spiral (Sb/Sc/Sd) galaxies appears to be dominated by discrete evolved stellar sources, mainly accreting binaries, while in early-type (E/S0) galaxies the hot gaseous component is a more significant source, and bulge-dominated (Sa) spirals contain a mixture of the two types of emission (Kim, Fabbiano and Trinchieri 1992).

Some of the discrete X-ray sources found within galaxies – O-type stars, supernova remnants and MXRBs – will only be found in regions of active or very recent star-formation. The MXRBs are of particular interest due to their very high luminosities (a few such binaries may dominate the X-ray emission of an entire galaxy), and very flat/hard spectra ($f_\nu \propto \nu^{-0.3}$ approximately, up to energies of ~ 20 keV). Hence the fact that Sc/Sd spirals galaxies possess harder X-ray spectra ($kT > 3$ keV) than ellipticals ($kT \sim 1.5$ keV) favours the hypothesis that massive binaries account for a significant fraction of their X-ray emission. MXRBs are formed from very massive stars with short lifetimes, and their X-ray emitting lifetimes are even shorter ($\sim 10^5$ years), so if they dominate the total X-ray emission of late-type galaxies, the evolution of the total X-ray luminosity of these galaxies may quite closely trace the evolution of the star-formation rate. However, this may not be the case for elliptical galaxies where X-ray emission is not primarily associated with ongoing star-formation.

Despite the differences in the dominant emission mechanisms, elliptical and spiral galaxies tend to show similar ratios between their X-ray and optical luminosites at the present day. Most galaxies have been found to follow an approximate linear relation between X-ray and blue-band luminosity (see eg. Fabbiano 1989, Giacconi and Zamorani 1987) which corresponds to a monochromatic flux ratio $f_\nu(2\text{keV})/f_\nu(B) \sim 10^{-6.6}$. As will be discussed in more detail in Section 6.6, if this ratio is typical we would expect most galaxies as faint as $18 \leq B \leq 23$ not to be individually detectable on our ROSAT images.

However, it is known that some galaxies, particularly cluster-dominating ellipticals such as M87 in Virgo, have L_X/L_B ratios higher than this typical ratio by factors of order ~ 100, and as noted above, the enhanced star-formation rates at higher redshifts are likely to be accompanied by increased X-ray emission from MXRBs (see eg. Griffiths and Padovani 1990). It is therefore possible that a proportion of the galaxies in our dataset, perhaps including those of both elliptical and spiral/irregular morphology, could possess

very high L_X/L_B ratios, and would therefore be individually detected on our ROSAT images. Follow-up optical spectroscopy will enable the properties of any very X-ray luminous galaxies which may be detected to be studied in more detail.

A further possibility is that rich clusters of galaxies, which may be comparable in their X-ray luminosities to QSOs (for a Coma-type cluster, $L_X \sim 10^{44-45}$ ergs s^{-1}), could be detected at high redshifts, perhaps providing information about the nature and extent of their evolution.

1.9 The Contribution of Faint Galaxies to the X-Ray Background

Even if normal galaxies and rich clusters are not found to be significantly correlated with the bright X-ray sources it seems certain that they must contribute at some level to the $\sim 65\%$ of the XRB which remains unresolved in our data.

The origin of this diffuse component has not as yet been fully explained. The hypothesis that a diffuse inter-galactic medium of very hot gas is the principal source can now be excluded, as this would produce distortions in the cosmic microwave background spectrum which are not detected by the COBE satellite (Wright et al. 1993). Upper limits on such distortions require a uniform gaseous medium hot enough to fit the XRB spectrum ($kT \sim 40$ keV) to have a density no more than $\sim 1\%$ of that needed to generate the entire background flux. The diffuse background must then be produced by large numbers of faint discrete sources, the weakness of its small-scale fluctuations requiring these to have a surface density exceeding ~ 5000 deg^{-2} (Hamilton and Helfand 1987)

As the resolved $\sim 35\%$ of the XRB flux is so greatly dominated by AGN emission there seems little doubt that less luminous AGN must account for a significant fraction of the remainder. The X-ray and blue-band luminosities of AGN increase strongly with redshift, but as the rate of evolution is now fairly well determined, at least for the more luminous AGN (Boyle et al. 1993, Boyle et al. 1994), their total contribution to the XRB can be estimated reasonably accurately by integrating the expected X-ray emission from AGN out to high redshifts. In this way Boyle et al. (1994) estimated the X-ray flux from QSOs out to $z = 4$ would account for 34–53% of the total 1–2 keV flux. As galaxies are generally less luminous than AGN, less is known about their properties at high redshifts, particularly when we are considering X-ray evolution rather than that seen in the optical bands, so that an equivalent estimate of the XRB contribution from galaxies will be more model-dependent.

By assuming a constant X-ray/B-band flux ratio, the mean value for a sample of local elliptical and spiral galaxies observed using *Einstein*, and normalizing the blue flux using the B-band number counts of Tyson (1988), Giacconi and Zamorani (1987) estimated that $B \leq 27$ galaxies would produce at least 13% of the 2 keV background. Griffiths and Padovani (1990) estimated that star-forming galaxies at $z \leq 3$ could account for 20–30% of the XRB at 2 keV, with a 'moderate' rate of X-ray luminosity evolution derived from the far infra-red evolution of IRAS galaxies, and $> 50\%$ of the XRB if they evolve as rapidly as AGN.

Some indication of the relative AGN and star-forming galaxy contributions to the unresolved background may also be given by its spectral energy distribution. This has been found to possess a flatter spectral index (between $f_\nu \propto \nu^{-0.4}$ and $f_\nu \propto \nu^{-0.7}$) than most of the individually studied QSOs resolved on the same areas (typically $f_\nu \propto \nu^{-1}$). However, the SED of the XRB at 1–10 keV energies can be reasonably well fitted by a summation of a component with ($f_\nu \propto \nu^{-1}$), typical of the detected QSOs, and another with a flatter MXRB-like spectrum ($f_\nu \propto \nu^{-0.3}$), with these two components

being approximately equal at 0.5–2.0 keV energies (Shanks et al. 1991, Treyer et al. 1992). The autocorrelation and cross-correlation functions described below may provide another, independent, estimate of the two components.

As with our attempts to investigate the redshift distribution of $B \geq 24$ galaxies, when the sources in question are too faint to be studied (or in this case even detected) individually, correlation techniques can still provide useful information.

After removing all sources above the $\sim 4\sigma$ level from the ROSAT images, an autocorrelation function (ACF) can be calculated for the fluctuations between the photon counts in the remaining pixels. X-ray sources outside our galaxy (i.e. galaxy clusters, QSOs and galaxies) are all clustered on some scale, and we would expect this clustering to produce a signal in the diffuse background ACF comparable to the $\omega(\theta)$ of its components. In general, rich clusters of galaxies are themselves more strongly clustered than QSOs which in turn appear to be more clustered than galaxies. The rich clusters are expected to be a relatively minor component of the total XRB flux, so the ACF amplitude will depend approximately on the size of the QSO contribution relative to that of galaxies, as well as on the redshift distribution of both types of source.

Georgantopoulos et al. (1993), calculated the ACF of the unresolved XRB for the two QSF fields imaged with ROSAT, and found significantly less signal than would be expected if the background was produced entirely by AGN (at $0 < z < 4$). These results appeared to set an upper limit of 40% on the AGN component at 0.5–2.0 keV, and required the remaining 60% or more to be produced by sources no more clustered than normal galaxies. However, as we shall discuss later (Chapter 6), some uncertainty remains about the true clustering strength of QSOs at high redshifts relative to that of galaxies.

In this thesis we shall perform a similar ACF analysis on the unresolved XRB – the inclusion of our new deeper image should improve the statistics – and compare the results with models of QSO clustering and with the $\omega(\theta)$ of galaxies on AAT plates of the same areas of sky. Georgantopoulos et al. (1993) estimated that if the non-QSO component of the XRB was composed of normally clustered galaxies, these could only dilute the fluctuations in the XRB to produce a sufficiently weak ACF if distributed out to at least $z \sim 3$. As a similar $N(z)$ is predicted by PLE models for the faint blue galaxies producing the excess in the number counts, it may be particularly useful to compare our ACF results with our faint galaxy $\omega(\theta)$ ampitudes, in order to verify whether faint blue galaxies (which may possess very high X-ray luminosities as a result of their rapid star-formation rates) are sufficiently weakly clustered on the sky to be able to account for the non-QSO component of the XRB.

A more direct estimate of the X-ray flux from $B \leq 23$ galaxies not detected as discrete X-ray sources can be found by cross-correlating the galaxies on these AAT plates with the unresolved XRB. If a signal is seen in this cross-correlation the existence of a faint galaxy contribution would be established directly, rather than as an inferred 'non-QSO component', and its strength could then be used to estimate a mean X-ray to B-band flux ratio and an X-ray volume emissivity for the galaxies in the sample.

An analysis of this type was recently performed by Lahav et al. (1993), who cross-correlated $z \leq 0.06$ galaxy catalogues with the XRB fluctuations on the same area of sky. By extrapolating an emissivity derived from their cross-correlation amplitude to $z = 5.0$, Lahav et al. (1993) estimated that non-evolving galaxies could account for $30 \pm 15\%$ of the XRB.

Ideally, an estimate of the X-ray flux produced by faint galaxies would combine deep X-ray imaging with optical CCD imaging to sufficient depths to detect galaxies

to their maximum redshift. In the absence of such data at present we must similarly extrapolate our result to high redshifts, but the fainter limit ($B = 23$) of our galaxy dataset should lead to an estimate of the total galaxy contribution less dependent on the evolution model than that of Lahav et al. (1993). Additionally, the comparison of the two sets of cross-correlation results may give some indication of the evolution in the X-ray properties of the galaxy population between $0 \leq z \leq 0.06$ and the $z \sim 0.6$ limits reached by our AAT plate galaxy dataset.

1.10 Outline of Thesis

Chapters 2, 3 and 4 are concerned with an analysis of the clustering of galaxies on deep CCD images, and comparison of the results with various models.

In Chapter 2 we derive the $\omega(\theta)$ amplitude of galaxies, and its scaling with magnitude limit, from a CCD survey detecting several thousand faint galaxies to limits of $B_{ccd} = 25.0$ and $R_{ccd} = 23.5$. These results are compared with the predictions of simple PLE and non-evolving models, assuming stable clustering.

In Chapter 3 we also consider models in which galaxy clustering evolves with look-back time, and the possible effects of galaxy merging on $N(z)$ and the $\omega(\theta)$ amplitude. The results from the previous Chapter, together with an analysis of the dependence of $\omega(\theta)$ on galaxy colour, are compared with these models.

In Chapter 4 we calculate a $\omega(\theta)$ amplitude of the galaxies on one of the deepest CCD images ever obtained, extending our investigation of the scaling to a limit of $B_{ccd} = 27.0$. We compare both the clustering and the number counts of very faint galaxies with various models to obtain information about $N(z)$ at faint limits, the maximum redshift to which galaxies can be detected in the B-band, and the form of the galaxy luminosity function at high redshift.

In Chapters 5, 6 and 7 we discuss ROSAT X-ray observations, including the cross-correlation of ROSAT data with photographic datasets. As less is known at present about the X-ray properties of faint galaxies than is known about galaxy clustering, the emphasis of this section is more on the presentation of new results than comparisons with detailed models.

In Chapter 5 we investigate in detail the cross-correlation between individually detected X-ray sources and faint galaxies, to determine what proportion of these are sufficiently X-ray luminous to be detected along with QSOs. We present the results of spectroscopic investigation of a number of candidates for X-ray detected faint galaxies, together with an assessment of how many of these are likely to be the genuine sources.

In Chapters 6 and 7 we consider the X-ray background in three deep ROSAT images with the detected sources removed, leaving only the unresolved component.

In Chapter 6 we analyse the fluctuations in this background, which will reflect the strength of clustering of the main sources of the flux. We compare our results with the clustering properties of faint galaxies and QSOs in an attempt to set constraints on the relative contributions of these two types of source to the total unresolved X-ray flux.

In Chapter 7 we investigate the contribution of faint galaxies to the X-ray background directly. Cross-correlating several thousand $B \leq 23$ galaxies detected on AAT plates with the unresolved background will enable us to estimate the total X-ray emission of $B \leq 23$ galaxies. This will be compared with previous results at shallower limits to estimate the rate of X-ray luminosity evolution, and extrapolated to high redshifts and/or faint optical magnitudes to estimate the total contribution from all galaxies,

to the faintest limits, to the X-ray background. This estimate will be compared with the constraints set on the background's composition in the fluctuation analysis of the previous Chapter. The mean X-ray/optical flux ratio derived from the cross-correlation will also be compared with the L_X/L_B ratios of the detected X-ray luminous galaxies investigated in Chapter 5. Comparison of the two sets of results will be used to derive information about the X-ray luminosity function of galaxies, the proportion of galaxies with very high X-ray luminosities being indicated by the numbers individually detected, and the L_X distribution of the galaxy population as a whole being investigated by means of its cross-correlation with the unresolved background.

In our concluding Chapter (8) we review the results obtained in both sections of the thesis, and discuss their implications about the processes of galaxy evolution. We discuss the possible connections between the galaxy clustering and X-ray results, and suggest ways in which we might better verify our results and interpretations, extend our investigations to fainter and/or more distant objects, and address some of the new questions about galaxy evolution which will inevitably be raised by the results presented here.

Chapter 2

Galaxy Clustering to B=25 and R=23.5

2.1 Introduction

In this Chapter we investigate the angular two-point correlation function, $\omega(\theta)$, of the galaxies observed in a CCD survey reaching limits of $B_{ccd} = 25.0$ and $R_{ccd} = 23.5$. The aim is to determine whether the large excess observed in the numbers of faint ($B \geq 23$) blue galaxies relative to non-evolving predictions results from an increase in the L^* luminosity with redshift, enabling high redshift ($z > 1$) galaxies to be seen within our survey limits – or from an increase of the number density, ϕ^*, of galaxies at somewhat lower redshifts, giving an approximately non-evolving redshift distribution with a raised normalization.

We therefore interpret our $\omega(\theta)$ results by comparing them with models representing these two 'extreme' possibilities – a model in which the galaxy redshift distribution maintains a no-evolution form at all magnitude limits, and a pure luminosity evolution model in which a much larger proportion of the galaxies in our dataset would be at $z > 1$. We also compare the pure luminosity evolution model with recently published redshift data, and with the $\omega(\theta)$ amplitudes of our $B_{ccd} \leq 24.5$ galaxies divided by colour at $B - R = 1.5$ into red and blue subsamples.

2.2 Observational Data

Our sample consists of 4540 galaxies observed in the blue passband and 3627 observed in the red passband, the magnitude limits of the survey being $B_{ccd} = 25.0$ and $R_{ccd} = 23.5$. The magnitudes and positions of each galaxy used in the following analysis were taken from a data catalogue of observations made in 1986 using the 2.4m Isaac Newton Telescope (INT), with the RCA chip at prime focus giving a pixel size 0.74 arcsec. The number counts from this data were presented and discussed by MSFJ. Twelve fields were observed in both the blue and red passbands and two more in the red only. The CCD frame size is 0.1033 × 0.0638 degrees, giving a total observed area of 284 arcmin^2 in the blue and 331 arcmin^2 in the red. The data catalogue listed all galaxies with 'total' magnitudes brighter than $B_{ccd} = 25.0$ or $R_{ccd} = 23.5$, incompleteness becoming significant only in the faintest half-magnitude intervals, where it is estimated as 25% by MSFJ. The fields are generally widely separated (with a minimum separation of 40^m of R.A.) and at intermediate galactic latitudes (41–63°). Their positions, chosen at random, are given in Table 1 of MSFJ.

Our magnitudes relate to those obtained using photographic passbands approximately as $B_{ccd} \simeq b_J + 0.09$ and $R_{ccd} \simeq r_F + 0.13$, for the mean colours of our survey galaxies. For details of the photometry, we refer the reader to MSFJ.

2.3 Calculating $\omega(\theta)$

The correlation function, $\omega(\theta)$, was calculated for each of the CCD frames separately. For each frame, the centroid positions and magnitudes of all N_g galaxies brighter than a chosen magnitude limit were read from the data catalogue. The separations of all $\frac{1}{2}N_g(N_g-1)$ possible pairs of galaxies were calculated and counted in logarithmic bins, each of width $\Delta(\log\,\theta) = 0.2$.

In addition 10000 points were assigned random positions in a 2-dimensional co-ordinate space corresponding to the frame area. The separations between the galaxies and the randoms, taking the real galaxies as the centres and so giving $10000N_g$ pairs in total, were similarly binned.

The estimate $\omega_e(\theta_n)$ for each bin was then calculated as

$$\omega_e(\theta_n) = \frac{N_{gg}(\theta_n)}{N_{gr}(\theta_n)}\frac{2N_r}{(N_g-1)} - 1$$

where $N_{gg}(\theta_n)$ = number of galaxy-galaxy pairs in bin n,

$N_{gr}(\theta_n)$ = number of galaxy-random pairs in bin n,

N_g = number of galaxies on the frame brighter than the limiting magnitude,

N_r = number of random points (10000 in this analysis),

and the bins of angular separation are defined as $10^{0.2(n-1)} \leq \theta_n < 10^{0.2n}$ arcsec.

The individual frame $\omega_e(\theta_n)$ values were then averaged at each θ_n point to give a mean correlation function. The error bars assigned to this mean $\omega_e(\theta)$ are simply the standard deviations of the mean of the individual frame $\omega_e(\theta_n)$ values at each angular separation θ_n. Figure 2.1 shows the angular correlation functions for all $B_{ccd} \leq 25.0$ and all $R_{ccd} \leq 23.5$ galaxies in this survey. A log-linear scale is used, as the observed $\omega_e(\theta)$ becomes negative at the largest angles considered due to the 'integral constraint' effect discussed below.

In deriving $\omega(\theta)$ amplitudes from our data, we assume in this thesis that the true $\omega(\theta)$ follows a $\theta^{-0.8}$ power law, as estimated from a number of previous surveys, over the range of angular separations covered by our estimate $\omega_e(\theta)$. A significant departure from this power-law form has only been observed at angular separations significantly larger than our CCD frame size of $\sim$ 0.1 deg (see, e.g., Infante 1990). However, for the small area of a CCD frame the bias in the estimate for $\omega(\theta)$ due to the well-known 'integral constraint' is a large effect. This results from the need to use the sample itself to estimate the mean density of galaxies at that magnitude limit (see, e.g., Peebles 1980), and causes the estimate, $\omega_e(\theta)$ to be biased low relative to the true $\omega(\theta)$ by the amount C where

$$C = \frac{1}{\Omega^2}\int\int \omega(\theta)d\Omega_1 d\Omega_2$$

On the basis of previous surveys, we assume

$$\omega(\theta) = A\theta^{-0.8}$$

Using this form for $\omega(\theta)$, and taking into account the difficulty of distinguishing galaxies that are separated by less than a few arcsec, a numerical integration of the above equation over the CCD frame area Ω gives

$$C = 16.1A$$

As the estimated correlation function, $\omega_e(\theta)$, corresponds to $A\theta^{-0.8} - C$, we simply fit '$A(\theta^{-0.8} - 16.1)$' to our $\omega_e(\theta)$ data to determine a best-fitting amplitude A. A least-squares method in which each θ_n point has been weighted using the field-to-field variance in $\omega_e(\theta_n)$ was used. Each θ_n was taken as the logarithmic centre of the corresponding bin. The $\omega_e(\theta_n)$ data for $10 \leq \theta \leq 400$ arcsec separations only were used in the amplitude fitting, as merging of images reduces the observed $\omega_e(\theta)$ at separations of a few arcsec or less. Figure 2.2 shows the same data as Figure 2.1 but corrected for the integral constraint by adding $16.1A$, with the fitted function as $A\theta^{-0.8}$.

The simplest way of assigning an error bar to each amplitude would be to take the error from the least-squares fitting program, but this may lead to an underestimate as the values of $\omega(\theta_n)$ at each of the θ_n points are not completely independent. Instead, a series of amplitudes were obtained by fitting the function described above to each of the individual frame correlation functions (weighting each θ_n point as before). The amplitude error for each magnitude limit was then taken as the standard deviation of the mean of the relevant set of individual frame amplitudes.

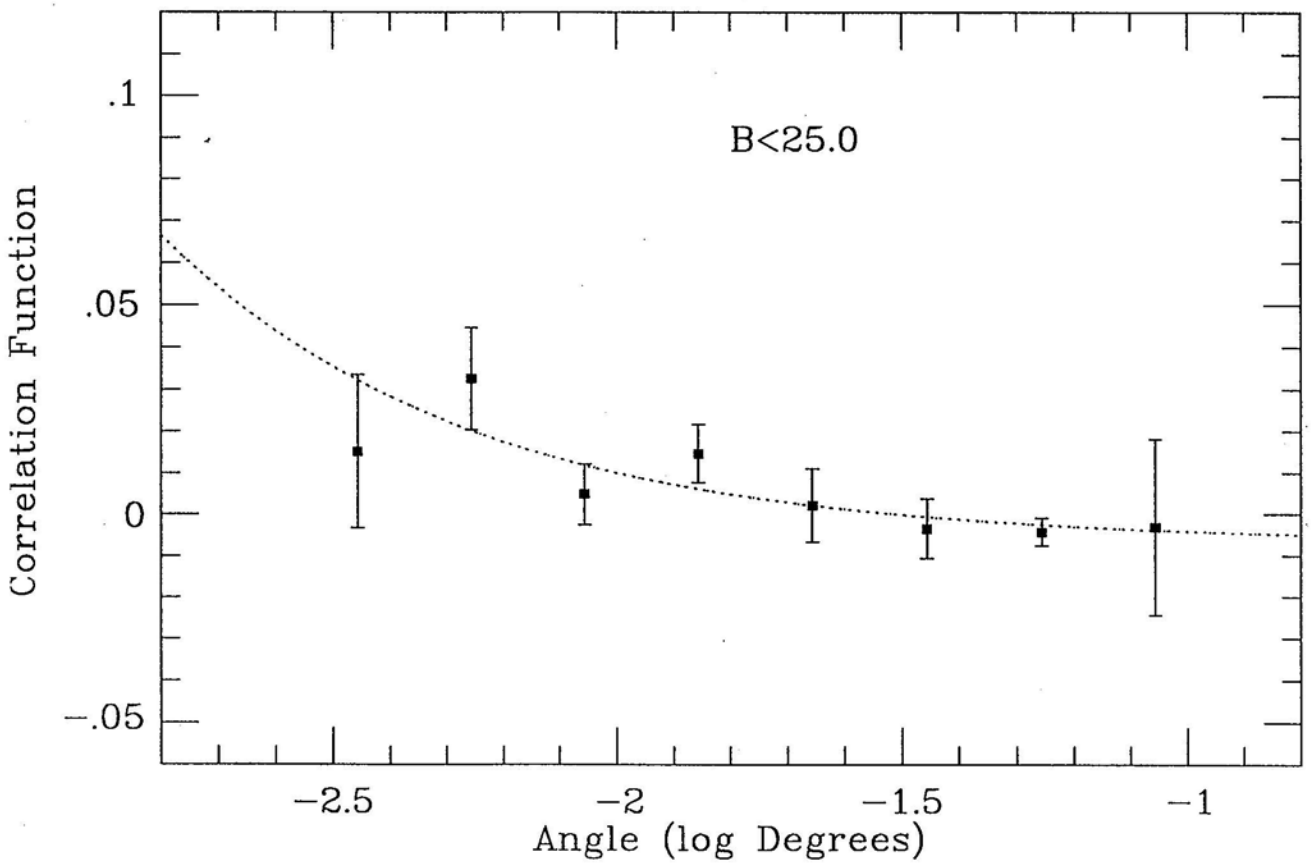

Figure 2.1a Observed angular correlation function, with field-to-field errors, for all $B_{ccd} \leq 25.0$ galaxies on the 12 CCD fields imaged in the blue band. The closest-fitting function of the form '$A(\theta^{-0.8} - 16.1)$', used as described in Section 2.3 to estimate the $\omega(\theta)$ amplitude, A, is shown as a dotted line.

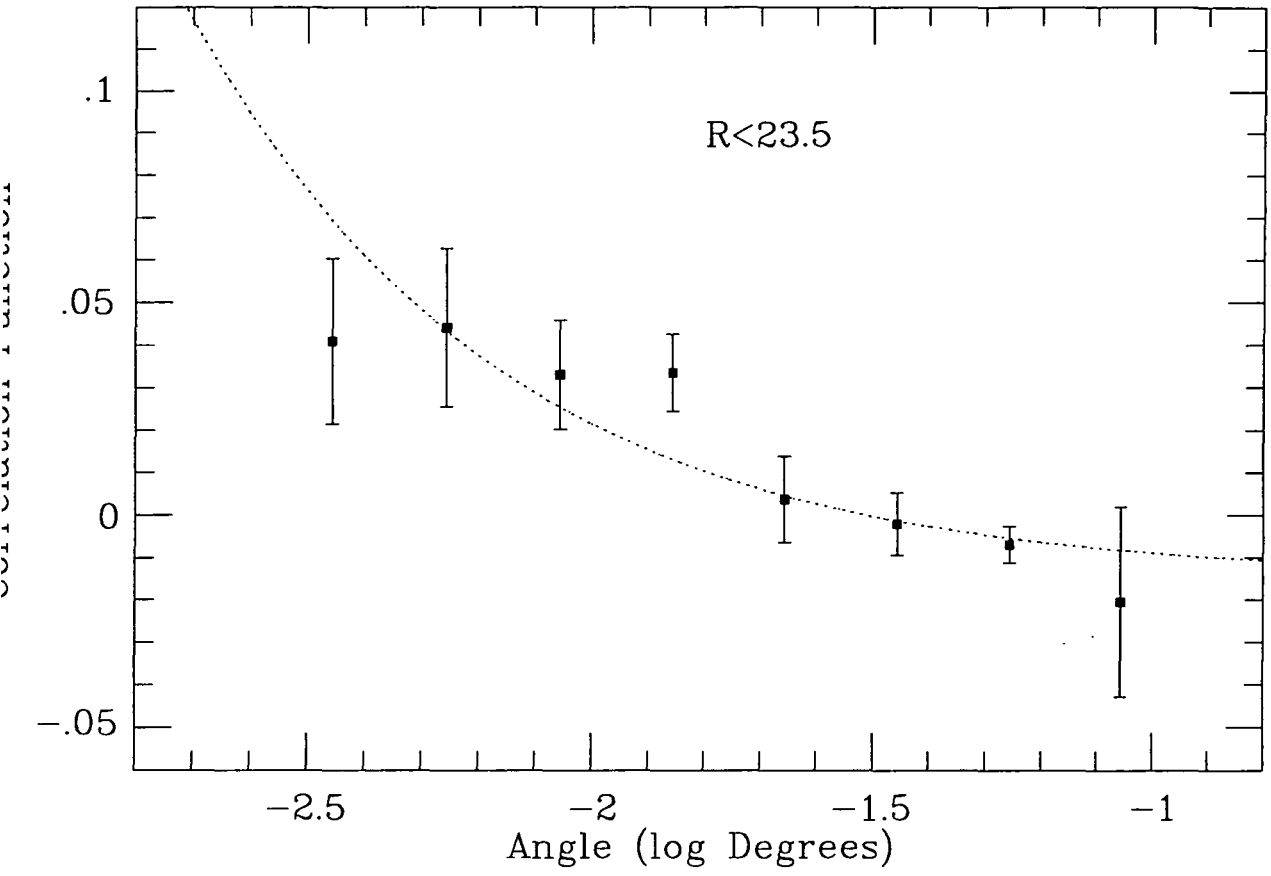

Figure 2.1b Observed angular correlation function, with field-to-field errors, for all $R_{ccd} \leq 23.5$ galaxies on the 14 CCD fields imaged in the red band. The closest-fitting function of the form '$A(\theta^{-0.8} - 16.1)$', used as described in Section 2.3 to estimate the $\omega(\theta)$ amplitude, A, is shown as a dotted line.

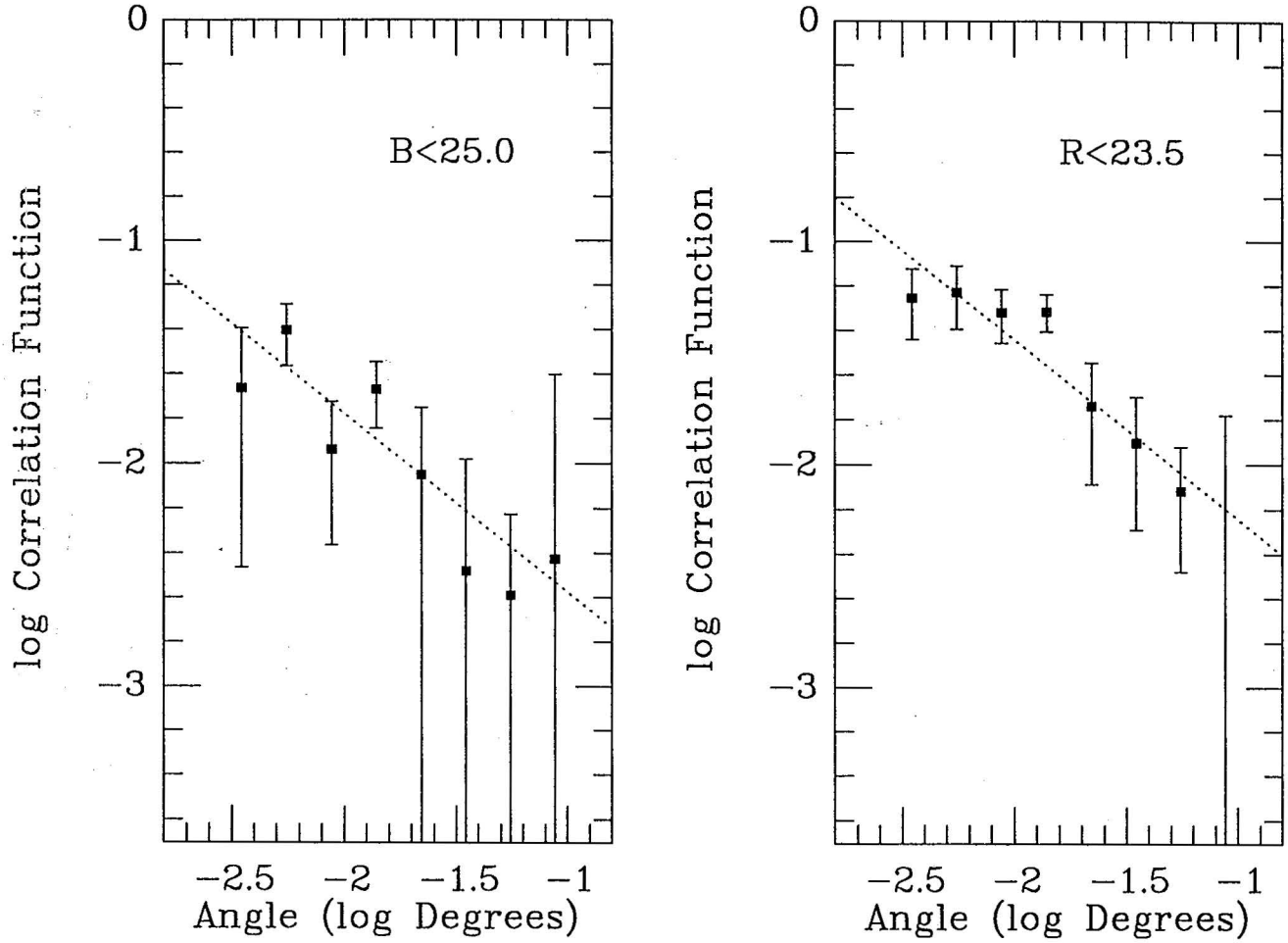

Figure 2.2 The same angular correlation function data and best-fitting functions as shown on Figure 2.1, with an integral constraint correction of '16.1 A' added on to each data point. The functions fitted to the data then become simply $\theta^{-0.8}$ power-laws of amplitude A, and are shown on this log-log plot as straight dotted lines.

2.4 $\omega(\theta)$ Results

Our survey is sufficiently large that meaningful constraints can be placed on the $\omega(\theta)$ amplitudes from brighter subsets of the catalogue, enabling us to investigate the scaling with depth of these amplitudes over magnitude limits in the range $23.25 \leq B_{ccd} \leq 25.00$ and $22.00 \leq R_{ccd} \leq 23.50$. For the magnitude limits chosen in the blue and red passbands, the integral number counts and the correlation amplitudes are given in Table 2.1.

Figures 2.3 and 2.4 show our $\omega(\theta)$ amplitudes for the blue-limited and red-limited samples, together with previously published $\omega(\theta)$ amplitudes from photographic surveys.

The photographic b_J and r_F magnitudes have been approximately converted to the equivalent B_{ccd} or R_{ccd}. Additionally, for 5 of the 8 UKST plates used by Stevenson et al. (1985) a correction of +0.21 has to be made to the b_J magnitudes (see Jones et al. 1991); the UKST data plotted in Fig. 2.3 are then the mean correlation amplitudes of these 8 plates, with a mean correction of $+0.^m13$ applied to the published magnitude limits. The UKST and AAT Jones amplitudes are as given by JSF, where the results have been corrected for the effects of star contamination, but were plotted against galaxy number density rather than against limiting magnitude.

Additionally, the more recent $\omega(\theta)$ results from the CCD survey of Couch et al. (1993) are plotted on Figure 2.4, which shows the mean correlation amplitudes of the two areas surveyed. The VR magnitude system used by these authors was converted, using our mean colours, into our red magnitude system as $R_{ccd} = VR - 0.35$.

It can be seen that our results are in agreement with all of the photographic surveys in the blue band to within the statistical errors. In the red band the scatter between observers is a little higher – JSF obtained rather lower amplitudes than Infante. Our own red-band results are intermediate, and very similar to those of Couch et al. (1993). Overall it is clear that our correlation amplitudes, as well as our number counts (see MSFJ), lie in the middle of the range previously encompassed by photographic data to the faint limits of such surveys.

B_{ccd} Limit	Density deg^{-2}	$\omega(\theta)$ amplitude
23.25	9091	24.62 ± 13.72
23.50	12594	20.32 ± 7.98
23.75	16577	16.88 ± 4.81
24.00	22090	12.81 ± 4.77
24.25	29563	7.665 ± 2.621
24.50	38123	5.568 ± 2.157
24.75	47480	4.127 ± 2.209
25.00	57406	4.214 ± 2.044

R_{ccd} Limit	Density deg^{-2}	$\omega(\theta)$ amplitude
22.00	10610	19.97 ± 11.74
22.25	13428	13.67 ± 6.02
22.50	16658	15.98 ± 4.89
22.75	20755	13.95 ± 3.44
23.00	26174	14.83 ± 3.43
23.25	32568	11.75 ± 3.35
23.50	39310	9.086 ± 2.843

Table 2.1 The integral galaxy number counts, in galaxies deg^{-2}, and $\omega(\theta)$ amplitudes (with field-to-field errors), in units of 10^{-4} (deg)$^{-0.8}$, of the galaxies brightward of a series of magnitude limits in our $B_{ccd} \leq 25.0$ and $R_{ccd} \leq 23.5$ CCD datasets.

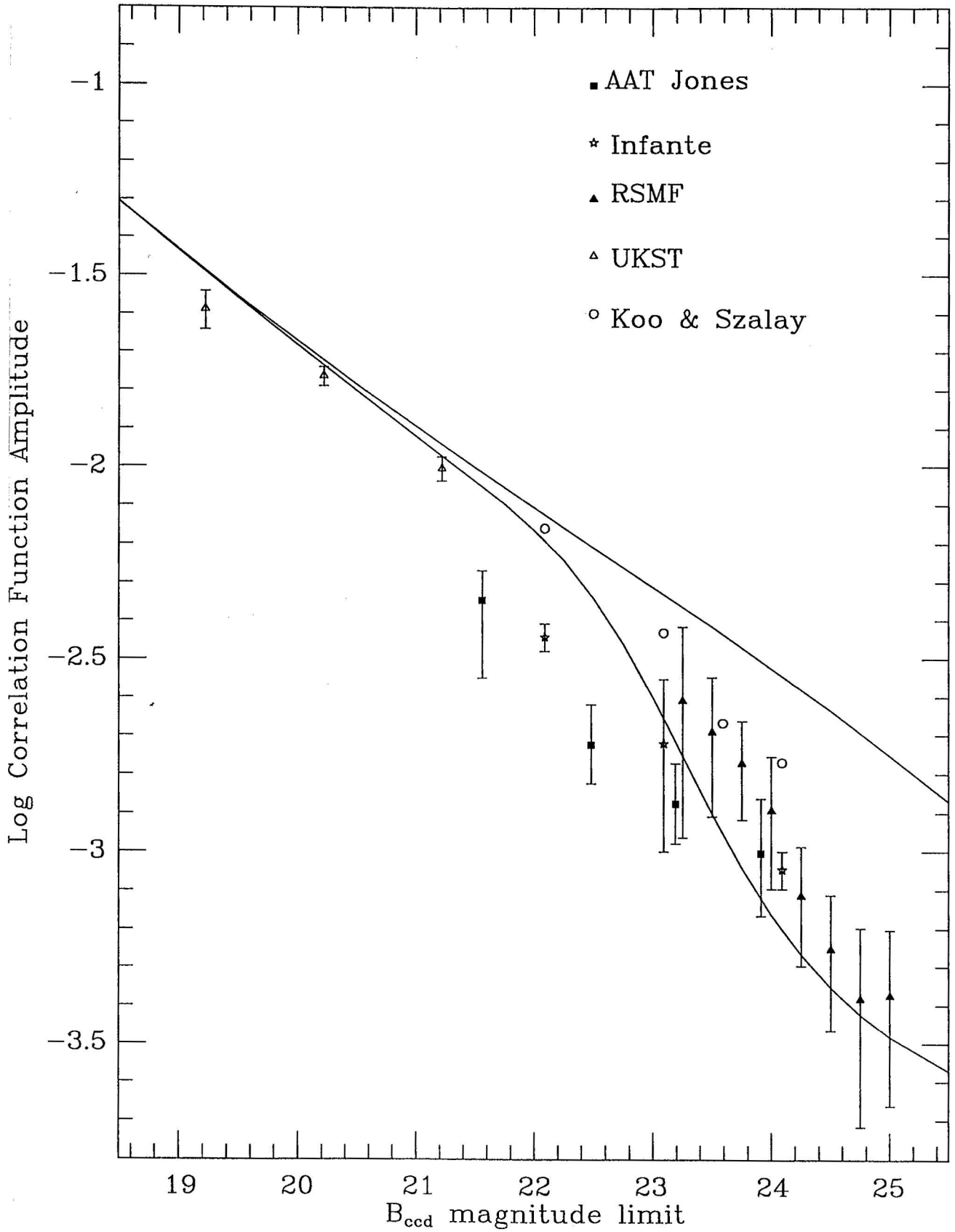

Figure 2.3 Galaxy $\omega(\theta)$ amplitudes obtained from the AAT photographic surveys of Jones et al. (1987), Infante (1990), Koo and Szalay (1984), from the UKST data of Stevenson et al. (1985), and from the 12 CCD frames of our $B_{ccd} \leq 25.0$ survey (RSMF). These are compared with the predictions of a non-evolving model (upper curve) and our Bruzual pure luminosity evolution model (lower curve), over a range of blue magnitude limits. The models shown here assume stable clustering, $q_0 = 0.05$ and $z_{max} = 4$.

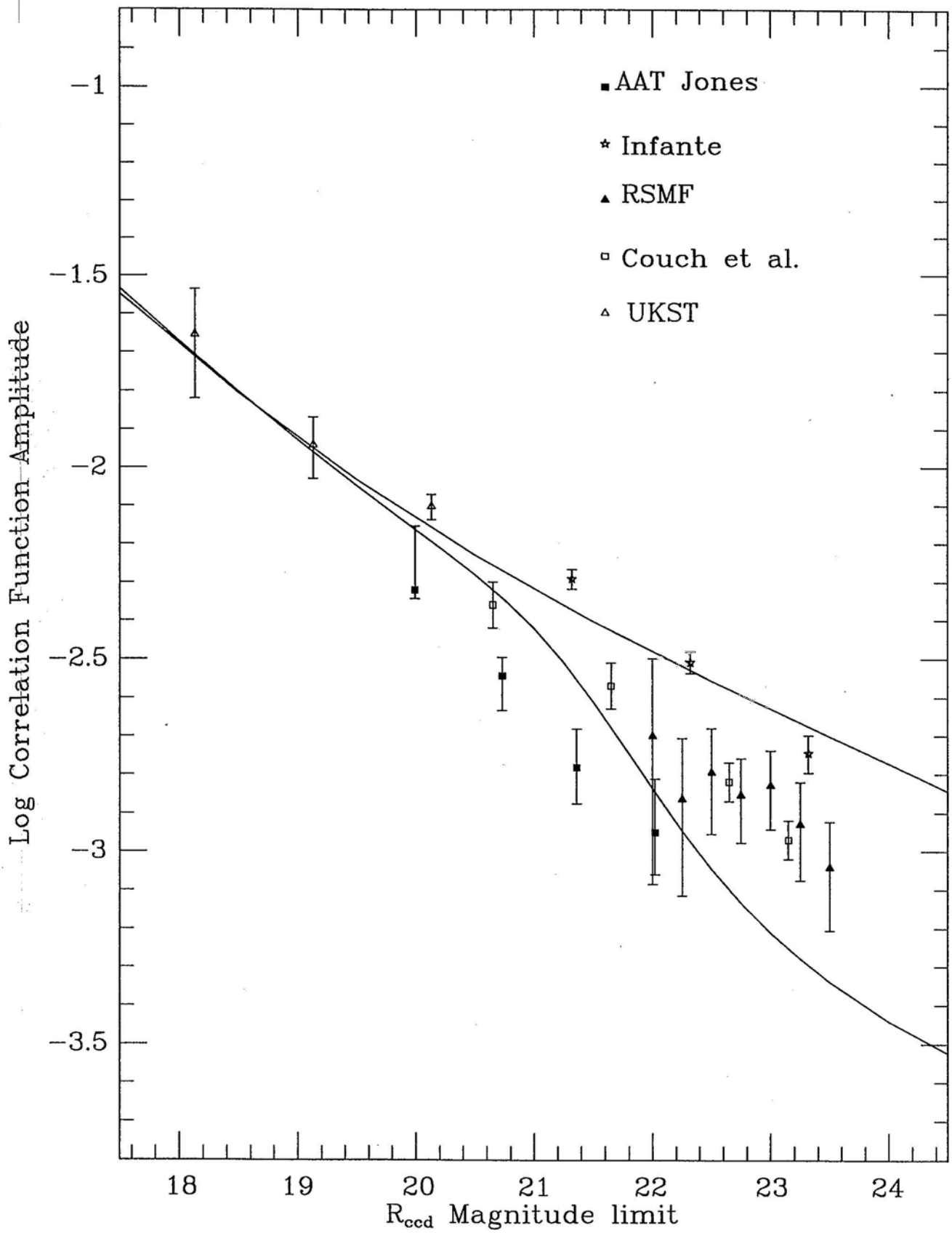

Figure 2.4 Galaxy $\omega(\theta)$ amplitudes obtained from the AAT photographic surveys of Jones et al. (1987) and Infante (1990), from the UKST data of Stevenson et al. (1985), from the 14 CCD frames of our $R_{ccd} \leq 23.5$ CCD survey (RSMF), and from the Couch et al. (1993) $VR \leq 23.5$ CCD survey. These are compared with the predictions of a non-evolving model (upper curve) and our Bruzual pure luminosity evolution model (lower curve), over a range of red magnitude limits. The models shown here assume stable clustering, $q_0 = 0.05$ and $z_{max} = 4$.

2.5 $N(z)$ and $\omega(\theta)$ from No-Evolution and PLE Models

Figures 2.3 and 2.4 also show the $\omega(\theta)$ amplitudes predicted by the no-evolution (upper) and PLE (lower) models described in Section 1.4. The blue-band PLE model incorporates the Bruzual (1981) $\mu = 0.5$ model of exponentially decreasing star-formation rate for the early type galaxies, giving very strong L^* evolution at $z > 1.5$. The red-band PLE model, as used by MSFJ, incorporates somewhat stronger evolution for early-type galaxies than Bruzual's $\mu = 0.5$ model. As the evolving and non-evolving models differ only in the evolution corrections applied to L^* as a function of redshift, they converge in the bright or shallow limit, but differ greatly at our faint limits. The models plotted here are computed using $q_0 = 0.05$, as we require a low (≤ 0.15) value of q_0 to fit the faint ($B > 24.5$) galaxy counts with any PLE model, and we are aiming to determine whether L^* evolution alone can fit all the observational data.

Figure 2.5 shows $N(z)$ as given by the no-evolution model for a series of magnitude limits. Non-evolving models underpredict the number counts at the depth of our survey, in both passbands. However, as far as the $\omega(\theta)$ scaling is concerned, such a model can approximately represent some models in which galaxy evolution is dominated by merging and/or starbursting in low-redshift dwarf galaxies – resulting in $N(z)$ at $B \sim 24$ limits possessing a similar form to a non-evolving galaxy $N(z)$, being increased only in normalization (see Section 1.6).

Figure 2.6 shows $N(z)$ as given by the Bruzual PLE model for the same magnitude limits. The strong luminosity evolution of this model enables high redshift galaxies to be seen at relatively bright apparent magnitudes. The resulting $N(z)$ is bimodal at $23 \leq B \leq 25$, with a very broad second peak, centred on $z \simeq 1.85$, composed of $L \sim L^*$ galaxies undergoing initial starbursts. According to this model, the very blue 'flat-spectrum objects' appearing at $B \sim 24$ would be the high redshift galaxies comprising this second peak. In MSFJ's red band PLE model, there is similar but slightly weaker luminosity evolution, producing a second peak in $N(z)$ which is smaller at the faint limits of our survey than in the blue-band model, but lies at a similar redshift.

The modelled correlation amplitude is derived from the modelled $N(z)$ using the Limber's formula integration, as described by e.g. Phillipps et al. (1978). We assume a 3-dimensional two-point correlation function of the form $(r/r_0)^{-\gamma}$, with $\gamma = 1.8$ (see Groth and Peebles 1977 and Peebles 1980, also Section 3.2), and a normalization of the clustering strength given by a fit of our models to the Zwicky catalogue results, which corresponds to a correlation radius of $r_0 = 4.3\mathrm{h}^{-1}\mathrm{Mpc}$, where $\mathrm{h} = (H_0/100\mathrm{km\ s^{-1}Mpc^{-1}})$, consistent with the estimate of r_0 given by Peebles (1980).

In deriving a $\omega(\theta)$ amplitude from $N(z)$, it was also assumed that clustering is stable in proper (physical) co-ordinates, as would be expected for gravitationally bound and virialized systems, and that galaxies of all morphologies and intrinsic luminosities have the same strength of clustering. It must be emphasized that any conclusions about the redshift distribution on the basis of correlation amplitudes depend on these assumptions. Possible departures from these assumptions (e.g. the gravitational collapse of clusters) are likely to have less influence on $\omega(\theta)$ at these limits than the very strong effects of luminosity evolution, but clustering evolution will be considered further in Chapter 3.

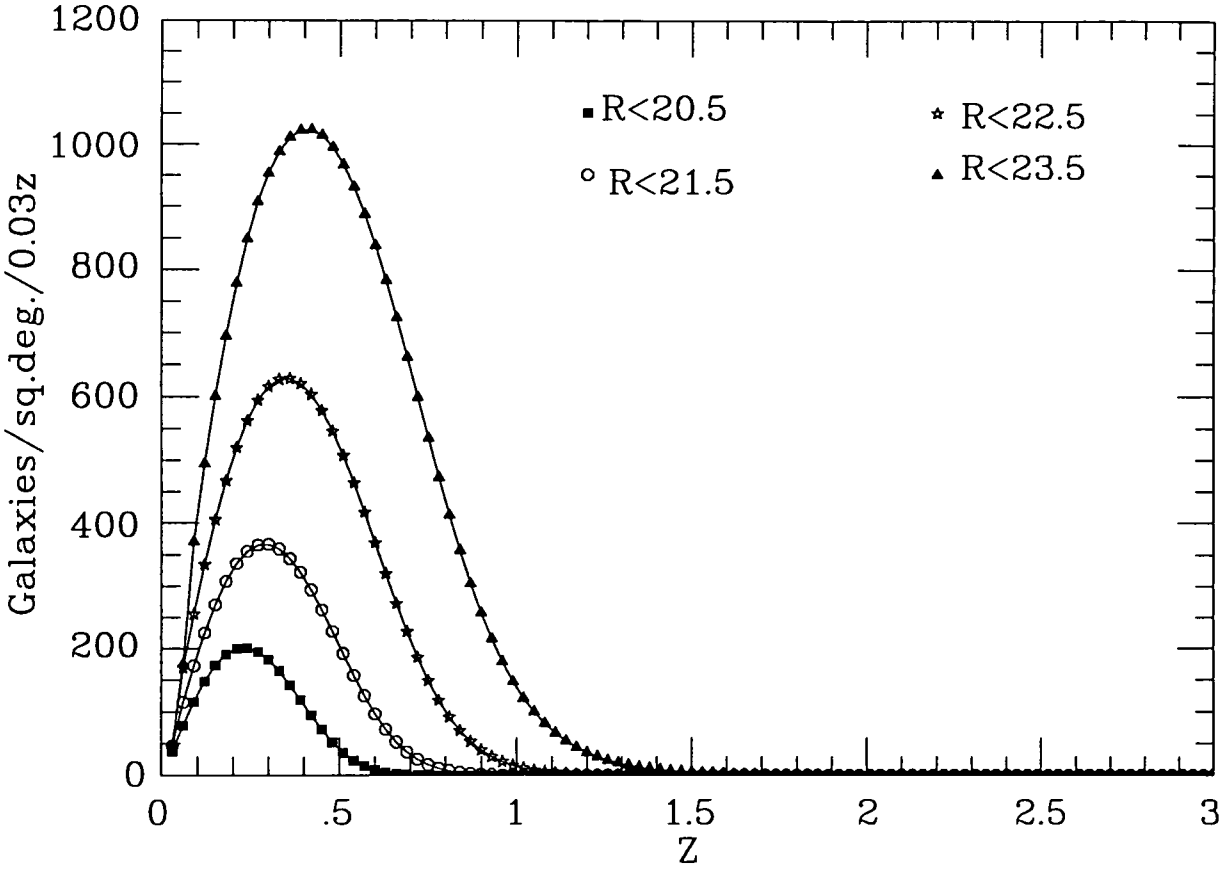

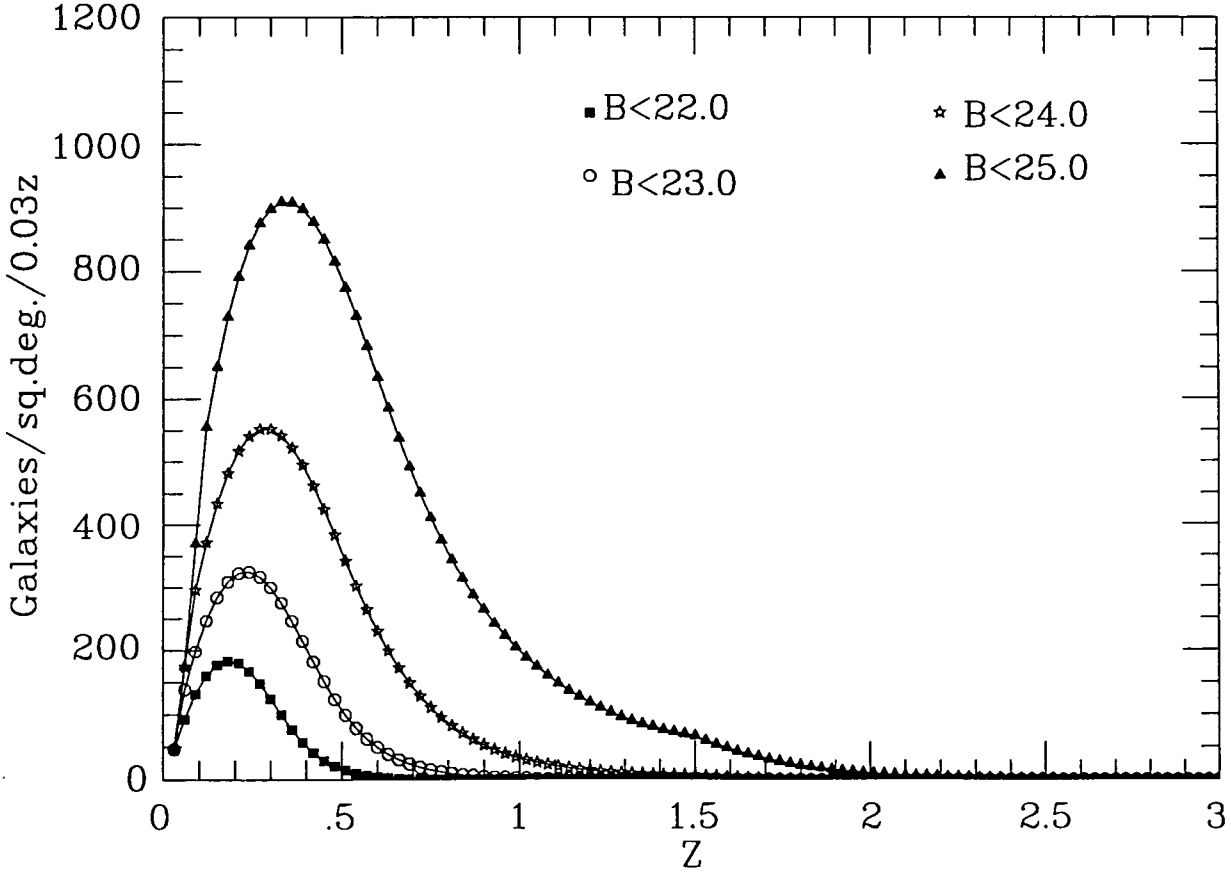

Figure 2.5 Redshift distributions predicted by our no-evolution models, with $q_0 = 0.05$, for a range of blue magnitude limits from $B_{ccd} \leq 22.0$ to $B_{ccd} \leq 25.0$, and a range of red magnitude limits from $R_{ccd} \leq 20.5$ to $R_{ccd} \leq 23.5$.

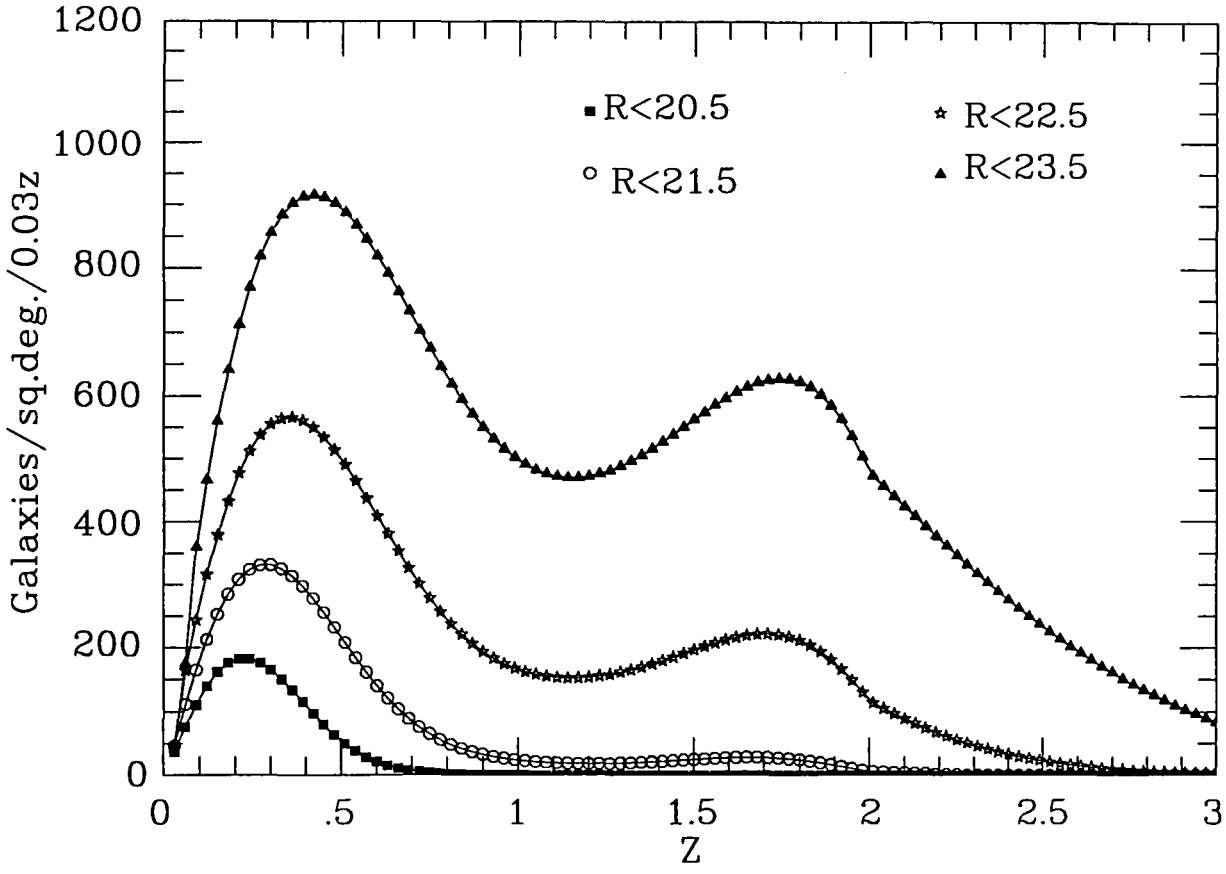

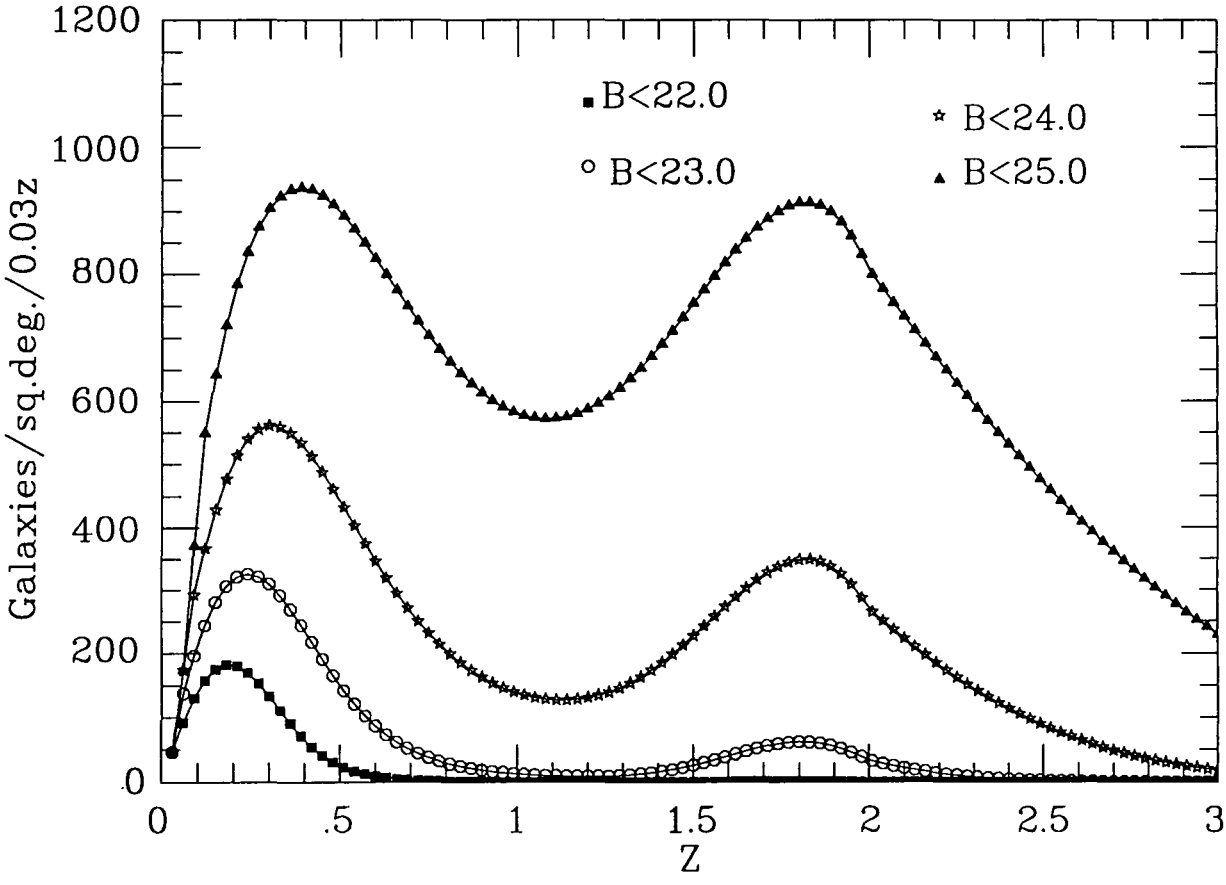

Figure 2.6 Redshift distributions predicted by our Bruzual PLE models, with $q_0 = 0.05$, for a range of blue magnitude limits from $B_{ccd} \leq 22.0$ to $B_{ccd} \leq 25.0$, and a range of red magnitude limits from $R_{ccd} \leq 20.5$ to $R_{ccd} \leq 23.5$.

2.6 Comparison with Models

It is clear from Figures 2.3 and 2.4 that our correlation amplitudes do not follow the no-evolution scaling in either passband, being lower at $B_{ccd} > 23$ and at $R_{ccd} > 22$. The non-evolving $N(z)$ model is strongly rejected by at least 4σ at $B_{ccd} = 24.5$.

In the blue band our results are fitted reasonably well by the Bruzual PLE model. In the red band where there is more scatter between the results of different observers, our amplitudes fall off with magnitude limit a little less steeply than the PLE model prediction. Our results therefore suggest that MSFJ's red-band model may have somewhat overestimated the amount of evolution at $z \sim 2$ for early types. However, the non-evolving model is still rejected by 2σ at $R_{ccd} = 23.5$ and therefore the $\omega(\theta)$ results suggest that some luminosity evolution is seen in the red band (assuming no evolution of clustering) as well as in the blue band, confirming the conclusions of MSFJ based on the galaxy counts.

Our conclusions are essentially in agreement with those of Koo and Szalay (1984), Stevenson et al. (1985) and JSF, in that the $\omega(\theta)$ amplitude at the faint limit of photographic surveys is significantly lower than would be expected for a model in which clustering is stable in proper co-ordinates and the redshift distribution maintains a no-evolution form. We find the $\omega(\theta)$ amplitude to fall even further below no-evolution predictions faintward of the photographic limits of $B \sim 24$ and $R \sim 23$. The PLE model described above would explain this dilution of clustering as resulting from the appearance of a population of high redshift galaxies at these magnitude limits. We find the scaling of $\omega(\theta)$ with magnitude limit to be as expected if the rise in galaxy number counts above the no-evolution prediction is primarily a result of luminosity (L^*) rather than density (ϕ^*) evolution.

2.7 Comparison with $B \leq 24$ Galaxy Redshift Surveys

To a limit of $B \leq 24$, the excess in the galaxy number counts above no-evolution predictions is a factor of ~ 2.5, even with the relatively high normalization of our models. As can be seen by comparing Figures 2.5 and 2.6, the PLE models explain this excess as being made up almost entirely of galaxies at higher redshifts than the median of a no-evolution $N(z)$. For this particular model, a significant extension of $N(z)$ beyond the no-evolution form is only expected faintward of $B \simeq 22.5$, the limit of the $\sim 95\%$ complete redshift survey of Colless et.al. (1990). This survey found a no-evolution $N(z)$, with $z_{median} = 0.32$, which is consistent with both our models at this magnitude limit. However, a number of observers have recently obtained redshifts for significant numbers of galaxies as faint as $B = 24$, where the models differ greatly. We now consider whether the high proportion of $z > 1$ galaxies at $B_{ccd} = 24$ in our pure luminosity evolution model is consistent with these spectroscopic results.

Firstly, Lilly, Cowie and Gardner (1991, hereafter LCG) examined three small (70 arcsec square) and widely separated regions in which a total of 22 galaxies were detected to $B_{AB} = 24.1$ (approximately $B_{ccd} = 24.14$); spectroscopic redshifts were given by Cowie, Songaila and Hu (1991) for 11 of these. The other redshifts were estimated from U'BVI colours. The median redshift for $B_{AB} \leq 24.1$ was estimated at the surprisingly low value of 0.40, only slightly higher than our no-evolution prediction of 0.36. Four galaxies in the sample were thought on the basis of their colours to be at $z > 1$, three of these being 'flat-spectrum' objects with a very blue $B - I$ colour. Such a colour would result from active star-formation at $1.3 \leq z \leq 3$ (see eg. Koo 1990).

We now compare these results with our Bruzual model $N(z)$ for $B_{ccd} \leq 24.14$. We can predict not only the expected number of galaxies in a chosen redshift interval but also the field-to-field variance, which is higher than the Poisson value because of galaxy clustering. A $\omega(\theta)$ amplitude is estimated for the galaxies in each interval by performing the Limber's formula integration for that portion of the modelled $N(z)$ in the relevant interval. If the mean number of galaxies observed on each field is N and the galaxy $\omega(\theta)$ amplitude is A, the field-to-field variance in N will be

$$\mu_2 = N + N^2 \frac{A}{\Omega^2} \int \int \omega(\theta) d\Omega_1 d\Omega_2$$

integrated doubly over the field area Ω, which for a square field of side θ degrees gives

$$\mu_2 = N + 2.24 N^2 A \theta^{-0.8}$$

where N and A are provided by our model for each redshift interval. For the total of three fields the prediction will be $3N \pm (3\mu_2)^{0.5}$ galaxies observed.

Our PLE model predicts that there will be 14.44±4.75 $z < 1$ galaxies and 16.23±4.23 with $z \geq 1$, whereas LCG observed 18 and 4 respectively. The resulting χ^2 is 8.92, and for two degrees of freedom the probability of $\chi^2 \geq 8.92$ is 1.16% (ie. approximately a 2.5σ rejection in Gaussian terminology).

Glazebrook et al. (1993) more recently presented the results of a much larger but less complete galaxy redshift survey. This covered the magnitude range $22.5 \leq B \leq 24.0$ on two fields, $22.5 \leq B \leq 23.3$ on a third and $22.5 \leq B \leq 23.0$ on a fourth, the faint limits being chosen to give $\sim 70\%$ completeness on each field. The survey identified 58 galaxies at $z < 1$ and only one at $z > 1$, together with two $z > 1$ objects thought to be QSOs, and four stars. The median of the measured galaxy redshifts was 0.46, again only a little higher than the no-evolution prediction.

Glazebrook et al. (1993) interpreted their results as favouring a merging-dominated model, in particular the 'b=4 Q=4' model described by Broadhurst, Ellis and Glazebrook (1993). We discuss models of this type in more detail in Chapters 3 and 4. In this particular model, the blue-band L^* remains constant, resulting in a low median redshift of $z_{median} = 0.51$ at Glazebrook's survey limit, but the very rapid increase in ϕ^* with redshift (caused by merging), is sufficient in itself to fit the high number counts.

However, redshifts could not be obtained for 24 objects examined in the survey, and therefore a substantial ($\sim$ 30%) high-redshift component at $23 \leq B \leq 24$ could still have been present. As in the LCG survey, the unidentified objects were generally very blue in $B - R$ colour, indicating that they are star-forming galaxies, so that the failure to detect the expected OII(3727Å) emission line anywhere blueward of $\lambda \sim 8000$Å (the reddest wavelengths observed in the galaxy spectra) suggests high redshifts of $z > 1.1$. Interestingly, the highest galaxy redshift obtained in the survey was $z = 1.108$ for a blue, star-forming galaxy with its strong OII 3727Å emission line shifted close to the red limit of the observed spectral region.

As the dimensions and magnitude limits of the fields examined by Glazebrook et al. differ, to compare their results with our PLE model we predict the numbers of $z < 1$ and $z \geq 1$ galaxies expected, with corresponding variances including the clustering term, for each field separately. The total of these means and variances was then normalized to the number of objects (85 excluding stars) in the survey.

Our PLE model then predicted 40.37±18.08 galaxies to be at $z < 1.0$ and 44.63±8.70 to be at $z \geq 1.0$. If all unidentified objects are assumed to be at $z \geq 1$ the resulting

χ^2 is 5.057. As we have normalized the model to give the same total number as the survey, the χ^2 test is left with only one degree of freedom, for which the probability of $\chi^2 \geq 5.057$ is 2.45% (ie. a 2.25σ rejection).

Hence, although both surveys do suggest that the proportion of $z > 1$ galaxies is lower than the 50–55% predicted by our PLE model at these magnitude limits, in neither case is the rejection of this model very strong (i.e. $> 3\sigma$). If most of the blue galaxies at $23.0 \leq B \leq 24.0$ for which redshifts could not be measured are indeed at $z > 1.1$, as the authors of both redshift survey papers consider most likely, a model in which $\sim$ 30–35% rather than 50–55% of the galaxies in a $B \leq 24.0$ sample are at $z > 1$ is entirely consistent with spectroscopic observations. As our PLE model actually underpredicts slightly the observed $\omega(\theta)$ amplitude at $B_{ccd} \leq 24.0$, a slightly smaller high-redshift component (eg. 30–35% at $22.5 \leq B \leq 24$) could still explain the low $\omega(\theta)$ amplitudes without invoking any departure from stable clustering.

Further faintward, in the range $24.0 \leq B_{ccd} \leq 24.5$, the $\omega(\theta)$ amplitude continues to fall steeply, decreasing by a factor of ~ 2 when $24.0 \leq B \leq 24.5$ galaxies are added to a $B \leq 24.0$ sample. Under the assumption of stable clustering, which is still consistent with observations, a very large proportion ($\sim$ 50%) of $24.0 \leq B \leq 24.5$ galaxies must be at $z \geq 1.0$, and therefore the true brightening of L^* at high redshifts can only be slightly ($\leq 0.5^m$) less than that in Bruzual's $\mu = 0.5$ model. We therefore predict that future spectroscopic surveys will find large numbers of $1 \leq z \leq 3$ flat-spectrum galaxies less than 0.5^m beyond the limits reached by the redshift surveys described above.

We conclude that a PLE model with slightly more moderate L^* evolution than Bruzual's $\mu = 0.5$ model could be consistent with the redshift data, the $\omega(\theta)$ scaling, and (at least in a low q_0 Universe) the high number counts.

2.8 The Colour Dependence of $\omega(\theta)$ at $B = 24.5$

The $\omega(\theta)$ analysis of a galaxy sample divided by colour may provide information about galaxy evolution additional to that given by the scaling of $\omega(\theta)$ with magnitude limit. Luminosity evolution in galaxies is always associated with colour evolution, as a result of the shorter lifetimes of hotter, bluer stars. The colours of the reddest galaxies in our sample, those with $(B - R)_{ccd} \geq 1.50$, indicate that these are observed while undergoing little star formation. These 'passive' galaxies cannot be much more luminous than their present-day counterparts, so we would expect the redshifts of the reddest galaxies to lie approximately within a no-evolution $N(z)$, regardless of the evolutionary model. Hence the extension of $N(z)$ to high redshifts, and therefore the steep decline in the $\omega(\theta)$ amplitude, predicted by PLE models at $B \sim 24$ would be associated only with the galaxies of bluer colours.

To verify whether the colour dependence of $\omega(\theta)$ in our galaxy dataset, as well as the scaling of $\omega(\theta)$ with blue magnitude limit, agrees well with a stable clustering PLE model, we now calculate $\omega(\theta)$ separately for red and blue subsamples of our galaxy sample limited at $B_{ccd} = 24.5$, and compare our results with the $\omega(\theta)$ amplitudes predicted by our Bruzual PLE model for these two subsamples.

The $B_{ccd} \leq 24.5$ galaxies on our 12 CCD frames (observed in both blue and red passbands) were divided into two subsamples – the 701 'red' galaxies with $(B - R)_{ccd} \geq 1.5$ and a larger 'blue' subsample of 2314 galaxies with $(B - R)_{ccd} < 1.5$. Galaxies with $B_{ccd} \leq 24.5$ not detected at all in the red band were placed in the $(B-R)_{ccd} < 1.5$ subset, i.e. were assumed to be at $R_{ccd} > 23.0$. This is not unreasonable as our incompleteness is only significant at $R_{ccd} > 23.0$ and $B_{ccd} > 24.5$ (see MSFJ). We then calculated $\omega(\theta)$

separately for the blue and red subsamples, fitting $\theta^{-0.8}$ power-laws and obtaining field-to-field errors for the resulting amplitudes, exactly as described in Section 2.3 for the full magnitude-limited samples.

The red and blue galaxies were found to have significantly differing correlation functions, as shown in Figure 2.7. For the red galaxies we measured

$$\omega(\theta) = (24.156 \pm 6.907) \times 10^{-4}(\mathrm{deg})^{-0.8}$$

This is in good agreement with the no-evolution $N(z)$, stable clustering prediction for all $B \leq 24.5$ galaxies.

For the bluer galaxies, we obtained a much lower correlation amplitude of

$$\omega(\theta) = (5.016 \pm 3.745) \times 10^{-4}(\mathrm{deg})^{-0.8}$$

similar to that of $\omega(\theta) = (5.568 \pm 2.157) \times 10^{-4}(\mathrm{deg})^{-0.8}$ measured for the full $B_{ccd} \leq 24.5$ sample, and the Bruzual PLE model prediction at this limit.

The cross-correlation between the red and blue galaxies, taking the red galaxies as the centres in the calculation, was consistent with zero, being best-fitted by a power-law of amplitude $(-0.134 \pm 8.899) \times 10^{-4}(\mathrm{deg})^{-0.8}$.

Our analysis therefore indicates, at 2.5σ significance (field-to-field errors), that red galaxies at this limit are more clustered on the sky than are bluer galaxies, and at 2.2σ significance that the red galaxies are more correlated with each other than with the blue galaxies.

To compare these results with our PLE model, we must now consider in more detail the effect of dividing the PLE model $N(z)$ by galaxy colour. In the models of MSFJ, galaxies were classified into five types with different rest-frame colours, k-corrections and Bruzual model evolution corrections. We would observe colours as red as $(B-R)_{ccd} \geq 1.50$ for E/S0 and Sab galaxies evolving according to the $\mu = 0.5$ model in the redshift ranges $0.01 \leq z \leq 0.96$ and $0.06 \leq z \leq 0.86$ respectively. Sbc galaxies, following Bruzual's evolution model for spirals, would have $(B-R)_{ccd} \geq 1.50$ at $0.17 \leq z \leq 0.51$, whereas at no redshift would Scd or Sdm galaxies appear as red as this. Hence the red $(B-R \geq 1.50)$ galaxies will all be at $z < 1$, at any magnitude limit, as blue-band luminosity evolution sufficient to enable $z > 1$ galaxies to be seen at $B \leq 24.5$ would also shift their colours blueward to $(B-R)_{ccd} < 1.5$.

The $B \leq 24.5$ galaxy $N(z)$ given by our PLE model was divided, using these redshift ranges, into the separate red and blue galaxy redshift distributions shown in Figure 2.8 (the sharp discontinuities result from the use of only five galaxy colour types). The red galaxy $N(z)$, with $z_{mean} = 0.45$, is similar to that given by a no-evolution model at this magnitude limit, so if clustering is stable, the $\omega(\theta)$ amplitude for red galaxies only should be similar to the no-evolution prediction. The blue galaxy $N(z)$ given by our PLE model at the same limit of $B \sim 24.5$ contains both late type galaxies at $z < 1$ and giant galaxies undergoing their initial starbursts at $1 \leq z \leq 3$. As blue, star-forming galaxies would be seen at all redshifts from $z = 0$ to $z \sim 3$, the blue galaxy $N(z)$ in our PLE model is much more extended (with $z_{mean} = 1.48$) than that of the red galaxies. If the $z > 1$ blue galaxies correspond to the present-day $L \sim L^*$ galaxy population at earlier epochs, we would expect the intrinsic clustering properties to be similar to the $z < 1$ red galaxies, but as a result of their much more extended $N(z)$, the blue galaxies in a PLE model would give much lower $\omega(\theta)$ amplitude than the red subsample.

Limber's formula integration of the red galaxy $N(z)$, assuming $q_0 = 0.05$ and stable clustering, predicts a $\omega(\theta)$ amplitude of $25.798 \times 10^{-4}(\mathrm{deg})^{-0.8}$, and for the much more

extended blue galaxy $N(z)$ only $3.369 \times 10^{-4}(\mathrm{deg})^{-0.8}$. The PLE model, with stable clustering, is therefore in very good agreement ($\chi^2 = 0.25$) with our observations.

We find that the $\omega(\theta)$ amplitude of red galaxies, which would lie within an approximately no-evolution $N(z)$, fits a non-evolving $N(z)$ model with stable clustering. This indicates that the clustering of at least the early-type galaxies (i.e. the E/S0/Sab types which would comprise most of the red subsample) must have remained approximately stable since the $z \sim 0.5$ epochs at which they are seen, and therefore excludes an extremely rapid evolution of the clustering of all galaxies as a possible cause of the steep $\omega(\theta)$ scaling at $23 \leq B \leq 25$. As the drop in $\omega(\theta)$ amplitude below the no-evolution prediction is associated only with blue galaxies, it must result from either a much more extended $N(z)$ or a much weaker intrinsic strength of clustering for the blue galaxies at $23 \leq B \leq 24.5$ in comparison to the 'passive' red galaxies. If the flat-spectrum objects appearing faintwards of $B \simeq 23$ are intrinsically as clustered as normal galaxies, they must be broadly distributed in redshift over the $1 \leq z \leq 3$ range, as in our PLE model.

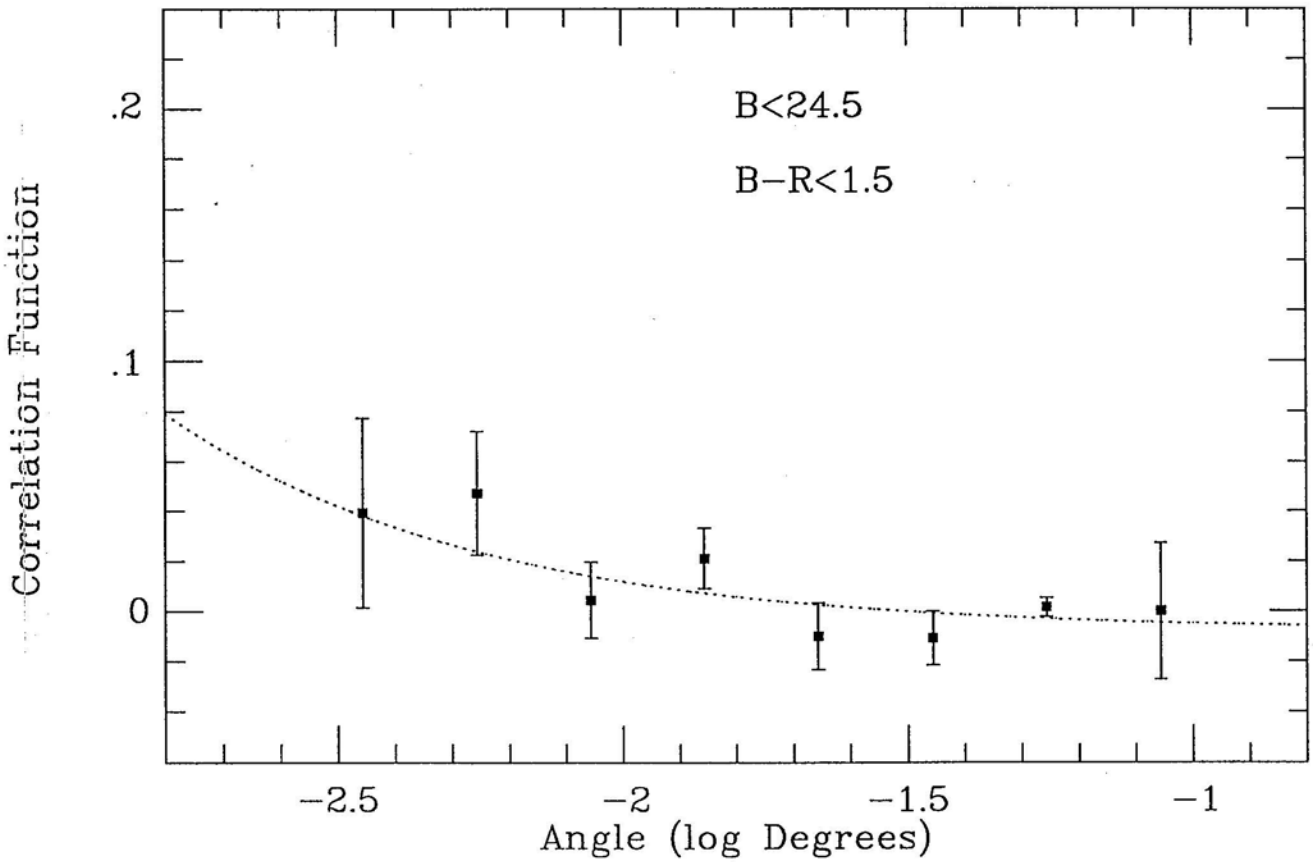

Figure 2.7a The observed angular correlation function, $\omega(\theta)$, of the blue ($B-R < 1.5$) galaxies detected on our 12 blue-band CCD frames with blue magnitudes $B_{ccd} \leq 24.5$. The data are shown with field-to-field errors and the best-fitting function of the form '$A(\theta^{-0.8} - 16.1)$' (dotted line).

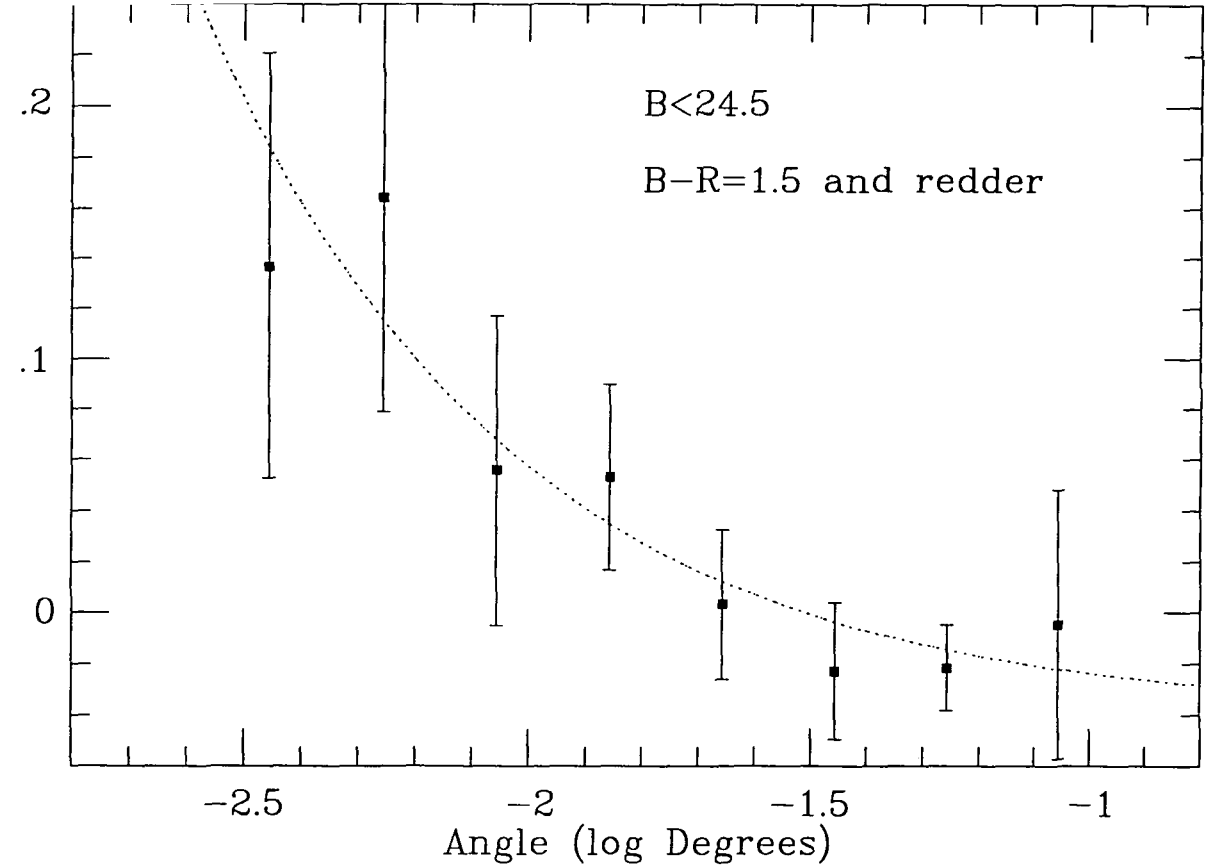

Figure 2.7b The observed angular correlation function, $\omega(\theta)$, of the red ($B-R \geq 1.5$) galaxies detected on our 12 blue-band CCD frames with blue magnitudes $B_{ccd} \leq 24.5$. The data are shown with field-to-field errors and the best-fitting function of the form '$A(\theta^{-0.8} - 16.1)$' (dotted line).

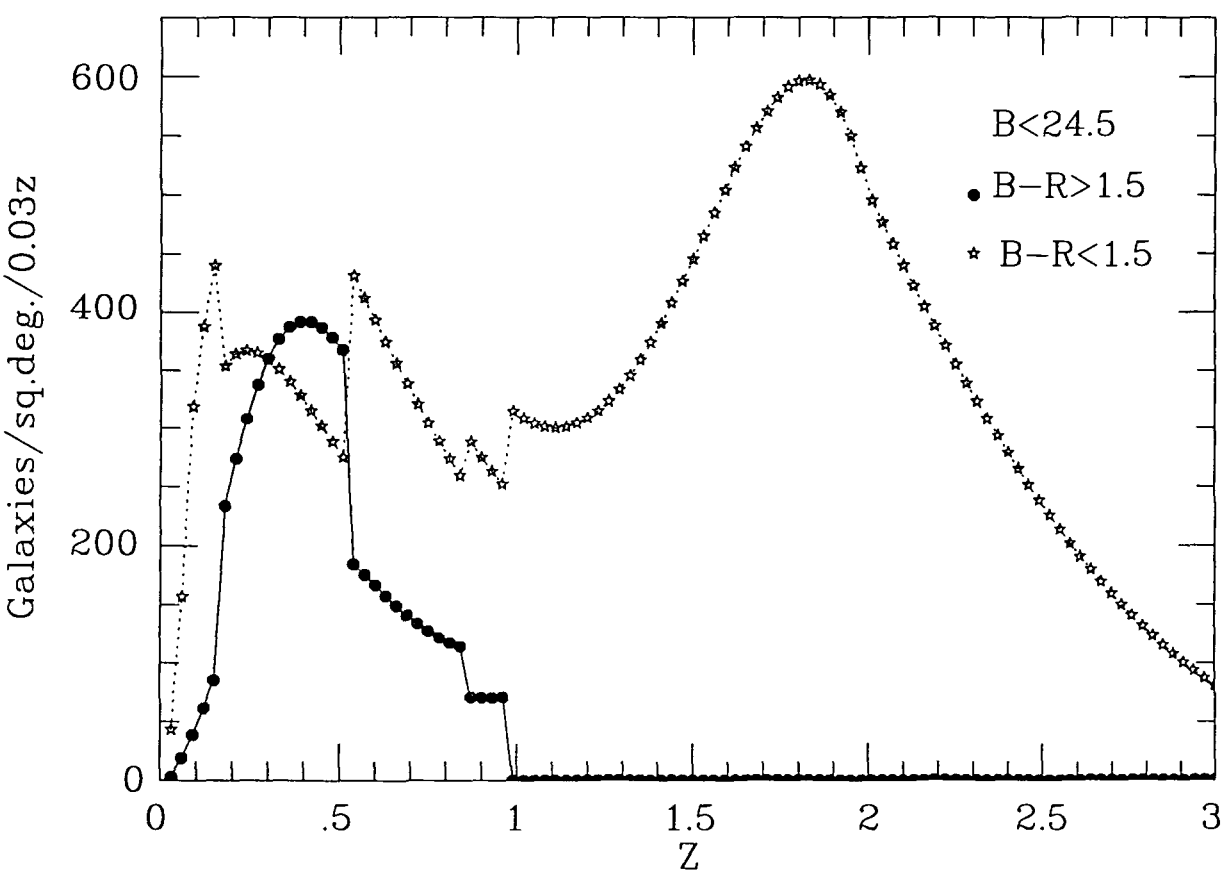

Figure 2.8 Redshift distributions predicted by our Bruzual PLE model, with $q_0 = 0.05$, for galaxies with blue magnitudes $B_{ccd} \leq 24.5$, divided into galaxies with blue ($B - R < 1.5$) and red ($B - R \geq 1.5$) colours.

2.9 Summary and Conclusions

(i) The scaling of the $\omega(\theta)$ amplitudes in both the blue and red passbands was determined from CCD data. The model of pure luminosity evolution described in MSFJ, with a Bruzual $\mu = 0.5$ model of exponentially decreasing star-formation rate used for the early types, was found to fit the blue-band $\omega(\theta)$ scaling well. A model in which $N(z)$ maintains a no-evolution form at limits of $B_{ccd} = 24$ and fainter is strongly rejected, if we assume no evolution of galaxy clustering relative to a stable clustering model.

(ii) Our $\omega(\theta)$ results for red-limited samples suggest that some luminosity evolution is also seen in the red band at $R_{ccd} > 22$.

(iii) In the $B_{AB} \leq 24.1$ redshift survey of LCG and the $22.5 \leq B \leq 24.0$ redshift survey of Glazebrook et al. (1993), fewer high-redshift galaxies were found than would be expected from our Bruzual PLE model, which predicts $\sim 50\%$ of galaxies at these magnitudes to be at $z \geq 1$. However, these redshift surveys, being relatively small and/or incomplete, can only reject the Bruzual PLE model at the $\sim 2.5\sigma$ level. A model predicting a slightly lower ($\sim$ 30–35%) proportion of $22.5 \leq B \leq 24.0$ galaxies to be at $z \geq 1.0$ would be consistent with both the spectroscopic results and the low $\omega(\theta)$ amplitudes, without invoking any departure from stable clustering. Our lower $\omega(\theta)$ amplitude at $B_{ccd} \leq 24.50$ suggests that, if clustering is stable, the proportion of $z > 1$ galaxies increases further to $\sim 50\%$ at this limit, and therefore the true brightening of L^* at high redshift is only slightly ($\leq 0.5^m$) less than that in Bruzual's $\mu = 0.5$ model.

(iv) Red, i.e. $(B-R)_{ccd} \geq 1.5$, galaxies were found to be significantly more clustered on the sky than the bluer galaxies at a limit of $B_{ccd} = 24.5$. The high $\omega(\theta)$ amplitude of the red galaxies is similar to no-evolution predictions, indicating that the clustering of the galaxy population as a whole, or at least that of E/S0/Sab morphological types, has been approximately stable since the epoch corresponding to $z \sim 0.5$. The bluer galaxies possessed a much lower $\omega(\theta)$ amplitude, similar to the PLE model prediction, and no significant cross-correlation was detected between red and blue galaxies.

The simplest explanation of this colour dependence is that the $N(z)$ of blue galaxies at $B \leq 24.5$ is much more extended than both the red galaxy $N(z)$ and that given by a no-evolution model. In our Bruzual PLE model, the blue galaxy subsample would consist of star-forming giant galaxies at $1 \leq z \leq 3$ in addition to late-type galaxies at lower redshifts, whereas the red galaxies would all lie at $z < 1$. With stable clustering, this PLE model gives a very good fit to the $\omega(\theta)$ amplitudes of both the blue and red galaxies in our $B_{ccd} \leq 24.5$ sample.

(v) We conclude that both the scaling with magnitude limit and the colour dependence of the galaxy $\omega(\theta)$ amplitude are most easily explained if the very blue (flat-spectrum) galaxies appearing at $B > 23$ are at $1 \leq z \leq 3$. Flat-spectrum galaxies would therefore be the progenitors of the present-day giant galaxies, undergoing rapid star-formation at these earlier epochs as indicated by their colours (Tyson 1988, Koo 1990, MSFJ). An alternative explanation, discussed further in Chapter 3 following, is that these blue galaxies are at somewhat lower redshifts and very weakly clustered in comparison to other galaxies.

Chapter 3

Clustering Evolution and non-PLE Models

3.1 Introduction

In the galaxy clustering analysis of Chapter 2, we found the $\omega(\theta)$ amplitude of faint ($23 \leq B \leq 25$) galaxies to be much lower than predicted by a model without significant evolution of either the luminosity or the clustering of galaxies. We interpreted this as indicating a very extended (out to $z \sim 3$) redshift distribution for galaxies at these magnitude limits, resulting from strong luminosity evolution at $z > 1$. We now consider the other possible explanation for the low $\omega(\theta)$ amplitudes – that galaxies were intrinsically less clustered at earlier cosmological epochs.

Our results are compared with the no evolution $N(z)$ model considered previously, but combined with a simple model of gravitational clustering evolution. We also describe models which have been proposed to explain the high number counts through an increase in the number density of galaxies with redshift, rather than a brightening of the luminosity L^* as in the PLE models. We consider in particular the merging-dominated model proposed by Broadhurst, Ellis and Glazebrook (1993), and a 'disappearing dwarf' model in which the excess blue galaxies lie at low redshifts. We compare these models with our $\omega(\theta)$ results, both the scaling with magnitude limit at $23 \leq B_{ccd} \leq 25$ and the colour dependence of $\omega(\theta)$ at $B_{ccd} \leq 24.5$. We estimate the extent to which evolution of clustering is required for non-PLE models with low median redshifts to be consistent with our $\omega(\theta)$ results, and discuss the other constraints which we may be able to set on non-PLE models when the physical processes of galaxy and clustering evolution are also considered.

3.2 Clustering Evolution

Consider the three-dimensional correlation function of galaxies in proper (physical) co-ordinates r as a function of redshift z,

$$\xi(r, z) = (\frac{r_0}{r})^{\gamma}(1+z)^{-(3+\epsilon)}$$

The correlation radius r_0 is the separation, at $z = 0$, at which the probability of finding another galaxy is twice than expected from a random distribution. Observations have indicated a power-law slope $\gamma = 1.8$, and for galaxies the correlation radius has usually been found to be $r_0 \sim 4.0$–5.5 h^{-1} Mpc.

Clustering analysis in three dimensions – using redshift data as well as positions on the sky – has suggested that $\xi(r)$ may have a somewhat more complicated form than a simple power-law, but the observed variations in r_0 with radial separation are largely smoothed out in the projection of $\xi(r)$ into $\omega(\theta)$, so that $\omega(\theta) \propto \theta^{-0.8}$ remains a good approximation at the small angular separations ($\theta \leq 0.1$ deg) considered here (see e.g. Shanks et al. 1989). Hence in this thesis we normalize our $\omega(\theta)$ models with an 'effective' r_0 of 4.3 h^{-1} Mpc determined by fitting the models to the $\omega(\theta)$ amplitudes of nearby galaxies (i.e. the Zwicky catalogue), rather than using r_0 obtained from $\xi(r)$ analysis.

We now consider the possible change in $\xi(r)$ with redshift, parameterized here by ϵ. More complicated models, in which the slope γ also changes with redshift, are considered by Neuschaefer (1992), but here we shall confine our discussion to the evolution of the amplitude of $\xi(r)$ on small scales (i.e. $r < r_0$).

In a static Universe, small variations in density would tend to increase exponentially with time for as long as the the linear approximation $\Delta\rho << \langle\rho\rangle$ remains valid. However, as discussed by Peebles (1980), the expansion of the Universe will tend to slow this process, so that in an $\Omega = 1$ Universe, low-amplitude inhomogeneities will increase with time only as $t^{2/3}$, i.e. as $(1+z)^{-1}$, and the increase will be even slower than this in a low-q_0 Universe.

However, the small separations ($r \sim 1$ Mpc) probed by our $\omega(\theta)$ analysis correspond to $r \leq r_0$ in the correlation function $\xi(r)$, where $\Delta\rho > \langle\rho\rangle$ and linear approximations no longer apply. Dense clusters of galaxies will be approximately virialized and evolving very slowly in physical co-ordinates. If galaxy clustering in general is dynamically bound and stable at small scales, the clustering pattern will remain fixed in proper co-ordinates, neither expanding with the Universe nor collapsing. This gives $\epsilon = 0$ in the $\xi(r,z)$ formula, with the remaining change as $(1+z)^{-3}$ being due to the change in the background density.

The above equation can also be written as

$$\xi(ra^{-1}) = (\frac{r_0}{ra^{-1}})^{\gamma} a^{\alpha}$$

where $a = (1+z)^{-1}$, the scale factor of the Universe. In the comoving co-ordinate system (ra^{-1}) the background density does not change, so $\alpha = 0$ corresponds to a clustering pattern fixed in comoving co-ordinates. As $\alpha = 3 + \epsilon - \gamma$, for a power-law $\gamma = 1.8$ the comoving model corresponds to $\epsilon = -1.2$, and high redshift galaxies are significantly more clustered than in the stable model. For example, at $z = 1$ the clustering in the two models would differ by a factor

$$\frac{\xi_{comoving}(r)}{\xi_{stable}(r)} = (2.0)^{1.2} = 2.3$$

A comoving clustering model represents the extreme case in which gravity is neglected entirely so that the pattern of galaxy clustering expands with the Universe, which may be an appropriate assumption when we consider very large scale structures. We might expect approximately comoving clustering, perhaps even on relatively small scales, if the mean density is as high as $\Omega = 1$, as this would require the galaxy distribution to be biased, i.e. more strongly clustered than the underlying distribution of mass. If $\Omega = 1$, dark matter must form over 90% of the mass of the Universe, and if this dark matter is more uniformly distributed than the galaxies, the influence of the gravitational attraction between the galaxies on the evolution of galaxy clustering evolution will be diluted. On the basis of the n-body simulations of Davis et al. (1985), biased models of galaxy formation in an $\Omega = 1$ Universe predict little growth of clustering relative to a comoving model on scales larger than $r \sim 1$ h^{-1}Mpc.

However, the observed low $\omega(\theta)$ amplitude of faint galaxies obviously does not favour a comoving model for the small-scale clustering of galaxies – if there is any evolution relative to the stable model it must be in the opposite direction, as was concluded by Efstathiou et al. (1991), Neuschaefer (1992), and Couch et al. (1993) from $\omega(\theta)$ analysis of various deep galaxy surveys. Phillipps et al. (1978) considered three simple models of clustering evolution – comoving, stable and collapsing. Considering a departure from

stable clustering in the opposite direction, weaker clustering at earlier epochs would correspond to $\epsilon > 0$ or $\alpha > 1.2$. For example, in the collapsing ($\beta = -1$) model of Phillipps et al. (1978), galaxy clustering collapses at the same rate at which the Universe expands, giving $\epsilon = 1.2$ and $\alpha = 2.4$.

Melott (1992) derived a growth rate for $\xi(r)$ of $\alpha = 6/(n+5)$, where n is the index of the assumed primordial power-spectrum, $P(k) \propto k^n$, and obtained growth rates for small-scale clustering in good agreement with this formula from numerical simulations of gravitational clustering evolution in an $\Omega = 1$ Universe. For $n = 0$ clustering is approximately stable, whereas increasingly negative values (more power on large scales) result in increasingly rapid growth rates. Melott (1992) favoured $n = -1$ as the $P(k)$ index most appropriate on small scales, which would give a more moderate growth rate of $\epsilon \sim 0.3$. The more extreme ($\epsilon = 1.2$) collapsing model of Phillipps et al. (1978) would, on the basis of Melott's formula and simulations, require $n < -2$. Therefore it seems reasonable to regard $\epsilon = 1.2$ as an upper limit to clustering growth rates produced by gravitational collapse.

We now predict, using Limber's formula, the $\omega(\theta)$ amplitudes expected for our no-evolution redshift distributions, with the addition of an $\epsilon = 1.2$ evolution of clustering. Figure 3.1 shows this model, together with the $\omega(\theta)$ results and stable clustering models from Figure 2.3. It is clear that adding $\epsilon = 1.2$ clustering evolution to a non-evolving model has much less effect on the predicted $\omega(\theta)$ amplitude of $23 \leq B \leq 25$ galaxies than does strong L^* evolution. Galaxies with a no-evolution $N(z)$ would need to be clustered only about $\sim \frac{1}{4}$ as strongly as present-day galaxies (with $r_0 \simeq 4.3$ h^{-1}Mpc and a stable clustering model assumed), to give the observed low $\omega(\theta)$ amplitude at $B = 24.5$. At the relatively moderate redshifts of the no-evolution $N(z)$, (ie. $z \sim 0.4$), this would require extremely rapid ($\epsilon > 3$) clustering evolution, far more than would be expected from simple gravitational evolution.

However, in addition to the possible effects of luminosity evolution and gravitational clustering evolution, it has been suggested that the influence of environment on the star-formation histories of dwarf galaxies might also affect the $\omega(\theta)$ scaling. For example, Babul and Rees (1992) suggested that some dwarf galaxies might begin forming stars at relatively late epochs, and that when this occurs in low-density regions, the first wave of supernova explosions may be sufficient to blow away the entire gas content of the dwarf galaxy. This would prevent further star-formation, so the dwarf galaxy would fade rapidly after its initial starburst. Whereas, when dwarf galaxies form in dense clusters the much higher pressure of the surrounding intergalactic medium might contain the gas within the dwarf galaxy and allow star-formation to continue. Hence in this model, the 'unclustered' dwarfs 'self-destruct' and fade from view while those in clusters survive to the present day. The gradual disappearence of an intrinsically weakly clustered population of galaxies could have the same effect on the $\omega(\theta)$ scaling as a rapid growth of the strength of clustering of all types of galaxy, and may produce an effective rate of clustering evolution exceeding $\epsilon = 1.2$, even if the clustering of each separate galaxy population remains approximately stable.

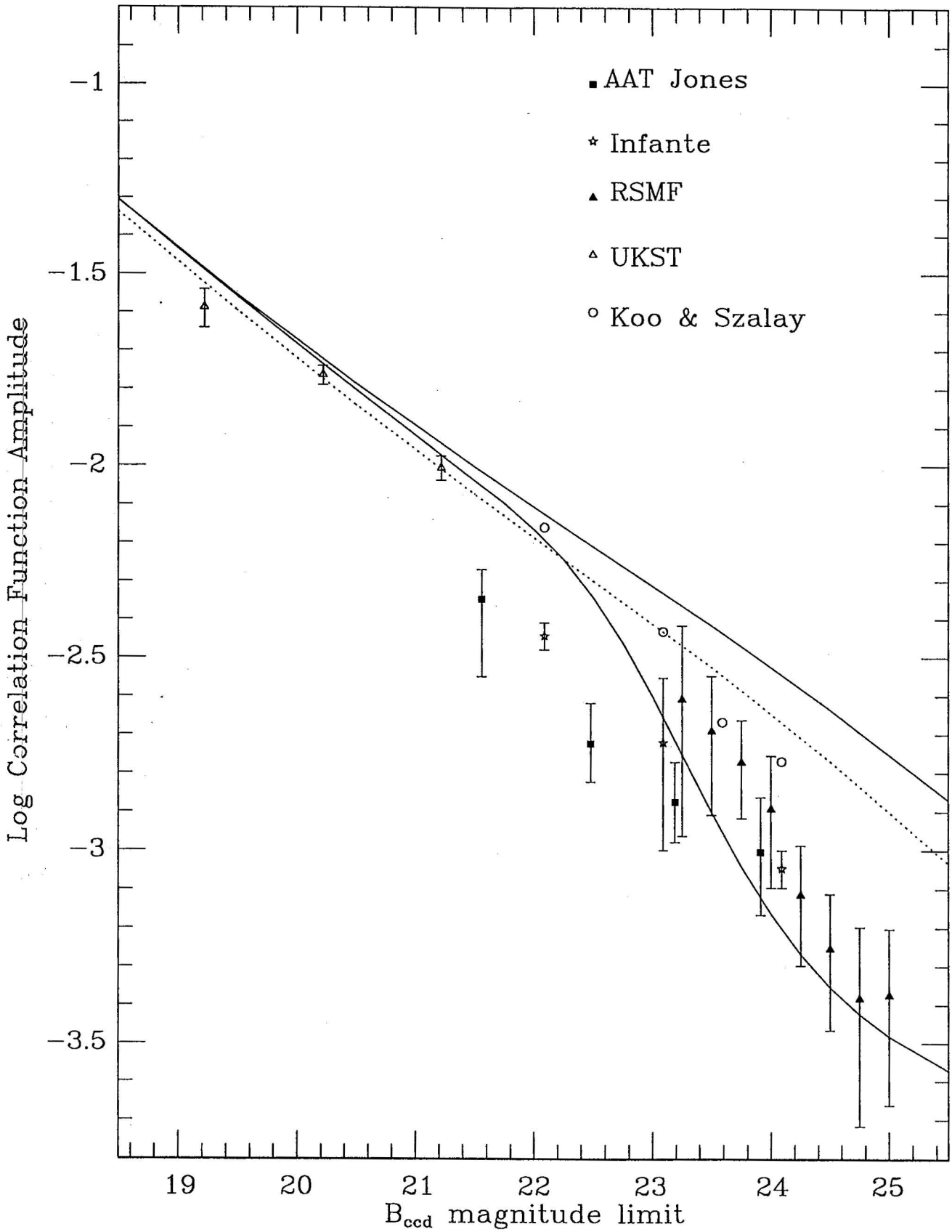

Figure 3.1 Galaxy $\omega(\theta)$ amplitudes obtained from the AAT photographic surveys of Jones et al. (1987), Infante (1990), and Koo and Szalay (1984), from the UKST data of Stevenson et al. (1985), and from the 12 CCD frames of our $B_{ccd} \leq 25.0$ survey (RSMF). These are compared with the predictions of a non-evolving model (upper solid curve), and our Bruzual PLE model (lower solid curve), over a over a range of blue magnitude limits, with stable clustering. The dotted line shows the no-evolution model with the addition of $\epsilon = 1.2$ evolution of the clustering. All three models shown here assume $q_0 = 0.05$ and $z_{max} = 4$.

3.3 Merging Models

Up to this point we have simply represented models in which galaxy evolution is dominated by merging as producing a no-evolution redshift distribution. However, the stellar populations within merging galaxies are undergoing spectral evolution, as in PLE models, but were distributed amongst a larger number of smaller galaxies at earlier epochs. In comparison to galaxies in a PLE model, the smaller masses and correspondingly lower luminosities of merging galaxies reduce the redshift to which they are visible at a given magnitude limit, and consequently $N(z)$ will tend to be less extended, but will not necessarily be identical to a no-evolution $N(z)$.

The merging process incorporated into the models of Broadhurst, Ellis and Glazebrook (1993, hereafter BEG) is essentially the '$M^* - \phi^*$' evolution initially proposed by Rocca-Volmerange and Guiderdoni (1990), to enable the high galaxy counts of Tyson (1988) to be accomodated in an $\Omega = 1$ Universe. In models of this type, discussed in more detail by Guiderdoni and Rocca-Volmerange (1991, hereafter GRV), the faint-end slope of the luminosity function remains constant, but the comoving number density increases as a function of look-back time

$$\phi^*(t) = f(t)\phi_0^*$$

The characteristic mass of the galaxy mass function decreases as

$$M^*(t) = f(t)^{-1} M_0^*$$

so as to conserve the comoving mass density of galaxies. The (L^*/M^*) ratio increases with redshift – exactly as L^* increases in a PLE model – as a result of the younger stellar populations and/or more rapid star-formation at earlier epochs. The 'GRV' merging models incorporated a range of exponential timescales for SFR evolution ranging from 1 Gyr for E/S0 types to 10 Gyr for Sdm types – very similar to those in the spectral evolution models of Bruzual (1981) and Bruzual and Charlot (1993) – but the more simplified 'BEG' model used a single mean timescale for the blue-band (L^*/M^*) evolution of all galaxy types.

It must be emphasized that, whereas the brightening of (L^*/M^*) with redshift in Bruzual-type models is derived from the reasonably well-understood physical processes of stellar evolution, the merging models of GRV and BEG are not based on any physical model of the merging process, being merely parameterizations of the change in ϕ^* and α with redshift which have been adjusted to fit the observed number counts and redshift distributions. An alternative and complementary approach is to simulate the entire physical process of the formation, merging and spectral evolution of galaxies from the early Universe to the present day, within a chosen cosmological model, and from the luminosity function of the galaxies in different time stages in these models derive number counts and redshift distributions to compare with observations. Some recent attempts to do this are described by White and Frenk (1991), Carlberg and Charlot (1993), Lacey et al. (1993) and Cole et al. (1994). We discuss the results of these physical merging models later, in Section 4.8, after first considering the simple parametric models.

In the 'BEG' model, both $f(t)$ and $(L^*/M^*)(t)$ were parameterized as exponential increases with look-back time, and for $\Omega = 1$ BEG found the number counts and $N(z)$ observations to be best fitted if the (L^*/M^*) evolution and the merging both followed $\tau = 0.25\ \mathrm{H}_0^{-1}$ timescales.

As these timescales are the same, the blue-band L^* remains constant – the effects of merging (M^* decreasing with z) and spectral evolution (L/M increasing with z) cancel

out. As only ϕ^* then increases with look-back time in the 'BEG' model, it can be described as a pure density evolution model (for a blue-limited sample).

The mean K-band luminosity of the galaxies is more sensitive to the change in mean galaxy mass than to increased star-formation activity, so L^*_K might *decrease* with redshift in a merging-dominated model. Hence a K-limited redshift survey might be a good test of merging-dominated models, as these would predict that z_{mean} would be even lower than the non-evolving prediction, for a sufficiently deep K-limited sample (see BEG). However, K-band observations with optical spectroscopy have yet to reach the depths required ($K \sim 20$) to determine whether or not this is the case.

The '$M^* - \phi^*$' evolution in the 'BEG' model is actually very extreme – each present-day galaxy would have existed as, on average, 5.6 pre-merging 'fragments' at $z = 1$ and this 'breakup' totally cancels out the effects of enhanced star-formation on the blue-band L^*. On the other hand, in the GRV version the galaxies are broken up into only 2.8 fragments at $z = 1$, and with this more moderate rate of merging some brightening of L^* with redshift can still occur.

We represent the 'BEG' model here using our non-evolving model, with the same k-corrections and $z = 0$ luminosity functions as previously, but a density normalization increasing as

$$\phi^*_z = \phi^*_0 \exp(4T(z)/H_0^{-1})$$

where look-back time

$$T(z) = \frac{2}{3} H_0^{-1}(1 - (1+z)^{-3/2})$$

for $q_0 = 0.5$. For this model we assume $q_0 = 0.5$ in the modelling of $N(z)$ and $\omega(\theta)$, as the merging model fits the number counts with this value. The resulting redshift distributions are shown in Figure 3.2. As density evolution increases the normalization of a non-evolving $N(z)$ by a larger factor in its high-redshift tail, the mean redshift is somewhat higher than for the non-evolving model, increasingly so at fainter limits. However, even to $B = 25$ the merging model $N(z)$ is much less extended than that produced by pure luminosity evolution, with most of the number count excess at $z < 1$ rather than at $1 < z < 3$.

Figure 3.3 shows the observed $\omega(\theta)$ amplitudes together with three models, all computed using $q_0 = 0.5$.

(i) The no-evolution model.

(ii) The 'BEG' merging model with stable clustering.

(iii) The 'BEG' merging model with the addition of $\epsilon = 1.2$ clustering evolution.

In comparison to the $q_0 = 0.05$ non-evolving model (shown on Figure 2.3), a higher q_0 increases the predicted $\omega(\theta)$ amplitude slightly at faint limits, as a result of the smaller angular diameter distances of high redshift galaxies, but the q_0-dependence is weak for non-evolving models as most $B < 25$ galaxies are still at $z < 1$.

The addition of even the 'BEG' model's very rapid ϕ^* evolution to a non-evolving model clearly has much less effect on the $\omega(\theta)$ amplitudes than does the strong L^* evolution in the Bruzual models, although both enable the number counts to be fitted. Neither gravitational clustering evolution nor density evolution alone appear to be able to explain the low $\omega(\theta)$ amplitudes. A model combining the two processes, as shown here, can predict $\omega(\theta)$ amplitudes at faint limits sufficiently low to be at least marginally consistent with observations, but could be regarded as rather extreme. Only if the co-moving number density increases with redshift at the maximum rate allowed by the

number counts, and galaxy clustering becomes stronger with time at about the maximum rate predicted by any gravitational model, is it possible to explain the low $\omega(\theta)$ amplitudes without significant evolution of L^*, and the resulting model still appears to fit the overall scaling of $\omega(\theta)$ over the whole $19 \leq B \leq 25$ range less well than a stable clustering PLE model.

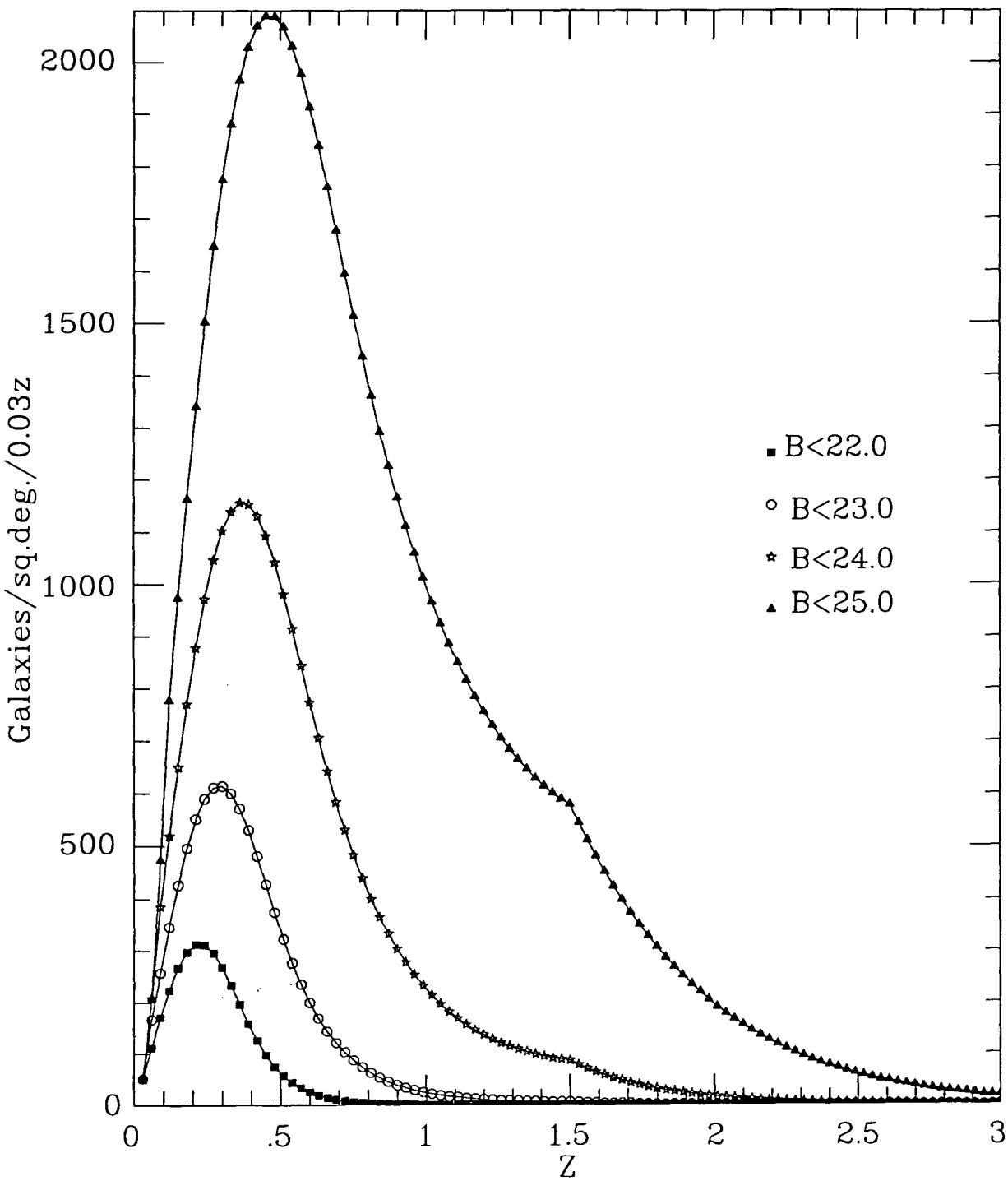

Figure 3.2 Redshift distributions predicted by the 'BEG' pure density evolution model, with $q_0 = 0.5$, for a range of blue magnitude limits from $B_{ccd} \leq 22.0$ to $B_{ccd} \leq 25.0$.

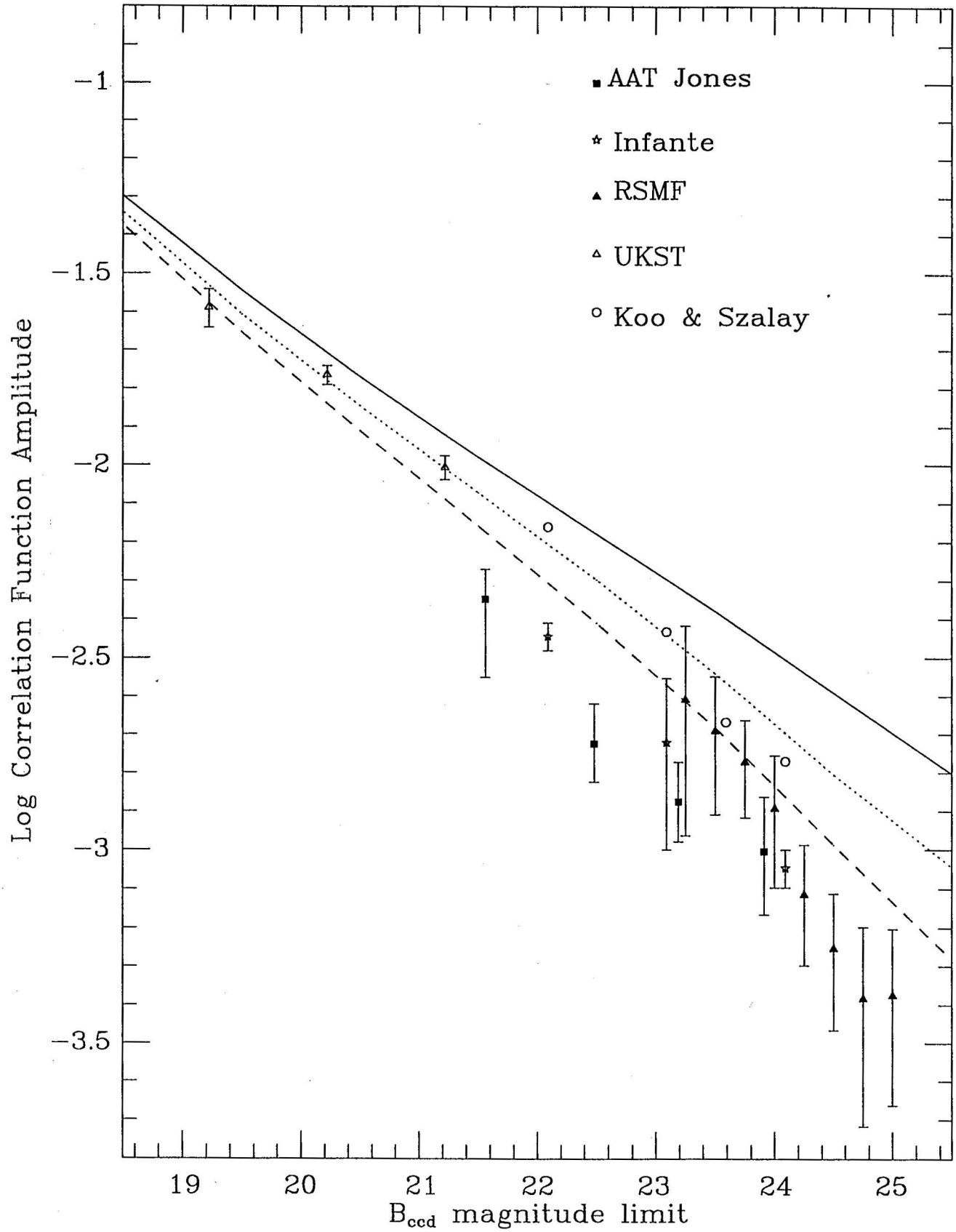

Figure 3.3 Galaxy $\omega(\theta)$ amplitudes obtained from the AAT photographic surveys of Jones et al. (1987), Infante (1990), Koo and Szalay (1984), from the UKST data of Stevenson et al. (1985), and from the 12 CCD frames of our $B_{ccd} \leq 25.0$ survey (RSMF), compared with the predictions of a non-evolving model (solid line) with stable clustering, the 'BEG' pure density evolution model with stable clustering (dotted line), and the 'BEG' pure density evolution model with the addition of $\epsilon = 1.2$ evolution of the clustering (dashed line). All three models shown here assume $q_0 = 0.5$ and $z_{max} = 4$.

3.4 Constraints from the Colour Dependence of $\omega(\theta)$

We found in Chapter 2 that the steep decline of the $\omega(\theta)$ amplitude as a function of magnitude limit between $B \sim 23$ and $B \sim 25$ was well fitted by a PLE model with stable ($\epsilon = 0$) clustering. We also found in Section 2.8 that the low $\omega(\theta)$ amplitude at $B \sim 24.5$ was associated only with the bluer galaxies in the sample, while the redder galaxies were clustered as strongly as the no-evolution prediction, again as predicted by a stable clustering PLE model.

However, in Section 3.3 above, we found that the scaling of $\omega(\theta)$ amplitudes with magnitude limit might also be consistent with a very different model – pure density evolution – if the assumption of stable clustering is relaxed, although the required clustering evolution is very rapid. Hence the scaling of $\omega(\theta)$ with magnitude limit may not be sufficient in itself to rule out non-PLE models. We now consider whether the observed colour dependence of $\omega(\theta)$, which is explained very well by PLE models, can help to exclude or at least set additional constraints on non-PLE models.

In a model of galaxy evolution dominated by merging (e.g. the 'BEG' model), the 'excess' blue galaxies would be those galaxies undergoing bursts of star-formation triggered by merging. Each merger would cause a blue galaxy to 'appear' amongst red galaxies, and then gradually redden again over much longer timescales after the merger/starburst. In merging-dominated models we might expect the intrinsic clustering properties of blue and red galaxies to be fairly similar, and we would also expect blue galaxies to be intrinsically as correlated with red galaxies as the red galaxies are with each other. The excess blue galaxies at $B \sim 24.5$ would lie at lower redshifts in a merging model than in a PLE model, resulting in more similar redshift distributions for blue and red galaxies. Hence merging models would predict less difference in $\omega(\theta)$ amplitudes between red and blue galaxies than would PLE models, and would also predict a cross-correlation between the red and blue galaxies similar in amplitude to the $\omega(\theta)$ of the red and blue galaxy subsamples.

We assume for now that red and blue galaxies possess the same intrinsic clustering properties, not being segregated into 'separate populations', and consider in more detail the 'BEG' density evolution/merging model. Dividing the $N(z)$ given by this model at a $B \leq 24.5$ limit by colour, assuming the evolution of galaxy colours with redshift to be the same as given by the Bruzual models, gives the redshift distributions shown in Figure 3.4. Limber's formula integration of these two redshift distributions, with $q_0 = 0.5$ and $\epsilon = 1.2$ clustering evolution, predicts a $\omega(\theta)$ amplitude of $28.069 \times 10^{-4}(\mathrm{deg})^{-0.8}$ for the red galaxies and $7.822 \times 10^{-4}(\mathrm{deg})^{-0.8}$ for the blue galaxies.

As a result of the rapid merging process, the excess blue galaxies in the BEG model generally lie at lower redshifts than in a PLE model. However, $N(z)$ for blue galaxies in the BEG model is still significantly more extended ($z_{mean} = 0.78$) than that of the red galaxies ($z_{mean} = 0.41$), at limits as faint as $B = 24.5$. This results from the effect of the strong density evolution on blue late-type galaxies, which dominate the sample at $0.5 < z < 1.2$ as a result of their small k-corrections, increasing their numbers in this redshift range. In combination with strong clustering evolution, reducing the amplitude of $\xi(r)$ by a factor of ~ 2.3 at $z = 1$, this strong density evolution can produce a significant colour dependence of the $\omega(\theta)$ amplitude, which is less than that predicted by the PLE model, but sufficient to be consistent ($\chi^2 = 0.88$) with observations.

Furthermore, even if red galaxies are intrinsically as correlated with blue galaxies as they are with each other, as might be expected in a merging model, the 'mismatch' of the redshift distributions would reduce the observed (projected) cross-correlation between the two subsamples to an amplitude lower than the red galaxy $\omega(\theta)$. As our 2σ upper

limit on the cross-correlation amplitude, $17.664 \times 10^{-4}(\mathrm{deg})^{-0.8}$, is only 27% lower than our red galaxy $\omega(\theta)$ amplitude, merging models in which the blue galaxy $N(z)$ is even moderately more extended than the no-evolution form (eg. with $z_{mean} \simeq 0.78$ as given by the 'BEG' model) may still be consistent, within the large statistical errors, with our failure to detect any cross-correlation between red and blue galaxies.

However, if we simply divide the no-evolution $N(z)$ for $B \leq 24.5$ galaxies by expected colour, the resulting redshift distributions for blue and red galaxies are quite similar, as shown in Figure 3.5. With extremely rapid clustering evolution of $\epsilon = 3$, about the minimum necessary for a no-evolution $N(z)$ to be consistent with the low $\omega(\theta)$ amplitude of all $B \leq 24.5$ galaxies, Limber's formula integration of the no-evolution redshift distributions gives $16.862 \times 10^{-4}(\mathrm{deg})^{-0.8}$ for the red galaxies and $10.495 \times 10^{-4}(\mathrm{deg})^{-0.8}$ for blue galaxies, much less of a dependence on colour than is observed. Hence if both blue and red galaxies lie within a no-evolution $N(z)$ at this magnitude limit, we would require that either:

(i) The rates of clustering evolution must differ greatly between types of galaxy, with extremely rapid ($\epsilon > 3$) growth of clustering for blue galaxies but approximately stable clustering ($\epsilon \sim 0$) for red (passive) galaxies. However, it does not seem plausible that gravitational evolution of the clustering could be so strongly dependent on the properties of the galaxies involved, or as rapid as $\epsilon = 3$ for any form of galaxy.

(ii) Most of the blue galaxies producing the excess in the number counts at $B \sim 24$ must be members of an additional population of blue dwarf galaxies ('hidden' within the no-evolution $N(z)$, but no longer visible at the present day) which are intrinsically much less clustered than other galaxies and uncorrelated with the redder galaxies at the same redshifts. We discuss this possibility in more detail in Section 3.5 below.

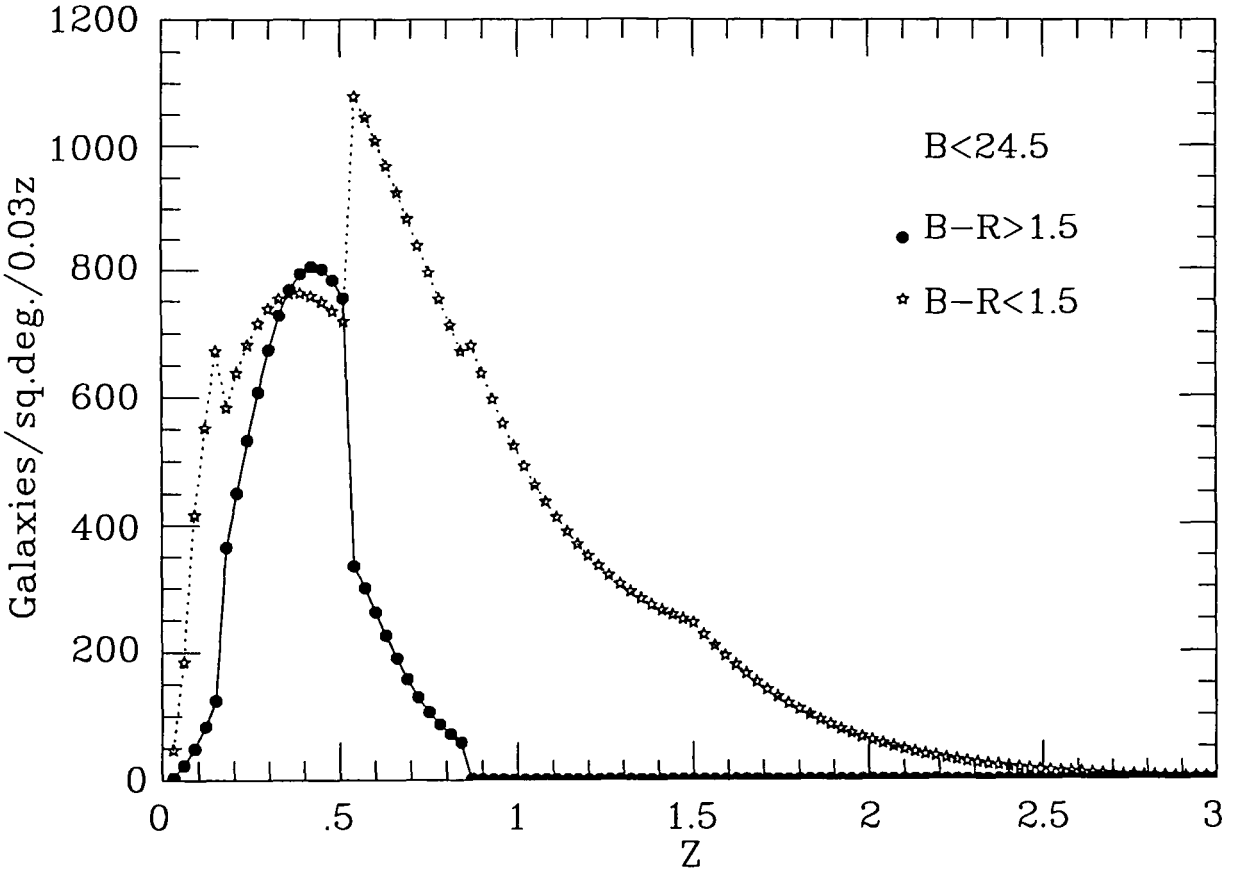

Figure 3.4 Redshift distributions predicted by the 'BEG' pure density evolution model for blue ($B-R < 1.5$) and red ($B - R \geq 1.5$) galaxies with blue magnitudes $B_{ccd} \leq 24.5$.

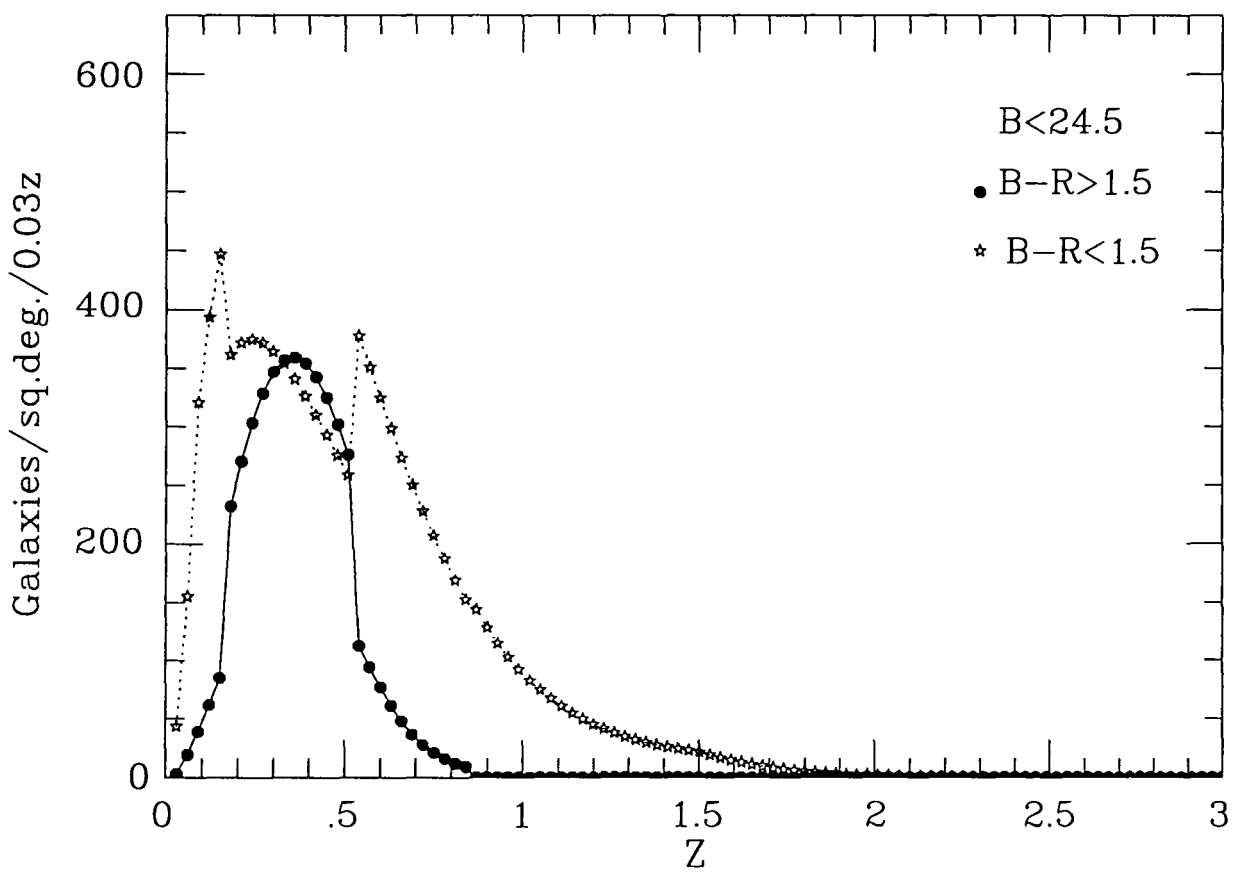

Figure 3.5 Redshift distributions predicted by the no-evolution model for blue ($B - R < 1.5$) and red ($B - R \geq 1.5$) galaxies with blue magnitudes $B_{ccd} \leq 24.5$.

3.5 Low Redshift Dwarfs vs. High Redshift Giants at $B \sim 24.5$

Although our $\omega(\theta)$ results may be insufficient to exclude the 'BEG' merging model if we allow the possibility of very rapid ($\epsilon \geq 1.2$) clustering evolution, there are considerable doubts about whether clustering could evolve as rapidly as this, particularly in combination with merging. Roukema and Yoshii (1993) recently found that in their N-body simulations, galaxy merging slowed the growth of clustering – a relatively moderate process of merging, giving an approximately $\phi^* \propto (1+z)$ density evolution, resulted in clustering evolution of $\epsilon = -0.4 \pm 0.3$ – i.e. clustering which is stable or slightly stronger at earlier epochs, whether the power spectrum is $n = 0$ or as negative as $n = -2$.

If these models of clustering evolution combined with merging are correct, the $\omega(\theta)$ results would quite definitely exclude the 'BEG' merging model (see the $\epsilon = 0$ 'BEG' model in Figure 3.3). Furthermore, as we shall discuss in more detail in Section 4.8, the rapid merging in the 'BEG' model acts on all galaxies equally, those of high luminosity ($L \sim L^*$) as well as dwarfs. It is difficult to reconcile such a rapid merging of $L \sim L^*$ galaxies at relatively recent epochs with the observation that the majority of present-day $L \sim L^*$ galaxies possess spiral arms and thin disks, which would have been disrupted by recent major merging events.

It might seem that a model in which late starburst processes cause a population of *unclustered* low-redshift dwarf galaxies to dominate the galaxy counts at $B > 23$ but 'disappear' at brighter magnitudes might be able to explain the high number counts and the low $\omega(\theta)$ amplitude of faint blue galaxies, more easily than merging models for the following reasons:

(i) No drastic departure from stable clustering for each galaxy population is required to give the steep $\omega(\theta)$ scaling, which would result instead from a change with magnitude limit in the ratios of two populations with different clustering properties.

(ii) Even if red and blue galaxies lie at the same redshifts at $B \sim 24$, we can explain a strong colour dependence of $\omega(\theta)$ if the environment in which a dwarf galaxy forms influences its luminosity evolution and therefore its colour, so that the galaxy populations which are seen with red and blue colours at $z \sim 0.4$ possess significantly different intrinsic clustering amplitudes. A difference in r_0 between the two galaxy populations at all redshifts since the time of their formation seems more physically plausible than requiring more rapid gravitational clustering evolution for the bluer galaxies – instead it is the weak clustering of the blue dwarf population which causes their rapid luminosity evolution between $z \sim 0$ and $z \sim 0.5$, and therefore their very blue colours at the $z \sim 0.4$ redshifts where they are bright enough to be seen.

(iii) If the blue galaxies producing the excess in the number counts at $B > 23$ can 'disappear' from shallower surveys through a 'self-destruction' process in which they remain *physically separate* from the 'normal' galaxies which survive to the present day, the total number density of galaxies could decrease greatly between $z \sim 0.4$ and $z = 0$ without producing any changes in the 'surviving' galaxies, whereas the removal of the excess galaxies through physical merging into the 'surviving' galaxies could alter their colours and morphologies to an extent which might be in conflict with the observed morphologies and colours of galaxies at the present day.

With many free parameters (i.e. different clustering strengths for different galaxy populations), a 'disappearing dwarf' model of this type, cannot easily be excluded by $\omega(\theta)$ analysis in the absence of complete redshift data. However, our results provide additional constraints on such models – requiring that if $N(z)$ still has a no-evolution form at $B \leq 24.5$, the disappearing dwarf population must be *very* weakly clustered, and would have to comprise at least $\sim 50\%$ of all galaxies seen at $B \sim 24$ (i.e. most or

all of the excess in the number counts) to reduce the overall $\omega(\theta)$ amplitude sufficiently, i.e. to $\sim \frac{1}{4}$ the non-evolving prediction. A sufficiently large population of unclustered low-redshift dwarfs to explain the $\omega(\theta)$ scaling and number count excess would have to undergo a very extreme degree of fading in the blue band since $z \sim 0.35$ epochs to fit within the present-day luminosity function of galaxies. If these galaxies instead merged into ellipticals, the blue stellar populations in these dwarfs would still have to fade very rapidly, or the present-day colours of ellipticals would be bluer than observed.

According to Dalcanton (1993), if all the excess in the galaxy number counts at $B \sim 24$ was made up of dwarf starburst galaxies with redshifts as low as the no-evolution $N(z)$, their stellar populations would have to fade by $\Delta B \simeq 3.5^m$ between $z \simeq 0.35$ and the present day, regardless of whether these dwarf galaxies subsequently 'self-destructed' or merged with larger galaxies. Even for a galaxy forming all its stars in a single burst, such rapid fading would not be possible unless the Initial Mass Function of the stellar population generated in the starburst was extremely 'top-heavy', with a power-law closer to $\psi(M) \propto M^{-0.35}$ than to the 'normal' $\psi(M) \propto M^{-2.35}$ IMF. An initial burst population formed with a 'normal' IMF would take at least 9 Gyr after the halting of star-formation to fade by $\Delta B \simeq 3.5^m$. Hence if all galaxies possess the normal IMF, then starbursting blue galaxies at $z < 1$ can only account for part of the excess in the number counts.

Large numbers of 'disappearing dwarf' galaxies at redshifts of $z \sim 1$ or higher, with the same IMFs as other galaxies but with much longer timescales in which to fade, do remain a possibility. However, these would only be seen at rather fainter magnitudes of $B \sim 27$ (see Chapter 4). Any $z > 1$ star-forming galaxies with apparent magnitudes as bright as $B \sim 24$ would be much more massive and intrinsically luminous objects – the progenitors of present-day giant ellipticals and spirals, rather than starbursting dwarf galaxies destined to fade to invisibility.

Both the $\omega(\theta)$ results and considerations of stellar evolution timescales suggest strongly that, unless positive evidence is found for either large numbers of weakly clustered blue dwarf galaxies undergoing starbursts with 'top-heavy' IMFs, and/or for a combination of large amounts of recent merging with a rapid growth of clustering (i.e. $\epsilon \geq 1.2$), most of the excess blue galaxies at $B \sim 24.5$ must lie at high redshifts ($1 \leq z \leq 3$), as predicted by our PLE model.

3.6 Summary and Conclusions

(i) As alternatives to pure luminosity evolution models, we considered clustering evolution and an increase in ϕ^* with redshift as possible explanations for the low $\omega(\theta)$ amplitude of $B \sim 24.5$ galaxies. Both processes were found to have relatively small effects on $\omega(\theta)$ in comparison to those of strong L^* evolution at high redshifts. However, a combination of very rapid clustering evolution ($\epsilon = 1.2$) with very rapid ϕ^* evolution (an exponential increase with $\tau = 0.25 H_0^{-1}$) could reduce the $\omega(\theta)$ amplitude at $B \sim 24.5$ sufficiently to be consistent with observations, although this fits the overall scaling of $\omega(\theta)$ over the $19 \leq B \leq 25$ range less well than the Bruzual PLE model.

(ii) If rapid merging processes convert the luminosity evolution caused by increased star-formation activity into an effective density evolution, as in the 'BEG' model, the excess blue galaxies will lie at somewhat lower redshifts ($0.5 \leq z \leq 1$ rather than at $1 \leq z \leq 3$). However, the blue galaxy $N(z)$ given by this pure density evolution model still extends somewhat more deeply than either a no-evolution $N(z)$ or the $N(z)$ of red galaxies, at limits as faint as $B \sim 24.5$. Although the colour dependence of

$N(z)$ is much less in the 'BEG' model than in the Bruzual PLE model, the addition of clustering evolution will increase its effect on $\omega(\theta)$. With the addition of $\epsilon = 1.2$ clustering evolution, the 'BEG' model predicts a colour dependence of the $\omega(\theta)$ amplitude which, although less than that predicted by a PLE model, is sufficient to be consistent with our results within the statistical errors. Furthermore, the more extended $N(z)$ for blue galaxies in the 'BEG' model may enable this merging-dominated model to remain consistent with our upper limit on the cross-correlation between the red and blue subsamples.

However, it is clear that all our observations – the dependence of $\omega(\theta)$ on colour, the lack of a red galaxy/blue galaxy cross-correlation, and the steep scaling of $\omega(\theta)$ of all galaxies with magnitude limit – are most easily explained if the excess faint blue galaxies lie at high redshifts. As pure density evolution models predict these galaxies to be at lower redshifts than do PLE models, they inevitably explain our results less easily than PLE models, requiring very rapid clustering evolution to be even marginally consistent with observations. If, as argued by Roukema and Yoshii (1993), merging processes would slow the growth of clustering, giving $\epsilon \leq 0$, our $\omega(\theta)$ results can exclude merging-dominated pure density evolution models, and require either strong L^* evolution at $z > 1$, or strong density evolution caused by the rapid fading of an *unclustered* blue dwarf population.

(iii) Our results are only consistent with a no-evolution $N(z)$ for the blue galaxies at $B \sim 24.5$ if they belong to a separate 'blue dwarf' population, intrinsically very weakly clustered and uncorrelated with 'normal' galaxies at the same redshifts. With a no-evolution $N(z)$, these unclustered galaxies would have to comprise at least $\sim 50\%$ of the galaxies seen at $B \sim 24.5$ (i.e. most or all of the excess in the number counts) to produce the observed low $\omega(\theta)$ amplitude, and to 'disappear' from shallower $B < 22.5$ surveys where the $\omega(\theta)$ amplitude is 'normal'. Being neither the progenitors of present-day giant galaxies, nor their pre-merging components, these blue dwarf galaxies must instead have faded to invisibility after undergoing starbursts.

However, if the entire number count excess is made up of galaxies undergoing starbursts at redshifts within the no-evolution $N(z)$, it is doubtful whether these galaxies could fade sufficiently within the relatively short period of time since $z \sim 0.35$ epochs to fit within the present-day luminosity function and colour distribution of galaxies (see Dalcanton 1993). Such rapid fading would only appear to be physically possible if these low-redshift starburst galaxies formed stellar populations with an extremely 'top-heavy' Initial Mass Function compared to the $\psi(M) \propto M^{-2.35}$ IMF of other galaxies. When both the low $\omega(\theta)$ amplitudes of faint blue galaxies and the timescales of stellar evolution are taken into account it seems more probable that most of the very blue galaxies seen at $B \sim 24$ are starbursting at much higher redshifts ($1 \leq z \leq 3$), giving an extended $N(z)$ for blue galaxies much closer to that predicted by PLE models.

Chapter 4

Galaxy Clustering and Counts to $B = 27$

4.1 Introduction

In this chapter we extend our analysis of faint galaxy clustering to $B_{ccd} = 27.0$, using a sample of 1442 galaxies detected on a single CCD frame to this limit. The data consisted of a large number of short (25–30 minute) exposures on the INT, stacked together to give an image with a total effective exposure time of 21 hours. Our survey reached even fainter limits than the previous deep CCD survey of Tyson (1988), although covering a smaller area. The surface density of detected faint galaxies reached $3 \times 10^5 \mathrm{deg}^{-2}$, with the differential number counts continuing to rise as $\frac{d(logN)}{dm} \simeq 0.3$ at our faint limit.

Here we calculate a $\omega(\theta)$ amplitude for the galaxies on this deep image, again with the aim of investigating the redshift distribution. We compare this with our $\omega(\theta)$ results from the $B_{ccd} \leq 25.0$ survey discussed in the previous two Chapters, and with the results of the Efstathiou et al. (1991) analysis of the galaxy clustering on the deep Tyson (1988) CCD frames, at an intermediate limit of $B = 26$.

In Chapter 2 we discussed the steep fall in $\omega(\theta)$ amplitude observed for magnitude limits in the range $23 < B < 25$. We now examine the possibility that the $\omega(\theta)$ scaling levels out at a minimum amplitude, which would indicate that galaxies are seen out to their maximum redshifts, at magnitude limits of $B > 24.5$. This might be expected if galaxies undergo the strong L^* evolution already implied by the steep decline in $\omega(\theta)$ amplitude at $23 \leq B \leq 24.5$. The minimum amplitude reached by $\omega(\theta)$ would depend on q_0 and on the maximum redshift, hence we compare the observed $24.5 \leq B \leq 27.0$ $\omega(\theta)$ amplitudes with those expected for a range of values of these parameters.

Once the maximum redshift has been reached, $N(z)$ cannot become any more extended at even fainter limits, and so the differential number counts of galaxies can only continue to rise beyond this point with a gradient following the faint-end slope of the luminosity function. For the faint end slope of $\alpha = -1.25$ typically seen locally, PLE models predict that the steep counts gradient of $\frac{d(logN)}{dm} \simeq 0.5$ seen at $B \sim 24$ should flatten to only $\frac{d(logN)}{dm} \simeq 0.1$ at $B \sim 26$. However our deep count data show a steeper slope of $\frac{d(logN)}{dm} \simeq 0.3$ at $25 \leq B \leq 27.5$.

As possible explanations for this discrepancy, we then consider – taking into account both the number counts and $\omega(\theta)$ scaling – the 'BEG' pure density evolution/merging model, and an alternative model combining Bruzual's L^* evolution with a steepening with redshift of the faint-end slope of the luminosity function. Finally, we discuss the results of new physical simulations of galaxy formation and merging.

4.2 Observational Data

The observational data discussed in this Chapter consisted of a total of 60 individual 25–30 minute exposures of a single field, obtained using the RCA CCD camera at the prime focus of the Isaac Newton Telescope. This configuration is the same as that used for the $B_{ccd} \leq 25.0$ survey of MSFJ, giving a pixel size of 0.74 arcsec, and the field chosen was the same as Field 13 of the earlier survey, centered on

RA = $00^h20^m00^s$, Dec = $00°02'58''$ (equinox 1950.0).

In equinox 2000.0 co-ordinates this is

RA = $00^h22^m33.79^s$, Dec = $00°19'35.8''$.

Galactic longitude and latitude are 107.57° and −61.68° respectively.

The reduction of this data is described in more detail by Metcalfe, Shanks, Fong and Roche (1994). The individual CCD exposures were stacked to give a single CCD frame with an effective exposure time of approximately 21 hours, and an area of 0.0950×0.0545 deg (i.e. slightly smaller than each frame in the $B \leq 25.0$ survey). On this area, 1595 images were detected to an estimated 3σ limit of $B_{ccd} = 27.0$. However, the dataset used for this $\omega(\theta)$ analysis excluded four 41 × 41 pixel areas centred on bright stars, as these could have been contaminated by spurious faint images. This reduced the number of objects in our dataset to 1442, within the remaining area of $4.927 \times 10^{-3}\mathrm{deg}^2$.

The surface density of these galaxies, $2.93 \times 10^5\mathrm{deg}^{-2}$, is a factor of 5.1 greater than was detected to $B_{ccd} = 25.0$ in our earlier survey. These very high number counts are discussed further in Section 4.6. A further 689 images were detected at $27.0 < B_{ccd} \leq 27.5$, but these are not included in the $\omega(\theta)$ analysis, as spurious detections, patchy incompleteness, sensitivity gradients etc. may become serious faintward of the 3σ limit and $\omega(\theta)$ would be quite sensitive to such effects.

Simulations of deep CCD images were generated, using our $q_0 = 0.05$ PLE model, in order to test the image detection routines etc., as described in more detail by Metcalfe et al. (1994). The results suggested that less than 5% of our $B_{ccd} \leq 27.0$ images are spurious noise detections, but also that our incompleteness exceeds 10% faintward of $B_{ccd} = 24.5$ and may be as high as $\sim 40\%$ in the $26.5 < B_{ccd} \leq 27.0$ interval. Metcalfe et al. (1994) concluded that this data is reasonably reliable (i.e. that almost all detected galaxies are genuine) to the $3\sigma/B_{ccd} = 27.0$ limit, and that the true surface density of $B \leq 27.0$ galaxies is $\sim 4 \times 10^5\mathrm{deg}^{-2}$.

4.3 Calculating $\omega(\theta)$ and Estimation of Errors

The correlation function $\omega(\theta)$ of the 1442 galaxies on the deep CCD frame was calculated as described in Section 2.3 for the less deep frames, with the number of random points used in the analysis (N_r) increased to 30000 so as to remain much larger than the number of real galaxies (N_g). The random points were scattered over the deep frame area, excluding the four 'holed' areas surrounding bright stars. The integration used to estimate the integral constraint (see Section 2.3) gave $C = 17.5A$, which is slightly higher than the value of 16.1 used for the MSFJ data as a result of the slightly smaller area of the deep frame.

As our deep dataset consisted of only one field, we cannot, as previously, derive errors for each $\omega(\theta_n)$ value and the fitted $\omega(\theta)$ amplitude from their observed field-to-field variation. We therefore devised a simple clustering simulation program which could be adjusted by trial and error to generate a set of 1442 (x,y) co-ordinates with a similar $\omega(\theta)$ to the data, and then run repeatedly so that statistical errors could be estimated from the variations in $\omega(\theta)$ within a series of simulations. The program generated a six-level hierarchy of clustering, using the methods described by Shanks (1979), except that only 1 in 10 of the clustered points generated by the simulation was included in the simulated dataset so as to weaken the clustering to a similar level as seen in the real data.

We then calculated $\omega(\theta)$ from 8 simulated datasets, obtaining a mean simulation $\omega(\theta_n)$ with a simulated field-to-field error given by the scatter in the 8 $\omega(\theta_n)$ values at

each angular separation θ_n. The function '$A(\theta^{-0.8} - 17.5)$' was fitted to the $\omega(\theta)$ of each of the 8 simulated fields, using the simulated field-to-field error bars for weighting, to give a set of 8 amplitudes A. The field-to-field error on the amplitude obtained from a single-field sample can then be estimated as the σ_{n-1} standard deviation of these 8 simulated field $\omega(\theta)$ amplitudes, giving $\pm 1.525 \times 10^{-4}(\mathrm{deg})^{-0.8}$.

The error bars from the simulations were then assigned to the $\omega(\theta_n)$ values from the real data, and used in weighting a least-squares fit of the function '$A(\theta^{-0.8} - 17.5)$', which gave the $\omega(\theta)$ amplitude of our real $B_{ccd} \leq 27.0$ galaxy dataset as

$$\omega(\theta) = (2.791 \pm 1.525) \times 10^{-4}(\mathrm{deg})^{-0.8}.$$

4.4 $\omega(\theta)$ Results at $24.5 \leq B \leq 27.0$

Figure 4.1 shows $\omega(\theta)$ calculated from our $B_{ccd} \leq 27.0$ data, with the simulated field-to-field error bars and the fitted power law $2.791 \times 10^{-4}(\theta^{-0.8} - 17.5)$.

Contamination of the data by randomly distributed noise images would dilute the clustering of real galaxies, but as noise detections are thought to comprise $< 5\%$ of the images at this limit, the resulting underestimation of the true $\omega(\theta)$ amplitude will not exceed $\sim (1 - 0.95^2) \sim 10\%$. Hence the real galaxies at these faint limits must be clustered on the sky very weakly – if we assume the simulation error to be reasonably accurate, our detection of any clustering above $\omega(\theta) = 0$ is only $\sim 2\sigma$ for the small area of the survey. However, our $B_{ccd} \leq 27.0$ result is also similar to, and within 1σ of, the $\omega(\theta)$ amplitudes we measured at considerably brighter limits of $B_{ccd} = 24.75$ and $B_{ccd} = 25.0$, i.e. $(4.127 \pm 2.209) \times 10^{-4}(\mathrm{deg})^{-0.8}$ and $(4.214 \pm 2.044) \times 10^{-4}(\mathrm{deg})^{-0.8}$ respectively.

The deep CCD survey of Tyson (1988) is intermediate between our $B_{ccd} \leq 25.0$ and $B_{ccd} \leq 27.0$ data in both depth and area, covering 107 arcmin^2 (equivalent to approximately 5 of our frames), on 12 small CCD frames.

Efstathiou et al. (1991) analysed the clustering of the 3631 galaxies with $24.0 \leq B_J \leq 26.0$ detected in the Tyson survey. After correction for the integral constraint, $\omega(\theta)$ was estimated as 0.0191 ± 0.006 (field-to-field errors) for an interval of angular separation centred on 30 arcsec. For a $\theta^{-0.8}$ power-law, this corresponds to

$$\omega(\theta) = (4.157 \pm 1.303) \times 10^{-4}(\mathrm{deg})^{-0.8},$$

almost identical to our results at $B_{ccd} = 24.75$–25.0 limits. Efstathiou et al. (1991) similarly interpreted their results as suggesting that $N(z)$ for $24 < B < 26$ galaxies extends out to $z \simeq 3$, and that small-scale galaxy clustering is stable rather than comoving.

Figure 4.2 shows the $\omega(\theta)$ amplitudes from our deep survey and the Tyson (1988) data, together with the $B \leq 25$ results discussed earlier. The non-evolving and PLE models plotted here show the effects of varying q_0, and the cut-off redshift discussed in Section 4.5 following.

Neuschaefer (1992) examined the clustering of galaxies on another CCD survey reaching $B \sim 25$, and also concluded that $\omega(\theta)$ for $24 \leq B \leq 25$ galaxies was significantly lower than predicted by models without evolution of either luminosity or clustering. As the galaxies were divided into magnitude slices and $\omega(\theta)$ fitted with varying power-laws (not $\theta^{-0.8}$), the Neuschaefer results are difficult to compare exactly with our own, and are not plotted on this graph. However, the Neuschaefer (1992) $\omega(\theta)$ appeared to reach a minimum at magnitudes of $B \sim 24.5$–25, where its value at 1 arcmin separations is approximately 0.02, corresponding to $\omega(\theta) \sim 7.5 \times 10^{-4}(\mathrm{deg})^{-0.8}$ for a $\theta^{-0.8}$ power-law, and although Neuschaefer's $\omega(\theta)$ amplitude at $B \sim 25$ appears to be a little higher than

our result, the general trend in $\omega(\theta)$ amplitude with magnitude limit is obviously similar to that seen in our own data.

In summary, while the statistics on $\omega(\theta)$ estimates for $B > 24$ galaxies are poor at present, the combination of all available data does suggest that the $\omega(\theta)$ amplitude as a function of magnitude limit falls steeply in the range $23.0 < B < 24.5$, but at $B \sim 25$ a minimum value of $\omega(\theta) \simeq 4 \times 10^{-4}(\mathrm{deg})^{-0.8}$ is reached. As the statistical errors on $\omega(\theta)$ from our single deep field are large, the most significant indication of this trend may be given by the comparison of our $B_{ccd} \leq 25.0$ results with those from the Tyson fields. We assume for now that a levelling out of the $\omega(\theta)$ scaling is genuinely observed, and discuss the interpretation of this result in the following Section.

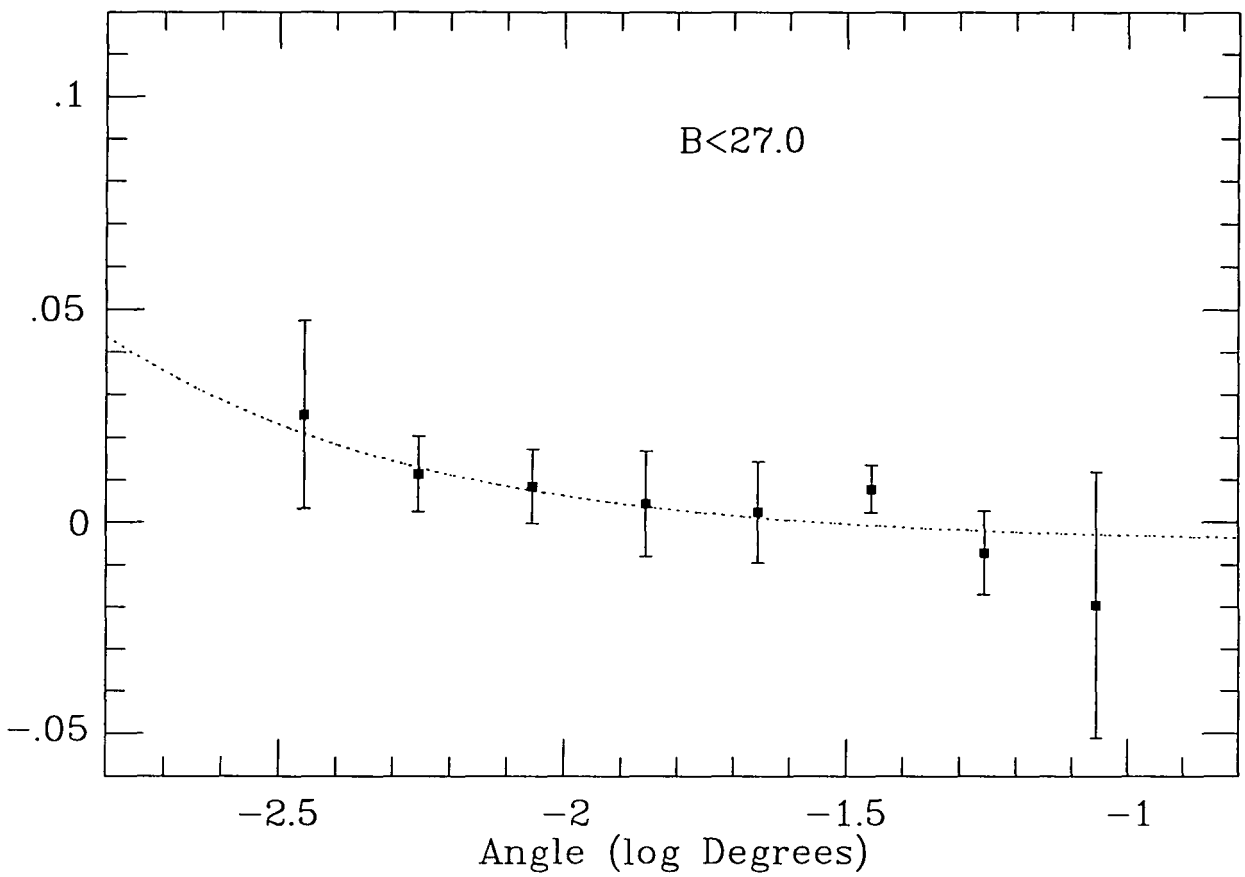

Figure 4.1 The angular correlation function $\omega(\theta)$ of the $B_{ccd} \leq 27.0$ galaxies on the deep 21hr CCD frame, shown with error bars from simulations and the fitted function '$A(\theta^{-0.8}) - 17.5$'.

4.5 Interpretation of the $24.5 \leq B \leq 27.0$ $\omega(\theta)$ Results

If galaxies undergo strong luminosity evolution at high redshifts, as in Bruzual's PLE models, with the effects on $N(z)$ produced by any merging processes being much less significant, the observed $\omega(\theta)$ scaling is exactly as would be expected. In such models, giant early-type galaxies in their initial phases of rapid star-formation would become visible at $1 \leq z \leq 3$ within a fairly narrow range of magnitude limits centred on $B \sim 24$ (see Figure 1.5). Consequently, the $\omega(\theta)$ amplitude declines steeply in this range. However, once a magnitude limit is reached where galaxies are seen out to their maximum redshifts, $N(z)$ cannot become any more extended on going to even fainter limits, and so the $\omega(\theta)$ scaling levels out at a minimum amplitude.

In Figure 4.2 we compare the observed $\omega(\theta)$ amplitudes with our PLE model predictions for $z_{max} = 4$, $z_{max} = 3$ and $z_{max} = \infty$ (i.e. no-cut off), with both $q_0 = 0.5$ and $q_0 = 0.05$. In our PLE models with $3 \leq z_{max} \leq 4$, galaxies would become visible out to the cut-off redshift at $B \sim 25$, so the modelled $\omega(\theta)$ scaling levels out at this magnitude limit. The asymptotic minimum value of the $\omega(\theta)$ amplitude at faint magnitudes will be lower for lower values of q_0, and lower for higher maximum redshift limits. The amplitude at which the measured $\omega(\theta)$ scaling levels out is evidently in the range we predict for stable clustering, $0 \leq q_0 \leq 0.5$ and $3 \leq z_{max} \leq 4$.

For $H_0 = 50$ km s^{-1}Mpc^{-1} and $q_0 = 0.05$, an angular separation of 1 arcmin corresponds to 0.72 Mpc at $z = 2$, but with $q_0 = 0.5$ it would correspond to only 0.49 Mpc. At 0.49 Mpc, $\xi(r)$ will have twice its 0.72 Mpc value, so the effect of q_0 on the $\omega(\theta)$ amplitude becomes quite strong for the evolving models at faint limits, where $z_{median} \sim 2$.

If the clustering is assumed to be stable, the asymptotic low value of the $\omega(\theta)$ amplitude at faint limits could in principle enable an estimation of q_0. Unlike the constraints on q_0 from number counts, this would be independent of both luminosity evolution and density evolution, but the statistical errors of present data may be too large to set useful constraints. Efstathiou et al. claim that their result may be too low for $\Omega = 1$ and a redshift cut-off at $z = 3$, unless the faint blue galaxies are intrinsically weakly clustered, whereas we find the $\omega(\theta)$ results cannot exclude any value of Ω from 0 to 1. However, Efstathiou et al. have used a higher normalization of the clustering, $r_0 = 5.5$h^{-1}Mpc, in their model as opposed to our $r_0 = 4.3$h^{-1}Mpc, and it is probably this which accounts for the difference in interpretation.

For a blue-limited sample, a reasonable value for the maximum redshift to which we would expect galaxies to be seen is $z_{max} = 4$ (as used in most of the models in this thesis). Star-forming galaxies are very luminous at $1000 \leq \lambda \leq 4000$Å but emit much less light at wavelengths shortward of the Lyman limit of 912Å (see e.g. Guhathakurta 1991), so would not be visible in the blue band at $z > 4$ where the $\lambda < 912$Å region of the spectrum would be redshifted into the blue ($\lambda \simeq 4500$Å) passband.

Additionally, a cut-off in $N(z)$, sharp or more gradual, must occur at the typical redshift of galaxy formation. In the Bruzual models used here $z_{formation} = 4.7$, but the true value is very uncertain and may not necessarily be higher than the Lyman cut-off redshift for the blue band. Guhathakurta (1989) found that most of the $B < 27$ galaxies detected in the blue-band by Tyson (1988) were also visible in the near-ultraviolet U-band, where the Lyman limit cut-off would occur at $z \simeq 3$, and so concluded that no more than $\sim 7\%$ of these faint galaxies could lie at $z > 3$. This result may therefore suggest $z_{formation} < 4$.

On the other hand, a lower limit on $z_{formation}$ may be set by the observed upper limits on the diffuse extragalactic background light at ultraviolet wavelengths. It has

been claimed (Pagel 1993) that the upper limits at $\lambda \sim 2000$Å require most of the metal content of the Universe to have been produced at $z > 1$, so that Lyman limit cut-off in the spectra of the star/metal-forming galaxies would be redshifted to longer wavelengths of $\lambda \sim 3000$Å, where the upper limits on the UV background intensity are much higher. Therefore UV observations also suggest $1 \leq z \leq 3$ for the flat-spectrum (initial starburst) objects, with $3 \leq z_{max} \leq 4$, although the nature and cause of the redshift cut-off remain uncertain at present.

Figure 4.3 shows median redshift plotted against $\omega(\theta)$ amplitude for our PLE models computed over a wide range of magnitude limits with both $q_0 = 0.05$ and $q_0 = 0.5$, but with no cut-off in $N(z)$ at high redshift, i.e. $z_{max} = \infty$.

Although the angular diameter distance of galaxies increases little beyond $z \sim 1$, and indeed decreases at $z > 1.25$ for $q_0 = 0.5$ and at $z > 2.84$ for $q_0 = 0.05$ (Figure 1.9), the $\omega(\theta)$ amplitude as a function of the median redshift of the sample continues to decrease even when $z_{median} > 2$, as the variance of the redshifts is still increasing and so causing further dilution of the clustering by projection. However, the median redshift itself tends to an upper limit at faint magnitudes - for these models never exceeding $z_{median} = 2.16$ in the $q_0 = 0.5$ geometry, whereas for $q_0 = 0.05$ it can reach $z_{median} \sim 5$.

The cause of this is apparent from Figure 1.8. In the shallow (Euclidean) limit the comoving volume element increases with redshift as $\frac{dV_{com}}{dz} \propto z^2$ in all cosmological geometries, but in a $q_0 = 0.5$ Universe it increases much more slowly than this beyond $z \sim 1$, and reaches a maximum at $z = 1.78$. In low-q_0 geometries the volume element reaches its maximum at much higher redshifts, but still increases much more slowly with redshift than the Euclidean relation beyond $z \sim 2$. Indeed, in all cosmologies except that dominated purely by a cosmological constant (ie. $\Omega = 0$, $\Lambda = 1$, $q_0 = -1$) the increase in volume element with redshift must fall below $\frac{dV_{com}}{dz} \propto z^2$ at sufficiently high redshifts.

Hence an 'effective' $N(z)$ cut-off is reached at the magnitude limit where $z_{median} \sim 2$, for $q_0 = 0.5$, and at somewhat higher but still finite redshifts if q_0 is low. If, at very faint limits, the sample becomes dominated by $z \geq 2$ galaxies, the $\omega(\theta)$ scaling with magnitude limit must level out eventually even without a sharp cut-off in $N(z)$, as can be seen from the $z_{max} = \infty$ models plotted in Figure 4.2.

The levelling out of the $\omega(\theta)$ scaling at $B \sim 25$ therefore indicates that an upper redshift limit for galaxies has been reached, and/or that for galaxies at this magnitude limit $z_{median} > 1.5$. The low $\omega(\theta)$ amplitude at $24.5 \leq B \leq 27$ limits also indicates that (if clustering is assumed stable), $z_{median} > 1$ for galaxies at $B > 24.5$, and that these galaxies must also be broadly distributed in redshift, from $z = 0$ to $z \sim 3$.

This is in good agreement with the observations, described by Tyson 1991, that most of the faint blue galaxies seen close to two high-mass clusters at $z = 0.39$ and $z = 0.46$ appear gravitationally lensed, with the degree of lensing indicating $z_{mean} > 0.9$ for galaxies at $24 < B < 27$. Therefore, on the basis of both our $\omega(\theta)$ results and the lensing observations, $N(z)$ for the $B \leq 27$ galaxies on our deep CCD frame is likely to resemble our PLE model $N(z)$ shown in Figure 4.10.

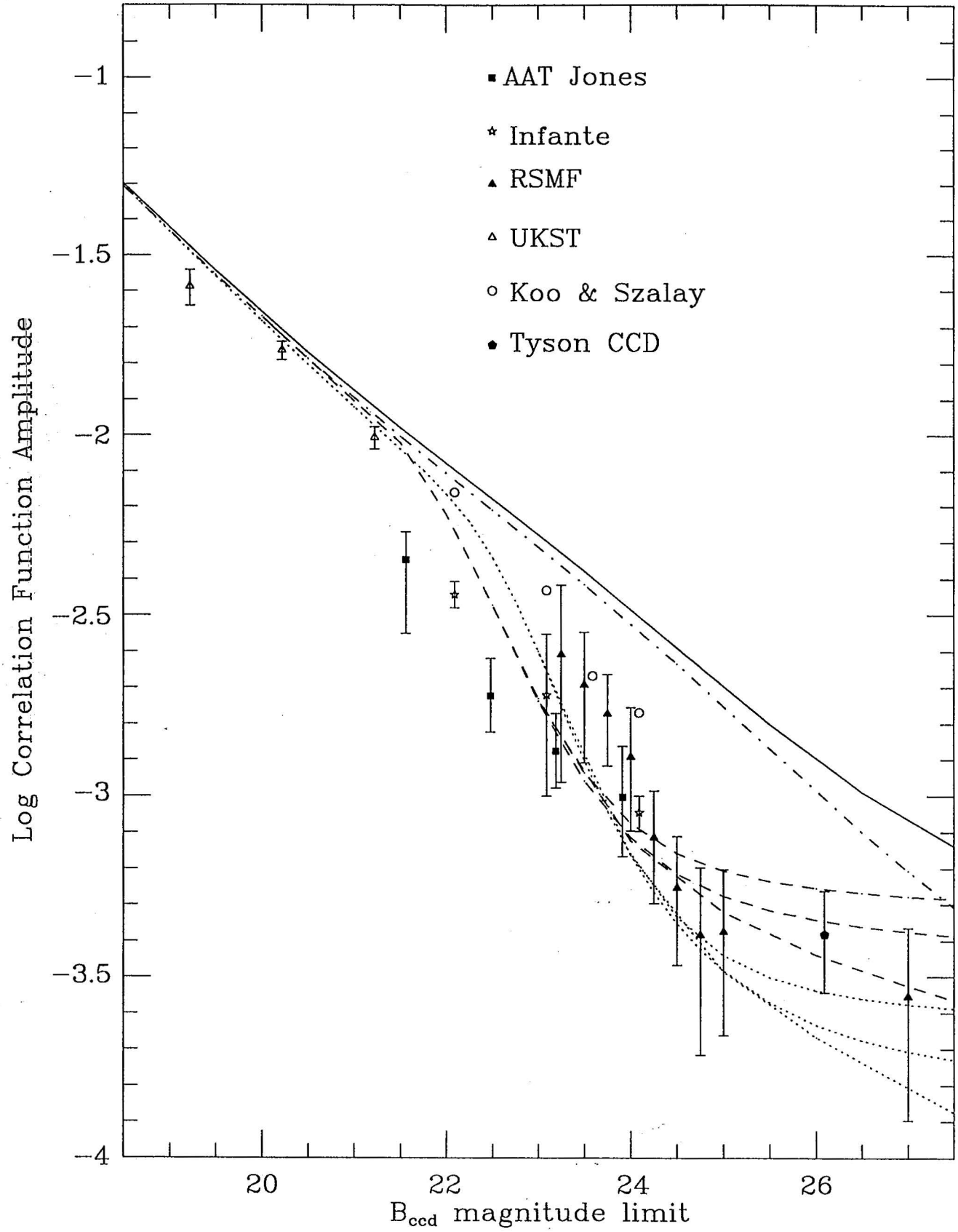

Figure 4.2 Galaxy $\omega(\theta)$ amplitudes obtained from the AAT photographic surveys of Jones et al. (1987), Infante (1990), Koo and Szalay (1984), from the UKST data of Stevenson et al. (1985), from the Tyson (1988) deep CCD survey, from the 12 CCD frames of our $B_{ccd} \leq 25.0$ survey (RSMF) and the single frame we extended to $B_{ccd} = 27.0$. These are compared with the predictions of a non-evolving model with $q_0 = 0.5$ (solid line) and with $q_0 = 0.05$ (dot-dash line), both assuming $z_{max} = 4$, and with our Bruzual PLE models . The three dashed and three dotted lines show the Bruzual PLE models with $q_0 = 0.5$ (dashed) and and $q_0 = 0.05$ (dotted), and three values of the maximum redshift, $z_{max} = 3$ (upper), $z_{max} = 4$(middle) and $z_{max} = \infty$ (lower). All 8 models plotted here assume stable clustering.

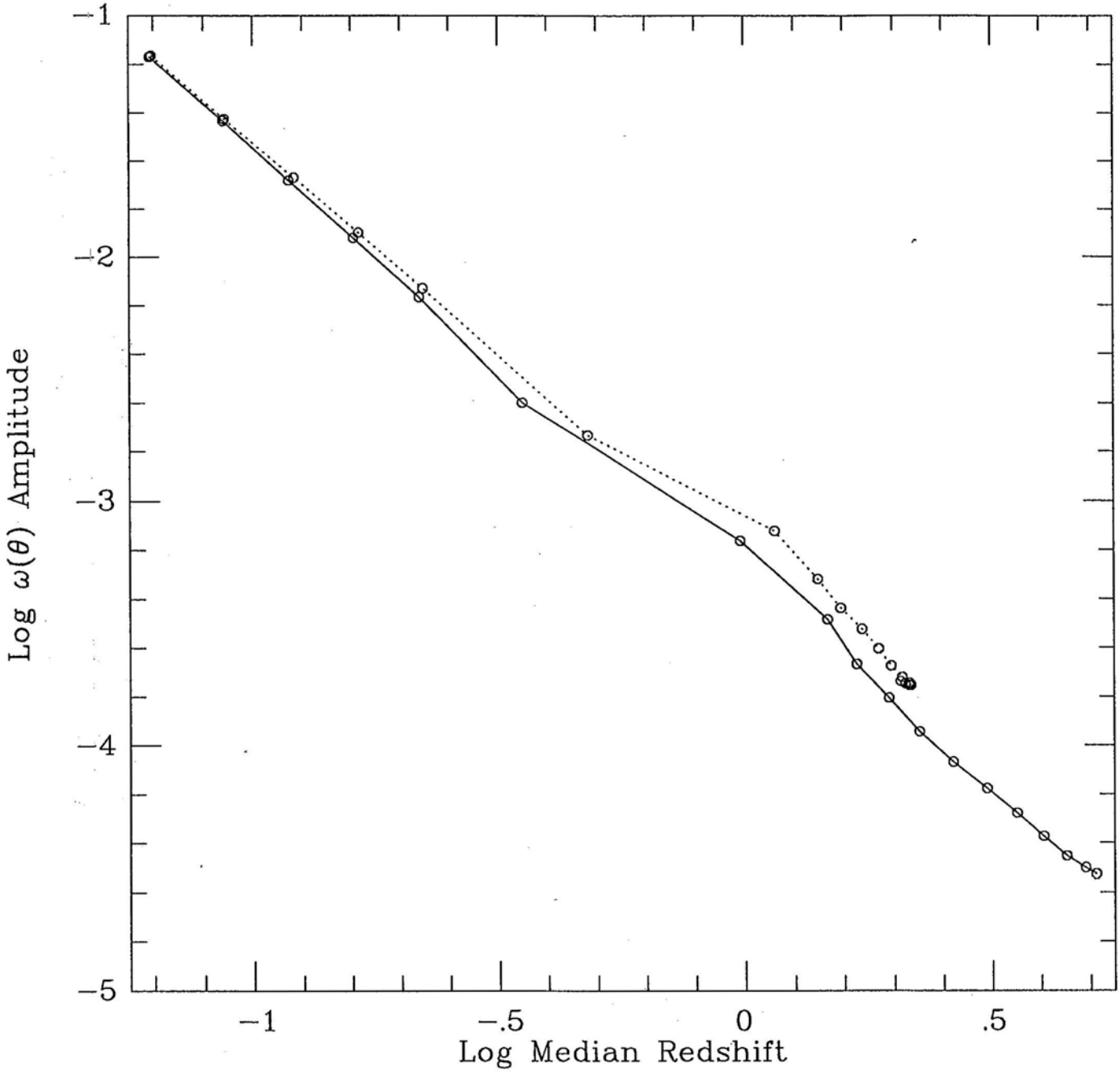

Figure 4.3 The $\omega(\theta)$ amplitude predicted by our PLE models with $q_0 = 0.5$ (dotted line) and $q_0 = 0.05$ (solid line), assuming stable clustering and $z_{max} = \infty$. These are plotted against the median redshift in the modelled redshift distributions, at a series of magnitude limits indicated on the graph as open circles at one magnitude intervals, from $B_{ccd} = 18.0$ to $B_{ccd} = 35.0$.

4.6 Galaxy Number Counts to $B \sim 27.5$

Where $N(z)$ can still become more extended to higher redshifts, the galaxy number count increases steeply, giving a gradient $\frac{d(logN)}{dm} \simeq 0.47$ at $20 < B < 25$. However, faintward of the magnitude B_{zmax}, at which $L \sim L^*$ galaxies are seen out to their maximum redshift z_{max}, the galaxy number count obviously cannot increase further as a result of galaxies becoming visible at even higher redshifts. Any galaxies detected at $B > B_{zmax}$ must be less luminous galaxies, on the faint-end slope of the luminosity function, within the same cosmological volume, i.e. at $0 \leq z \leq z_{max}$. The differential number counts at $B > B_{zmax}$ therefore 'look down' the faint-end of the luminosity function, following its slope as

$$\frac{d(logN)}{dm} = -0.4(\alpha + 1)$$

A typical faint-end slope of $\alpha = -1.25$ would give only $\frac{d(logN)}{dm} = 0.1$ at $B > B_{zmax}$, and even the steeper $\alpha = -1.5$ of Sdm galaxies only $\frac{d(logN)}{dm} = 0.2$. Indeed at very faint limits the galaxy number counts *must* flatten to $\frac{d(logN)}{dm} < 0.4$, to avoid a divergence of the sky brightness (Olber's Paradox), so there is no doubt that a decrease in the count slope will be observed at *some* magnitude faintward of $B \sim 24.5$.

As discussed by, for example, Fukugita et al. (1990), the magnitude B_{zmax} is sensitive to the amount of L^* evolution, whereas the number count at B_{zmax} is a good indicator of the total volume available for galaxies (if the comoving number density is conserved), and therefore the cosmological geometry. If PLE models are a good approximation, it should therefore be possible to disentangle the effects of L^* evolution and q_0, once number counts have been obtained to the limit at which a turnover in their gradient is seen (i.e. B_{zmax}).

The first survey to reach depths at which this might be possible was that of Tyson (1988), whose raw (uncorrected) differential galaxy counts appeared to reach a maximum of $\sim 10^5 \mathrm{deg}^{-2}\mathrm{mag}^{-1}$ at $25.5 < B < 27.0$. Estimates of the incompleteness in the Tyson galaxy counts, given by analysis of simulated CCD frames, were used to derive a 'corrected count'. This suggested that the true galaxy count continues to increase at $B > 26$, although less steeply than at brighter magnitudes, and may reach $\sim 3 \times 10^5 \mathrm{deg}^{-2}\mathrm{mag}^{-1}$ at $B = 27$, higher than many models would predict.

Interpreting the Tyson counts on the assumption of pure luminosity evolution, Guiderdoni and Rocca-Volmerange (1990) found that a $q_0 \simeq 0.05$ PLE model fitted well but any PLE model with $q_0 = 0.5$ greatly underpredicted these counts and was strongly rejected. We similarly find our Bruzual PLE model with $q_0 = 0.05$ to fit the Tyson counts reasonably well, but with $q_0 = 0.5$ it underpredicts all observed counts at $B > 24.5$. The strong q_0 dependence of number count models at faint limits results entirely from the much larger volume available for galaxies in a low-q_0 Universe, by a factor of 3.80 between $q_0 = 0.05$ and $q_0 = 0.5$ geometries if galaxies are seen out to $z = 4$ (see Figure 1.8).

As an alternative to the $q_0 = 0.05$, $\Lambda = 0$ geometry used in most models in this thesis, a spatially flat Universe with a slightly higher matter density and a 'moderate' cosmological constant (eg. $\Omega = 0.3$, $\Lambda = 0.7$) possesses similar distance/volume elements particularly in the important range $1 \leq z \leq 2$ (Peebles 1984). Hence in a 'moderate Λ' cosmology, the galaxy counts and $\omega(\theta)$ amplitudes given by our galaxy evolution models would be quite similar to the $q_0 = 0.05$ predictions, and such a spatially flat model might be more consistent with inflationary cosmological theories.

Fukugita et al. (1990) went somewhat further, arguing that the high Tyson counts favoured the even larger volume elements of a Λ-dominated cosmology, with $\Omega \sim 0.1$ and $\Lambda = 0.9$ giving $q_0 = -0.85$ and a flat geometry. This more 'extreme' interpretation of the high number counts is simply the result of the lower normalization (local ϕ^*) of the Fukugita et al. (1990) count models relative to GRVs normalization and that used here for our own models. As discussed in Section 1.5, the K-band counts, which are insensitive to evolution of the star-formation rate, appear to confirm our higher normalization as being appropriate.

Our deep CCD survey also found differential galaxy counts of $\sim 10^5$ deg^{-2}mag^{-1} at $25.5 < B_{ccd} < 26.0$. Being more complete than the Tyson data at $B > 26$, our data gave an uncorrected count increasing further to 1.7×10^5 deg^{-2}mag^{-1} at $26.5 < B_{ccd} < 27.0$ and 2.6×10^5 deg^{-2}mag^{-1} at $27.0 < B_{ccd} < 27.5$. The data may be less reliable beyond our 3σ limit of $B_{ccd} = 27$, but an even deeper WHT image, covering a small subset of the INT frame, gave a very similar raw count in the $27.0 < B_{ccd} < 27.5$ range (see Metcalfe et al. 1994). Applying incompleteness corrections to our data, estimated from the results of the Metcalfe et al. (1994) simulations (run using the $q_0 = 0.05$ Bruzual model), gives 'corrected' counts of 2.6×10^5 deg^{-2}mag^{-1} at $26.5 < B_{ccd} < 27.0$ and 3.8×10^5 deg^{-2}mag^{-1} at $27.0 < B_{ccd} < 27.5$.

Figure 4.4 shows the raw and corrected Tyson (1988) and Metcalfe et al. (1994) counts, together with the predictions of $q_0 = 0.5$ and $q_0 = 0.05$ non-evolving and PLE models, the 'BEG' merging model (Section 3.3), and a model in which the faint-end slope of the luminosity function is steeper at higher redshifts (see Section 4.7 below). The error bars on the Metcalfe et al. deep data are estimated field-to-field errors which include both the Poisson variance and that produced by the observed clustering of these galaxies. Our raw counts are quite close to Tyson's *corrected* counts, confirming that the corrections were not overestimated and that the true count is indeed significantly in excess of $q_0 = 0.5$ PLE model predictions.

The galaxy number counts at $B \sim 26$ would then appear consistent with any one of the following possibilities:

(i) $q_0 = 0.5$ with significant merging/density evolution, in addition to the normal luminosity evolution.

(ii) Low-q_0 or 'moderate' (eg. flat with $\Omega \sim 0.3$) Λ cosmology, strong luminosity evolution, high local ϕ^*.

(iii) Λ-dominated cosmology, strong luminosity evolution, but a lower local ϕ^*.

At $B > 26$ the corrected counts exceed even the $q_0 = 0.05$ PLE model, and even our raw count appears to be increasing with a somewhat steeper gradient.

As the normalization appropriate for number count models may still be somewhat uncertain, the steepness of the gradient may be a more significant observation. To investigate this further, we now estimate $\frac{d(logN)}{dm}$ for the data shown on Figure 4.4, by evaluating the difference Δ (log N) between the logarithms of counts in adjacent half-magnitude bins and dividing by Δm (ie. 0.50). The estimation of $\frac{d(logN)}{dm}$ from number count data obviously suffers greater statistical errors than the counts themseves, but does allow us to investigate the evolution independently from the local normalization.

The observed gradients are shown in Figure 4.5 and compared with $\frac{d(logN)}{dm}$ given by the $q_0 = 0.05$ Bruzual model, the 'BEG' model and the steepening α model. The Bruzual model gives a very high gradient of $\frac{d(logN)}{dm} \sim 0.6$ at $\bar{B} \simeq 23$, exceeding that seen in the data, as a result of the dominance of the model by a single evolutionary timescale ($\mu = 0.5$), producing a larger 'bump' in the counts than is actually observed. However,

once z_{max} is reached at $B \sim 24.5$, the predicted gradient decreases steeply towards $\frac{d(logN)}{dm} \sim 0.1$–$0.15$ at $B = 27$ (corresponding to the faint-end slope of the LF), whereas our deep count data show only a slight flattening of the gradient to $\frac{d(logN)}{dm} \sim 0.3$. The gradients from the data exceed the PLE model predictions at $B > 26$ with at least 2σ significance, and are in much better agreement with the 'BEG' and the steepening α models. These models both give steep gradients of $\frac{d(logN)}{dm} \sim 0.25$–$0.30$ at $26 < B < 27$, but for quite different reasons.

In the 'BEG' merging model, $L \sim L^*$ galaxies 'break up' rapidly on going back in time, so that each present-day galaxy existed as at least ~ 10 pre-merging fragments at high redshifts. As we would not detect these much smaller galaxies at z_{max} until much fainter limits of $B > 27$ are reached, $\frac{d(logN)}{dm}$ would remain relatively steep in the $25 < B < 27$ range, where the high redshift limit would not yet have been reached. However, although both the combination of rapid merging with rapid clustering evolution and the presence of low-redshift 'disappearing dwarfs' with very weak clustering can predict low $\omega(\theta)$ amplitudes at $B \sim 24.5$, these models cannot account for the levelling out of the scaling which may be observed at even fainter limits. In both these models, $N(z)$ would still become more extended from $B \sim 24.5$ to $B \sim 27$, and the effects of this change in $N(z)$ on $\omega(\theta)$ would be increased further by the rapid clustering evolution and/or the increasing dominance of the unclustered dwarf population at fainter limits, so that the $\omega(\theta)$ amplitude would continue to decrease very steeply from $B \sim 24.5$ to $B \sim 27$.

The observed levelling out of the $\omega(\theta)$ scaling at $B > 24.5$ can only be explained by a strong brightening of L^* at $z > 1$ similar to that in Bruzual's PLE model, enabling $L \sim L^*$ galaxies to become visible out to z_{max} at brighter magnitudes of $B \sim 25$. Whether these $L \sim L^*$ galaxies are seen throughout the relatively small $0 \leq z \leq z_{max}$ volume of a $q_0 = 0.5$ Universe, the larger volume of a low-q_0 Universe, or the largest possible volume of the Λ–dominated cosmology, the continuation of a steeply rising number count (ie. $\frac{d(logN)}{dm} > 0.2$) to even fainter limits (ie. $B > 26$) can only be explained by introducing 'extra' *low-luminosity* (ie. $L < L^*$) dwarf galaxies at high redshifts.

The apparent discrepancy between the steep number counts at $B > 25$ (favouring merging-dominated evolution) and the $\omega(\theta)$ scaling (favouring pure luminosity evolution) is therefore resolvable if:

(i) The luminosity of $L \sim L^*$ galaxies evolves as in our PLE models, so that a high redshift population becomes visible at $23 < B < 25$, and that $B_{zmax} \sim 25$.

and

(ii) Merging or other forms of evolution occur in a *luminosity-dependent* fashion, increasing the numbers of dwarf galaxies relative to the numbers of $L \sim L^*$ galaxies at higher redshifts (i.e. steepening the faint-end slope α). If the high-redshift population possesses a luminosity function with $\alpha \simeq -1.75$, a count slope of $\frac{d(logN)}{dm} \sim 0.3$ could continue indefinitely beyond B_{zmax}.

Hence we further consider 'steepening α' models and their physical interpretation in Sections 4.7 and 4.8 below.

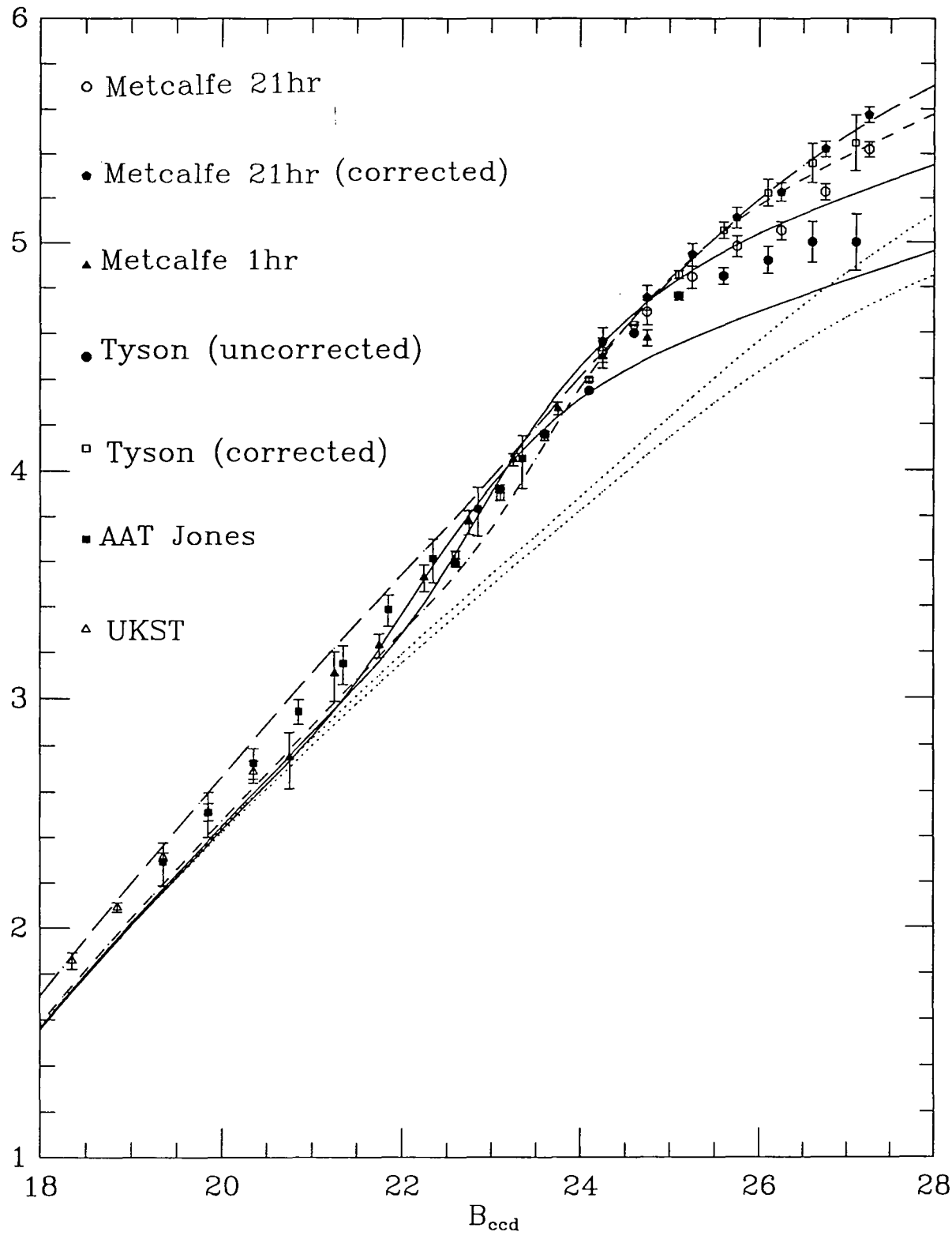

Figure 4.4 Faint ($18 \leq B \leq 28$) galaxy counts from the AAT photographic survey of Jones et al. (1991), from the UKST data of Stevenson et al. (1985), from the Tyson (1988) deep CCD survey, and from the 1 hr CCD data of MSFJ and the 21 hr deep CCD data of Metcalfe et al. (1994). The counts from the Tyson (1988) and Metcalfe et al. (1994) data are shown with and without corrections for incompleteness. The graph compares these with the non-evolving models (dotted) and Bruzual PLE (solid) models for both $q_0 = 0.5$ (lower) and $q_0 = 0.05$ (upper), the 'BEG' pure ϕ^* evolution model with $q_0 = 0.5$ (long dashes) and our 'steepening α' model with $q_0 = 0.05$ (short dashes).

4.7 Evolution of the Faint-End Slope of the Luminosity Function

A model in which α steepens with redshift was proposed by BES to explain the results of their $B \leq 21.5$ redshift survey, which found $N(z)$ to have a no-evolution form, although with a somewhat raised normalization produced by 'extra' star-forming dwarf galaxies within the same redshift range as the no-evolution $N(z)$. The suggested physical interpretation was that galaxies underwent bursts of star-formation activity, perhaps associated with merging or other interactions, much more frequently at relatively recent epochs ($z \sim 0.2$) than at present. The starbursts in this model produced a much greater brightening relative to the total galaxy luminosity when occurring in dwarf galaxies. The effect of this on the luminosity function was a steepening of α with redshift, with little change in L^* out to $z \sim 0.7$, giving a no-evolution form for $N(z)$ at $B \leq 21.5$ with a somewhat raised number and proportion of blue galaxies. At these relatively shallow limits, the post-starburst fading required to give a no-evolution $N(z)$ is no more than $\Delta(B) \simeq 2^m$, which is within the upper limits of fading rates for 'normal IMF' post-starburst stellar populations. However, it is unclear whether the BES spectroscopic observations require even this relatively 'mild' luminosity-dependent evolution, as the results may still be consistent with a PLE model if the luminosity function of bluer galaxies possesses a slope as steep as $\alpha = -1.5$ locally, as in the models used here (see MSFJ).

GRV considered the effects of merging and/or luminosity-dependent evolution on the luminosity function parameters (ϕ^*, L^*, α) in more detail, combining this with physical models of the spectral evolution caused by evolution of the star-formation rate. In the GRV models these two processes are considered separately, with the merging process acting on a Schechter *mass* function (parameterized by ϕ^*, M^* and α) to redistribute the stars amongst a larger number of smaller galaxies at earlier epochs. This was done by increasing ϕ^* or steepening α with redshift, while decreasing one of the other parameters so as to conserve the total mass $\int M\phi(M)\ \mathrm{d}M$.

The spectral evolution acts on the luminosity/mass ratio which converts this mass function into a luminosity function. Hence the total luminosity of the galaxies within each morphological type evolves with redshift as in a PLE model. This ensures that the luminosity evolution is consistent with the physical processes of star-formation and stellar evolution, which may not be the case for the more extreme 'disappearing dwarf' models needed to give a no-evolution $N(z)$ at $B \sim 24$ and fainter, which require galaxies now extremely faint to have been be several magnitudes brighter at relatively recent epochs (see Section 3.5).

Three representative merging processes were considered by GRV, the first two being '$M^* - \phi^*$' and '$M^* - \alpha$' evolution which, respectively, increase ϕ^* or steepen α with redshift. The compensating reduction in M^*, to conserve the total comoving mass density of galaxies, cancels out to some extent the brightening of the blue-band L^* with redshift caused by spectral evolution. The '$M^* - \phi^*$' and '$M^* - \alpha$' processes are approximately represented by the 'BEG' model and the 'BES' model respectively. The third process described is '$\phi^* - \alpha$' evolution, which steepens the faint-end slope α at higher redshift, with a corresponding reduction in ϕ^* to conserve the comoving mass density. The merging produces no change in M^*, so that L^* brightens with redshift as much as in a PLE model.

We therefore represent this process here using the same luminosity evolution as in our Bruzual PLE model. We again assume a low q_0 of 0.05, and use the same luminosity functions at $z = 0$ as in our other models except that, to introduce extra very small galaxies into the model, the low-luminosity cut-off was moved to 14 magnitudes faintward

of M^*, corresponding to the size of a small globular cluster. The faint-end slope α steepens with look-back time from the present day values (Table 1.1) towards $\alpha = -2$ for all types in the limit of $z = \infty$, following an exponential timescale $\tau = \frac{2}{3}H_0^{-1}$. If look-back time $T(z)$ is approximated by the $q_0 = 0$ relation

$$T(z) = H_0^{-1}(1 - (1+z)^{-1})$$

a faint-end slope of α_0 at $z = 0$ then evolves as

$$\alpha(z) = \alpha_0 - (2 + \alpha_0)\exp(-1.5(1+z)^{-1})$$

A zero-redshift slope $\alpha_0 \simeq -1.25$ would then steepen to $\alpha \simeq -1.7$ at $z = 2$, approximately the slope suggested by $\frac{d(logN)}{dm}$ at $B > 26$.

To conserve the total comoving mass density within each morphological type, ϕ^* undergoes a compensatory evolution. For the low-luminosity cut-offs used here, if the faint-end slope steepens from $\alpha = -1.25$ to $\alpha - 1.70$, ϕ^* must decrease by a factor of 2.4, but this redistribution of about half the mass within present-day giant galaxies into very large numbers of very small galaxies increases the comoving *number* density by a factor of 50.

As shown on Figure 4.4, the model gives a reasonable fit to the number counts, in particular to the steep slope at faint limits. With $q_0 = 0.5$ this model underpredicts the $B > 25$ counts, but to a lesser degree than a $q_0 = 0.5$ PLE model. As shown by GRV, '$\phi^* - \alpha$' evolution does enable a very good fit to the counts within the $\Omega = 1$ Universe if it is combined with somewhat stronger luminosity evolution, as found in the GRV models with relatively low redshifts of galaxy formation ($2 \leq z_{formation} \leq 5$). As any steepening of α will help to fit the steep count slope at $B > 25$, it is not surprising that GRV found the number count data to favour the '$M^* - \alpha$' and '$\phi^* - \alpha$' processes over '$M^* - \phi^*$' evolution. GRV also claimed that the redshift data may favour, in particular, the '$M^* - \alpha$' (ie. 'BES'-type) merging model as this produces a redshift distribution most similar to the no-evolution form at $B \leq 24$. However, as we discussed in Section 2.6, $B \leq 24$ redshift surveys still allow, and the $\omega(\theta)$ results strongly suggest, a substantial ($\sim 30\%$) $z > 1$ population to be present at this limit. The combination of the number counts and $\omega(\theta)$ results, from our surveys and the Tyson (1988) data, favours instead the '$\phi^* - \alpha$' merging process, which allows L^* to brighten as in the PLE models so that some high redshift galaxies are visible at $B \sim 24$.

Figure 4.6 shows the redshift distributions given by our 'steepening α' model at a series of magnitude limits from $B \leq 22$ to $B \leq 25$. The $\omega(\theta)$ amplitudes derived from this model are shown in Figure 4.7, together with the $q_0 = 0.05$ non-evolving and PLE models, and the $q_0 = 0.5$ 'BEG' model, with stable clustering assumed in all cases. The addition of '$\phi^* - \alpha$' evolution to the PLE model reduces the proportion of $z > 1$ galaxies in a $B \leq 24.0$ sample from 50% to 34% (Figure 4.8), a proportion which is in better agreement with the unidentified fraction in the Glazebrook et al. (1993) spectroscopic survey results while remaining sufficient to fit the $\omega(\theta)$ results without invoking any departure from stable clustering. In contrast, the 'BEG' model, in which the 'excess' galaxies lie mostly at $z < 1$ at $B \sim 24$, requires very strong clustering evolution to fit the $\omega(\theta)$ amplitudes to $B = 24.5$ and fails to predict the levelling out of the scaling which may be observed at even fainter limits.

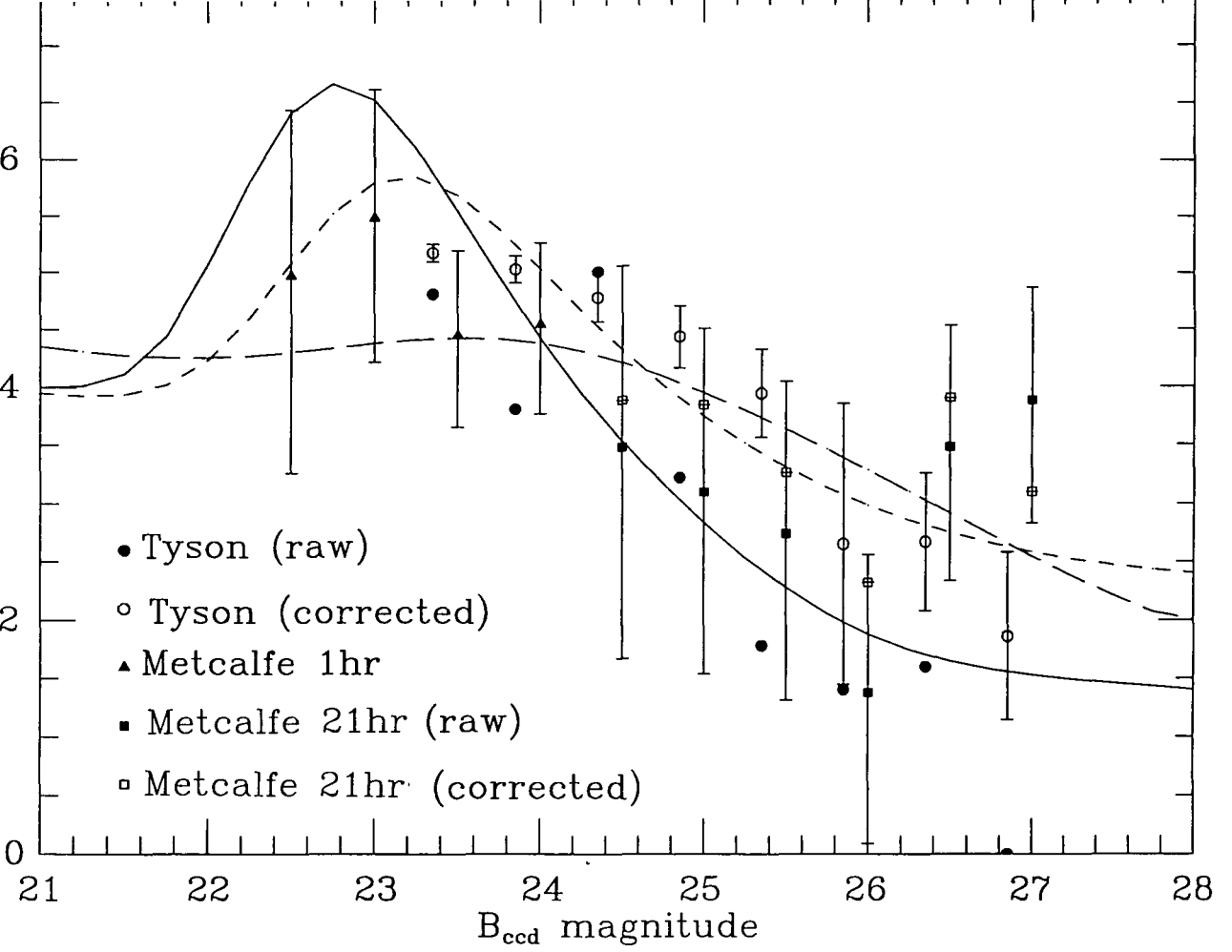

Figure 4.5 The gradient of the differential number counts of galaxies, $\frac{d(logN)}{dm}$, as a function of blue magnitude. The gradients are calculated from the 1 hr CCD number counts of MSFJ, and from – with and without the corrections for incompleteness shown on Figure 4.4 – the 21 hr CCD data of Metcalfe et al. (1994) and the Tyson (1988) number counts. These are compared with the count gradients predicted by the Bruzual PLE model with $q_0 = 0.05$ (solid line), the 'BEG' pure ϕ^* evolution model with $q_0 = 0.5$ (long dashes) and our 'steepening α' model with $q_0 = 0.05$ (short dashes).

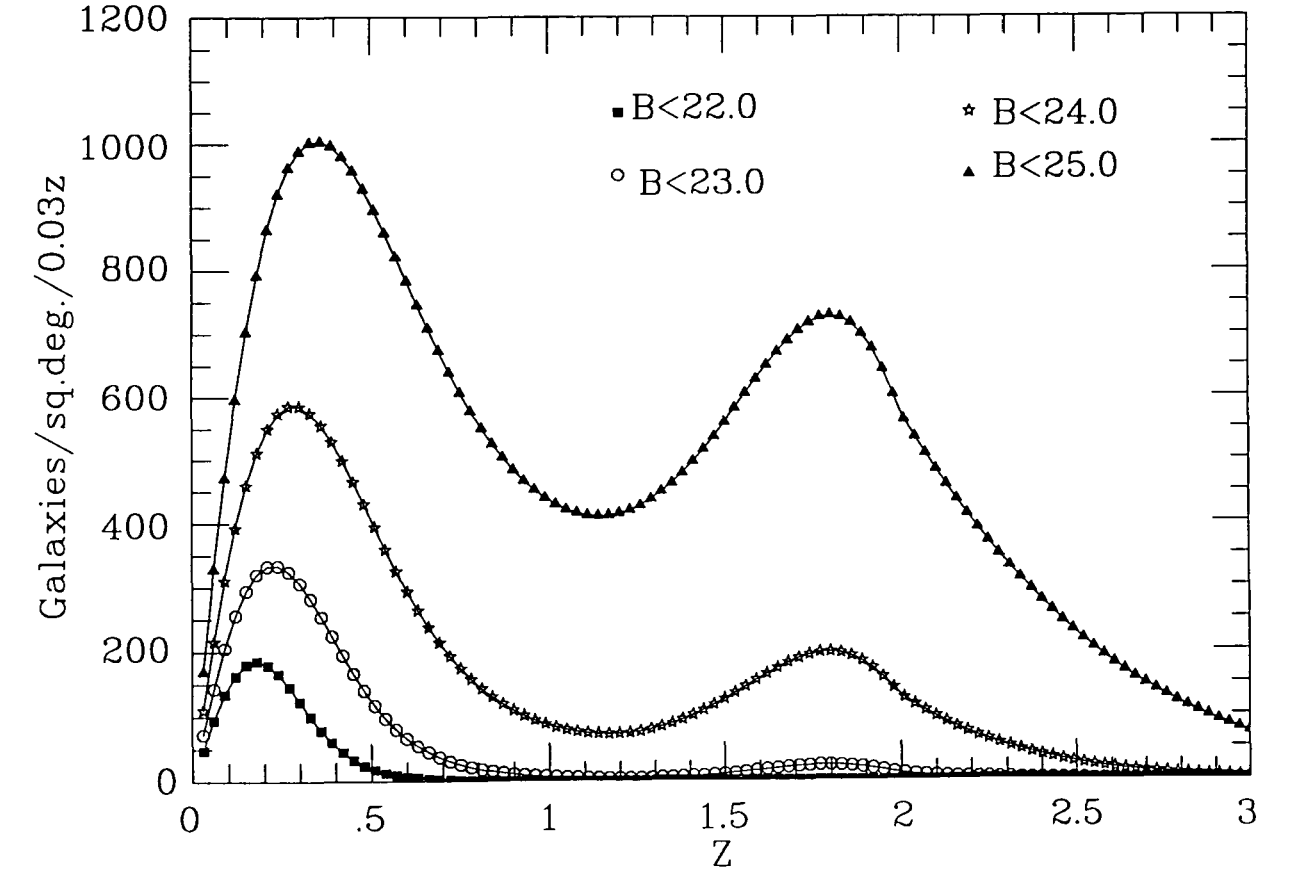

Figure 4.6 Redshift distributions predicted by our 'steepening α' model (which also incorporates strong L^* evolution), with $q_0 = 0.05$, for a range of blue magnitude limits from $B_{ccd} \leq 22.0$ to $B_{ccd} \leq 25.0$.

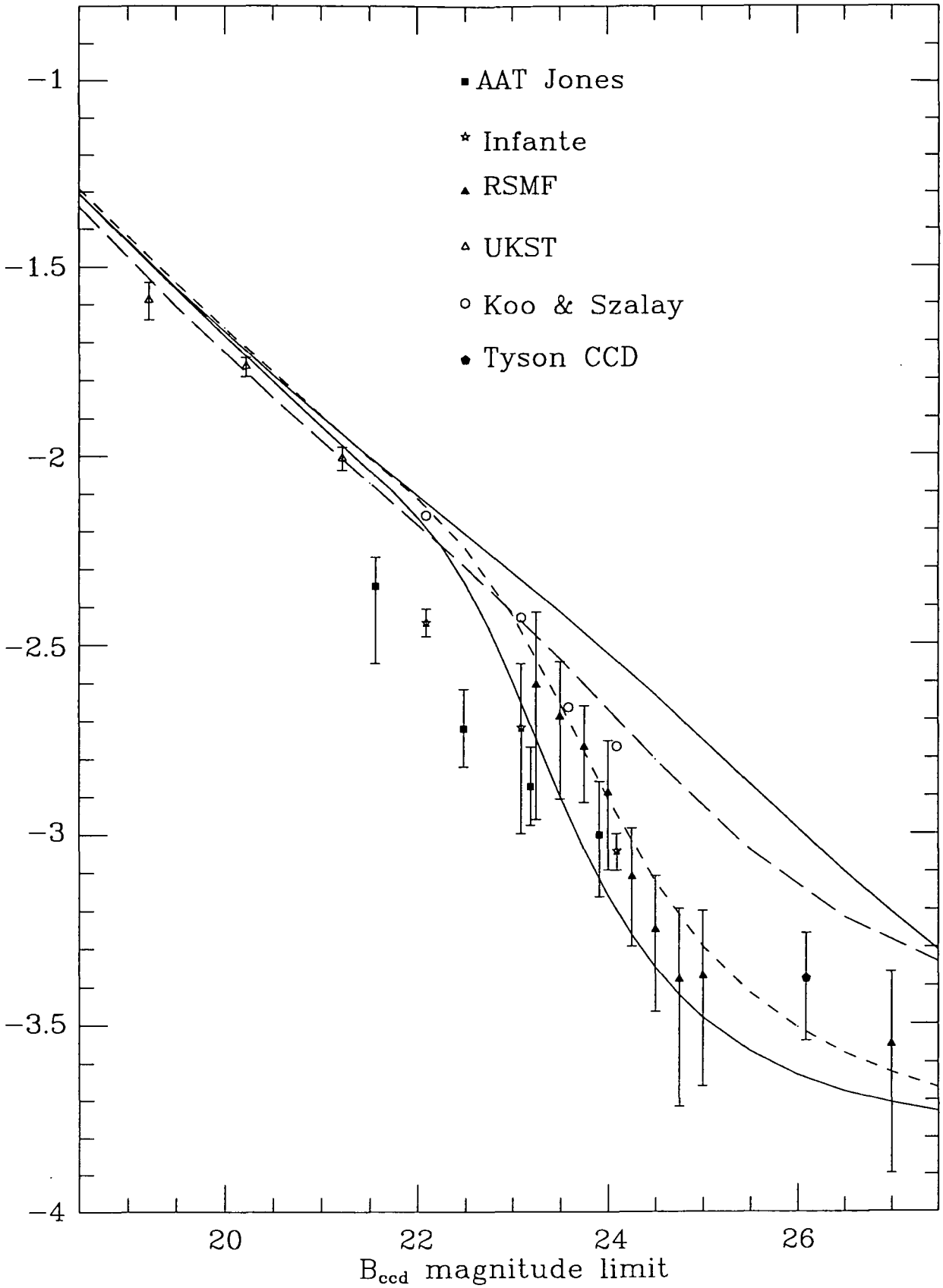

Figure 4.7 Galaxy $\omega(\theta)$ amplitudes obtained from the AAT photographic surveys of Jones et al. (1987), Infante (1990), Koo and Szalay (1984), from the UKST data of Stevenson et al. (1985), from the Tyson (1988) deep CCD survey, from the 12 CCD frames of our $B_{ccd} \leq 25.0$ survey (RSMF) and the single frame we extended to $B_{ccd} = 27.0$. These are compared with the predictions of a non-evolving model (solid line, upper), our Bruzual PLE model (solid line, lower), and our 'steepening α' model (short-dashed line), all with $q_0 = 0.05$, and the 'BEG' ϕ^* evolution model with $q_0 = 0.5$ (long-dashed line). All four models assume stable clustering and $z_{max} = 4$.

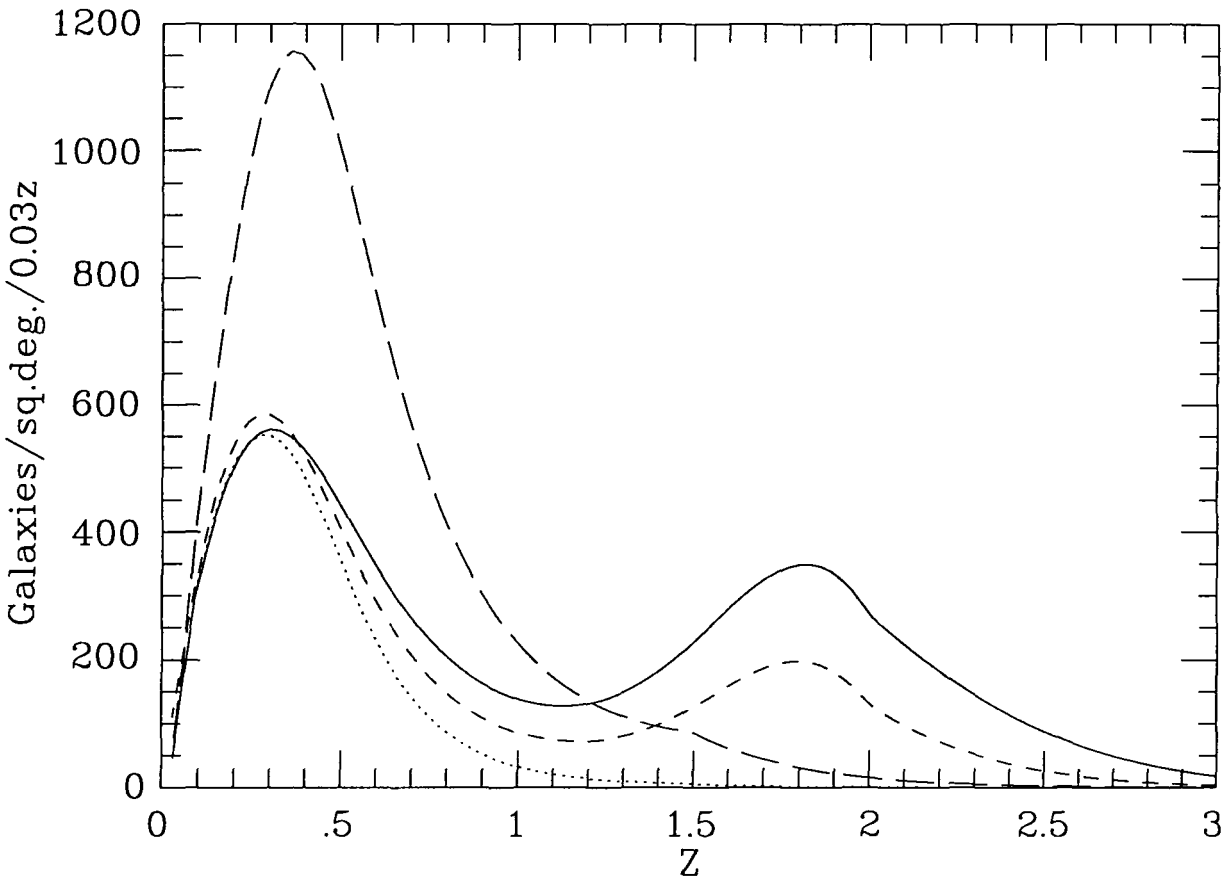

Figure 4.8 The redshift distribution predicted for all $B_{ccd} \leq 24.0$ galaxies by our no-evolution (dotted line), Bruzual PLE (solid line) and 'steepening α' (short-dashed line) models, all computed with $q_0 = 0.05$, and by the 'BEG' pure density evolution model with $q_0 = 0.5$ (long-dashed line).

4.8 Physical Causes of α and ϕ^* Evolution

The differences between L^* evolution, ϕ^* evolution and our suggested combination of L^* and α evolution are best illustrated by considering the changes they produce in the luminosity function. Figure 4.9 shows the luminosity function of all galaxy types at $z = 2$, for galaxies evolving as in the PLE, 'steepening α', and 'BEG' density evolution models.

In the PLE and 'steepening α' models, very luminous (i.e. $M_B < -23$, corresponding to $B < 23.75$ for $q_0 = 0.05$) giant starbursting galaxies are found at this redshift, appearing as a 'second peak' in the $B \sim 24$ $N(z)$. When '$\phi^* - \alpha$' merging is added to the Bruzual evolution to give the 'steepening α' model, the numbers of high-redshift galaxies seen at $B = 24$ are somewhat reduced – but the numbers of $M_B > -21.5$ galaxies (corresponding to $B > 25.25$ at $z = 2$) are increased, so at fainter magnitudes ($B > 25$) the $z \simeq 1.85$ peak in $N(z)$ is increased (Figure 4.10) and the count slope steepened (Figure 4.4).

The very rapid '$M^* - \phi^*$' evolution of the 'BEG' model results in a luminosity function at $z = 2$ with even more $-14 > M_B > -21$ galaxies than in our 'steepening α' model, but very few more luminous than $M_B = -22$. In this model, *all* present-day giant galaxies, as well as those of lower luminosities, are 'broken up' into many (8.6 on average) pre-merging components at this redshift, so their absolute (and apparent) magnitudes are $\sim 2^m$ fainter than in the other two models considered here. Consequently, high redshift galaxies in this model only begin to appear in large numbers at very faint limits of $B \sim 27$ (compare Figure 4.8 and Figure 4.10).

However, the $\omega(\theta)$ results strongly suggest that many giant galaxies at $z \sim 2$ already exist with masses similar to their present-day counterparts, so as to be sufficiently luminous to appear in, and dilute the clustering of, galaxy samples with relatively bright magnitude limits of $B \sim 24$.

Furthermore, it may be possible to exclude the the BEG parameterization of the merging process, designed simply to fit the number counts and redshift distributions of faint galaxies, on the basis of very different observations – the observed morphologies of present-day galaxies. The merging of similarly sized galaxies would occur very frequently in the BEG model, with most of the galaxies seen today having undergone such an interaction since the epoch corresponding to $z \sim 0.4$ (one exponential merging timescale). However, the majority of $L \sim L^*$ galaxies are observed to possess thin disks and spiral arms which would be disrupted by a merger with any other galaxy of comparable mass (see e.g. Larson 1990).

Although mergers of similar large galaxies may be important in building-up cluster-dominating giant ellipticals, the thinness of *spiral* galaxy disks sets severe constraints on the amount of mass they could have acquired through recent mergers with other galaxies. According to Tóth and Ostriker (1992), the structure of the disk of our own Galaxy indicates that no more than 4% of the total mass within the radius of the solar orbit could have been supplied through merging in the past 5 Gyr. This would suggest that, in most cases, only dwarf galaxies of very low mass ($M \leq 4 \times 10^9 M_\odot$) have merged with the much more massive ($M \geq 10^{11} M_\odot$) $L \sim L^*$ spiral galaxies – and that only a small minority (a few percent) of large galaxies could have undergone major mergers, changing their mass and luminosity by factors of order unity, since $z \sim 1$ epochs.

Both these problems with non-mass-dependent (i.e. '$M^* - \phi^*$') merging models are avoided if merging processes are described better by the '$\phi^* - \alpha$' model – in which the accretion of very small galaxies onto large galaxies, which would suffer relatively little

disruption as a result, is a much more common process than the coalescence of similarly sized objects.

GRV estimated that the accretion of dwarfs onto giant galaxies, as a result of dynamical friction, would occur at a rate of the order of ~ 1 Gyr^{-1} at the present day and much more freqently at earlier epochs, the rate increasing with redshift at least as rapidly as $\sim (1+z)^{1.5}$. In contrast, observations of galactic interactions and the results of n-body simulations (Carlberg and Couchman 1989) suggest merging rates between giant galaxies of no more than ~ 0.02 Gyr^{-1}, in agreement with the constraints discussed above from the thinness of spiral disks. When Carlberg and Charlot (1992) combined the mass-dependent merging process of the Carlberg and Couchman (1989) simulations with Bruzual-type models of the SFR evolution, the predicted evolution of the luminosity function out to $z \sim 2$ was a combination of a strong brightening of L^* and a steepening of the faint-end slope – very similar to the GRV '$\phi^* - \alpha$' model and the steepening α model discussed here. This would suggest that real, physical merging processes would indeed produce the inferred steepening of the LF, without cancelling out the brightening of L^* produced by increased star-formation.

The Cole et al. (1994) simulations of galaxy formation in an $\Omega = 1$ CDM Universe also predict a change in the faint-end slope, from $\alpha \simeq -1.5$ at $z = 0$ to $\alpha \simeq -1.8$ at $z \sim 2$, resulting from the merging of dwarf galaxies. However, the merging process within this model is more similar to the '$M^* - \alpha$' model of GRV than to the '$\phi^* - \alpha$' model, and largely cancels out any brightening of L^*_B with redshift. In the Cole et al. model, as in the BEG model, there are no extremely luminous ($M_B < -23$) giant galaxies at $z \sim 2$, and the faint blue galaxies would lie at $z \sim 1$. In this model supernovae reheat most of the cool gas in dwarf galaxies, reducing the fraction which remains available for star-formation, and giving very long SFR evolution timescales, rather than blowing out all the gas and halting star-formation completely (we discuss the star-formation histories of dwarf galaxies further in Section 8.3.3). This combination of strong suppression of star-formation in dwarf galaxies and a late formation epoch ($z \sim 1$) for giant galaxies results in a predicted mean age of only 9 Gyr for the stellar populations of giant ellipticals, but the very red colours of these galaxies suggest ages of at least 14 Gyr.

The 'self-destruction' of dwarf galaxies soon after formation, due to 'winds' from the first wave of supernovae blowing away most of the gas content and preventing further star-formation (see Babul and Rees 1992), may also have played a part in reducing the comoving number density of visible low-mass galaxies since $z \sim 2$ epochs. If such events occurred mainly at $z > 0.5$, rather than at the low redshifts which would be required to give a no-evolution $N(z)$ at $B \sim 24.5$ (see Section 3.6), a large degree of fading ($\sim 2.5^m$–3.5^m) of the post-starburst stellar population would be possible between the starburst epoch and the present day (see e.g. Dalcanton 1993). Hence, if initial starbursts do often cause the 'self-destruction' of low-mass galaxies, the subsequent fading of these galaxies could be significant in causing the inferred evolution of the faint-end slope, in addition to the accretion of dwarfs onto large galaxies. The choice of these two possible 'fates' for an 'excess' dwarf galaxy may then depend on the environment in which it initially forms.

In the Lacey et al. (1993) model of tidally triggered galaxy formation in an $\Omega = 1$ CDM Universe, winds from supernovae do remove most of the gas from dwarf galaxies, resulting in a significant flattening with time of α. However, although this model does predict some brightening of L^* (in all passbands) between $z = 0$ and $z = 2$, the combination of a very steep LF ($\alpha \simeq -1.6$ even at $z = 0$) and a late formation redshift for large galaxies gives a low median redshift of only $z_{median} = 0.39$ for $24 \leq B \leq 25$ galaxies. This model also fails to account for the red colours of present-day giant ellipticals.

It is clear that, for the interpretation of the number counts, colours and $\omega(\theta)$ amplitudes of galaxies at these very faint limits, the Bruzual-type models of spectral evolution must be incorporated into accurate physical models including all the processes of galaxy formation, merging, interactions and supernova feedback. We find that the physical models of Cole et al. (1994) and Lacey et al. (1993) predict a steepening of the faint-end slope with redshift in approximate agreement with our observations, and suggest plausible physical mechanisms, but both our $\omega(\theta)$ scaling and the red colours of ellipticals suggest that giant galaxies already existed at higher ($z \geq 2$) redshifts than in either of these $\Omega = 1$ CDM models. Reconciling these models with observations may require lowering the value of Ω, with or without the inclusion of a cosmological constant, so that large galaxies would form earlier (note also that a reduction in the M/L ratio by a factor of 5 is needed for galaxies in the Cole et al. model to fit the observed Tully-Fisher relation) and/or the replacement of some or all of the Cold Dark Matter with baryons, which again would lead to higher formation redshifts for large galaxies (note that the predicted median redshift of $23 \leq B \leq 27$ galaxies increases with increased baryon fractions in the CDM models of White and Frenk 1991).

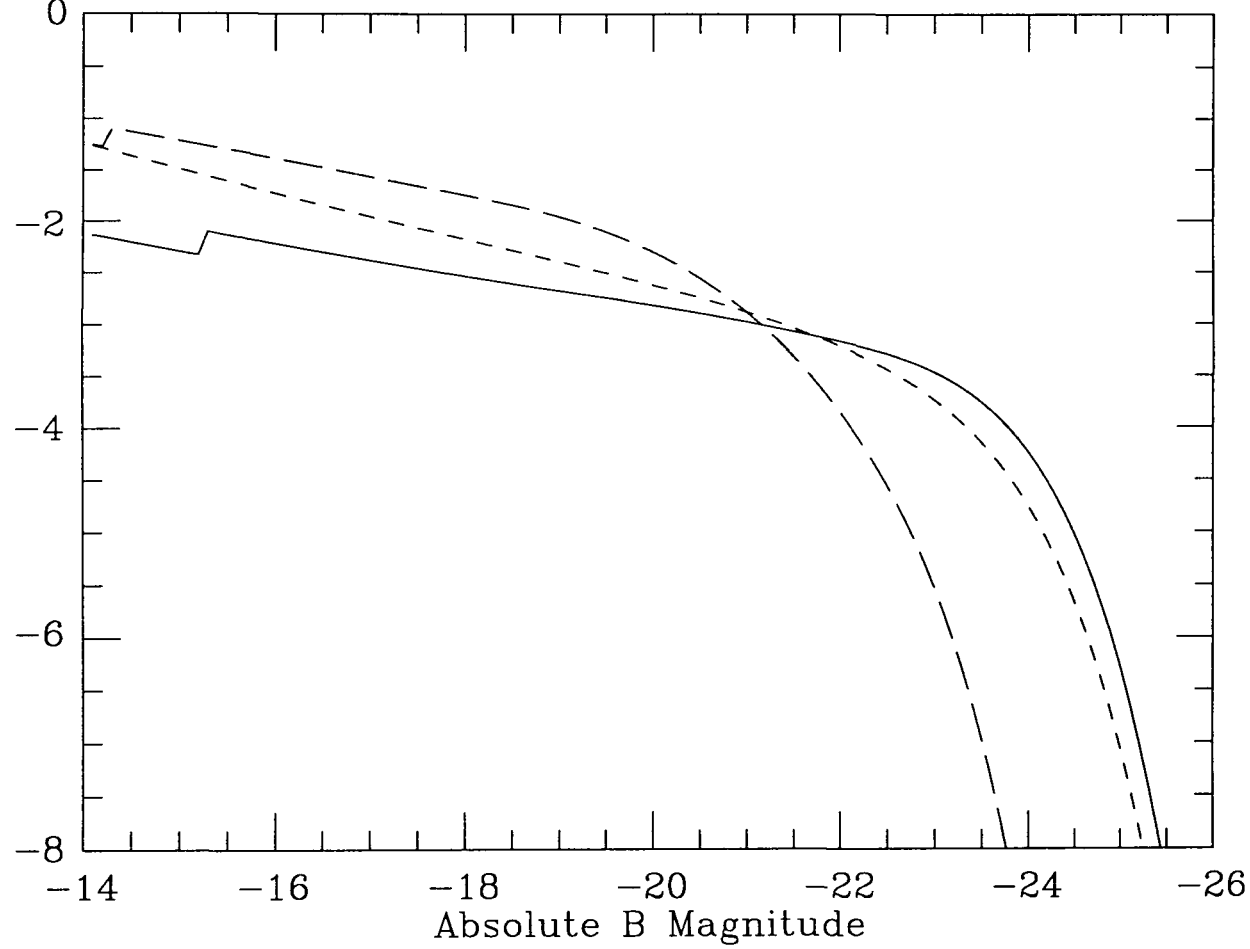

Figure 4.9 Luminosity functions for all galaxies at $z = 2$, as predicted by our Bruzual PLE model (solid line), our 'steepening α' model (short-dashed line), and the 'BEG' ϕ^* evolution model (long-dashed line).

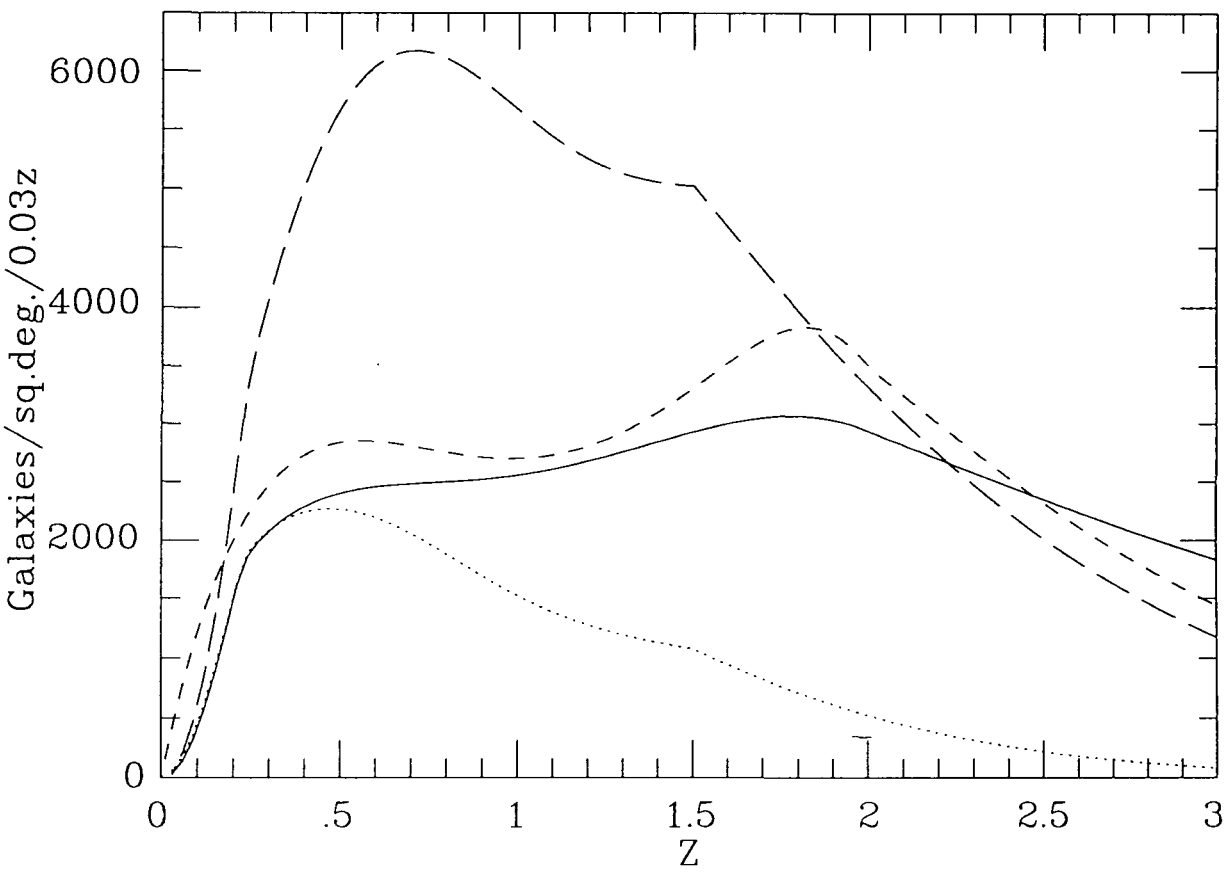

Figure 4.10 The redshift distribution predicted for all $B_{ccd} \leq 27.0$ galaxies by our no-evolution (dotted line), Bruzual PLE (solid line) and 'steepening α' (short-dashed line) models, all computed with $q_0 = 0.05$, and by the 'BEG' pure density evolution model with $q_0 = 0.5$ (long-dashed line).

4.9 Summary and Conclusions

(i) The clustering of the galaxies detected on a single CCD frame reaching a very faint limit of $B_{ccd} = 27.0$ was analysed, and a $\omega(\theta)$ amplitude estimated. The clustering was found to be very weak, but similar to that seen in two independent samples of galaxies with brighter limits of $B = 25$ and $B = 26$. Hence the steep decline in $\omega(\theta)$ amplitude observed between the magnitude limits of $B = 23$ and $B = 24.75$ may not continue further faintward, where the $\omega(\theta)$ scaling appears to level out at a minimum amplitude of $\sim 4 \times 10^{-4}(\mathrm{deg})^{-0.8}$.

(ii) The apparent levelling out of the $\omega(\theta)$ scaling at $B \sim 25$ suggests that galaxies are seen out to their maximum redshifts at this magnitude – either due to the epoch of galaxy formation or the redshifting of the Lyman limit into the blue band at $z = 4$, and/or that $z_{median} > 1.5$ at $B > 25$ and an 'effective' redshift cut-off has been reached due to the reduction in the size of the comoving volume element ($\frac{dV_{com}}{dz}$) at even higher redshifts.

The $\omega(\theta)$ amplitudes measured at $24.75 \leq B \leq 25.0$ limits from our data and the Tyson (1988) survey are consistent with those expected if clustering is stable, the redshift maximum is approximately $3 \leq z_{max} \leq 4$, and Ω has any value from 0 to 1. These $\omega(\theta)$ results are in good agreement with our PLE model, as was the case at $23 \leq B \leq 25$. Therefore the redshift distribution of the galaxies on our deep CCD image is likely to be similar to that given by this model for the same $B \leq 27.0$ magnitude limit (Figure 4.10), with the galaxies broadly distributed in redshift from $z = 0$ to at least $z \sim 3$.

(iii) Our CCD data gives a high galaxy number count at $B \sim 26$, which is in excess of PLE model predictions in a $q_0 = 0.5$ Universe, but can be fitted by PLE models in a low-q_0 or a Λ-dominated cosmology. However, in the range $25 \leq B \leq 27.5$ we find our galaxy counts, which exceed the raw counts of Tyson (1988), to increase with a surprisingly steep gradient of $\frac{d(logN)}{dm} \sim 0.3$. Faintward of the magnitude at which galaxies can be seen out to z_{max}, the slope of their differential number counts will reflect the faint-end slope of the galaxy luminosity function. The $\omega(\theta)$ results strongly suggest that z_{max} is reached at $B \sim 25$, as would be expected if L^* brightens with redshift as much as in our PLE models. The steep count gradient would then indicate that, at high redshifts ($z \sim 2$), the galaxy luminosity function possesses a steep faint-end slope of $\alpha \simeq -1.75$, compared to $\alpha \simeq -1.25$ seen locally.

In combination with the strong L^* evolution inferred from the $\omega(\theta)$ scaling, this suggests that the galaxy luminosity function may be undergoing a mass/luminosity-dependent evolution, similar to that in the '$\phi^* - \alpha$' model of GRV, in which the faint-end slope α steepens with redshift but the characteristic galaxy mass is not affected. The L^* luminosity would then evolve as in a PLE model, so that high redshift galaxies would appear in surveys at similar magnitudes – in slightly smaller numbers at $23 \leq B \leq 24$ (giving better consistency with redshift surveys than PLE models), but in larger numbers at $B > 26$ (explaining the steep count gradient). Combining '$\phi^* - \alpha$' evolution with the evolution of L^* given by our Bruzual model improves the fit to the steep number counts at $25 \leq B \leq 27.5$, while still explaining the observed $\omega(\theta)$ scaling without requiring any departure from stable clustering.

Chapter 5

Cross-correlation of X-Ray Sources with Faint Galaxies

5.1 Introduction

In this chapter we aim to identify individual, faint ($16 \leq B \leq 23$) galaxies as X-ray sources, through an analysis of the positional cross-correlation of X-ray sources detected using ROSAT and the galaxies on photographic plates covering the same areas of the sky. The nature of the discrete sources contributing to the extragalactic X-ray flux can be studied by resolving as many sources as possible out of the background on deep high-resolution X-ray images, followed by spectroscopic investigation of optical counterparts corresponding to the detected X-ray sources. The high-resolution X-ray imaging capabilities of the *Einstein* and, more recently, ROSAT satellites have enabled the origin of a substantial fraction of the soft X-ray background (XRB) to be investigated in this way.

On a long exposure of the XRB on the Pavo field, obtained using the *Einstein* High Resolution Imager, Griffiths et al. (1992) detected 17 discrete sources above a flux limit $S(0.1\text{–}3.0 \text{ keV}) \sim 10^{-14}$ ergs cm^{-2}s^{-1}. Spectroscopic investigation of the sources identified 14 of these as QSOs, at a median redshift of 0.94. The detected QSOs accounted for $\sim 15\%$ of the total 0.1–3.0 keV X-ray background intensity. Two of the remaining X-ray sources were identified as star-forming, narrow emission-line galaxies, both at $z = 0.4$, and the other as a cluster-dominating early-type galaxy at $z = 0.13$.

Using the ROSAT Position Sensitive Proportional Counter (PSPC), a series of deep (20–50 ksec exposure time) images have been obtained on fields previously surveyed for UV-excess quasars by Boyle et al. (1990). These observations are the first part of an ongoing X-ray survey aiming to cover all 10 fields of the UVX QSO catalogue. On the basis of the earlier *Einstein* surveys, most of the optically identified QSOs would be expected to be detectable on the ROSAT images, thus enabling ~ 10 or more sources on each field to be identified immediately and aiding the investigation of those remaining by providing an accurate astrometric transform between the optical and X-ray datasets.

The contents of the first ROSAT image in this survey, of the field known as QSF3, are described by Shanks et al. (1991). In the central 0.35 deg^2, 39 discrete sources were detected. Follow-up spectroscopy with AUTOFIB at the Anglo-Australian Telescope (AAT) identified 24 of these as QSOs with a median redshift of 1.52, giving a lower limit of 30% for the QSO contribution to the total 0.5–2.0 keV flux. Only one of the remaining sources was unambiguously identified as a galaxy – an elliptical at $z = 0.180$. However, when spectroscopy was extended to fainter ($4\text{–}5\sigma$ detected) sources on QSF3, and to a second field (QSF1) also within the area of the QSF Schmidt plate, a further seven galaxies appeared to be associated with X-ray sources (Griffiths et al. 1993). Five X-ray detected galaxies, including galaxies on both ROSAT fields within the QSF Schmidt plate area, were found to be at the same redshift of $z = 0.312$, suggesting the presence of a large-scale (~ 10 h^{-1} Mpc) structure. Two of the X-ray detected galaxies (including one at $z = 0.312$) possessed strong, narrow emission lines in their optical spectra, probably indicative of starburst activity, but the others appeared to be early-type galaxies without ongoing star-formation.

Griffiths and Padovani (1990) and Treyer et al. (1992) have suggested that star-forming galaxies could form an increasingly large percentage of the X-ray sources identified at fainter flux limits. It is evident from both *Einstein* and ROSAT observations that

QSOs, rather than galaxies, dominate the component of the XRB most easily resolvable into discrete sources. However, results from the deepest surveys now suggest that a wide variety of types of galaxy are beginning to show up in the X-ray source counts at $S(0.5\text{–}2.0\ \mathrm{keV}) \simeq 5 \times 10^{-15}$ ergs $\mathrm{cm}^{-2}\mathrm{s}^{-1}$, i.e. the source detection limit attained on a $\sim$ 30 ksec ROSAT PSPC image.

In this chapter we shall be attempting to estimate the numbers of galaxies within the $\sim$ 35% component of the 0.5–2.0 keV background which was resolved into discrete sources in this ROSAT survey. The remaining, unresolved $\sim$ 65% appears as a very uniform background, and we investigate its nature and origin in the two chapters following.

We extend the search for X-ray emitting galaxies to 3 further UVX survey fields now imaged by ROSAT – one of these having been given an exposure time of $\sim$ 50 ksec, almost twice that used previously. Fluctuation analysis of the QSF3 unresolved XRB (Georgantopoulos et al. 1993) suggested that there were larger numbers of sources just faintward of the limit for resolution than would be expected if these consisted entirely of AGN, assuming AGN to possess an X-ray luminosity function as described by Boyle et al. (1993). Therefore, the aim of obtaining a longer exposure on one field was both to detect less luminous QSOs and thus to better determine the form and evolution of the QSO X-ray luminosity function, and to search for possible new populations of faint X-ray sources including normal and starburst galaxies.

AAT photographic plates were available for 3 of the 5 fields imaged using ROSAT, including the 50 ksec image, enabling the identification of fainter ($B \simeq 23$) optical counterparts for the X-ray sources than was possible with the UK Schmidt Telescope plates used previously. However, at $B \sim 23$ the surface density of normal galaxies exceeds $\sim 10^4$ deg^{-2}, leading to a confusion problem as we would expect to find one faint galaxy within each resolution element of a ROSAT image (i.e. within a radius $\sim$ 20 arcsec of each source) simply by chance. Hence when attempting to identify normal galaxies at these faint magnitudes as X-ray sources, we cannot simply match the source and galaxy positions within a 20 arcsec radius 'error box'. It is necessary to compute the number of source/galaxy pairs expected by chance, and subtract this from the observed number, as in the cross-correlation analysis described below. In this way, even when the identification of individual galaxies as X-ray sources becomes uncertain (i.e. the excess of pairs above the chance expectation is less than a factor of $\sim$ 2) the proportion of galaxies in the X-ray source counts can still be estimated.

5.2 Observational Data

5.2.1 X-Ray Data

The X-ray data used in this thesis consists of images obtained using the ROSAT PSPC. The images consist of counts of 0.5–2.0 keV photons in square pixels of side 15 arcsec. In the investigations of the extragalactic XRB described in this thesis, we did not include the 0.1–0.5 keV photons to which the PSPC is also sensitive, as a much larger proportion of these are thought to originate within our own Galaxy. As the sensitivity and resolution (FWHM $\simeq$ 25 arcsec) of the PSPC remain approximately constant out to 10 arcmin from the image centres, but deteriorate increasingly rapidly at larger off-axis angles, we use only (at most) the central 40 × 40 arcmin areas of each of our ROSAT images.

Table 5.1 lists the field centres, all of which lie within the QSF and SGP areas used in the Boyle et al. (1990) QSO survey. The QSF1, QSF3, SGP2 and SGP3 fields

were imaged with the ROSAT PSPC for 30 ksec and the GSGP4 field for 60 ksec. The effective exposure times, also listed here, are slightly less due to rejection of parts of the data contaminated by cosmic rays.

5.2.2 UK Schmidt Telescope (1.2m) Data

Our optical dataset includes COSMOS scans of two blue-band UK Schmidt Telescope plates used in the Boyle et al. (1990) survey, each covering a large, $\sim$ 14 deg^2 area. For the SGP field the plate used was J3721, with a sky brightness $\mu_J^{sky} = 22.90$ mag arcsec^{-2}. The corresponding zero-point for the galaxy magnitudes in these COSMOS scans of UKST plates is $\mu^{sky} + 1.35$. In addition, we have a red-band UKST plate of the SGP field – R2775, with $\mu_R^{sky} = 21.52$ mag arcsec^{-2}. The two plates have been 'matched' to give $B - R$ colours for most objects in the blue-band dataset.

The QSF field is covered by the J2672 plate, with $\mu_J^{sky} = 22.29$ mag arcsec^{-2}. For further details of these Schmidt plates, refer to Boyle et al. (1990).

5.2.3 Anglo-Australian Telescope (4m) Data

For three of our five fields we now have COSMOS scans of AAT plates which reach at least two magnitudes deeper than the UKST data. Each AAT plate covers only one ROSAT field – 40 arcmin corresponds to about 157mm on an AAT plate compared to 36mm on a UKST plate. Our deep GSGP4 ROSAT image covers the same area of sky as the J1888 AAT plate, which was previously used for number counts and $\omega(\theta)$ analysis by Stevenson et al. (1985) and Jones et al. (1991). A red-band AAT plate (R1996) was also available for this field, providing $B - R$ colours for most of the objects in the J1888 dataset used here. For further details of these two plates see Jones et al. (1991), who give $\mu_J^{sky} = 22.16$ mag arcsec^{-2} for J1888 and $\mu_R^{sky} = 20.64$ mag arcsec^{-2} for R1996, the values used here to zero-point the galaxy magnitudes (for AAT plates the COSMOS zero-point is $\mu_J^{sky} + 3.06$).

The QSF3 field was covered by the J2719 plate and SGP2 by J2801. The reduction of these two plates followed essentially the same procedures of star-galaxy separation etc. as described by Jones et al. (1991) for J1888. The derivation of astrometric transforms is described below in Section 6.5.1. Zero-points were estimated by comparing magnitudes from the COSMOS scans of the AAT plates with those of the same stars and galaxies in the QSF and SGP UKST datasets – this gave $\mu_J^{sky} = 22.26$ mag arcsec^{-2} for J2719 and $\mu_J^{sky} = 21.92$ mag arcsec^{-2} for J2801.

5.3 Detection and Spectroscopic Investigation of X-Ray Sources

Source detection algorithms were applied to each of the five ROSAT images (see e.g. Shanks et al. 1991), giving centroid positions and fluxes for all discrete, point-like sources above $\sim 4\sigma$ significance. Table 5.2 gives the total number detected in each field. Some of these are QSOs previously identified in the Boyle et al. (1990) UVX survey – the X-ray positions of these were used to derive astrometric transforms to enable candidate optical counterparts to the remaining sources to be located on the UKST plates and the J1888 AAT plate.

Field	Equinox 2000.0		Galactic co-ordinates		Exposure time
	R.A.	Dec.	Longitude	Latitude	(seconds)
GSGP4	00 57 29.0	-27 38 13	234.034	-88.565	48955
SGP2	00 52 04.9	-29 05 26	298.828	-88.032	24494
SGP3	00 54 59.3	-28 19 43	269.927	-88.565	21062
QSF1	03 42 10.3	-44 54 45	252.089	-51.745	26155
QSF3	03 42 13.5	-44 07 44	250.848	-51.905	27358

Table 5.1 Positions of the centres of the five ROSAT images used in this thesis, as both R.A. and Dec. co-ordinates and as galactic longitude and latitude, together with their effective exposure times in seconds.

Field	5σ detection limit	$\geq 4\sigma$ sources		$\geq 5\sigma$ sources	
	ergs $cm^{-2}s-1$	Total	Unidentified	Total	Unidentified
GSGP4	3.125×10^{-15}	100	51	61	26
SGP2	6.200×10^{-15}	67	40	30	14
SGP3	6.420×10^{-15}	53	21	30	6
QSF1	5.325×10^{-15}	73	38	37	10
QSF3	5.000×10^{-15}	63	34	36	11
TOTAL		356	184	194	67

Table 5.2 The 0.5–2.0 keV flux thresholds for the detection of individual X-ray sources in the central regions of our 5 ROSAT images, the total numbers of sources actually detected above 4σ and 5σ levels of significance, and the numbers of these detected sources which are not identified as either QSOs or stars in our own Galaxy, and which could therefore be faint galaxies.

Most of these candidate sources were then examined spectroscopically using the AUTOFIB multi-fibre system on the AAT. As expected, many were found to be high-redshift QSOs (with $z_{mean} \sim 1.5$), bringing the total number of QSOs detected in the 5 fields of the X-ray survey to at least 127 (for more information on the detected QSOs, see Boyle et al. 1994). When all sources identified by spectroscopy as either QSOs, BL Lac objects or stars within our own galaxy were excluded the total number of 4σ-detected sources on the 5 fields was reduced from 356 to 184. It is these unidentified sources we are concerned with here, as a large proportion (~ 100) appeared to be associated with galaxies on the photographic plates, and for 39 of these sources the optical counterpart closest to the X-ray position was firmly identified by spectroscopy as a normal, cD or starburst galaxy.

However, not all of these galaxies will be the true origin of the observed X-rays. Misidentification of galaxies as X-ray sources is particularly likely when the galaxy is faint ($B > 21$) or not closely coincident with the X-ray position (separation $\geq$ the ROSAT instrumental FWHM of $\simeq 25$ arcsec). In such cases the true X-ray source may be, for example, a QSO at an even fainter blue magnitude, perhaps invisible on the photographic plate. In cross-correlating the 184 unidentified sources with the galaxies, we therefore subtract the number of source/galaxy co-incidences expected by chance from the number actually observed, in order to estimate the true extent and significance of their association.

We shall also cross-correlate with galaxies the subset of these sources which have X-ray fluxes above 5σ detection limits, as if some of the fainter, 4–5σ sources are spurious, their exclusion may reduce the statistical errors in our estimate of the source/galaxy cross-correlation. Table 5.2 gives the flux limits for 5σ detection of sources at the centre of each of the images (sources more than 8 arcmin from the field centres would require somewhat greater fluxes to be detected above 5σ, the threshold increasing to almost four times the central value at 20 arcmin).

5.4 Cross-correlation with UKST Data

5.4.1 Method

To investigate the nature of the X-ray sources, their positions had to be converted to (x,y) co-ordinates on the SGP and QSF Schmidt plates. Astrometric transforms were already in existence for these plates from their earlier use in the Boyle et al. (1990) UVX QSO survey. Further transforms could then easily be set up for the 5 ROSAT images using the X-ray sources which already had fairly definite identifications with UVX QSOs or bright stars visible on the photographic plates. Although only point sources were used in this, the limited resolution of ROSAT in comparison to optical observations meant that positional errors in matching X-ray sources with their optical counterparts would be of the order of 10 arcsec.

The numbers of stars and galaxies (in magnitude bins, to a limit of $B = 21$) in annuli (of 5 arcsec width) around the position of each of the 184 unidentified X-ray sources were counted. The number of X-ray/optical pairs as a function of separation, $N_{xg}(\theta)$, was compared with the number expected in the absence of any correlation by placing 20000 points randomly over each of the five field areas (avoiding 'holed' areas of the plates which will contain no objects in the dataset used here) and similarly cross-correlating the X-ray sources with these.

A cross-correlation function $C_{xg}(\theta)$ of X-ray sources and galaxies was then calculated as

$$C_{xg}(\theta_i) = \frac{N_{xg}(\theta_i)}{N_{xr}(\theta_i)} \frac{N_r}{N_g} - 1$$

where $N_{xg}(\theta_i)$ is the number of source/galaxy pairs of separation $5(i-1) < \theta \leq 5i$ arcsec,

$N_{xr}(\theta_i)$ is the number of source/random pairs of separation $5(i-1) < \theta \leq 5i$ arcsec,

N_g is the number of galaxies, and

N_r is the number of random points (20000).

5.4.2 Results

When the list of 184 X-ray sources (detected above 4σ and not identified as stars or QSOs) were cross-correlated with the 1911 objects classed as $B \leq 21.0$ galaxies (on the total of 5 fields), 27 galaxies were seen within 20 arcsec of a source compared to 16.2 expected by chance (at $\theta > 20$ arcsec the cross-correlation was generally consistent with zero). This result corresponds to a 2.7σ rejection (with $\sqrt{N}$ statistics) of the hypothesis that these X-ray sources and galaxies are uncorrelated.

Alternatively, this could be expressed as indicating that 10.8 ± 5.2 of these 184 unidentified (ie. $5.8 \pm 2.8\%$) sources have genuine optical counterparts classed as $B \leq 21.0$ galaxies on either of the UKST plates. Although a positive and significant correlation is detected, only a very small proportion ($0.56 \pm 0.27\%$) of all $B \leq 21$ galaxies are bright enough at X-ray energies to be individually detectable on ROSAT images of this depth.

There is no overall cross-correlation between the unidentified sources and the 3194 images classed as $B \leq 21$ stars in the UKST dataset, with 20 star/source pairs at $\theta \leq 20$ arcsec compared to 26.2 expected by chance. Five of these stars matched with sources were found by spectroscopy to be misclassified galaxies (these are listed in Section 5.5 below). Hence there is a slight (2σ) anticorrelation between our sources and 'real' stars (including QSOs), but this is to be expected as sources identified as stars or QSOs have already been excluded from the analysis.

Table 5.3 shows the X-ray source/UKST galaxy pair counts divided up by field and into galaxy magnitude bins. For the SGP fields, where red data is available, the galaxies have also been divided into red ($B - R \geq 1.50$) and blue ($B - R < 1.50$) subsets. The greatest source/galaxy pair excess, in fact most of the total for the five fields, appears on the 50 ksec depth GSGP4 field, with 14 pairs seen compared to 5.4 expected. Looking at the dependence on galaxy colour, on the three SGP fields there were 12 blue galaxies seen within 20 arcsec of an X-ray source against 6.4 expected by chance, and for redder galaxies there were 7 seen compared to 3.7 expected. In both cases the excess correlation is a factor of ~ 2 for $B \leq 21.0$ galaxies, so there is no indication from these results that the X-ray emission of galaxies of the same blue magnitude depends significantly on their $B - R$ colour.

Table 5.3 also shows the source/galaxy pair counts when only the unidentified X-ray sources brighter than the 5σ detection limits on each ROSAT image are included. The overall result is that 11 galaxies are seen within 20 arcsec of a $\geq 5\sigma$ source compared to 6.4 expected by chance. This would indicate 4.6 ± 3.3 (ie. $6.9 \pm 5.0\%$) of these 67 brighter X-ray sources to have genuine optical counterparts classed as $B \leq 21.0$ galaxies. When $4\text{–}5\sigma$ sources are excluded from the analysis, the factor of ~ 2 excess in the number of source/galaxy pairs remains approximately constant, but the reduction in the number

of unidentified sources by a factor of 2.75 considerably worsens the statistics, so that the rejection of the hypothesis that X-ray sources and galaxies are uncorrelated is reduced in significance to 1.8σ. The sources detected at $4\text{–}5\sigma$ significance do not appear to be any less correlated with galaxies than the $\geq 5\sigma$ sources. Hence our results suggest that most of the $4\text{–}5\sigma$ detections are genuine X-ray sources, rather than random fluctuations in the background, and that for further investigation of X-ray sources, e.g. spectroscopy of the optical counterparts, it is worthwhile to include X-ray sources detected close to the $\sim 4\sigma$ flux limits.

Figure 5.1 shows the cross-correlation function of $\geq 4\sigma$ and $\geq 5\sigma$ unidentified X-ray sources with the $B \leq 21.0$ galaxies on the UKST plates. It can be seen that there is no correlation at separations much larger than the ROSAT image FWHM ($\simeq 25$ arcsec), suggesting that the X-ray emission of these sources is generally associated with individual galaxies rather than large galaxy clusters. At smaller separations $C_{xg} \sim 1$, giving the approximate twofold excess of galaxy/source pairs when summed to 20 arcsec.

Table 5.3 (Following page) The total numbers of galaxies seen on 5 areas of UKST plates corresponding to ROSAT images, and their cross correlation with unidentified X-ray sources detected above 4σ and above 5σ on the ROSAT images. The cross-correlation results are given by listing the numbers of these galaxies which are found to lie within 20 arcsec of the X-ray sources, and the numbers expected in these areas by chance. The results are divided up by the B magnitudes of the galaxies into $\Delta(B) = 1^m$ bins, and by field, and the galaxies on the SGP plate are further divided by colour at $B - R = 1.5$ into red (r) and blue (b) subsamples.

Magnitude range	Field	No. of galaxies	Galaxies ≤ 20 arcsec from an X-ray source			
			$\geq 4\sigma$ list		$\geq 5\sigma$ list	
			seen	expected	seen	expected
$B < 18$	GSGP4b	5	0	0.06	0	0.03
	GSGP4r	4	0	0.05	0	0.03
	SGP2b	2	0	0.02	0	0.01
	SGP2r	3	0	0.03	0	0.01
	SGP3b	3	0	0.01	0	0.00
	SGP3r	6	0	0.03	0	0.00
	QSF1	5	0	0.05	0	0.01
	QSF3	6	0	0.04	0	0.02
	TOTAL	34	0	0.29	0	0.11
$18 \leq B < 19$	GSGP4b	18	2	0.22	1	0.12
	GSGP4r	8	1	0.10	1	0.05
	SGP2b	23	0	0.21	0	0.08
	SGP2r	11	0	0.10	0	0.04
	SGP3b	23	0	0.10	0	0.02
	SGP3r	11	0	0.05	0	0.01
	QSF1	39	0	0.35	0	0.11
	QSF3	37	1	0.25	0	0.09
	TOTAL	170	4	1.38	2	0.52
$19 \leq B < 20$	GSGP4b	67	2	0.81	0	0.43
	GSGP4r	51	1	0.61	0	0.33
	SGP2b	41	0	0.37	0	0.14
	SGP2r	33	1	0.30	1	0.11
	SGP3b	41	0	0.18	0	0.03
	SGP3r	33	2	0.15	1	0.03
	QSF1	127	1	1.15	1	0.34
	QSF3	98	0	0.67	0	0.25
	TOTAL	491	7	4.24	3	1.66
$20 \leq B \leq 21$	GSGP4b	199	7	2.40	2	1.27
	GSGP4r	94	1	1.13	1	0.60
	SGP2b	159	1	1.43	1	0.54
	SGP2r	82	1	0.74	0	0.28
	SGP3b	135	0	0.59	0	0.10
	SGP3r	83	0	0.37	0	0.07
	QSF1	226	2	2.05	0	0.61
	QSF3	238	4	1.62	2	0.61
	TOTAL	1216	16	10.33	6	4.08

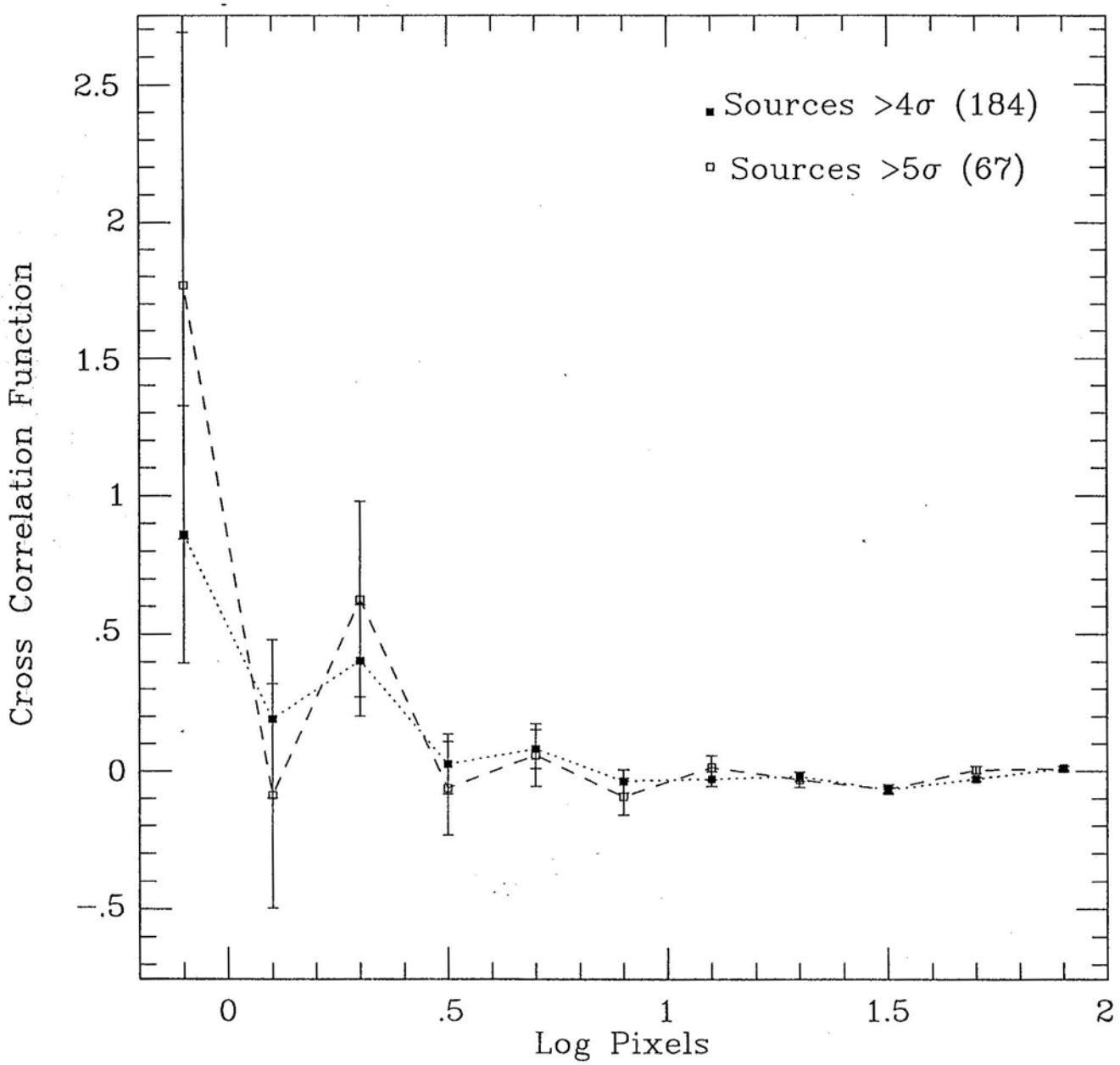

Figure 5.1 The cross-correlation function (with $\sqrt{N}$ error bars) of unidentified X-ray sources detected on 5 ROSAT images and the $B \leq 21.0$ galaxies on UKST plates of the same areas, plotted against the logarithm of the angular separation in units of ROSAT pixels (15 arcsec). The cross-correlation function is shown for the 184 sources detected above 4σ (filled squares, dotted line) and for the subset of these sources, numbering 67, detected above brighter 5σ flux limits (open squares, dashed line) on these images.

5.5 Cross-correlation with AAT Data

5.5.1 Method

The cross-correlation between X-ray sources and galaxies was similarly calculated using the galaxies on AAT plates, to a fainter magnitude limit of $B = 23$. As before, X-ray sources already identified as stars or QSOs were excluded, leaving 125 sources detected above 4σ and 51 above 5σ on the three fields for which the AAT data was available.

For each of the three AAT plates, a 6-coefficient astrometric transform was set up by identifying about 40 stars distributed over the area of the AAT plate and also seen on the corresponding UKST plate, with the Schmidt astrometry providing R.A. and Dec. for these stars accurate to 1–2 arcsec. These transforms were combined with the ROSAT image transforms (Section 5.4.1) to convert the positions of all $B \leq 23.0$ images on the plates to the corresponding (x,y) pixel co-ordinates on the ROSAT images (the reason for converting galaxy positions to ROSAT pixel co-ordinates, rather than converting source positions to plate (x,y) co-ordinates as was done for the UKST cross-correlation, was to enable these faint galaxies to be cross-correlated with the X-ray background – see Chapter 7).

Only ROSAT and AAT objects within a circle of radius 20 arcmin about each image centre were used. This radius excluded only one source, leaving 124 above 4σ and 51 above 5σ. The cross-correlation was calculated as described in Section 5.4.1 above, the source/galaxy pair counts again being compared with those expected by chance by correlating the X-ray sources with 20000 points scattered randomly over each of the circular areas, but avoiding 'holed' areas of the plates (which were generally of small dimensions, ~ 2 arcmin).

5.5.2 Results at $B < 21.0$

Table 5.4 shows the source/AAT galaxy pair counts divided up by field and into galaxy magnitude bins. For GSGP4, where a red AAT plate was also available, the galaxies were divided into blue ($B - R < 1.5$) and red ($B - R \geq 1.5$) subsets.

First of all, considering the $B < 21.0$ galaxies, numbering 1059 in total on the 3 AAT plate areas, we see 25 such galaxies within 20 arcsec of one of the $\geq 4\sigma$ unidentified sources compared to 12.6 expected by chance. This corresponds to a 3.50σ rejection of the hypothesis of no correlation, or to 12.4 ± 5.0 of these sources having genuine optical counterparts classed here as $B < 21.0$ galaxies. This result indicates that $1.17 \pm 0.47\%$ of the $B < 21.0$ galaxies seen on the three AAT plates are individually detectable on these ROSAT images. If the logarithm of the X-ray/B-band luminosity ratio of galaxies is hypothesised to follow a Gaussian distribution, these X-ray detected galaxies would all have log (L_X/L_B) ratios at least 2.27σ above the mean value for all galaxies. The median ratio for the X-ray detected 'top 1.17%' sample would be 2.52σ above the mean for all galaxies.

Again we see that the results from the deep GSGP4 field dominate the observed cross-correlation, with 15 galaxies being seen within 20 arcsec of one of the sources on this field, compared to 5.5 expected by chance. The overall result from the AAT data is slightly stronger than for the UKST data at the same magnitude limit, the reasons for this appearing to be that (i) the deep GSGP4 field (on which the largest number of galaxies were detected in X-rays) forms a larger proportion of the AAT dataset, (ii) four more $20 \leq B \leq 21$ galaxies in the AAT data were paired with sources on SGP2

than in the UKST data, perhaps due to chance differences in star-galaxy separation, magnitudes and astrometry.

As in the UKST data, there was no overall correlation with objects classed as $B < 21.0$ stars, only 11 of these being seen within 20 arcsec of a source compared to 13.9 expected by chance. One of these 11 was found by spectroscopy to be a galaxy (see Table 5.4), although misclassification of galaxies as stars appears to be less than in the Schmidt dataset.

When the $\geq 5\sigma$ sources only are used, there are 9 source/galaxy pairs seen for $B < 21.0$ galaxies, compared to 5.4 expected by chance. As in the cross-correlation with the UKST galaxies, the excess of $B < 21.0$ galaxies less than 20 arcsec from a source remains a factor of ~ 2 when the 4–5σ sources are excluded, but the reduction in the numbers of sources worsens the statistics, so when using the $\geq 5\sigma$ sources we obtain only a 1.6σ rejection of the hypothesis that these are uncorrelated with the galaxies.

Looking at the dependence on galaxy colour of the correlation on the GSGP4 field, we see at the $B < 21.0$ limit, 11 blue galaxies within 20 arcsec of a $\geq 4\sigma$ unidentified source compared to 3.4 expected, and 4 red galaxies compared to 2.1 expected. For sources above 5σ only these ratios become 3/1.8 and 4/1.2 respectively. As with the cross-correlation of X-ray sources with galaxies on the UKST plates, we find no significant difference between the cross-correlation results for red and blue galaxies.

Figure 5.2 shows the cross-correlation functions of $\geq 4\sigma$ and $\geq 5\sigma$ sources with $B < 21.0$ galaxies on the AAT plates, which are evidently very similar to those calculated using the Schmidt data.

5.5.3 Results at $21.0 \leq B \leq 23.0$

The above results still leave $\sim 90\%$ of the unidentified sources (~ 112 above 4σ or ~ 47 above 5σ) without optical counterparts at $B < 21$, hence we now consider their correlation with the even fainter objects visible on the deep AAT plates.

A total of 118 galaxies with $21 \leq B \leq 23$ are seen within 20 arcsec of a $\geq 4\sigma$ unidentified source, approximately one per source, but the surface density of these fainter galaxies is such that we would expect to see 101.0 source/galaxy pairs by chance. This gives a 1.7σ rejection of the hypothesis of no correlation, a result of only marginal significance, and would indicate 17.0 ± 10.9 of the X-ray sources to be $21 \leq B \leq 23$ galaxies. The deep GSGP4 field gives almost half of the total correlation, with 54 source/galaxy pairs compared to 45.8 expected, but as this is only a 1.2σ excess it is unclear, at any statistically significant level, whether GSGP4 continues to dominate our overall cross-correlation for these fainter galaxies.

As the 3 AAT plate areas used contain a total of 8620 galaxies with magnitudes $21 \leq B \leq 23$, only a very small proportion ($0.20 \pm 0.12\%$) of these can be sufficiently luminous in X-rays to be individually detected in this ROSAT survey even at the 4σ level. The L_X/L_B ratios of the X-ray detected $21 \leq B \leq 23$ galaxies would lie $\geq 2.9\sigma$ above the mean of all $21 \leq B \leq 23$ galaxies, with the median ratio of the X-ray detected galaxies being 3.1σ above the mean, in a Gaussian distribution of $\log(L_X/L_B)$.

The unidentified X-ray sources do show a significant correlation with objects classed as $21 \leq B \leq 23$ stars, (in contrast to the complete lack of correlation with stars at brighter magnitudes), with 39 being seen within 20 arcsec of a source compared to 22.0 expected by chance. The detection of a cross-correlation with objects classed as $21 \leq B \leq 23$ stars is of 3.6σ significance, considerably stronger than for galaxies in this range, as a result of both the higher amplitude of the cross-correlation with faint stars,

and the weakening of the significance of the cross-correlation with faint galaxies resulting from their higher surface density. Our results indicate than 17.0 ± 6.2 of these 'stars' are X-ray sources detected above 4σ, with most of the correlation (20 star/source pairs counted against 6.9 expected) being seen on the QSF3 field. At $B > 21$ the follow-up optical spectroscopy is less complete, so the likely cause of this correlation is that our list of unidentified X-ray sources still contains a few QSOs, which on account of their optical faintness have remained unidentified as such by spectroscopy, and which appear as faint 'stars' on the AAT plate.

More than half ($\sim 78/124$, $\sim 63\%$) of the unidentified X-ray sources detected above 4σ on the 3 AAT-observed fields remain unaccounted for by the cross-correlation with galaxies or stars even to a limit of $B = 23$. Many sources must therefore have optical counterparts (either faint galaxies or, more likely in most cases, faint QSOs) at fainter magnitudes of $B > 23.0$.

When only the sources detected above 5σ are considered, 53 source/$21 \leq B \leq 23$ galaxy pairs are seen compared to 43.4 expected, only a 1.5σ excess, and indicating 9.6 ± 7.3 of these 51 sources to be $21 \leq B \leq 23$ galaxies. Again, the cross-correlation changes little in amplitude, but becomes less statistically significant, if we use only the $\geq 5\sigma$ subset in our analysis – but the correlation of either source list with galaxies as faint as this is so weak that no significant conclusions can be reached from this comparison.

Looking at the dependence on galaxy colour of the correlation on the GSGP4 field, we find, for the fainter $21 \leq B \leq 23$ galaxies, 46 source/blue galaxy pairs against 38.0 expected by chance and 8 source/red galaxy pairs against 7.9 expected. For the 5σ limit these ratios become 27/20.2 and 7/4.2 respectively. As for $B > 21$ galaxies, no significant difference is evident, but this might be expected at $21 \leq B \leq 23$ where the overall cross-correlation is only a marginal result.

Figure 5.3 shows the cross-correlation functions of $\geq 4\sigma$ and $\geq 5\sigma$ sources with $21 \leq B \leq 23$ galaxies, which obviously show much less signal at small scales ($C_{xg}(0) \simeq 0.2$) than for brighter galaxies.

Magnitude range	Field	No. of galaxies	Galaxies $\leq$ 20 arcsec from an X-ray source			
			$\geq 4\sigma$ list		$\geq 5\sigma$ list	
			seen	expected	seen	expected
B < 18	GSGP4*b*	9	1	0.13	0	0.07
	GSGP4*r*	4	0	0.06	0	0.03
	SGP2	1	0	0.01	0	0.00
	QSF3	6	0	0.05	0	0.02
	TOTAL	20	1	0.25	0	0.12
18 $\leq$ B < 19	GSGP4*b*	13	1	0.19	0	0.10
	GSGP4*r*	13	2	0.19	2	0.10
	SGP2	29	0	0.34	0	0.12
	QSF3	12	0	0.11	0	0.04
	TOTAL	67	3	0.83	2	0.36
19 $\leq$ B < 20	GSGP4*b*	59	3	0.85	0	0.45
	GSGP4*r*	43	1	0.62	1	0.33
	SGP2	64	1	0.76	0	0.26
	QSF3	66	2	0.60	0	0.20
	TOTAL	232	7	2.83	1	1.24
20 $\leq$ B < 21	GSGP4*b*	156	6	2.25	3	1.20
	GSGP4*r*	86	1	1.24	1	0.66
	SGP2	244	6	2.88	2	1.00
	QSF3	254	1	2.31	0	0.79
	TOTAL	740	14	8.68	6	3.65
21 $\leq$ B < 22	GSGP4*b*	516	7	7.46	2	3.97
	GSGP4*r*	211	3	3.05	1	1.62
	SGP2	570	5	6.73	3	2.34
	QSF3	846	12	7.70	3	2.62
	TOTAL	2143	27	24.94	9	10.55
22 $\leq$ B $\leq$ 23	GSGP4*b*	2110	39	30.49	25	16.25
	GSGP4*r*	335	5	4.84	6	2.58
	SGP2	1510	23	17.81	5	6.19
	QSF3	2522	24	22.95	8	7.82
	TOTAL	6477	91	76.09	44	32.84

Table 5.4 The total numbers of galaxies seen on 3 areas of AAT plates corresponding to ROSAT images, and their cross correlation with unidentified X-ray sources detected above 4σ and above 5σ on the ROSAT images. The cross-correlation results are given by listing the numbers of these galaxies which are found to lie within 20 arcsec of the X-ray sources, and the numbers expected in these areas by chance. The results are divided by the B magnitudes of the galaxies into $\Delta(B) = 1^m$ bins, and by field, and the galaxies on the GSGP4 plate are further divided by colour at $B - R = 1.5$ into red (r) and blue (b) subsamples.

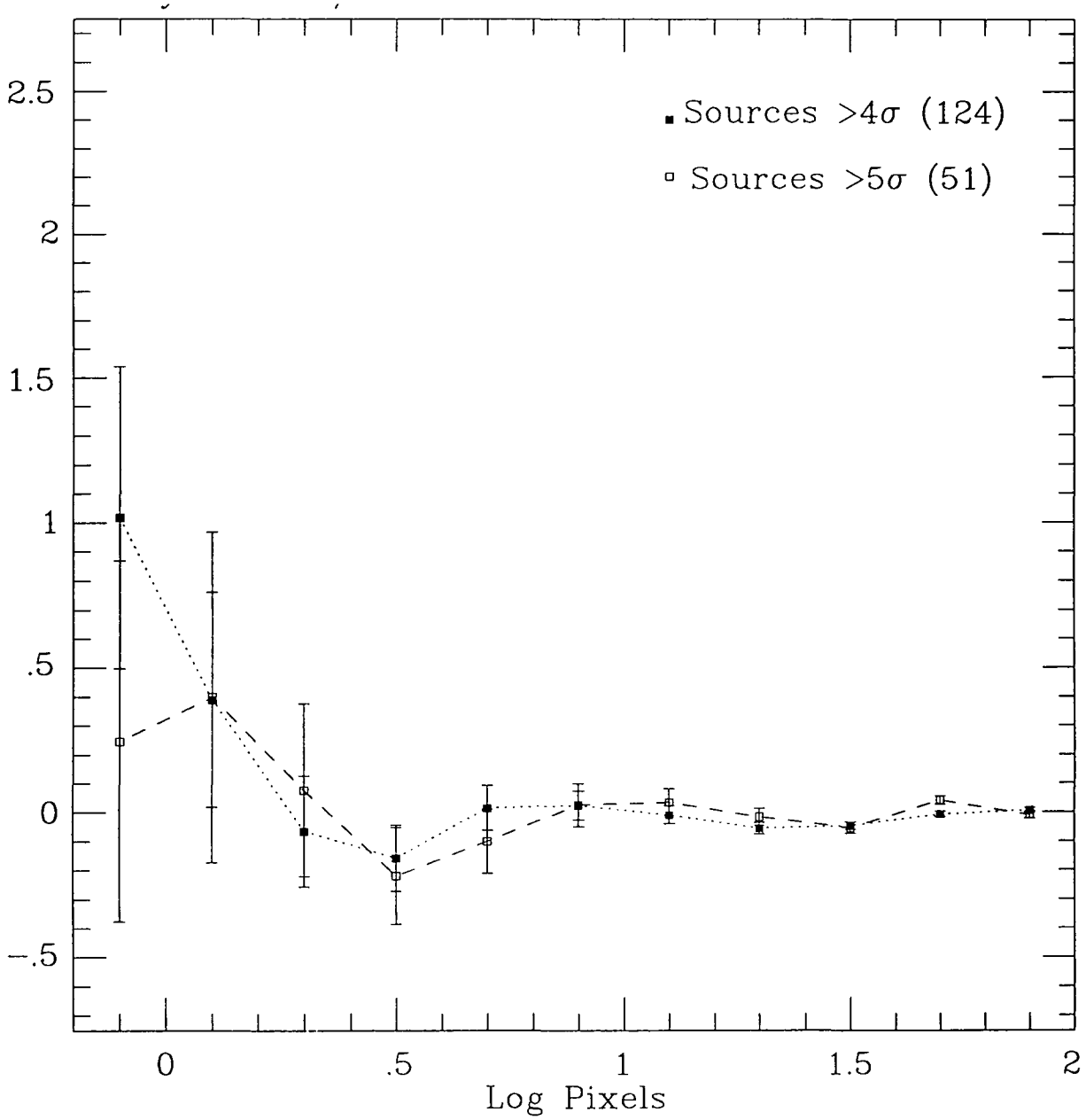

Figure 5.2 The cross-correlation function (with $\sqrt{N}$ error bars) of unidentified X-ray sources detected on 3 ROSAT images and the $B < 21.0$ galaxies on AAT plates of the same areas, plotted against the logarithm of angular separation in units of ROSAT pixels (15 arcsec). The cross-correlation function is shown for the 124 sources detected above 4σ (filled squares, dotted line) and for the subset of these sources, numbering 51, detected above brighter 5σ flux limits (open squares, dashed line) on these images.

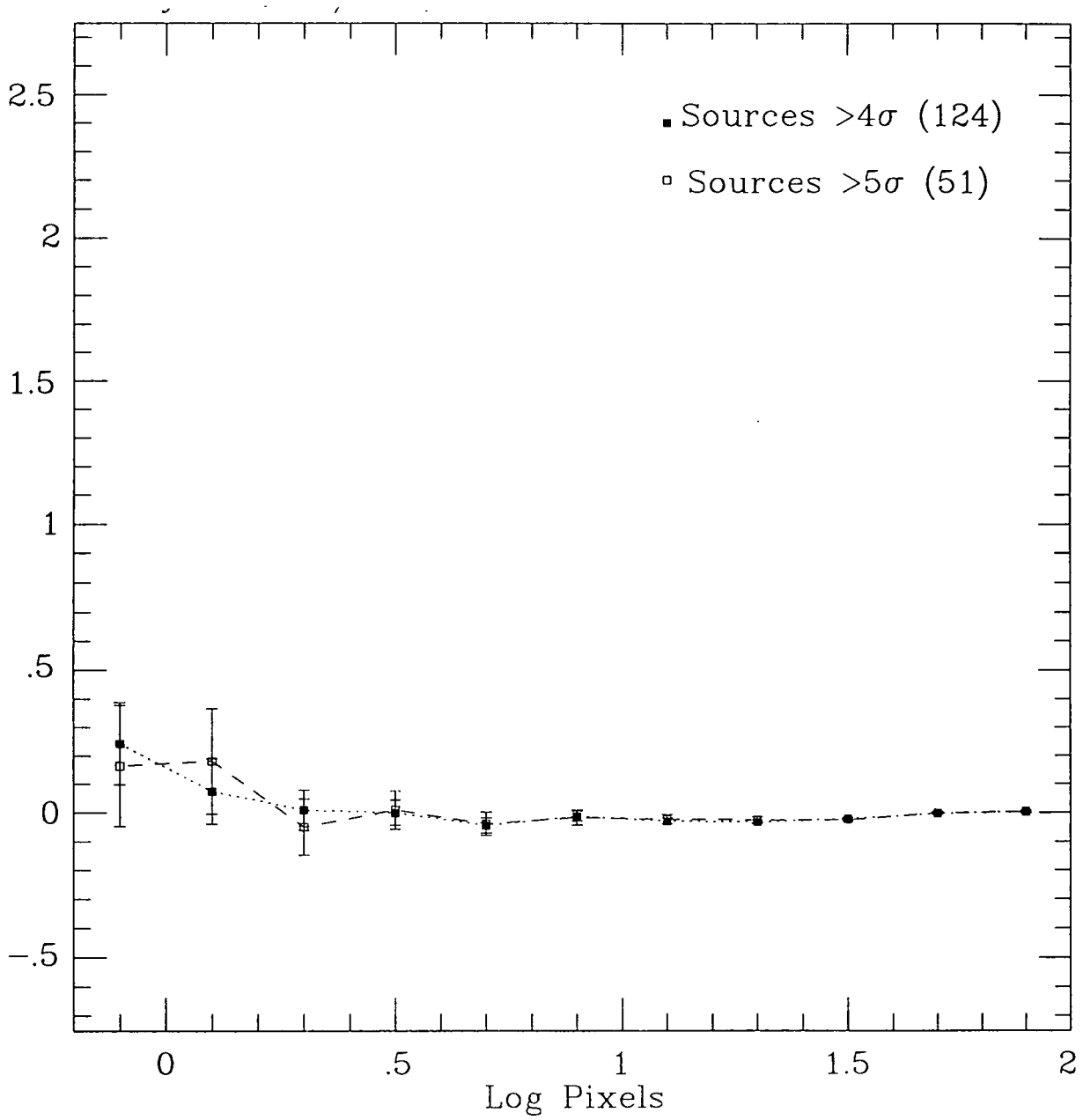

Figure 5.3 The cross-correlation function (with $\sqrt{N}$ error bars) of unidentified X-ray sources detected on 3 ROSAT images and the fainter galaxies, with $21.0 \leq B \leq 23.0$, on AAT plates of the same areas, plotted against the logarithm of angular separation in units of ROSAT pixels (15 arcsec). The cross-correlation function is shown for the 124 sources detected above 4σ (filled squares, dotted line) and for the subset of these sources, numbering 51, detected above brighter 5σ flux limits (open squares, dashed line) on these images.

5.6 Properties of Individual X-Ray Emitting Galaxies

5.6.1 Identification of X-Ray Emitting Galaxies

For a total of 39 X-ray sources on these five fields, the optical counterpart closest to the X-ray position was identified by spectroscopy as a galaxy, and its redshift measured at the same time. The cross-correlation results can give some indication of how many of these galaxies are the genuine X-ray sources.

Of the spectroscopically identified galaxies, 19 appear in the pair counts obtained using UKST, AAT or both optical datasets as $B \leq 21.0$ objects within 20 arcsec of the source position. The source/$B \leq 21.0$ galaxy pair count excess is approximately a factor of two at $\theta < 20$ arcsec, hence $\sim 50\%$ of these galaxies are likely to be the genuine X-ray sources, rather than chance co-incidences. This probability increases to $\sim 65\%$ for the $B < 20.0$ galaxies, for which the pair excess is a factor of 2.8 on the AAT fields.

Table 5.5 gives the R.A. and Dec. co-ordinates of these galaxies, from their positions on the photographic plates. There is evidently good agreement between the UKST and AAT plate astrometry, as the differences between the datasets in the positions obtained are only ~ 1 arcsec. The magnitudes from the two datasets are also closely similar (to $\sim 0.1^m$) except for one galaxy misclassified as a star on the Schmidt plate.

For the QSF fields our list includes three of the five $z = 0.312$ galaxies described by Griffiths et al. (1993) as X-ray luminous galaxies within a possible large-scale structure. The other two $z = 0.312$ galaxies, the $z = 0.180$ elliptical and an eighth galaxy (at $z = 0.238$), which were also listed as possible X-ray sources by Griffiths et al. (1993) are not included here as they are are offset from the source positions by more than 20 arcsec, the radius beyond which we detect no significant cross-correlation.

Only three galaxies fainter than $B = 21.0$ and within 20 arcsec of a $\geq 4\sigma$ detected source were successfully identified spectroscopically, all of these on GSGP4. These three are also listed here, although the cross-correlation of sources with normal galaxies as faint as this is of marginal significance, with only $\sim 20\%$ of pairings with X-ray sources being genuine. However, one of these galaxies (GSGP4X:100) has very strong, narrow emission lines and another (GSGP4X:32) is a cluster-dominating giant elliptical. Hence these two galaxies, belonging to categories of object likely to be more X-ray luminous than most galaxies, will have higher probabilities of being the detected X-ray sources than would be suggested by our cross-correlation with $21 \leq B \leq 23$ galaxies as a whole.

Source	Equinox 2000.0 optical positions			
	UKST		AAT	
	R.A.	Dec.	R.A.	Dec.
GSGP4X:17	00 56 33.947	-27 29 51.73	00 56 33.993	-27 29 51.18
GSGP4X:20			00 56 41.931	-27 46 57.67
GSGP4X:32			00 56 57.013	-27 40 29.43
GSGP4X:48	00 57 17.207	-27 21 46.41	00 57 17.201	-27 21 46.18
GSGP4X:54	00 57 21.192	-27 44 45.74	00 57 21.161	-27 44 45.95
GSGP4X:57			00 57 26.047	-27 43 36.77
GSGP4X:64	00 57 31.649	-27 23 18.45	00 57 31.748	-27 23 19.22
GSGP4X:69	00 57 36.782	-27 33 03.70	00 57 36.808	-27 33 04.01
GSGP4X:82	00 57 49.754	-27 23 04.79	00 57 49.816	-27 23 05.27
GSGP4X:86	00 57 55.658	-27 24 29.37	00 57 55.697	-27 24 31.21
GSGP4X:94	00 58 07.097	-27 34 34.85	00 58 07.097	-27 34 35.50
GSGP4X:100			00 58 13.520	-27 42 10.43
GSGP4X:109	00 58 24.490	-27 29 21.83	00 58 24.511	-27 29 22.56
GSGP4X:114	00 58 36.424	-27 48 47.22	00 58 36.415	-27 48 48.26
SGP2X:25			00 51 51.492	-29 04 18.09
SGP2X:49	00 52 18.124	-29 09 41.16		
SGP3X:6	00 54 03.658	-28 24 16.16		
QSF1X:20	03 41 20.752	-45 11 44.34		
QSF1X:33	03 41 48.926	-45 00 48.73		
QSF1X:64	03 43 06.206	-44 55 03.15		
QSF3X:39	03 42 09.444	-44 17 42.26	03 42 09.560	-44 17 43.97

Table 5.5 The R.A. and Dec co-ordinates of the optical positions of the galaxies we both examined spectroscopically and identified as probable X-ray sources (Section 5.6). These positions are derived from the UKST and AAT plate astrometric transforms, with the positions obtained from the UKST and AAT datasets listed separately (some of these galaxies appear in only one of these datasets). Both sets of co-cordinates are given for the galaxies which are seen in both datasets.

5.6.2 Luminosities and Spectral Classifications

Magnitudes, redshifts, X-ray fluxes and other data for the X-ray detected galaxies are given in Table 5.6. It is clear from the variation in colours and OII line widths that a wide range of galaxy types are represented here, probably the entire Hubble sequence. Where colours are available they cover the range typically seen in galaxy samples of this depth, and although the 3727Å OII emission line was not detected in 9 of the 22 spectra, for 5 galaxies its equivalent width exceeded 20Å, indicating rapid star-forming activity.

The total 0.5–2.0 keV flux produced by these 22 sources is 2.44×10^{-13} ergs cm^{-2}s^{-1}. In comparison, the 127 spectroscopically identified QSOs detected above 4σ on the same five ROSAT images produce in total a 0.5–2.0 keV flux of 2.83×10^{-12} ergs cm^{-2}s^{-1}, which exceeds the total flux of the 22 galaxies in this list by a factor of 11.6, illustrating the large extent to which QSOs dominate the resolved component of the XRB. However, the source/galaxy cross-correlation suggested that a further $\sim$ 14 faint ($21 \leq B \leq 23$) galaxies not included in this list were also 4σ-detected sources, so that the true QSO/galaxy ratio within the resolved component may be closer to $\sim (\frac{22}{36}) \times 11.6 \sim 7$. We discuss and compare the X-ray number counts of galaxies and QSOs in more detail in Section 5.7.

In Figure 5.4 the X-ray fluxes of the 22 galaxy and 127 QSO sources are plotted against the blue apparent magnitudes of the corresponding optical counterparts (using the AAT data where both UKST and AAT magnitudes are available).

Using the luminosity distances, $d_L(z)$, for the spectroscopically measured redshifts of each of the objects (assuming $H_0 = 50$ km s^{-1}Mpc^{-1} and $q_0 = 0.05$), we converted the apparent blue magnitudes m_B to absolute magnitudes (M_B) using the relation

$$M_B = m_B - 5(\log d_L(z) + 5),$$

and the X-ray (0.5–2.0 keV) fluxes, S_X, to X-ray luminosities, L_X, using

$$\text{Log } L_X = \log S_X + 2(\log d_L(z) + 5) + 40.08$$

giving the estimates of M_B and L_X listed in Table 5.7 and plotted on Figure 5.5. In both passbands the k-corrections were neglected, which would be appropriate for a spectral energy distribution $f_\nu \propto \nu^{-1}$. This power-law should reasonably well approximate the X-ray spectra of most sources in this energy range, and the optical spectra of the late-type galaxies and QSOs, so for these objects our estimates of M_B and L_X should be reasonably accurate despite the significant redshifts ($z > 0.15$) of most of the X-ray sources. However, for early-type galaxies, the listed estimates of M_B will be somewhat fainter than those which would be measured in the rest-frame blue-band, the difference increasing with redshift to as much as 1.5^m at $z \sim 0.5$ (see Section 1.3), on account of the steep drop in their spectral energy distributions blueward of $\lambda \simeq 4000$Å.

The absolute magnitudes of the galaxies identified with X-ray sources indicate that they are mainly $L \sim L^*$ galaxies rather than dwarfs. For the 21 detected galaxies (excluding the GSGP4X:32 cluster which we consider in Section 5.6.4 below), the mean M_B estimated as above is -20.89, and the mean redshift, $z_{mean} = 0.22$, is typical for a galaxy sample limited at $B \simeq 21$ (see e.g. BES). The 21 galaxies have high X-ray luminosities of $L_X \sim 10^{41.5}$–10^{43} ergs s^{-1} (the mean of log L_X being 42.2) – greatly exceeding, for example, the *Einstein* satellite estimates of $L_X \sim 10^{39.5}$ ergs s^{-1} for our own galaxy and for M31 (Fabbiano 1989).

The X-ray detected QSOs, which typically lie at much higher redshifts ($z_{mean} = 1.44$), are intrinsically much more luminous objects in both passbands. The mean M_B for the QSOs is -24.67 and the mean log L_X is 44.44, exceeding the mean optical and X-ray luminosities of the 21 galaxies by factors of 32.5 and 174 respectively. QSOs

therefore tend to have L_X/L_B ratios higher than even these X-ray selected galaxies, but there is considerable overlap in the ranges. For the galaxy cluster and two of our strong emission-line galaxies, the L_X/L_B ratio is at least as high as the typical QSO value.

Of the four galaxies in our X-ray detected sample with optical luminosities lower than $M_B = -20.0$, three (GSGP4X:48, GSGP4X:94, and SGP2X:25) show a strong OII emission line (W[OII] > 20Å). These could therefore be classified as starbursting dwarf galaxies, as detected in large numbers at these optical magnitudes in the spectroscopic surveys of BES and Colless et al. (1990). The other two X-ray detected galaxies with W[OII] > 20Å (GSGS4X:100 and QSF1X:33) are much more luminous galaxies at higher redshifts.

The BES spectroscopic survey included an area lying within our GSGP4 field, in which redshifts were measured for 60 galaxies with $b_J \leq 21.5$, and 37 of these were found to have W[OII] $\geq$ 20Å. None of the 60 BES survey galaxies lie within 20 arcsec of any of our X-ray sources. This might be expected for a sample of this size, as we detect only $\sim 1\%$ of all $B \sim 21$ galaxies on these ROSAT images. However, the failure of ROSAT to detect even one of the strong emission line galaxies may suggest that the proportion of starburst galaxies with very high L_X/L_B ratios does not greatly exceed the proportion with high L_X/L_B ratios in the galaxy population as a whole.

Indeed, the fraction of galaxies with strong emission lines in our X-ray selected sample is actually a little lower than that in the B-limited BES sample, and some of our galaxies show no evidence of any recent star-forming activity. Hence the unusually high X-ray luminosities of the galaxies in our X-ray selected sample do not appear to be associated in all cases with ongoing star-forming activity. A number of different mechanisms of X-ray emission are likely to be involved for the various types of galaxy represented.

If we now divide our X-ray detected galaxies, excluding the cluster, into 9 'star-forming galaxies' with W[OII] $\geq$ 10Å and 12 'passive galaxies' with W[OII] < 10Å, the two subsets are seen to possess similar mean X-ray luminosities (the mean log L_X = 42.22 for the star-forming galaxies compared to a mean log L_X = 42.18 for the passive galaxies), but there is some indication that the passive galaxies are on average slightly more luminous in the blue band (mean $M_B = -21.14$ compared to $M_B = -20.56$ for the star-forming galaxies). When the large k-corrections of early-type galaxies are taken into account this difference becomes more significant – for an E/S0 type at the mean redshift of $z = 0.22$, the k-correction (from MSFJ) is 0.98^m, so that the mean rest-frame blue absolute magnitude of the X-ray detected passive galaxies will be closer to $M_B = -22.12$, which is definitely above M_B^* in optical luminosity.

The absolute magnitudes of the 'star-forming' subset of our X-ray detected galaxies seem consistent with the hypothesis that spiral/irregular galaxies with high L_X/L_B ratios randomly sample the optical luminosity function of late-type galaxies, over the full range from dwarfs to giants. This would be expected if the relation between L_X and L_B for these galaxies is linear, but with a wide dispersion in L_X/L_B ratios.

However, the higher mean absolute magnitudes of our 'passive' subset of X-ray detected galaxies suggests that early-type galaxies with high L_X/L_B ratios tend to be those with the highest ($L_B > L_B^*$) optical luminosities. This would imply a non-linear relation $L_X \propto (L_B)^\epsilon$ with $\epsilon > 1$. There is indeed some indication from *Einstein* surveys (Fabbiano 1989) that, whereas spiral galaxies and $L_B \leq L_B^*$ ellipticals tend to follow a linear relation between L_X and L_B, for early-type galaxies at the highest optical and X-ray luminosities ($L_B > L_B^*$ and $L_X > 10^{41}$ ergs s^{-1}) this relation is closer to $L_X \propto (L_B)^{1.6}$. We discuss possible physical causes for this difference in Section 7.11.

The fact that our X-ray detected galaxies of early type tend to be those with $L_B > L_B^*$ (i.e. giant ellipticals) appears to agree with these *Einstein* survey findings, but a larger sample of X-ray detected galaxies than were identified on these ROSAT images would be required to investigate in detail the relation between the X-ray properties of galaxies and their morphological/spectral type.

ROSAT source	UKST		AAT		Redshift	W[OII]	0.5–2.0 keV flux
	B mag	B-R	B mag	B-R		Å	10^{-15} ergs cm^{-2}s^{-1}
GSGP4X:17	18.51	1.43	18.69	1.61	0.105		39.2
GSGP4X:20			21.54	1.96	0.382		3.51
GSGP4X:32			21.54	2.33	0.561		24.6
GSGP4X:48	20.61	0.61	20.49	0.76	0.155	37	30.0
GSGP4X:54	20.20	0.91	20.24	1.30	0.214	12	2.98
GSGP4X:57			19.81	1.06	0.161	19	2.84
GSGP4X:64	18.08	1.50	18.01	1.71	0.097		8.77
GSGP4X:69	20.49	1.65	20.52	1.74	0.213	7	8.53
GSGP4X:82	19.12	1.28	19.10	1.49	0.204	4	4.54
GSGP4X:86	18.18	1.48	18.16		0.161		4.36
GSGP4X:94	20.46	0.64	20.37	1.01	0.120	24	6.50
GSGP4X:100			22.17	1.51	0.597	51	5.80
GSGP4X:109	13.93s		16.78		0.098	4	4.83
GSGP4X:114	19.17	1.08	19.16		0.211	17	7.00
SGP2X:25			20.96		0.202	41	5.11
SGP2X:49	20.67s	1.56			0.106		6.73
SGP3X:6	19.02	2.45			0.258		20.1
SGP3X:33	19.10	1.70			0.195	8	11.8
QSF1X:20	19.66s				0.312		28.2
QSF1X:33	19.57s				0.312	60	5.66
QSF1X:64	19.89				0.253	11	8.52
QSF3X:39	19.57s		19.80s		0.312		4.48

Table 5.6 X-ray (0.5–2.0 keV) fluxes and optical data for the galaxies we both examined spectroscopically and identified as probable X-ray sources (Section 5.6). The optical data includes redshifts for all galaxies, and O(II) 3727Å equivalent widths for galaxies with spectra in which this emission line was strong enough to be detected (for the galaxies where no line-width is listed, W[OII] is probably less than $\sim$ 5Å), blue magnitudes and $B - R$ colours (for the fields where red-band data was also available), with the magnitudes and colours obtained from the UKST and AAT datasets listed separately. A letter 's' after a listed optical magnitude indicates that the galaxy was misclassified as a star on the respective optical dataset.

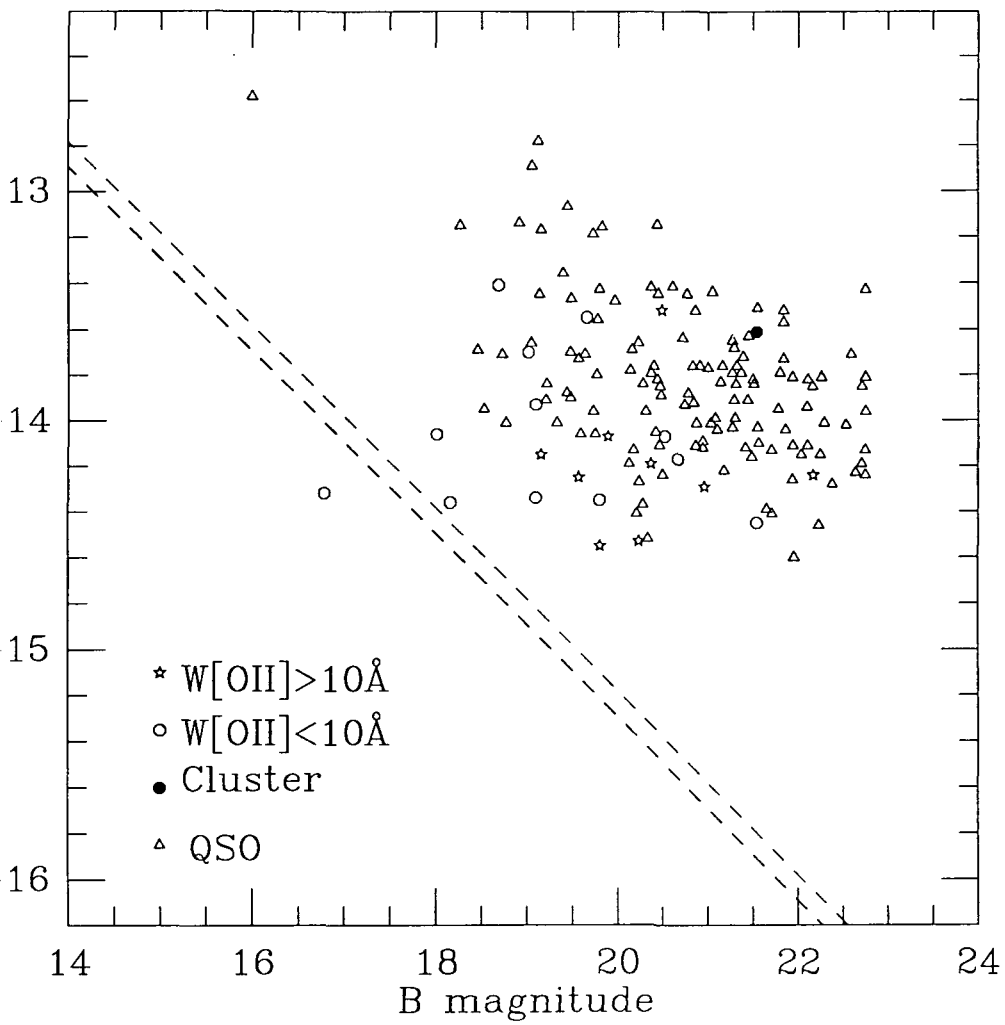

Figure 5.4 The 0.5–2.0 keV X-ray fluxes plotted against blue-band apparent magnitudes for our sample of spectroscopically examined X-ray sources, consisting of the galaxies identified as probable X-ray sources in Section 5.6 (divided by the equivalent width of the OII(3727Å) emission line in their optical spectra), the X-ray detected GSGP4X:32 cluster, and the X-ray detected QSOs on the same areas of sky. The dashed lines show the $\pm 1\sigma$ upper and lower limits on the mean X-ray/blue-band flux ratio we estimated for $18 \leq B \leq 23$ galaxies from their cross-correlation with the XRB (Chapter 7).

Source	Estimated M_B	Estimated log L_X (ergs s^{-1})	log (f_ν(2keV/f_ν(B))
GSGP4X:17	-20.41	42.31	-4.30
GSGP4X:20	-20.62	42.49	-4.21
GSGP4X:32	-21.60	43.73	-3.36
GSGP4X:48	-19.50	42.55	-3.70
GSGP4X:54	-20.51	41.85	-4.80
GSGP4X:57	-20.27	41.57	-4.99
GSGP4X:64	-20.91	41.59	-5.22
GSGP4X:69	-20.22	42.31	-4.23
GSGP4X:82	-21.54	41.99	-5.07
GSGP4X:86	-21.92	41.75	-5.47
GSGP4X:94	-19.04	41.66	-4.41
GSGP4X:100	-21.13	43.16	-3.74
GSGP4X:109	-22.16	41.34	-5.97
GSGP4X:114	-21.56	42.21	-4.86
SGP2X:25	-19.65	42.03	-4.28
SGP2X:49	-18.45	41.56	-4.27
SGP3X:6	-22.18	42.86	-4.46
SGP3X:33	-21.43	42.36	-4.66
QSF1X:20	-22.00	43.19	-4.06
QSF1X:33	-22.09	42.50	-4.79
QSF1X:64	-21.26	42.47	-4.48
QSF3X:39	-21.86	42.39	-4.80

Table 5.7 The 0.5–2.0 keV X-ray luminosities and blue-band absolute magnitudes, derived assuming $H_0 = 50$km s^{-1}Mpc^{-1} and $q_0 = 0.05$, and neglecting k-corrections, together with the ratio of X-ray to blue-band flux, expressed as log $f_\nu(2\text{ keV})/f_\nu(B)$, which is independent of H_0 and q_0, for the list of galaxies identified as probable X-ray sources (Section 5.6).

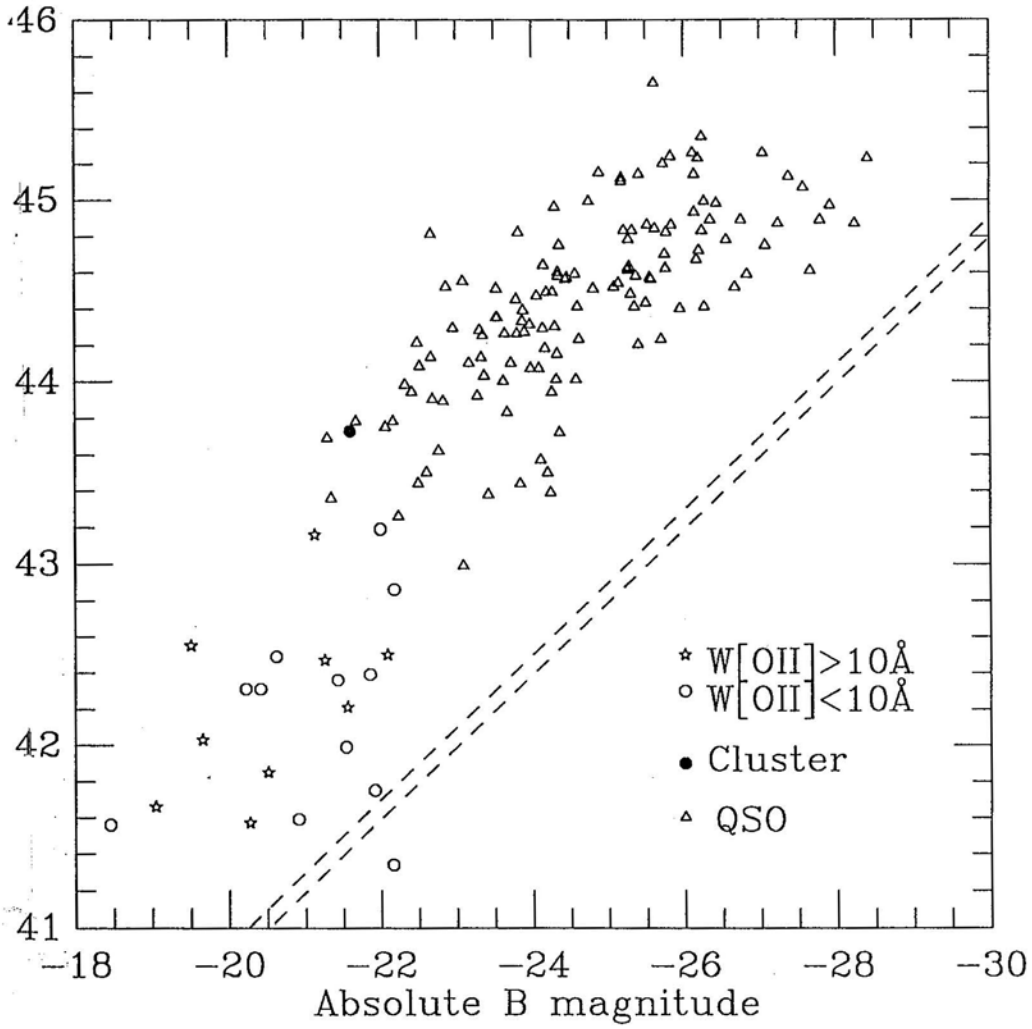

Figure 5.5 The 0.5–2.0 keV X-ray luminosities plotted against blue-band absolute magnitudes, derived assuming $H_0 = 50$ km s^{-1}Mpc^{-1} and $q_0 = 0.05$, and neglecting k-corrections, for our sample of spectroscopically examined X-ray sources, consisting of the galaxies identified as probable X-ray sources in Section 5.6 (divided by the equivalent width of the OII(3727Å) emission line in their optical spectra), the X-ray detected GSGP4X:32 cluster, and the X-ray detected QSOs on the same areas of sky. The dashed lines show the $\pm 1\sigma$ upper and lower limits on the mean L_X/L_B luminosity ratio we estimated for $18 \leq B \leq 23$ galaxies from their cross-correlation with the XRB (Chapter 7).

5.6.3 The X-Ray/Blue-band Flux Ratio

Figure 5.6 shows the monochromatic flux ratio $f_\nu(2\text{ keV})/f_\nu(B)$ plotted against redshift for the 22 galaxy and 127 QSO sources. This was estimated by again assuming a $f_\nu \propto \nu^{-1}$ spectral energy distribution which gave

$$f_\nu(2\text{ keV}) = 1.492 \times 10^{-18} S(0.5\text{–}2.0\text{ keV})\text{ Hz}^{-1}$$

Using the relation, given by LCG, between flux and the blue magnitude system used on these photographic plates (b_J);

$$\log f_\nu(B) = -0.4(b_J + 48.65)$$

we can estimate a logarithmic flux ratio

$$\log (f_\nu(2\text{ keV})/f_\nu(B)) = 1.63 + \log S + 0.4 b_J.$$

A galaxy with $B = 20.0$, for example, would require $f_\nu(2\text{ keV})/f_\nu(B) > 10^{-4.87}$ to be detected above our flux limit of $\log S \simeq -14.5$. It is therefore not surprising that the $f_\nu(2\text{ keV})/f_\nu(B)$ ratios of the galaxies in our X-ray selected sample (Table 5.7) are considerably higher than the $f_\nu(2\text{ keV})/f_\nu(B) \sim 10^{-6.6}$ ratio typical of normal galaxies (see e.g. Fabbiano 1989, Giacconi and Zamorani 1987).

In Chapter 7 we estimate a mean X-ray/B-band flux ratio for faint galaxies an order of magnitude higher ($f_\nu(2\text{ keV})/f_\nu(B) \simeq 10^{-5.6}$), by cross-correlating $18 \leq B \leq 23$ galaxies with the unresolved XRB. The dashed lines in Figures 5.4, 5.5 and 5.6 show the $\pm 1\sigma$ range of this estimate of the mean ratio. We see that this higher ratio is also exceeded by all the $B > 18.0$ galaxies detected individually on these ROSAT images.

The mean value of $\log (f_\nu(2\text{ keV})/f_\nu(B))$ is estimated as -4.67 ± 0.12 for the $B < 21.0$ galaxies in our X-ray detected sample, and -3.77 ± 0.25 for those with $21.0 \leq B \leq 23.0$. As noted in Section 5.5.2 above, comparing the numbers of $B < 21.0$ galaxies detected on these X-ray images, as given by the excess in the source/galaxy pair counts, with the total numbers of $B < 21.0$ galaxies on the photographic plates suggests that their logarithmic flux ratios, $\log (f_\nu(2\text{ keV})/f_\nu(B))$, are typically 2.5σ above the mean value of all galaxies, and for $21.0 \leq B \leq 23.0$ galaxies (see Section 5.5.3) this increases to 3.1σ. This could be explained if $\log (f_\nu(2\text{ keV})/f_\nu(B))$ for $0 \leq z \leq 0.6$ galaxies possesses a very broad, approximately Gaussian distribution, centred on the typical value for local galaxies of $\log (f_\nu(2\text{ keV})/f_\nu(B)) \simeq -6.6$, but with a very large dispersion of $\sigma \sim 0.8$ (so that, e.g. 2.5σ corresponds to a factor of ~ 100 in L_X/L_B).

Of the galaxies in our sample, the highest flux ratios are found for the cluster-dominating galaxy at $z = 0.561$ and for emission line galaxies at $z = 0.155$ and $z = 0.597$. As two of these sources lie at $z > 0.5$, Figure 5.6 may give the impression that the L_X/L_B ratio of galaxies tends to increase with redshift. However, L_X/L_B ratios similar to that estimated here for the $z = 0.561$ cluster have been obtained for massive, cluster-dominating galaxies at lower redshifts, including M87 in Virgo (Fabbiano 1989). Futhermore, at higher redshifts larger volumes are sampled, containing thousands of galaxies within the solid angle and magnitude limit of an AAT plate, and therefore it is more likely that galaxies in the extreme upper $\sim 0.1\%$ of the distribution of flux ratios will be detected. In contrast, typical $L \sim L^*$ QSOs are sufficiently luminous, in both X-ray and blue wavelengths, to be detected on both the ROSAT images and the AAT plates out to high redshifts, and therefore our survey is not biassed towards detecting QSOs with particularly high L_X/L_B ratios. The fact that no significant trend in L_X/L_B ratios with redshift is seen for QSOs simply reflects their very similar rates of luminosity evolution in the X-ray and blue passbands (Boyle et al. 1993).

The possibility does remain that the X-ray luminosity function of normal galaxies has undergone considerable brightening of its characteristic luminosity (L_X^*) even at

$z \sim 0.2$, and in this case less dispersion in the L_X/L_B ratios at a given redshift would be required to explain the detected cross-correlation. For example, in the case of the late-type, galaxies in our sample, with strong emission lines, an increase of L_X/L_B with redshift could be caused by increased star-formation activity (and consequently greater numbers of massive X-ray binaries) compared to galaxies seen locally. We discuss the possible X-ray luminosity evolution of galaxies in more detail in Sections 7.8 and 7.9.

X-ray surveys to fainter flux limits, with higher resolution imaging (FWHM < 5 arcsec) to reduce the confusion problem caused by the high surface density of faint galaxies, will be needed to determine the true form of the X-ray luminosity function of normal galaxies, and its evolution with redshift. This has been done already for the much more luminous QSOs (Boyle et al. 1993). However, as even galaxies with $L_X \sim 10^{42}$ ergs s^{-1}, such as those identified here, will be about two orders of magnitude fainter than QSOs at comparable redshifts, we may need to reach considerably fainter X-ray flux limits of $S \sim 10^{-15}$–10^{-16} ergs $cm^{-2}s^{-1}$ to quantify directly the X-ray luminosity evolution of galaxies.

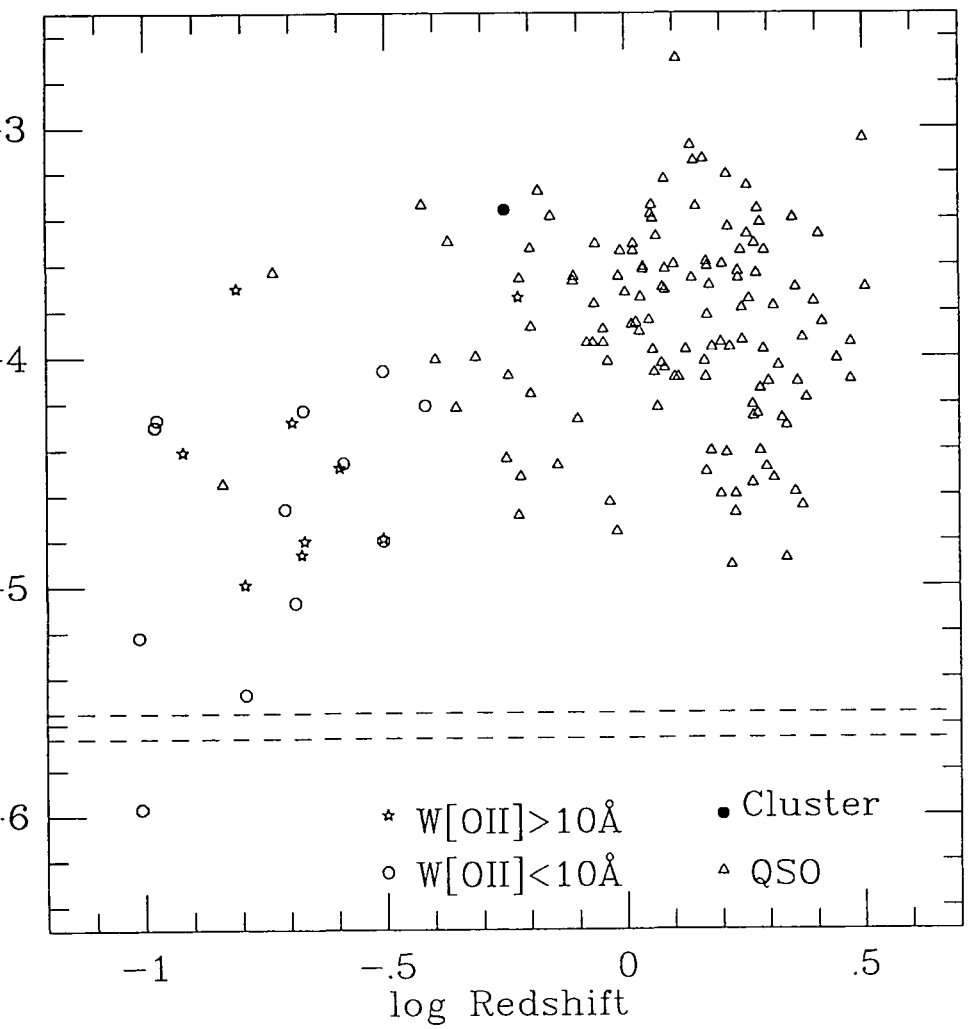

Figure 5.6 The logarithm of the monochromatic flux ratio $f_\nu(2\text{ keV})/f_\nu(B)$ plotted against the logarithm of the redshift for our sample of spectroscopically examined X-ray sources, consisting of the galaxies identified as probable X-ray sources in Section 5.6 (divided by the equivalent width of the OII(3727Å) emission line in their optical spectra), the X-ray detected GSGP4X:32 cluster, and the X-ray detected QSOs on the same areas of sky. The dashed lines show the $\pm 1\sigma$ upper and lower limits on the mean $f_\nu(2\text{ keV})/f_\nu(B)$ ratio we estimated for $18 \leq B \leq 23$ galaxies from their cross-correlation with the XRB (Chapter 7).

5.6.4 Detection of a High Redshift Cluster

One of the brighter X-ray sources, GSGP4X:32, was found to coincide (within 5 arcsec) with a giant elliptical at the centre of a remote ($z = 0.561$) cluster. The cluster was first discovered on an AAT plate of the area – optical observations including CCD photometry are described by Couch et al. (1985). It was found to be between half and two-thirds as rich as the Coma cluster, and more clumped in structure, and was given an Abell richness class of 1. The cluster possesses a 'central dominant' galaxy, more than $\sim 1^m$ brighter than any of the associated cluster galaxies, with a double nucleus (separation of the two components ~ 3.5 arcsec). Multiband (BVRI) photometry appeared to indicate a moderate amount of spectral evolution towards bluer colours, consistent with the Bruzual (1981) $\mu = 0.5$ model at this redshift.

Although the resolution of the ROSAT PSPC is inadequate to study the structure of the X-ray emission in detail, this source did appear to be somewhat extended (FWHM $\sim$ 50 arcsec), whereas all other X-ray sources on these five images were consistent with being point-like. After subtraction in quadrature of the ROSAT PSF width, the source FWHM was ~ 40 arcsec, corresponding at this redshift to 300–350 kpc (for $H_0 = 50$ km $s^{-1}Mpc^{-1}$ and $0.0 \leq q_0 \leq 0.5$).

The $z = 0.561$ cluster possesses a high X-ray luminosity estimated in the ROSAT band as

$$L_X \simeq 5.4 \times 10^{43} \text{ ergs s}^{-1}.$$

However, although this is the highest L_X of any of our 22 galaxy sources, it is not unusual for a rich cluster, as opposed to a single galaxy. Indeed the Coma cluster has a considerably higher X-ray luminosity, estimated from *Einstein* observations (Abramopoulos and Ku 1983) as

$$L_X(0.5\text{–}4.0 \text{ keV}) = 51.3 \times 10^{43} \text{ ergs s}^{-1}.$$

Thermal bremsstrahlung emission from hot gas produces an exponential spectral energy distribution of the form

$$f_\nu \propto \exp(-h\nu/kT).$$

Assuming an SED of this form with a gas temperature of $kT \simeq 7$–8 keV, typical of rich clusters such as Coma, the X-ray luminosity in the rest-frame energy band of 0.78–3.12 keV, which corresponds to 0.5–2.0 keV at $z = 0.561$, can be estimated as

$$L_X(0.78\text{–}3.12 \text{ keV}) \simeq 0.69 L_X(0.5\text{–}4.0 \text{ keV}),$$

Hence for a cluster identical to Coma at $z = 0.561$, the X-ray luminosity observed in the ROSAT band would be

$$L_X \simeq 35.4 \times 10^{43} \text{ ergs s}^{-1}.$$

The X-ray luminosity of clusters was estimated by Abramopoulos and Ku (1983) to relate to their richness N as $L_X \propto N^{1.2}$, so we would expect the GSGP4X:32 cluster, being of $\frac{1}{2}$–$\frac{2}{3}$ Coma richness, to produce 43–61% of its X-ray luminosity, i.e.

$$L_X \simeq (15.2\text{–}21.6) \times 10^{43} \text{ ergs s}^{-1}.$$

which is considerably higher than the observed luminosity. We estimate that the X-ray luminosity of GSGP4X:32 is only 25–36% of that expected for a cluster of similar richness at the present day. The relatively low L_X of this one cluster may indicate that there has been some increase in the X-ray luminosities of rich galaxy clusters in general since the epochs corresponding to $z \sim 0.5$, i.e. a negative evolution with redshift, although it is obvious that larger samples of X-ray detected clusters at these redshifts will be required to verify this. We discuss the X-ray luminosity evolution of clusters further in Section 8.4.2.

5.7 Galaxy Number Counts at 0.5–2.0 keV

In addition to cross-correlating X-ray sources with the galaxies divided by their optical magnitudes and/or colours, we can also cross-correlate the sources brightward of a given X-ray flux limit with the full ($B \leq 23.0$) galaxy sample. In this way we can derive an estimate of the galaxy number counts as a function of X-ray flux. As our dataset includes only those galaxies optically brighter than $B = 23.0$, the total X-ray band number count of galaxies may be underestimated somewhat. However, as we have found a much higher proportion of $B < 21$ galaxies to be correlated with the sources than is the case for $21 \leq B \leq 23$ galaxies, even fainter ($B > 23$) galaxies are likely to comprise only a small proportion of the total X-ray counts of galaxies until even fainter X-ray flux limits are reached.

The $\geq 4\sigma$ detected X-ray sources brighter than a series of flux limits from log $S = -13.6$ to log $S = -14.6$ were cross-correlated with all $B \leq 23.0$ galaxies on the three areas covered by AAT plates. The integral galaxy number count as a function of X-ray flux was then estimated by subtracting the numbers of galaxies expected within 20 arcsec of a source from the number actually counted ($N_{xg}(\theta \leq 20)$) for the sources brightward of each chosen flux limit. The excess number of galaxies near sources was then divided by the total area of 1.05 deg^2, to give a number count of 'correlated' galaxies, shown on Figure 5.7, with the statistical errors estimated as $\sqrt{N_{xg}(\theta \leq 20)}$. A statistically significant correlation is only seen at flux limits of log $S = -14.2$ and fainter.

The graph also shows the number count as a function of flux limit of the 18 identified galaxies (Tables 5.5, 5.6 and 5.7) which lie on the 3 fields covered by AAT plates. As these are mainly $B < 21$ galaxies, which show a more significant cross-correlation with X-ray sources than do $21 \leq B \leq 23$ galaxies, this number count will show smaller statistical errors than the count of 'correlated' galaxies, particularly at brighter flux limits. However, this identified galaxy count will be an underestimate at the fainter flux limits. Table 5.8 lists the two versions of the X-ray galaxy counts together with the mean redshift as a function of flux limit for the identified galaxies.

Figure 5.7 and Table 5.8 also include the number count and mean redshift data of the 72 spectroscopically identified QSOs detected above 4σ on the same 3 ROSAT fields. We only include the QSO data for these 3 fields, so the effect of the flux limits of the ROSAT images on the QSO number counts will be exactly the same as for the galaxies.

To $S \sim 10^{-14}$ ergs cm^{-2}s^{-1}, the galaxy and QSO counts both increase to fainter flux limits with approximately Euclidean gradients of $\gamma \simeq 1.5$ (i.e. $\frac{d(\log N)}{d(\log S)} = -1.5$). Between log $S = -14.4$ and log $S = -14.6$ the galaxy count gradient levels out somewhat, presumably as a result of incompleteness in the source detection, as the various 4σ limits of the fields are reached at log $S \sim -14.5$. To obtain an estimate of the galaxy count in the 0.5–2.0 keV band we therefore normalize to the count of correlated galaxies at a flux limit of log $S = -14.4$ (i.e. 27.2 ± 10.4 deg^{-2}), giving:

$$\log N(< S) = -1.5(\log S + 14) + 0.83^{+0.14}_{-0.21}$$

The dotted line on Figure 5.7 shows a count slope with this gradient ($\gamma = 1.5$) and normalization. This corresponds to a surface density of detected galaxies of 6.8 ± 2.6 deg^{-2} brighter than log $S = -14.0$, increasing to 38.4 ± 14.6 deg^{-2} at a flux limit of log $S = -14.5$, and 216 ± 82 deg^{-2} at log $S = -15.0$.

The QSO number count is higher than that of galaxies by a factor of 6.4 at log $S = -14.0$, but faintward of this flux limit the QSO count slope flattens considerably, to a log N–log S power-law index of $\gamma = 0.61$ at log $S = -14.1$ and $\gamma = 0.24$ at log

$S \leq -14.3$. Extrapolating the QSO counts with a $\gamma = 1.5$ slope beyond $\log S = -14.0$ predicts a surface density at $\log S = -14.4$ of 174.4 ± 25.7 deg^{-2}, while only 64.8 ± 7.9 deg^{-2} are identified at this limit.

The cross-correlation of unidentified X-ray sources with objects classed as $21 \leq B \leq 23$ stars (Section 5.5.3) suggested that the QSO count at the X-ray source detection limit is underestimated by 16.2 ± 5.9 deg^{-2} due to incompleteness in the optical spectroscopy. Adding this estimate to the density of identified QSOs gives 81.0 ± 9.8 deg^{-2}, which is still less than half the Euclidean extrapolation, the difference between the two being of 3.4σ significance. In contrast, the galaxy counts are not seen to fall significantly below the Euclidean slope until incompleteness of the source detection becomes significant at $\log S \leq -14.4$.

Hence the observed flattening of the QSO count gradient does not appear to be due entirely to incompleteness in either the X-ray source detection or the optical spectroscopy, and instead must reflect the fact that QSOs are seen out to a real or 'effective' (ie. caused by the comoving volume element reduction discussed in Section 4.5) redshift maximum at $\log S \sim -14$, where the mean redshift of spectroscopically identified QSOs is indeed seen to exceed $z_{mean} = 1.25$.

The galaxies we find to be correlated with detected X-ray sources are at much lower redshifts than the QSOs ($z_{mean} = 0.22$), so the galaxy $N(z)$ continues to become more extended and the galaxy counts continue to increase steeply to much fainter X-ray fluxes. In the blue band the galaxy counts increase as $\gamma = 1.1$–1.2 (i.e. $\frac{d(logN)}{dm} = 0.44$–$0.48$), until z_{max} appears to be reached at $B \sim 25$–26. Even steeper count slopes ($\gamma \simeq 1.5$) have been measured for the bluer galaxies only, and for U-limited samples of faint galaxies (Guhathakurta 1991). These gradients are perhaps more appropriate for comparison with X-ray observations, where the large B-band k-correction of early-type galaxies will not apply. Flattening of the number count slope is not seen in the blue-band until $\sim 5^m$ fainter than typical blue magnitudes of the X-ray detected galaxies discussed in Section 5.6 above, so we might expect the steep ($\gamma \sim 1.5$) increase in the galaxy counts in the ROSAT band to continue to at least $S \simeq 10^{-16}$ ergs cm^{-2}s^{-1}. This is predicted by the X-ray band galaxy count models of Griffiths and Padovani (1990), Treyer et al. (1992), and in Section 7.10 of this thesis.

In summary, comparing, as a function of X-ray flux limit, the cross-correlation of X-ray sources with galaxies and the correlation with QSOs indicates that QSOs are a much larger component (indeed, the dominant component) of the X-ray source counts than are galaxies to flux limits of $S(0.5$–2.0 keV$) = 10^{-14}$ ergs cm^{-2}s^{-1}, where they exceed the galaxies in number and flux contribution by a factor of at least ~ 6. However, at $S < 10^{-14}$ ergs cm^{-2}s^{-1}, number counts of QSOs level out, falling significantly below a Euclidean ($\gamma = 1.5$) extrapolation, whereas those of galaxies continue to rise steeply ($\gamma \sim 1.5$), and may continue to do so to fluxes a further 2 orders of magnitude faintward. We would therefore expect the ratio of galaxy flux to QSO flux to be much higher within the unresolved $\sim 65\%$ of the XRB, which contains the integrated emission of all sources faintward of the 4σ detection threshold. For an even deeper survey detecting sources to a flux limit of 10^{-15} ergs cm^{-2}s^{-1}, we predict the surface density of detected galaxies to reach $N \simeq 200$ deg^{-2}, perhaps exceeding that of QSOs.

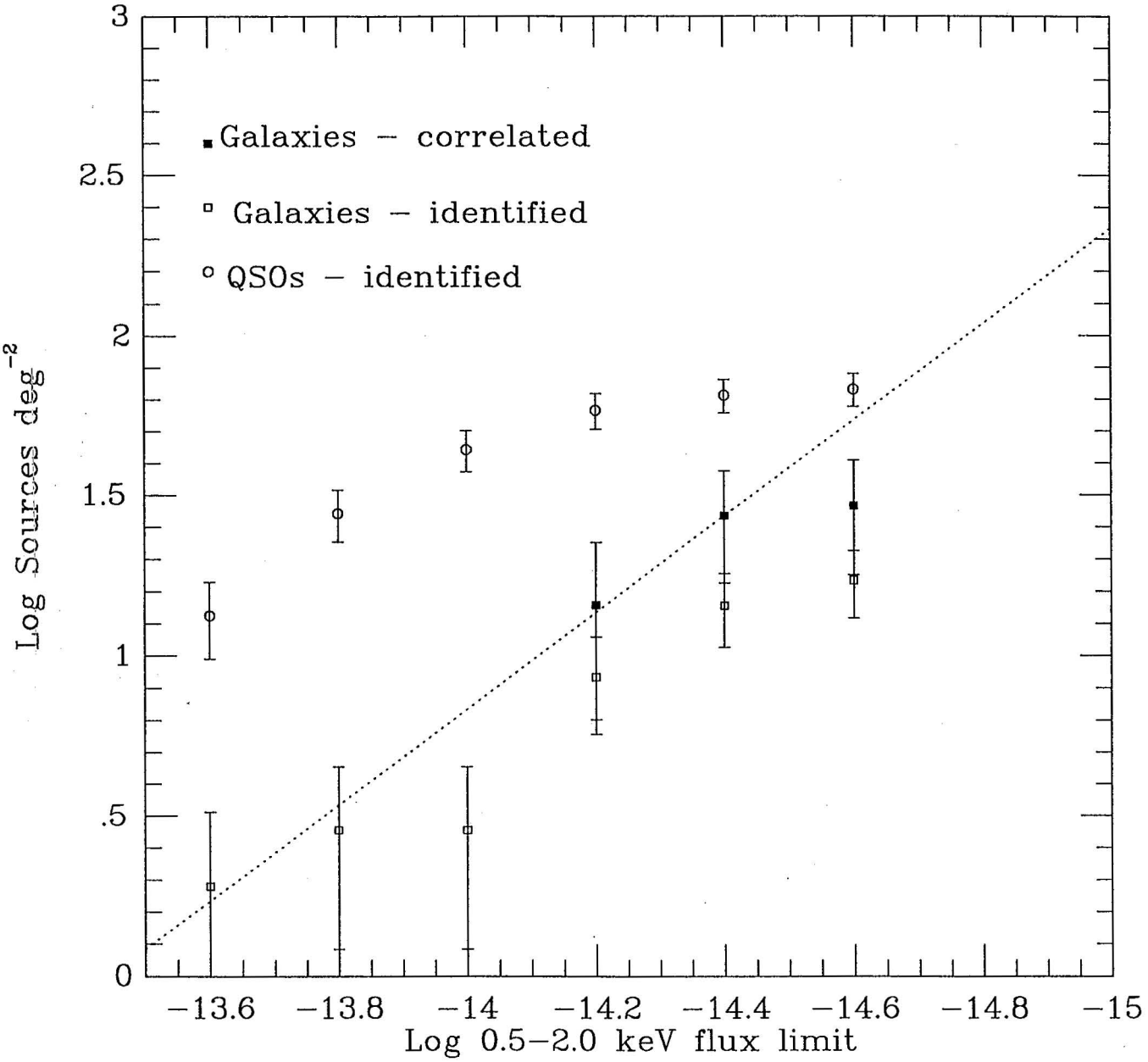

Figure 5.7 Integral X-ray number counts of sources detected on the GSGP4, SGP2 and QSF3 ROSAT images, in units of sources deg^{-2}, over a series of S(0.5–2.0 keV) flux limits from $10^{-13.6}$ to $10^{-14.6}$ ergs cm^{-2}s^{-1}. The counts shown are those of spectroscopically identified QSOs, the galaxies *identified* as probable X-ray sources from the list of Section 5.6, and an estimate of the total X-ray number count of $B \leq 23.0$ galaxies from the numbers found to be *correlated* with sources in Section 5.7. All three counts are shown with $\sqrt{N}$ errors. The dotted line shows a Euclidean slope normalized to the correlated galaxy count at $S = 10^{-14.4}$ ergs cm^{-2}s^{-1}.

Log Flux limit	Correlated Galaxies	Identified Galaxies		Identified QSOs	
	deg^{-2}	deg^{-2}	z_{mean}	deg^{-2}	z_{mean}
-13.6		1.905 ± 1.347	0.13	13.33 ± 3.56	0.93
-13.8		2.857 ± 1.650	0.27	27.62 ± 5.13	1.11
-14.0		2.857 ± 1.650	0.27	43.81 ± 6.46	1.26
-14.2	14.35 ± 8.02	8.571 ± 2.857	0.20	58.10 ± 7.44	1.35
-14.4	27.18 ± 10.35	14.29 ± 3.69	0.23	64.76 ± 7.85	1.40
-14.6	29.18 ± 11.35	17.14 ± 4.04	0.23	67.62 ± 8.02	1.41

Table 5.8 Integral X-ray number counts of sources detected on the GSGP4, SGP2 and QSF3 ROSAT images, in units of sources deg^{-2}, over a series of S(0.5–2.0 keV) flux limits from $10^{-13.6}$ to $10^{-14.6}$ ergs $cm^{-2}s^{-1}$, with $\sqrt{N}$ errors. The counts listed include (i) an estimate of of the total number X-ray number count of $B \leq 23.0$ galaxies from the numbers found to be *correlated* with sources in Section 5.7, (ii) the number count of galaxies *identified* as probable X-ray sources on these 3 fields, from the list of Section 5.6, and (iii) the spectroscopically identified QSOs detected on these 3 fields. For the galaxies and QSOs in number counts (ii) and (iii), which all have measured spectroscopic redshifts, the mean redshift as a function of flux limit is also listed.

5.8 The Source/Galaxy Cross-Correlation at a Constant Flux Limit

It was noted in Sections 5.4.2 and 5.5.2 that most of our observed positional correlation between X-ray sources and galaxies is seen on one of our five ROSAT fields, i.e. GSGP4. This is also apparent from Tables 5.5, 5.6 and 5.7, where 14 of the 22 galaxies we identify as probable X-ray sources lie on GSGP4 compared to 2 on SGP2, 2 on SGP3, 3 on QSF1 and 1 on QSF3.

Cross-correlation of X-ray sources with galaxies, as a function of their X-ray flux (Section 5.7 above), indicated that most of the observed correlation with galaxies was produced by the fainter sources in our list ($-14.0 > \log S \geq -14.4$), close to the 4σ limits for detection. Hence the obvious explanation for the much stronger result on GSGP4 would be the longer ROSAT exposure time, approximately twice that used for the other fields (Table 5.1), giving source detection limits fainter by a factor $\Delta(\log S) \sim 0.3$. However, other explanations may be possible. The GSGP4 area could be unrepresentative in some way – containing, for example, a large-scale association of unusually X-ray luminous galaxies, not seen in most other areas of the sky.

To investigate further the differences between our survey fields, we repeated our source/galaxy cross-correlation analysis using only the sources above a flux limit kept constant at $S(0.5\text{–}2.0 \text{ keV}) = 10^{-14}$ ergs cm^{-2}s^{-1} for all five fields. The use of this common flux limit, well above the 5σ detection limit in at least the central areas of all five ROSAT images (Table 5.2), may reveal whether there is any variation in the true strength of source/galaxy correlation between these areas of the sky, but limits our analysis to a much smaller number of sources.

Table 5.9 lists the total numbers of $S \geq 10^{-14}$ sources, and the numbers without identification as AGN or stars. In contrast to the numbers of $\geq 4\sigma$ and $\geq 5\sigma$ sources given in Table 5.2, the numbers above this common flux limit show no significant variation between the five fields. Table 5.9 also gives the numbers of $B < 21.0$ galaxies seen on the UKST plates within 20 arcsec of an unidentified $S \geq 10^{-14}$ source and the numbers expected by chance, in the absence of any positional correlation. The equivalent numbers are also given for $B < 21.0$ and $21.0 \leq B \leq 23.0$ galaxies on the AAT plates, for the three fields on which AAT data was available.

The ratio of $B < 21$ galaxies seen within 20 arcsec of an unidentified X-ray source to the number expected by chance remains a factor of just over 2 at this flux limit, although with the greatly reduced number of sources in comparison to the 4σ-limited sample the overall significance of the cross-correlation is only 2.4σ for the 5 UKST fields and 1.8σ for the 3 AAT fields. The fact that $B < 21$ galaxies appear to comprise a fraction $\sim 10\%$ of unidentified X-ray sources at all three flux limits considered (10^{-14}, 5σ and 4σ) may favour an approximately constant fraction of galaxies with high L_X/L_B ratios (i.e. the wide dispersion in $\log L_X/L_B$ proposed in Section 5.6.3 above) as the main cause of the source/galaxy correlation, rather than the sudden appearance of a high-L_X population at $z > 0.2$.

No significant cross-correlation is seen between $S > 10^{-14}$ sources and $21 \leq B \leq 23$ galaxies. For a source with an optical magnitude $B > 21$ to give an X-ray flux above 10^{-14} ergs cm^{-2}s^{-1}, a very high flux ratio of $f_\nu(2 \text{ keV})/f_\nu(B) > 10^{-3.97}$ would be required. In our detected sample, the galaxies GSGP4X:48 and GSGP4X:100 and the cluster GSGP4X:32 do appear to possess X-ray/optical flux ratios as high as this, but only the cluster, with a $B = 21.54$ central dominant galaxy, produces an X-ray flux $S > 10^{-14}$ ergs cm^{-2}s^{-1}. This single object would obviously not produce a statistically significant correlation above the errors of $\sim \sqrt{N_{pairs}} = 4.7$ in this analysis.

With the same flux limit used for all five X-ray images, no significant difference in

the source/galaxy cross-correlation remains between GSGP4 and the other four fields. Hence it would appear that the dominance of our results by the GSGP4 data is primarily or entirely a result of the longer X-ray exposure time. As discussed in Section 5.7 above, the total numbers of galaxies detected, unlike the numbers of QSOs, appear to increase with flux limit in the $-14.0 > \log S \geq -14.4$ range with a power law index greater than unity, and are likely to continue to do so to $\log S = -15.0$ and beyond.

For a galaxy count slope $\gamma = 1.5$, extending the flux limit by $\Delta(\log S) = 0.3$ will increase the number of detected galaxies by a factor of 2.8. Furthermore, at these faint limits, the numbers of detected QSOs will increase by a much smaller factor, so the proportion of unidentified X-ray sources which are not galaxies will decrease, resulting in smaller statistical errors in the cross-correlation. Our one 50 ksec exposure was therefore able to provide approximately as much data on the X-ray properties of faint galaxies as a total of $\sim$ 100 ksec exposure time divided amongst four other fields. We conclude from this that it is worthwhile for all future high-resolution X-ray surveys, at any range of photon energies, to include a very long exposure on a single field.

Field	$S \geq 10^{-14}$ sources		Galaxies $\leq$ 20 arcsec from an $S \geq 10^{-14}$ source					
	Total	Unidentified	$B < 21$ UKST		$B < 21$ AAT		$21 \leq B \leq 23$ AAT	
			seen	expected	seen	expected	seen	expected
GSGP4	27	8	2	0.65	3	0.98	6	8.09
SGP2	32	12	2	1.08	3	1.35	11	8.32
SGP3	27	7	2	0.44				
QSF1	31	7	0	0.69				
QSF3	30	8	2	0.63	0	0.56	5	5.56
TOTAL	147	42	8	3.49	6	2.89	22	21.97

Table 5.9 The total numbers of X-ray sources detected above a 0.5–2.0 keV flux limit of 10^{-14} ergs $cm^{-2}s^{-1}$ and the numbers not identified as stars or QSOs, and the cross-correlation between the unidentified sources and galaxies. The cross-correlation results are given by listing the numbers of these galaxies which are found to lie within 20 arcsec of the X-ray sources, and the numbers expected in these areas by chance. The results are given separately for each field – the use of a common flux limit for the five ROSAT datasets means that any differences between the results for the five fields will reflect real differences between these areas of the sky rather than differences in the ROSAT exposure times used for each image. For the AAT data, the cross-correlation results are given separately for the brighter ($B < 21$) and fainter ($21 \leq B \leq 23$) galaxies.

5.9 Summary

(i) A total of 184 X-ray sources (without identified QSO or stellar optical counterparts), detected using ROSAT, were cross-correlated with the positions of galaxies on photographic plates. A significant ($\sim 3\sigma$) cross-correlation was detected, indicating that the optical counterparts of ~ 12 of these X-ray sources were $B < 21.0$ galaxies.

(ii) The number of galaxies we found to be correlated with X-ray sources in our cross-correlation analysis indicated that $\sim 1\%$ of the galaxies at $B \leq 21$ and $z_{mean} = 0.22$ possess L_X/L_B luminosity ratios higher by factors of order ~ 100 than most galaxies seen locally. Our results therefore suggest that the L_X/L_B ratios of normal galaxies of both early and late types are widely dispersed, with $\sigma \sim 0.8$ in the logarithm of the ratio. The rate of X-ray luminosity evolution for galaxies is unknown at present, and if it is very rapid at even these moderate redshifts, a somewhat smaller dispersion in L_X/L_B ratios may be adequate to explain our observations.

(iii) The galaxies coinciding with these sources were examined spectroscopically, and were found to possess a wide range of spectral characteristics, covering the entire Hubble sequence from early to late types. The X-ray luminosities of these galaxies were estimated as $L_X \sim 10^{42}$ ergs s^{-1}, which is much higher (by factors of order ~ 100) than the X-ray luminosities of most normal galaxies. The late-type galaxies were typically of $L \sim L^*$ luminosity at optical wavelengths, whereas the X-ray detected early-type galaxies tended to be of somewhat higher than L^* optical luminosity ($M_B \sim -22$).

For the X-ray detected galaxies with strong narrow emission lines (W[OII] > 20Å), the high X-ray luminosities may result from the presence of large numbers of very luminous (but short-lived) massive X-ray binaries, formed in starbursts. However, strong emission line galaxies form less than half of the X-ray detected sample, and a number of spectroscopically examined $L_X \sim 10^{42}$ ergs s^{-1} galaxies show no evidence of ongoing or recent star-formation, so other mechanisms must account for the very strong X-ray emission in these cases.

(iv) A rich galaxy cluster at a high redshift of $z = 0.561$, previously identified on an AAT plate corresponding to the GSGP4 field, appeared on the ROSAT image as one of our brighter X-ray sources, appearing slightly extended in comparison to the other sources. The X-ray luminosity of the cluster was estimated from its flux and redshift to be $L_X(0.5\text{–}2.0 \text{ keV}) \simeq 5.4 \times 10^{43}$ ergs s^{-1}. Although this X-ray luminosity is higher than that of any of our detected single galaxies, it appears to be only about $\sim 30\%$ of that expected for a comparable large cluster seen locally (i.e. at the present day).

(v) The cross-correlation analysis also suggested that some (~ 17) of the X-ray sources are optically fainter ($21.0 \leq B \leq 23.0$) galaxies, but this result is much less significant ($\sim 1.7\sigma$). The cross-correlation analysis at this depth was badly affected by the confusion problem caused by the surface density of faint galaxies exceeding that of ROSAT PSPC resolution elements. The unidentified X-ray sources showed a more significant ($> 3\sigma$) cross-correlation with objects classified as $21 \leq B \leq 23$ stars, suggesting that ~ 17 of the unidentified sources were optically faint QSOs which spectroscopy had failed to identify.

(vi) The number counts of detected galaxies as a function of X-ray flux limit appear to be increasing with an approximately Euclidean ($\gamma = 1.5$) slope, reaching a surface density estimated as $N = 27.2 \pm 10.4$ deg^{-2} at our completeness limit of $S \simeq 10^{-14.4}$ ergs cm^{-2}s^{-1}. To a flux limit of $S \sim 10^{-14.0}$ ergs cm^{-2}s^{-1}, the X-ray number counts of QSOs also increase with a Euclidean slope, with a normalization higher than that of galaxies by a factor of ~ 7, so that the total flux from QSOs exceeds that from galaxies by a similar ratio within the resolved component of the 0.5–2.0 keV background.

However, faintward of $S \simeq 10^{-14.0}$ ergs cm^{-2}s^{-1}, where QSOs are seen out to their maximum redshifts and their mean redshift reaches $z_{mean} \simeq 1.25$, the QSO number count levels out significantly. The X-ray number count of galaxies appears to continue rising with a Euclidean slope. We would expect this, as galaxies will not be seen out to $z \sim 3$ until much fainter X-ray fluxes are reached. Hence the galaxy component of the X-ray source counts will increase relative to that of QSOs at fainter flux limits, and galaxies would account for a much larger component of the unresolved $\sim 65\%$ of the XRB than of the detected X-ray source counts.

Chapter 6

The Auto-Correlation Function of the X-Ray Background

6.1 Introduction

In this chapter we investigate the unresolved component of the X-ray background by calculating an autocorrelation function (ACF) of the fluctuations in its intensity over a wide range of angular scales. After excluding areas of our ROSAT images containing photons from sources detected above 4σ, we can use the ACF of the sub-4σ fluctuations in the remaining image area to investigate the clustering of X-ray sources faintward of the 4σ detection threshold.

Constraints on the number counts of X-ray sources at fluxes faintward of present detection limits have already been obtained by Hamilton and Helfand (1987) using *Einstein* data, and by Georgantopoulos et al. (1993) using ROSAT data. These authors investigated the P(D) distribution of the unresolved background – i.e. the frequency distribution of the number of photons D in each pixel. For a diffuse, absolutely uniform background P(D) would have a Poisson distribution. However, if the XRB contains discrete sources with fluxes greater than ~ 1 photon source^{-1} but less than the threshold for detection, these will create a 'clustering' of the X-ray photons on the scale of the point-spread function, whether or not the sources themselves are clustered, and consequently the variance and higher moments of P(D) will exceed the Poisson value.

The above authors compared P(D) with the predictions of models incorporating the point-spread functions of the respective instruments and assuming various forms for the number count relation log N–log S of sources faintward of the detection threshold. The P(D) analysis of both *Einstein* and ROSAT images of the unresolved XRB indicated the approximately Euclidean slope ($\gamma = 1.5$) of log N–log S found for detected sources at $S > 10^{-14}$ ergs cm^{-2}s^{-1} to flatten to $\gamma \simeq 1.2$ at fainter fluxes. A surface density of unresolved sources exceeding ~ 5000 deg^{-2} is then required to produce the entire X-ray background intensity.

The ACF differs from the P(D) distribution in that it measures only the second moment of the intensity fluctuations, but does so for a large range of scales from one pixel to the size of the image – the ACF is the intensity covariance as a function of separation between two pixels rather than simply the pixel-to-pixel variance. It therefore serves primarily as a probe of the clustering of the discrete sources themselves, rather than their number counts.

The ACF is given by

$$\omega_{ACF}(\theta) = \frac{\langle (I - \langle I \rangle)(I' - \langle I \rangle) \rangle}{\langle I \rangle^2}$$

where I and I' are the intensities detected in two pixels separated by angle θ on the sky, and $\langle I \rangle$ is the mean intensity for the whole image area. The ACF differs from the two-point angular correlation function $\omega(\theta)$ only in that

(i) The photons are binned into 15 arcsec pixels whereas the galaxies were detected within much smaller resolution elements (~ 1 arcsec) and not binned, but this will have little effect where θ is much larger than 15 arcsec.

(ii) The clustering of photons into discrete sources, if these are present, will produce a signal in the ACF (additional to that produced by the source clustering) at the small scales within the instrumental point-spread function ($\sim$ 25 arcsec for the ROSAT PSPC).

(iii) Any clustering of photons into sources will also produce statistical errors in the ACF larger than those estimated on the basis of photon pair counts, as individual, detected photons may not then be independent of each other (see Section 6.4).

(iv) Each X-ray photon, rather than each discrete source, is weighted equally. The brighter unresolved sources, given stronger weighting in the ACF, are likely to be fewer in number and at lower average redshifts (and therefore more strongly clustered on the sky) than fainter sources. Hence flux-weighting would tend to increase both the statistical errors in the ACF and any signal from source clustering, relative to the amplitude and error of $\omega(\theta)$ calculated with all sources weighted equally.

Discrete, extragalactic sources of X-rays – galaxies, galaxy clusters and the various types of AGN – are all clustered to some extent, with their projected clustering on the sky at small angular scales (i.e. a few arcminutes) approximately following $\omega(\theta) \propto \theta^{-0.8}$ power-laws of various amplitudes. If the XRB is produced by any combination of such sources, it should therefore be possible to obtain at least an upper limit on their $\omega(\theta)$ amplitude by fitting a $\theta^{-0.8}$ power-law to the ACF (at θ larger than the point-spread function). This will give an ACF amplitude, which will depend on both the redshift distribution and the intrinsic clustering properties of the sources.

On the basis of the measurements of QSO clustering described by Shanks and Boyle (1994), QSOs, if they follow a stable clustering model, appear to be more strongly clustered than normal galaxies would be at the same redshift. The ACF amplitude might then, as well as providing information about the the range of redshifts at which the X-ray flux is produced, constrain the relative contributions of QSOs and galaxies to the unresolved XRB. However, as we discuss further in Section 6.6, these estimates of the QSO clustering derive from measurements at physical separations of $r \sim 10$ h^{-1}Mpc, whereas our ACF amplitudes measure the clustering of X-ray sources at smaller scales of $r \sim 1$ h^{-1}Mpc, so we must treat any comparison of the two with caution.

Georgantopoulos et al. (1993) calculated autocorrelation functions for the QSF1 and QSF3 ROSAT images and were able to set a 2σ upper limit of 0.045 on the signal in the ACF at $1 \leq \theta \leq 3$ arcmin separations. For a $\theta^{-0.8}$ power-law, an upper limit of $\omega_{ACF}(2') \leq 0.045$ corresponds to

$$\omega_{ACF}(\theta) \leq 3 \times 10^{-3} (\mathrm{deg})^{-0.8}$$

If QSOs are as clustered on small scales as the Shanks and Boyle (1994) measurements indicate them to be at $r \sim 10$ h^{-1}Mpc, the Georgantopoulos et al. (1993) upper limit on the ACF is significantly lower than the ACF amplitude expected for a background produced entirely by QSOs, even if these are distributed out to $z \sim 4$. The Georgantopoulos et al. (1993) results would then set an upper limit on the QSO contribution to the unresolved XRB flux, f_{QSO}, of approximately $f_{\mathrm{QSO}} \leq 40\%$, but allow most of the XRB to be produced by normally clustered galaxies, if these are also distributed out to high redshifts.

In this Chapter, we shall repeat the ACF analysis of the QSF3 image, and extend this to the SGP2 image of comparable depth and to the GSGP4 image with approximately twice the exposure time. Our larger dataset (approximately twice the total exposure time used by Georgantopoulos et al. 1993) should improve the statistics on measurements of the ACF, providing either the detection of a signal or a stronger constraint on its upper limit.

We shall compare our ACF amplitude with the $\omega(\theta)$ amplitude of faint galaxies, to verify whether galaxies at any magnitude or redshift are sufficiently weakly clustered to produce the non-QSO fraction of the XRB, and with the models used by Georgantopoulos et al. (1993) to estimate possible constraints on $f_{\rm QSO}$. Finally, we shall discuss different models of QSO clustering at high redshifts and the extent to which $f_{\rm QSO}$ and f_{gal} can be constrained by ACF measurements and other observations, including P(D) analysis and the source counts discussed previously in Chapter 5.

6.2 Observational Data

In the ACF analysis we use the three ROSAT fields for which AAT photographic data is also available (GSGP4, SGP2 and QSF3), imaged in the 0.5–2.0 keV energy range. Figures 6.1, 6.2 and 6.3 show the 40 × 40 arcmin central areas of our three images. Only the central 16 arcmin radius circular area of each field is used here, to minimize the effect of the falloff in sensitivity and resolution at large off-axis angles. This is necessary as autocorrelation functions are very sensitive to large-scale gradients and the 'real' (non-instrumental) fluctuations are already known to be weak. These circular areas each contain 12972 ROSAT pixels, with the mean number of photons counted per pixel as listed in Table 6.1.

Sources detected above 4σ (Section 5.3) were removed by setting all pixels within an exclusion radius about the centroid of each source to a negative value. These pixels then were then ignored by the program making the various summations (Section 6.3 below) used in the calculation of the ACF. The exclusion radius used was that which would contain 98% of the photons detected from a point source. The radius used was 0.51 arcmin for sources within 8 arcmin of the field centre, but increases at large off-axis angles where the PSPC resolution is poorer, to 0.66 arcmin and 0.89 arcmin at off-axis angles of 12 and 16 arcmin respectively.

Figures 6.4, 6.5 and 6.6 show the 'holed' images, and Table 6.1 lists the numbers of pixels remaining in the 16 arcmin radius circular areas of each after source removal, and the mean numbers of photons per pixel before and after source removal. The reduction in the mean number of photons per pixel caused by removing pixels contained within $\geq 4\sigma$ detected sources indicated that sources detected above 4σ accounted for approximately 30%, 23% and 31% of the total 0.5–2.0 keV flux on GSGP4, SGP2 and QSF3 respectively.

Image	Pixels used	Mean photons pixel^{-1} ($\langle$N$\rangle$)	$\langle$N$\rangle\omega(0)$
GSGP4 *unholed*	12972	0.7836	3.357
GSGP4 *holed*	11191	0.5554	1.185
SGP2 *unholed*	12972	0.4895	2.444
SGP2 *holed*	11880	0.3746	1.031
QSF3 *unholed*	12972	0.4745	6.366
QSF3 *holed*	11884	0.3261	1.196

Table 6.1 For our GSGP4, SGP2 and QSF3 ROSAT images, both with all pixels included ('unholed') and with the pixels containing 4σ detected sources removed ('holed'), this table lists the number of ROSAT pixels used in our ACF analysis, the mean number of 0.5–2.0 keV photons, $\langle N \rangle$, detected in each of these pixels, and the product $\omega(0)\langle N \rangle$, ie. the ratio of the pixel-to-pixel variance in photon counts to the mean value (Section 6.3).

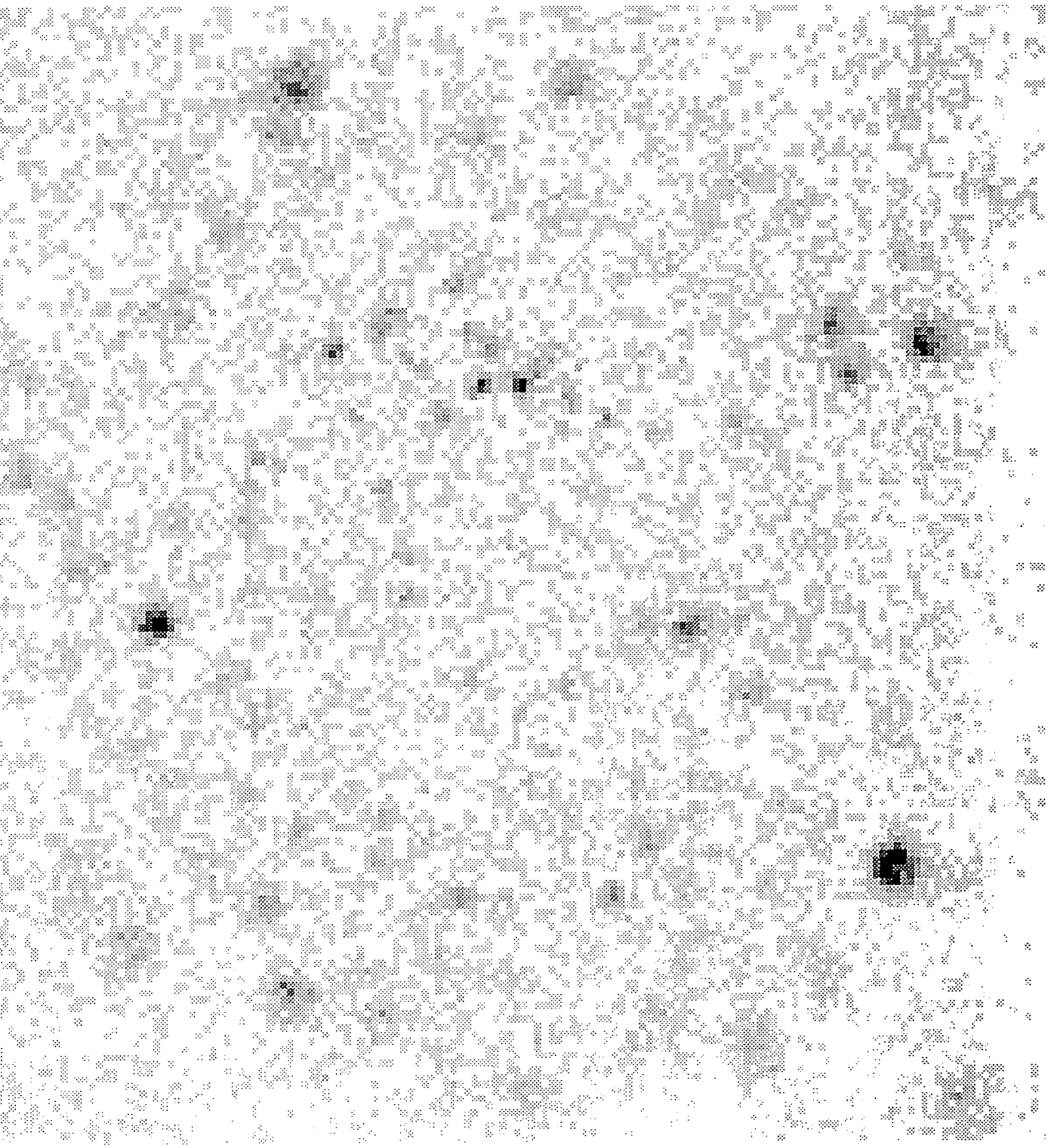

Figure 6.1 Grey-scale plot of the central 40×40 arcmin square area of our ROSAT image of the GSGP4 field, showing the 0.5–2.0 keV photon counts in pixels of side 15 arcsec.

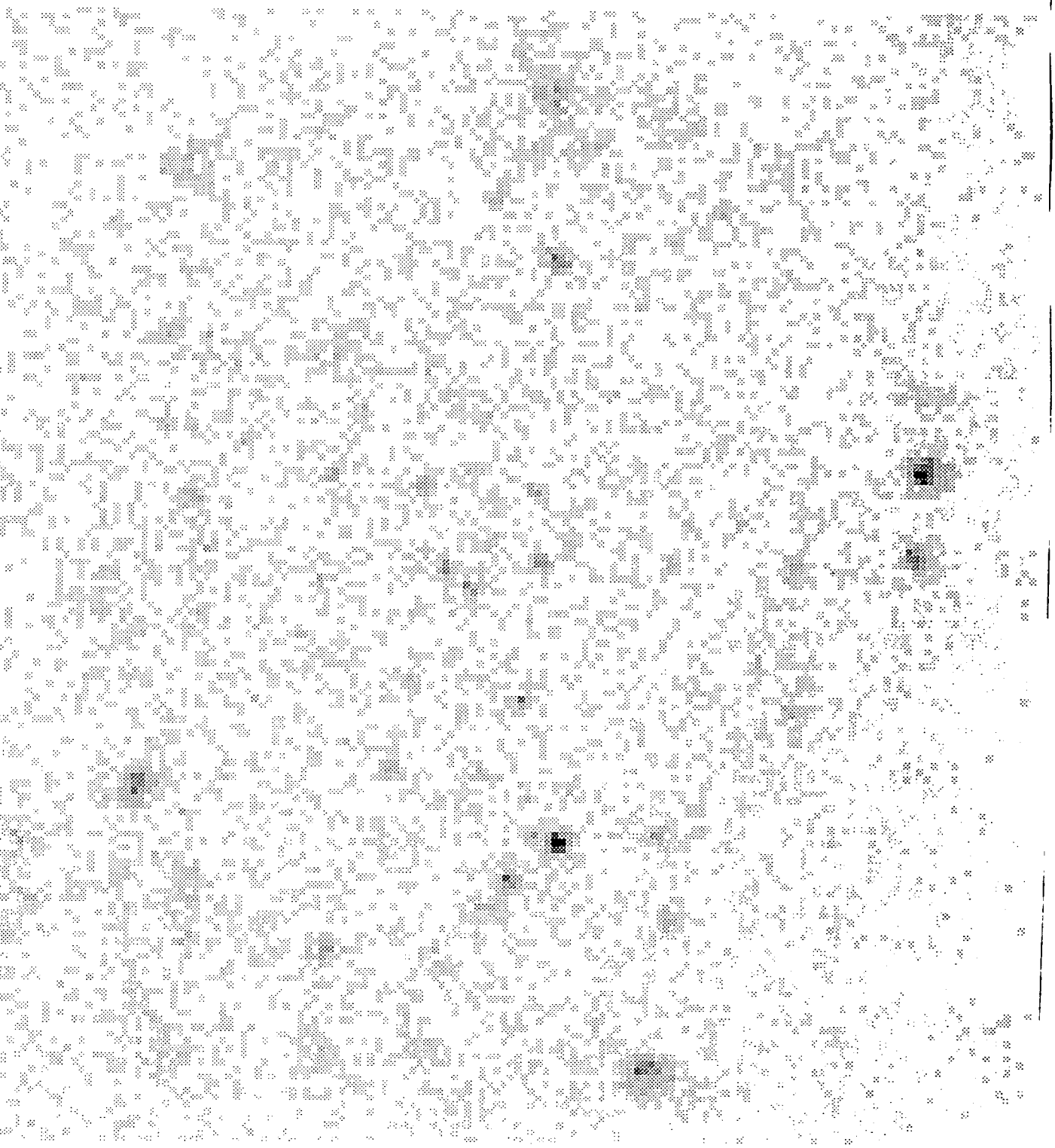

Figure 6.2 Grey-scale plot of the central 40×40 arcmin square area of our ROSAT image of the SGP2 field, showing the 0.5–2.0 keV photon counts in pixels of side 15 arcsec.

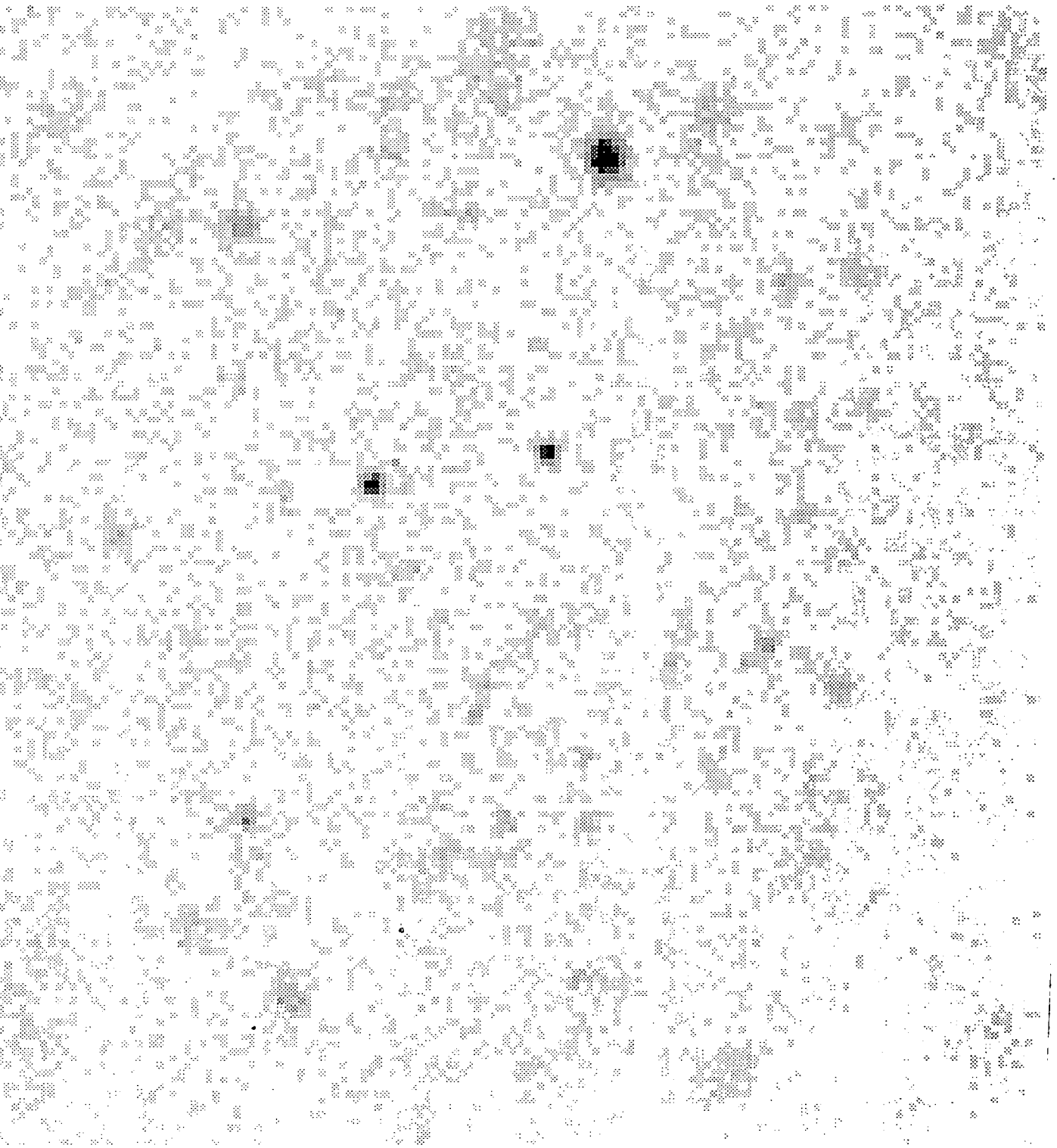

Figure 6.3 Grey-scale plot of the central 40 × 40 arcmin square area of our ROSAT image of the QSF3 field, showing the 0.5–2.0 keV photon counts in pixels of side 15 arcsec.

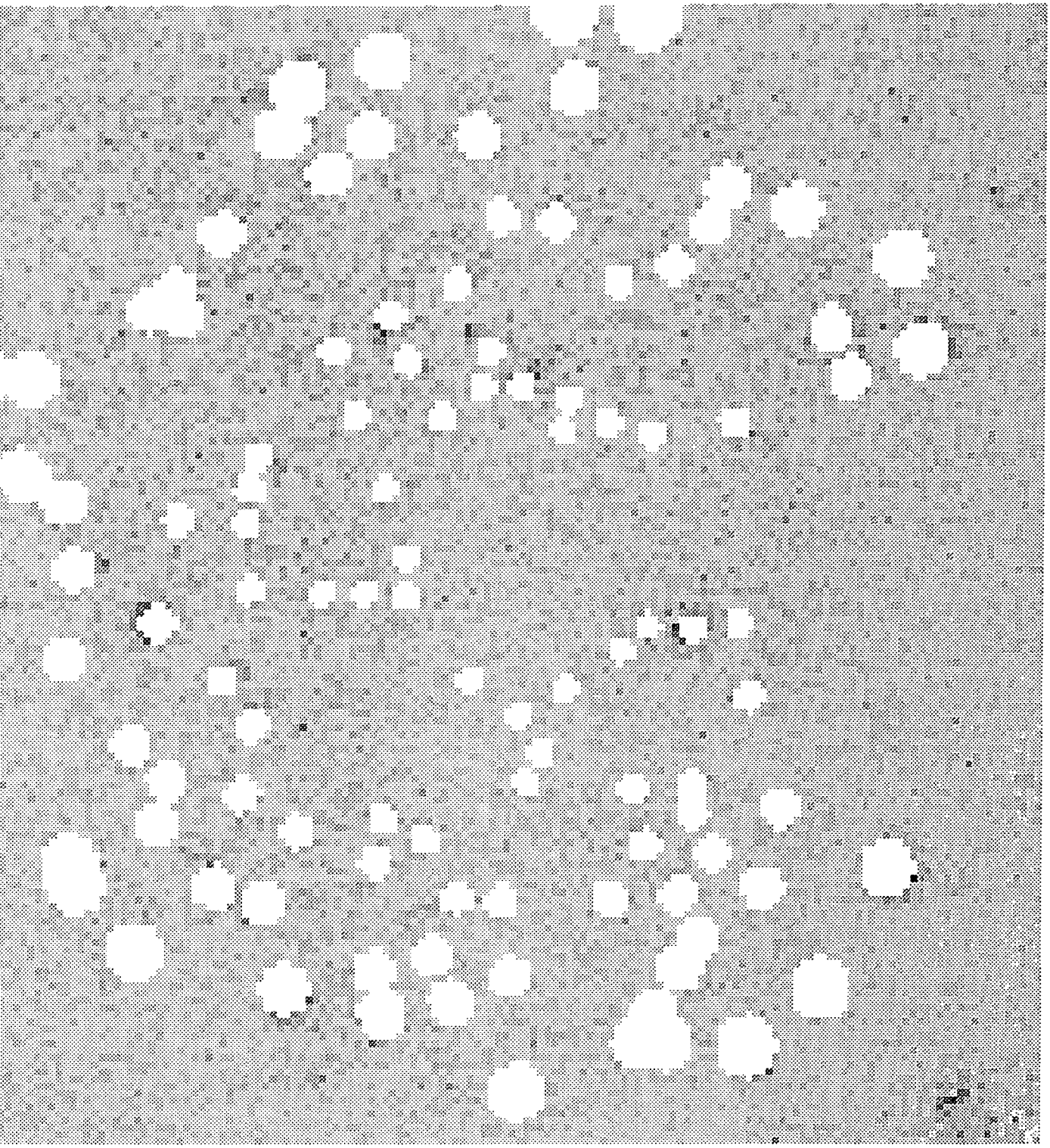

Figure 6.4 Grey-scale plot of the central 40×40 arcmin square area of our ROSAT image of the GSGP4 field, showing the 0.5–2.0 keV photon counts in pixels of side 15 arcsec, with pixels removed (see Section 6.2) which contain photons from discrete sources detected above 4σ. These 'holed' areas appear white on the plot.

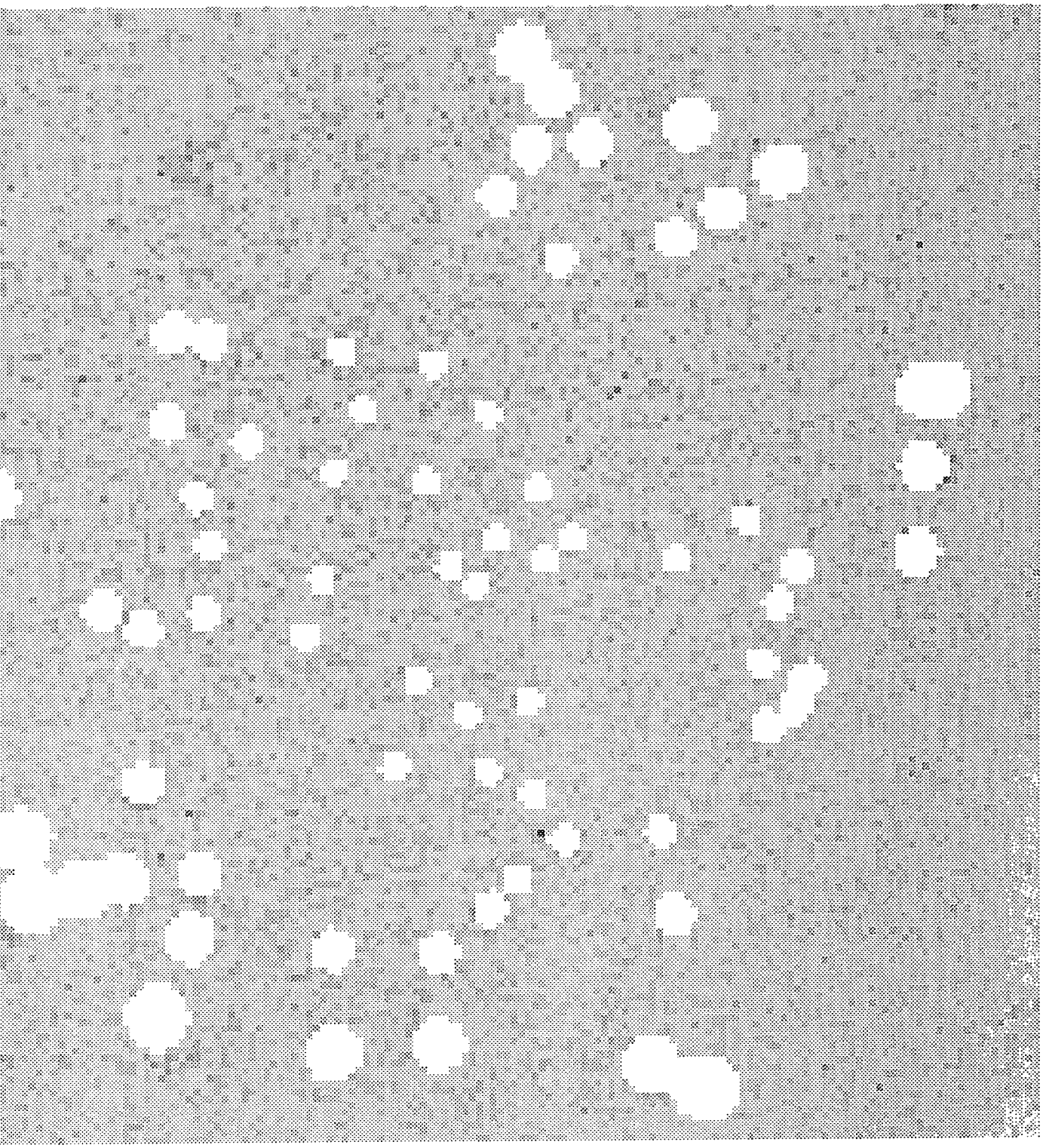

Figure 6.5 Grey-scale plot of the central 40 × 40 arcmin square area of our ROSAT image of the SGP2 field, showing the 0.5–2.0 keV photon counts in pixels of side 15 arcsec, with pixels removed (see Section 6.2) which contain photons from discrete sources detected above 4σ. These 'holed' areas appear white on the plot.

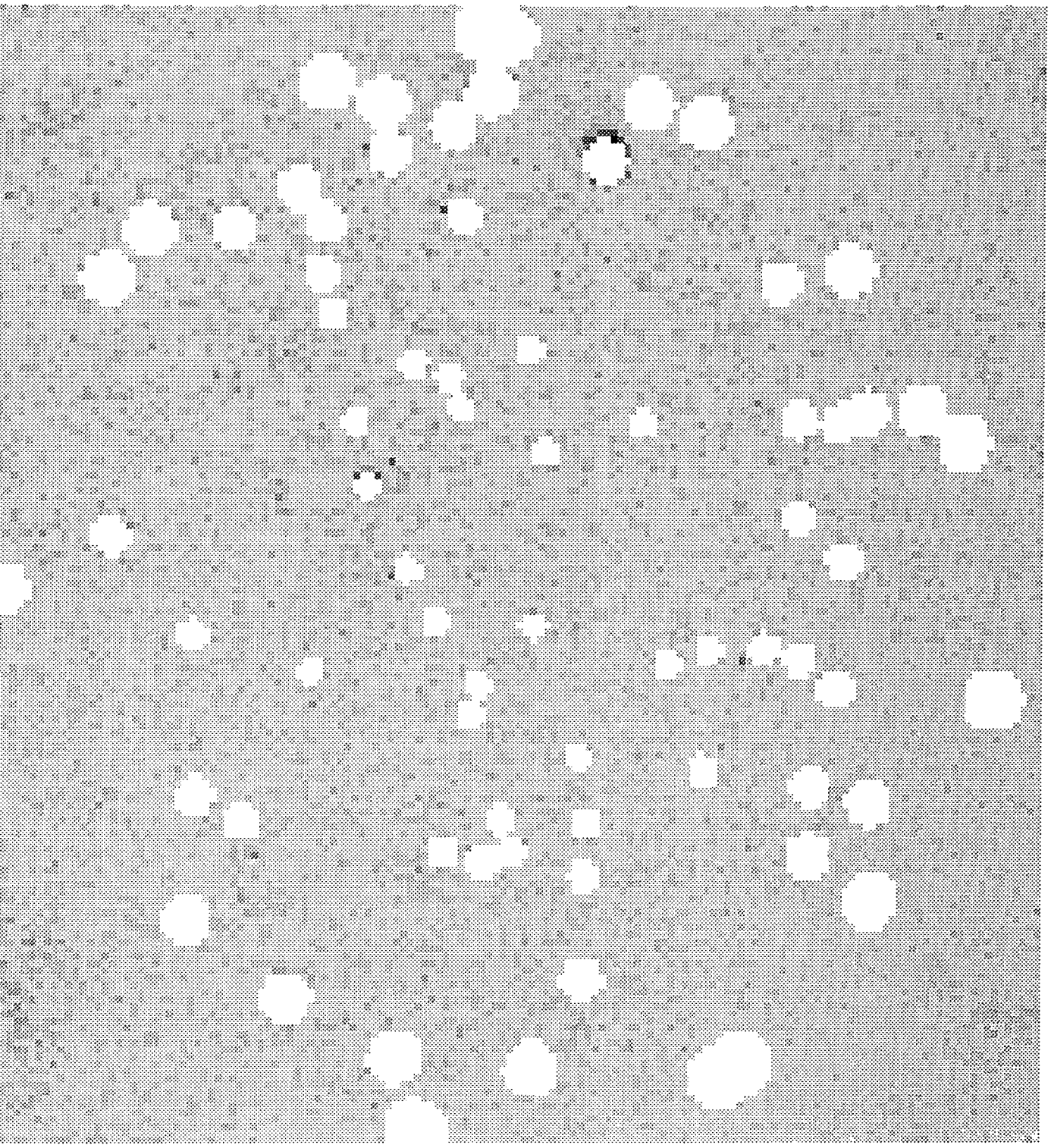

Figure 6.6 Grey-scale plot of the central 40 × 40 arcmin square area of our ROSAT image of the QSF3 field, showing the 0.5–2.0 keV photon counts in pixels of side 15 arcsec, with pixels removed (see Section 6.2) which contain photons from discrete sources detected above 4σ. These 'holed' areas appear white on the plot.

6.3 Calculating the Auto-correlation Function

Auto-correlation functions were calculated for the 3 holed and 3 unholed images by evaluating

$$\omega_{ACF}(\theta_n) = \frac{\sum N_i N_j(\theta_n)}{N_{pp}(\theta_n)\langle N\rangle^2} - 1$$

where $\langle N\rangle$ is the mean number of photons per pixel for all pixels used in the analysis, N_iN_j is the product of the photon counts in a pair of pixels i and j, and $\sum N_iN_j(\theta_n)$ is the product N_iN_j summed for all $N_{pp}(\theta_n)$ pairs of pixels separated by $10^{0.2(n-1)} \leq \theta < 10^{0.2n}$ where θ is in units of the pixelsize (15 arcsec).

The $n = 0$ bin corresponds to zero separation between the pixels, so that $N_iN_j(\theta_0)$ is simply N^2 and

$$\omega_{ACF}(0) = \frac{\langle N^2\rangle}{\langle N\rangle^2} - 1$$

The product $\langle N\rangle\omega_{ACF}(0)$, which is equivalent to $\frac{\langle N^2\rangle - \langle N\rangle^2}{\langle N\rangle}$, the second moment of P(D) divided by the first moment, will be unity for a diffuse, absolutely uniform background. A uniform background would give $\omega_{ACF}(\theta) = 0$ at all $\theta > 0$, but at zero separation there would be a positive signal $\omega_{ACF}(0) = \langle N\rangle^{-1}$ produced by the Poisson noise in the photon counts. Intensity fluctuations above the Poisson noise, on any scale within the image size, would increase $\langle N\rangle\omega_{ACF}(0)$ above unity, and would also increase the statistical errors in $\omega_{ACF}(\theta)$ by approximately the same factor (see Section 6.4 below).

6.4 Estimation of Errors

In the calculation of $\omega(\theta)$ for discrete sources such as galaxies, the Poisson error on the pair count in each bin of angular separation, $N_{gg}(\theta_i)$, is simply $\sqrt{N_{gg}(\theta_i)}$.

The error in $\omega(\theta_i)$, σ_ω, will be the pair count error multiplied by $(1+\omega(\theta_i))/N_{gg}(\theta_i)$, i.e.

$$\sigma_\omega = (1 + \omega(\theta_i))N_{gg}(\theta_i)^{-0.5}$$

In calculating the ACF we are counting pairs of photons rather than discrete sources. If the photons are effectively clustered into 'groups' of mean size n photons by the presence of fluctuations and/or discrete sources in the background, the distribution of these 'photon clusters' then being assumed Poissonian, the mean number of groups per pixel will be $\langle N\rangle/n$, with $\sigma_{groups} = \sqrt{(\langle N\rangle/n)}$.

The fluctuations therefore increase the variance of P(D) from $\langle N\rangle$ to $n\langle N\rangle$, so that n is equivalent to $\langle N\rangle\omega_{ACF}(0)$ as defined above.

A photon pair count N_iN_j corresponds to N_iN_j/n^2 pairs of 'groups', giving a Poisson error in $\omega(\theta_n)$ of

$$\sigma_\omega = n(1 + \omega(\theta_n))(\sum N_iN_j(\theta_n))^{-0.5}$$

Hence we can correct our ACF errorbars for the effects of fluctuations additional to the Poisson noise by simply multiplying by the factor $\langle N\rangle\omega_{ACF}(0)$ as measured for the image being analysed. If a large fraction of the photons are concentrated in a few bright sources the statistical errors of the ACF will be large, hence the exclusion of the bright sources not only removes any effect of their clustering from the ACF but

also greatly reduces the noise in the estimate for the underlying background – it can be seen (Table 6.1) that $\langle N \rangle \omega_{ACF}(0)$ is much closer to unity for the images with detected sources removed.

However, when $\omega(\theta)$ was calculated for galaxies (Chapter 2) it was seen that the Poisson $\omega(\theta)$ error underestimated the field-to-field variations, especially at large θ. This will generally be the case where $N_{gg}(\theta_i) > N_g$, i.e. the number of pairs counted exceeds the total number of independent objects in the dataset.

Lacking at present a sufficient number of ROSAT images to derive accurate field-to-field errors, we can instead use the analytic formula for estimating $\omega(\theta)$ errors given by Mo, Jing and Börner (1991). They find the error in the pair count $N_{gg}(\theta_i)$ to be well approximated by

$$\sigma_{gg} = \sqrt{[N_{gg}(\theta_i) + 4N_{gg}(\theta_i)^2/N_g]}$$

giving an error in $\omega(\theta_i)$ of

$$\sigma_\omega = (1 + \omega(\theta))/N_{gg}(\theta_i) \times \sqrt{[N_{gg}(\theta_i) + 4N_{gg}(\theta_i)^2/N_g]}$$

In assigning error bars to our ACF estimates we use this formula, corrected for the effective clustering of photons, to estimate the error on $\omega_{ACF}(\theta_n)$ as,

$$\sigma_\omega = \langle N \rangle \omega_{ACF}(0)(1 + \omega(\theta_i))/\sum N_i N_j(\theta_n)$$

$$\times \sqrt{[\sum N_i N_j(\theta_n) + 4\sum N_i N_j(\theta_n)^2/(N_{pix}\langle N \rangle)]}$$

where N_{pix} is the number of pixels in the image area considered.

6.5 ACF Results

The auto-correlation functions calculated for the three fields are shown in Figures 6.7, 6.8 and 6.9. The ACFs of 'unholed' (sources included) and 'holed' (sources removed) images are plotted as filled and open squares respectively. The 'unholed' image ACFs show a strong signal from the bright sources at $\theta \leq 10^{0.8}$ pixels (i.e. 95 arcsec), but when the detected sources are removed this is greatly reduced. However, some signal remains at $\theta \leq 40$ arcsec, indicating the presence of discrete unresolved sources fainter than the $\sim 4\sigma$ detection limit.

Figure 6.10 shows the ACFs for the three holed images plotted on the same graph but with a larger scale. Power laws of index $\theta^{-0.8}$ were fitted to these functions, over a range of θ at which the point-spread function has little influence ($10^{0.4} \leq \theta \leq 10^{2.0}$ pixels, i.e. $38 \leq \theta \leq 1500$ arcsec).

Evaluating $\int\int \theta^{-0.8} d\Omega_1 d\Omega_2$, with θ being the separation of the integration elements in degrees, over a 16 arcmin radius circle gave the result 3.85. Therefore, to give an amplitude A at one degree, corrected for the 'integral constraint' described in Section 2.3, the function actually fitted to the data was '$A(\theta^{-0.8} - 3.85)$'.

Table 6.2 shows the $\omega_{ACF}(\theta)$ amplitudes for the XRB on the 3 fields separately, with 1σ errors, and an error-weighted mean value. It can be seen that the correlation amplitudes obtained for the 3 fields, and the mean value, are all consistent with each other, and with zero, at the 1σ level. Hence we do not detect any significant clustering of the unresolved sources producing the 0.5–2.0 keV background, in agreement with the ACF results from the two fields investigated by Georgantopoulos et al. (1993), and we can set a somewhat lower 2σ upper limits on the ACF amplitude of

$$\omega_{ACF}(\theta) \leq 1.40 \times 10^{-3} (\mathrm{deg})^{-0.8}$$

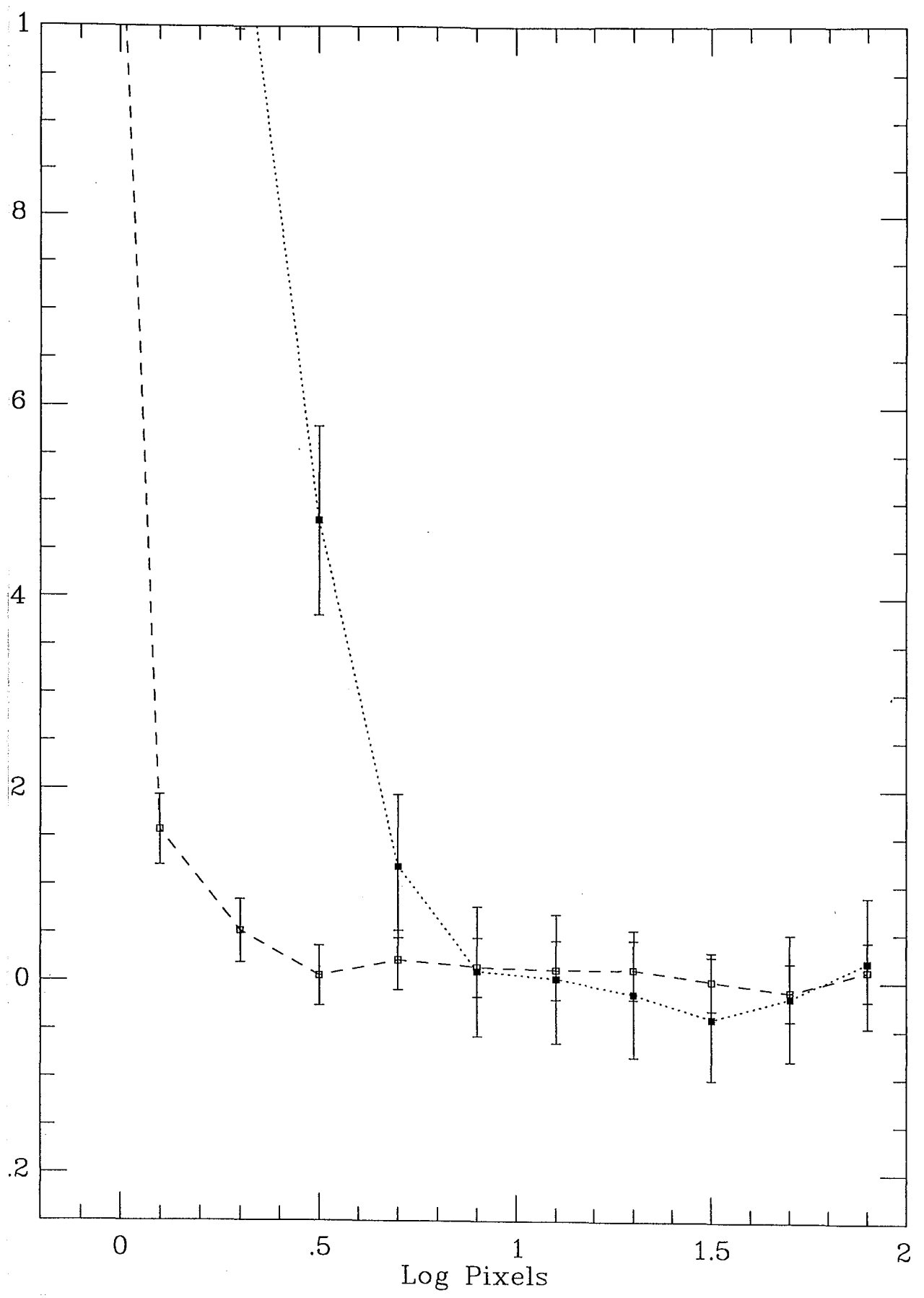

Figure 6.7 The auto-correlation function of the 0.5–2.0 keV X-ray background on our ROSAT image of the GSGP4 field, calculated for the full, 'unholed' image (solid squares, dotted line) and the 'holed' image (open squares, dashed line) with 4σ detected sources removed. The autocorrelation is shown as a function of the logarithm of angular separation, in units of ROSAT pixels (15 arcsec), with errors estimated as described in Section 6.4.

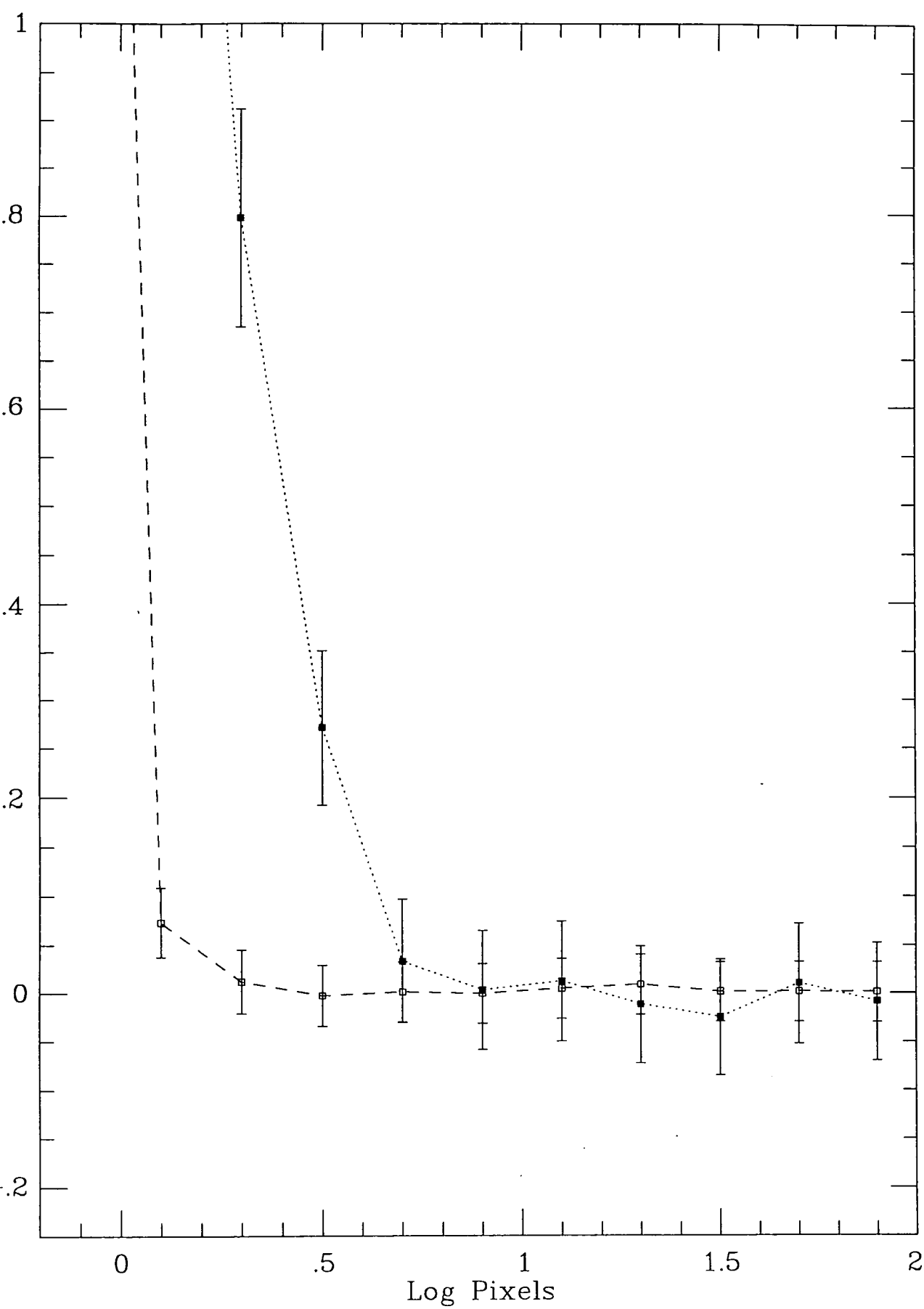

Figure 6.8 The auto-correlation function of the 0.5–2.0 keV X-ray background on our ROSAT image of the SGP2 field, calculated for the full, 'unholed' image (solid squares, dotted line) and the 'holed' image (open squares, dashed line) with 4σ detected sources removed. The autocorrelation is shown as a function of the logarithm of angular separation, in units of ROSAT pixels (15 arcsec), with errors estimated as described in Section 6.4.

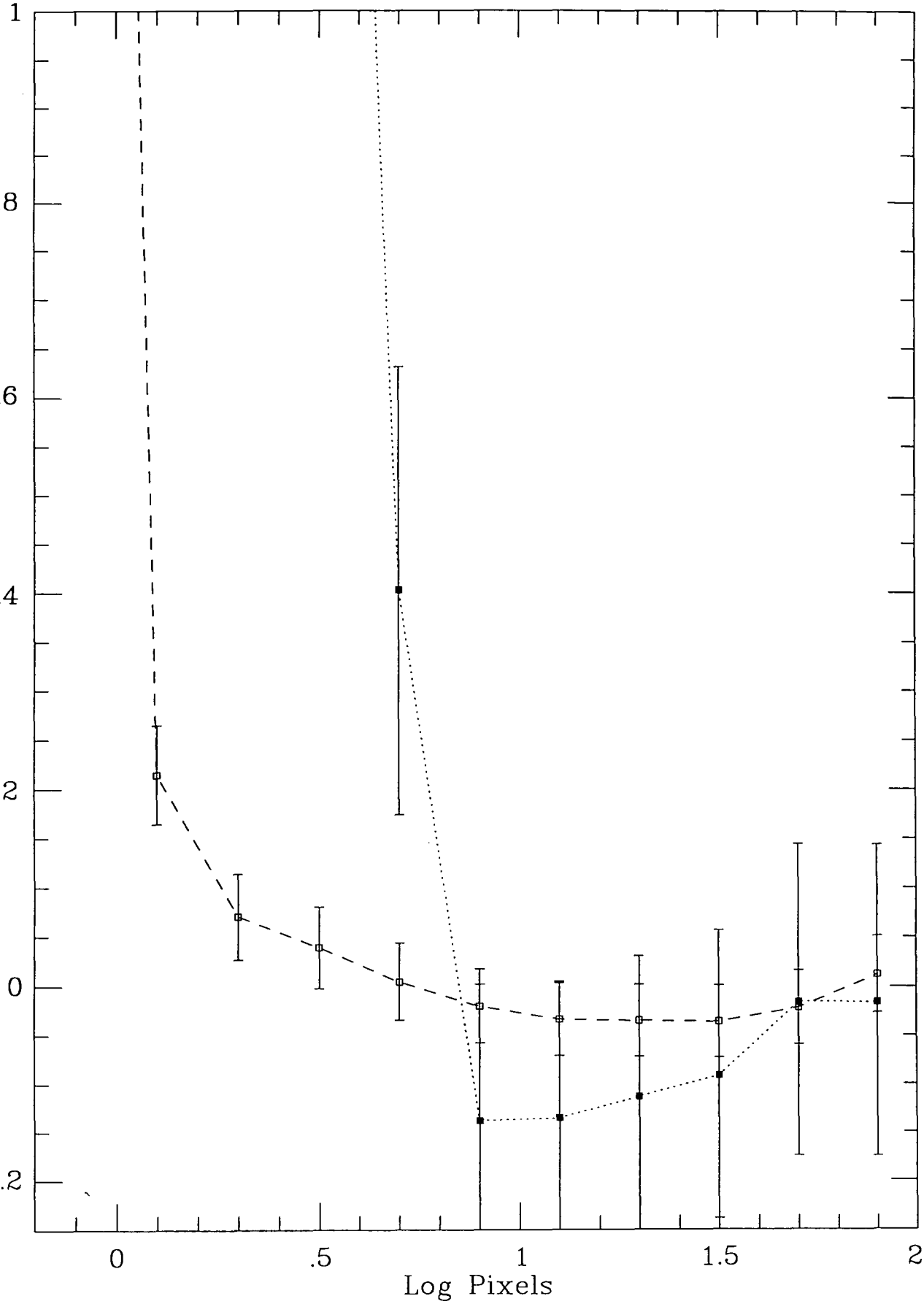

Figure 6.9 The auto-correlation function of the 0.5–2.0 keV X-ray background on our ROSAT image of the QSF3 field, calculated for the full, 'unholed' image (solid squares, dotted line) and the 'holed' image (open squares, dashed line) with 4σ detected sources removed. The autocorrelation is shown as a function of the logarithm of angular separation, in units of ROSAT pixels (15 arcsec), with errors estimated as described in Section 6.4.

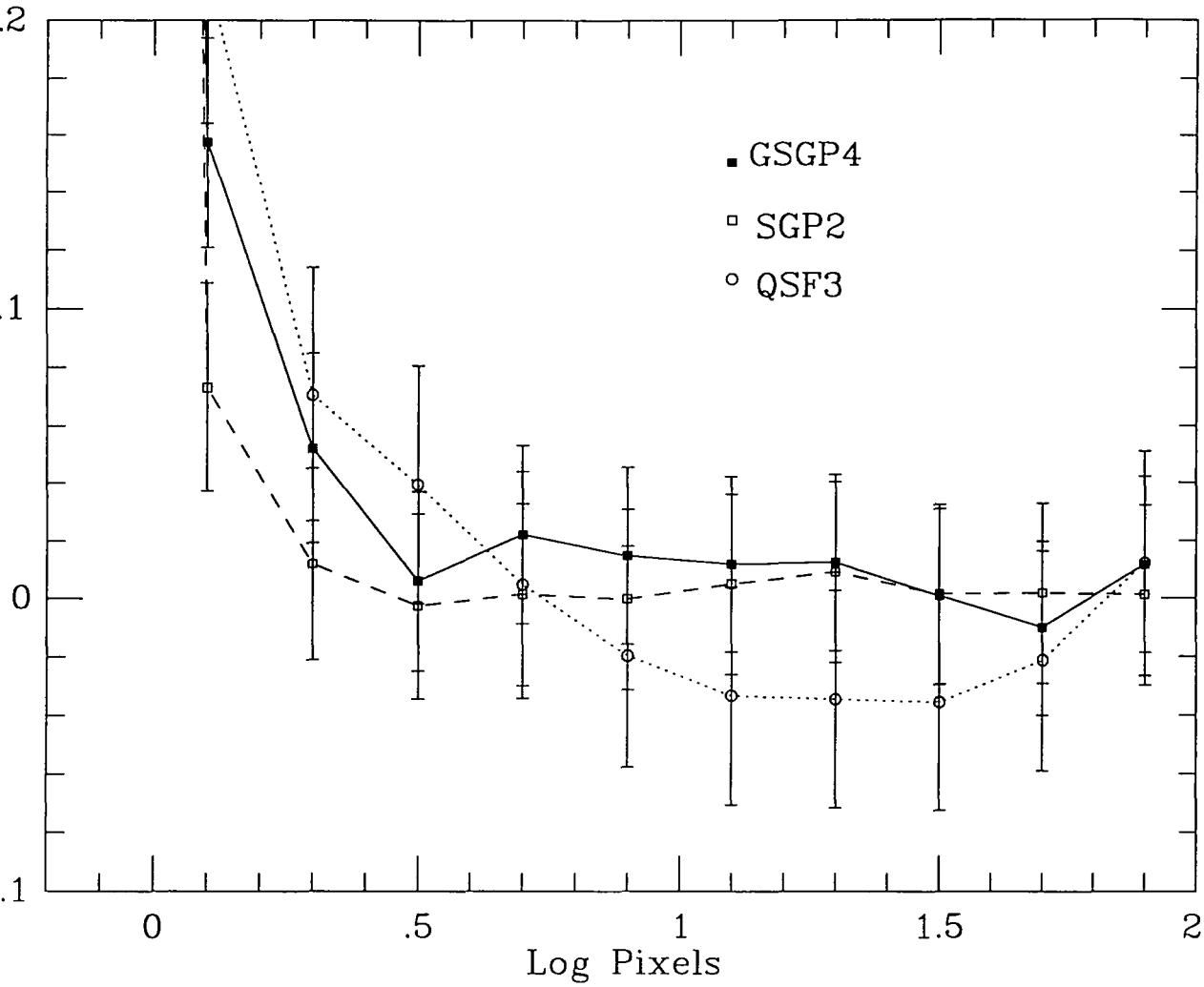

Figure 6.10 The auto-correlation functions of the 0.5–2.0 keV X-ray background, compared for ROSAT images of the GSGP4 (filled squares, solid line) SGP2 (open squares, dashed line) and QSF3 (open circles, dotted line) fields, with 4σ detected sources removed in all cases. The autocorrelation is shown as a function of the logarithm of angular separation, in units of ROSAT pixels (15 arcsec), with errors estimated as described in Section 6.4.

6.6 Comparison with the Clustering of Faint Galaxies

The correlation function $\omega(\theta)$ was also calculated for the $18.0 \leq B \leq 23.0$ galaxies found on the GSGP4, SGP2 and QSF3 AAT plates within circular areas of radius 16 arcmin centred on the ROSAT fieldcentres. The $\omega(\theta)$ analysis was carried out as described in Chapter 2, using 20000 random points for each area, and estimating the error bars using the formula from Section 6.4.

Figure 6.11 shows $\omega(\theta)$ for the galaxies on each field – the clustering appears similar (and weak) on QSF3 and SGP2, whereas the GSGP4 galaxy $\omega(\theta)$ shows more power on small scales. Fitting a function '$A(\theta^{-0.8} - 3.85)$' to give an amplitude at one degree corrected for the integral constraint appropriate for the area used, gives the amplitudes listed in Table 6.2 (with an error-weighted mean of the 3 fields). For GSGP4, and for the 3 fields combined, the detection of galaxy clustering is significant ($\sim 4\sigma$), and the estimated $\omega(\theta)$ amplitude is in agreement with that measured by Stevenson et al. (1985) and JSF from the full area of J1888 and other AAT plates, at the same $B \leq 23.0$ limit.

On each of the three fields, the $18.0 \leq B \leq 23.0$ galaxy $\omega(\theta)$ amplitudes are slightly higher than the amplitudes fitted to the ACF of the XRB, although the difference is nowhere statistically significant, being only 1.4σ (adding errors in quadrature) when the results from the 3 fields are combined. Correlation analysis of CCD data (Chapters 2, 3 and 4) indicated that the $\omega(\theta)$ amplitude of at least the bluer galaxies falls steeply faintward of $B = 23$, reaching $\omega(\theta) \sim 4 \times 10^{-4}(\mathrm{deg})^{-0.8}$ at $B_{ccd} = 25.0$. Figure 6.12 shows the ACF of the GSGP4 image with sources removed, $\omega(\theta)$ for the $B \leq 23.0$ galaxies on the same area of sky, and the $B_{ccd} \leq 25.0$ galaxy $\omega(\theta)$ from the 12 CCD frames of the MSFJ survey. We can see that, whereas the $\omega(\theta)$ of $B \leq 23.0$ galaxies is similar to or slightly higher than the ACF, the lower $\omega(\theta)$ of $B_{ccd} \leq 25.0$ galaxies is definitely below the ACF upper limits. We conclude from this that, although our ACF upper limits would allow a large contribution to the XRB from the galaxies seen on the AAT plates, the uniformity of the XRB would be more easily explained if as much or more of the XRB was produced by the less clustered 'flat spectrum' galaxies at $B > 23$. These galaxies would appear to be good candidates for the origin of a major component of the XRB, at least on the basis of their low $\omega(\theta)$ amplitudes, which indicate that they are sufficiently weakly clustered on the sky on arcminute scales to be capable of producing most of the XRB without causing fluctuations in excess of the observational upper limits.

For a more detailed comparison of the XRB ACF with the galaxy $\omega(\theta)$, we must take into account the fact that the ACF is weighted by the flux of each source, whereas in deriving the galaxy $\omega(\theta)$ amplitudes, galaxies with a wide range of apparent magnitudes were given equal weighting in the calculation. Unless the X-ray luminosity of the sources increases very rapidly with redshift (i.e. more rapidly than the luminosity distance $d_L(z)$), the brighter unresolved sources will tend to lie at lower redshifts and therefore be more clustered on the sky than fainter sources of the same type. A flux-weighted $\omega(\theta)$ amplitude estimated from the ACF would then to be higher than the normal number-weighted $\omega(\theta)$ amplitude.

To allow for this effect, we must replace the redshift distribution in Limber's formula by a flux redshift distribution $F(z)$, given by

$$F(z) = \rho(z)(1+z)^{1-\alpha}(d_L(z))^{-2}(\frac{dV_{com}}{dz})dz$$

where $\rho(z)$ is the X-ray emissivity at per unit comoving volume element at redshift z, α the spectral index, $d_L(z)$ the luminosity distance, and $\frac{dV_{com}}{dz}$ the comoving volume element.

First if all, we calculate $F(z)$ for non-evolving (i.e. $\rho(z)$ constant) galaxies, with spectral index $\alpha = 1$, distributed from $z = 0$ to $z = 4$. We perform the Limber's formula integration assuming the same normalization of galaxy clustering ($r_0 = 4.3$ h^{-1}Mpc) as used in Chapters 2, 3 and 4 of this thesis, and stable clustering. As a result of the weighting towards lower redshifts produced by the $(d_L(z))^{-2}$ term, most of the X-ray flux from galaxies with no X-ray luminosity evolution would be emitted from the galaxies at $z < 1$, producing a high flux-weighted clustering amplitude of $\omega_{ACF}(\theta) = 5.6 \times 10^{-3}(\mathrm{deg})^{-0.8}$ if $q_0 = 0.5$ and $\omega_{ACF}(\theta) = 4.0 \times 10^{-3}(\mathrm{deg})^{-0.8}$ if $q_0 = 0.05$

Our ACF upper limits can then strongly exclude non-evolving, normally clustered galaxies as the main source of the unresolved XRB. However, if galaxies are assumed to undergo strong X-ray luminosity evolution equal to that of QSOs in the models of Boyle et al. (1994) (see Section 7.9) the high-redshift component of $F(z)$ will be greatly increased. Galaxies with $r_0 = 4.3$ h^{-1}Mpc would then produce an ACF amplitude of only $\omega_{ACF}(\theta) = 7.21 \times 10^{-4}(\mathrm{deg})^{-0.8}$ if $q_0 = 0.5$, and only $\omega_{ACF}(\theta) = 3.39 \times 10^{-4}(\mathrm{deg})^{-0.8}$ if $q_0 = 0.05$, well within our observed upper limits.

We can use these Limber's formula calculations to express our ACF upper limit as upper limits on the correlation radius r_0 of the unresolved XRB sources. Non-evolving sources would require $r_0 \leq 2.0$ h^{-1}Mpc if $q_0 = 0.5$, or $r_0 \leq 2.4$ h^{-1}Mpc if $q_0 = 0.05$, to produce the entire XRB – clustering much weaker than that observed for galaxies. With QSO-like evolution, these limits are raised to $r_0 \leq 6.2$ h^{-1}Mpc if $q_0 = 0.5$, or $r_0 \leq 9.4$ h^{-1}Mpc if $q_0 = 0.05$. The clustering of normal galaxies lies well within these limits, although this may not be the case for the clustering of QSOs (see Section 6.7 following).

Carrera et al. (1991), and Soltan and Hasinger (1994) similarly interpreted upper limits on the XRB fluctuations, obtained from GINGA and ROSAT data respectively, in terms of upper limits on r_0. These authors obtained similar constraints on source clustering to those given here, finding that galaxy-like clustering was allowed, but only if there was some increase in X-ray luminosity with redshift. We conclude that the hypothesis that normally clustered galaxies distributed out to $z \sim 4$ produce the greater part of the unresolved XRB remains consistent with the ACF upper limits, if the X-ray emission from galaxies increases with redshift so that much of the XRB flux is produced at $z > 1$.

Field	$\omega(\theta)$ amplitude in units of $10^{-4}(\mathrm{deg})^{-0.8}$	
	X-ray Background	$18 \leq B \leq 23$ galaxies
GSGP4	6.515 ± 8.514	18.694 ± 4.438
SGP2	0.127 ± 8.700	6.710 ± 5.744
QSF3	3.197 ± 11.064	7.918 ± 4.393
Mean	3.345 ± 5.332	11.759 ± 2.743

Table 6.2 The $\theta^{-0.8}$ power-law amplitudes fitted to the ACF of the unresolved X-ray background (with detected sources removed), compared with the $\omega(\theta)$ amplitudes of the $18 \leq B \leq 23$ galaxies on the same areas. An error-weighted mean of the results from the three fields is also shown.

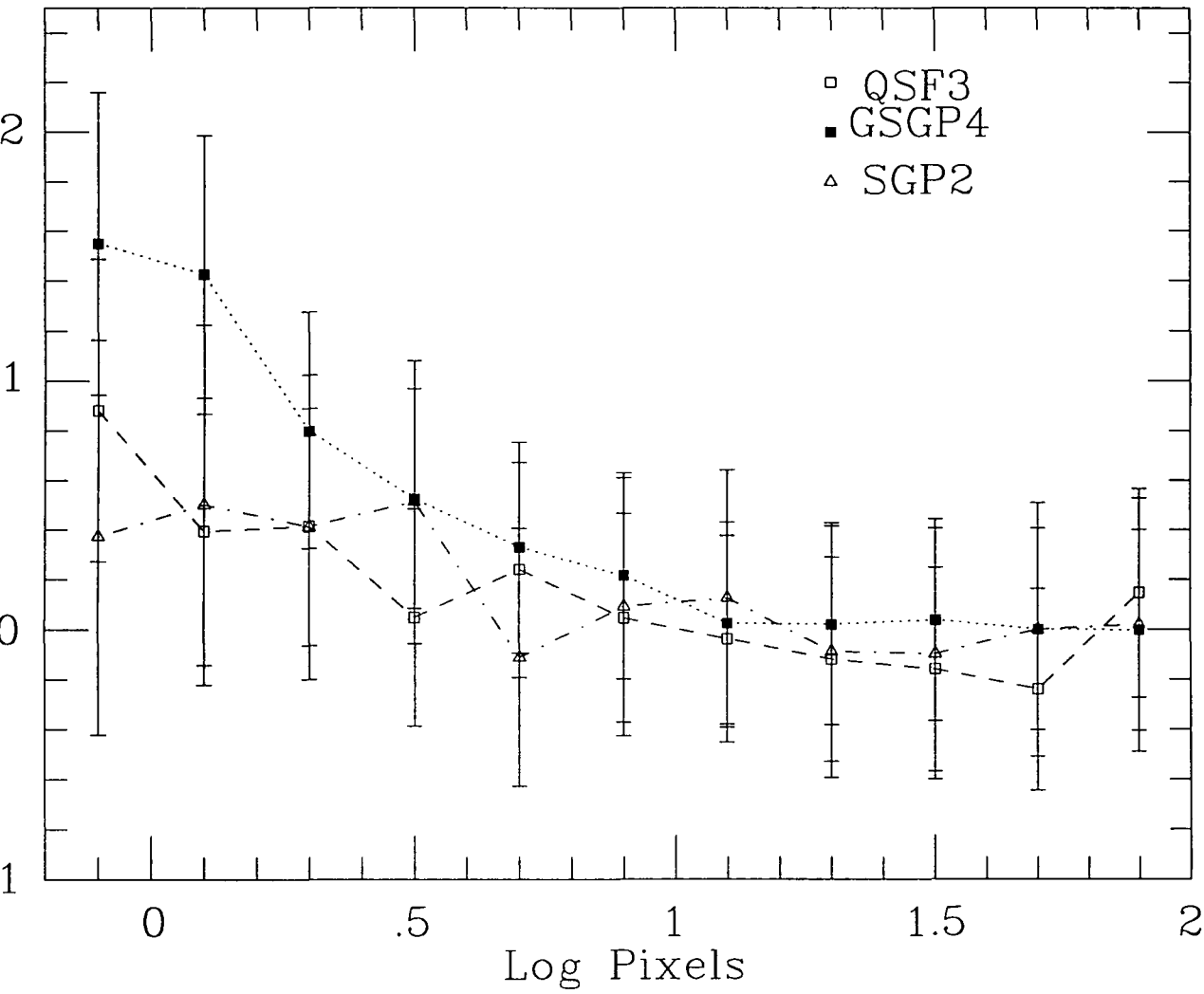

Figure 6.11 The angular correlation function, $\omega(\theta)$ of the $18.0 \leq B \leq 23.0$ galaxies (seen on AAT plates) on the same areas of sky as the ROSAT images used in calculating the XRB autocorrelation function. The graph shows the galaxy $\omega(\theta)$ for all 3 fields – GSGP4 (filled squares, dotted line), SGP2 (triangles, dot-dash line) and QSF3 (open squares, dashed line) – with the same logarithmic scale of angular separation as used for the XRB ACF, with θ in units of ROSAT pixels (15 arcsec). Errors were estimated as described in Section 6.4.

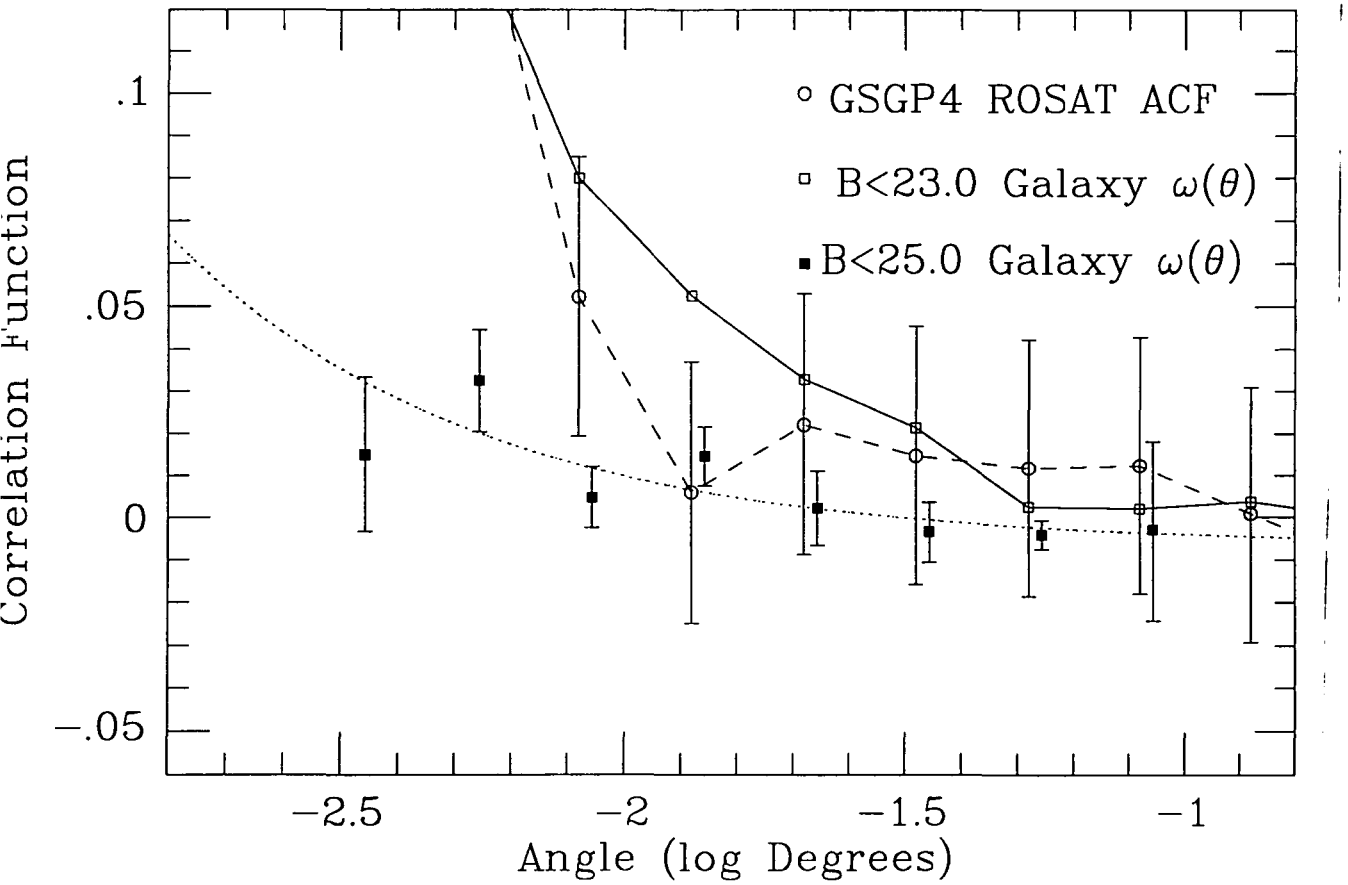

Figure 6.12 The autocorrelation function of the XRB on our GSGP4 image caompared with $\omega(\theta)$ of the $18.0 \leq B \leq 23.0$ galaxies on the corresponding area on the GSGP4 AAT plate, both with errors estimated as described in Section 6.4, and $\omega(\theta)$ of the $B_{ccd} \leq 25.0$ galaxies on our CCD survey (Chapter 2), with field-to-field errors and the fitted '$A(\theta^{-0.8} - 16.1)$' function (dotted line), with amplitude $A = 4.214 \times 10^{-4}(\mathrm{deg})^{-0.8}$.

6.7 Comparison with the Clustering of QSOs

Shanks and Boyle (1994) found that the clustering measured on $r \simeq 10$ h^{-1}Mpc scales in a sample of 700 QSOs with $z_{mean} \simeq 1.5$ could be reasonably well fitted by either a stable clustering model scaling from $r_0 \simeq 11$ h^{-1}Mpc at zero redshift, or a comoving clustering model scaling from $r_0 \simeq 6.6$ h^{-1}Mpc at zero redshift. These two models give similar strengths of QSO clustering at the median redshift of $z \sim 1.5$, where the difference between the two values of r_0 is approximately cancelled out by the difference between stable and comoving models. This is much stronger than the clustering of galaxies as measured at smaller ($r \sim 1$ h^{-1}Mpc) scales by our faint galaxy $\omega(\theta)$ amplitudes, which were well-fitted by a stable clustering model with a lower zero-redshift normalization of $r_0 \simeq 4.3$ h^{-1}Mpc.

We found in Section 6.6 above that our upper limits on the XRB fluctuations appear to be only slightly higher than the fluctuations predicted if the XRB was produced entirely by normally clustered galaxies. Hence if the intrinsic clustering of QSOs is significantly stronger than that of galaxies, as the Shanks and Boyle (1994) measurements might suggest, an XRB composed primarily of unresolved QSOs would contain significantly more fluctuations than observed, and it would be possible to use the ACF upper limits to set an upper limit on any QSO component in the unresolved XRB.

Georgantopoulos et al. (1993) predicted the XRB fluctuations on 2 arcmin scales produced by QSOs distributed out to $z = 4$, taking into account the observed luminosity evolution of QSOs and the flux-weighting of the ACF, for both the low-r_0/comoving and the high-r_0/stable models of QSO clustering described by Shanks and Boyle (1994). If QSOs produce a fraction $f_{\rm QSO}$ of the XRB flux, the fluctuations produced by the QSOs will scale approximately as $f^2_{\rm QSO}$, normalized by the intrinsic clustering strength of QSOs at their typical redshifts.

For both of these QSO clustering models, the 2σ upper limits on the ACF obtained by Georgantopoulos et al. (1993) from the two QSF fields gave the constraint $f_{\rm QSO} \leq 40\%$. With the lower 2σ limit given by the larger dataset used here, we can reduce the allowed QSO fraction still further to $f_{\rm QSO} \leq 30\%$.

However, any upper limit of $f_{\rm QSO}$ estimated from the upper limits on the ACF must be viewed with caution - as noted in Section 6.1 above, these models of QSO clustering are normalized to clustering measurements at relatively large physical separations ($r \sim 10$ h^{-1}Mpc), whereas we measure the ACF of the XRB and the $\omega(\theta)$ of galaxies on arcminute scales, corresponding at high redshifts to physical separations of only $r \sim 1$ h^{-1}Mpc.

This difference may be highly significant if the clustering evolution of galaxies and QSOs changes between a stable and a comoving model in the $1 \leq r \leq 10$ h^{-1}Mpc range. The small-scale clustering of QSOs, following a stable model, would then be weaker at high redshifts than the measurements at the larger scales within the comoving region would suggest, and much more similar to clustering of normal galaxies. Some evidence for this may be provided by the results of Ellingson, Yee and Green (1991), who measured the cross-correlation on small $r \leq 1$ h^{-1}Mpc scales between a sample of radio-quiet QSOs at $0.3 \leq z \leq 0.6$ and galaxies. This cross-correlation was estimated as $B_{gq} = 72 \pm 40$ Mpc$^{1.77}$ for $H_0 = 50$ km s^{-1}Mpc^{-1}, corresponding to a cross-correlation radius of $r_0 = 5.6^{+1.3}_{-2.2}$ h^{-1}Mpc, similar to the correlation radius of normal galaxies. Although the errors are large, this suggests that radio-quiet QSOs at these lower redshifts randomly sample the galaxy distribution. Furthermore, Georgantopoulos (1991) found the clustering of Seyfert AGN at low redshifts to be consistent with a $r_0 = 6.6$ h^{-1}Mpc model, which if scaled out to high redshifts with a comoving clustering evolution would

also fit the clustering of QSOs at $z_{mean} \sim 1.5$.

Shanks and Boyle (1994) argued that if the observed similarity of galaxy and QSO clustering properties at $0.3 \leq z \leq 0.6$ could be extrapolated to higher redshifts, and that high redshift QSOs are the progenitors of present-day Seyferts so must follow the same clustering model, these two results favoured their $r_0 = 6.6$ h^{-1}Mpc comoving model of QSO clustering. However, the very low $\omega(\theta)$ amplitudes measured for faint galaxies (Chapters 2, 3 and 4) require that the galaxy clustering at $r \sim 1$ h^{-1}Mpc scales be stable, rather than comoving, out to $z \sim 3$. At the faint magnitude limits ($B \sim 25$) at which galaxies are seen out to high redshifts, a comoving model for galaxy clustering would overpredict the observed galaxy $\omega(\theta)$ amplitudes, which are well-fitted by the stable model, by a factor of ~ 2.5, and could be rejected by at least 3σ. Hence if QSOs randomly sample the galaxy distribution on small scales, at $z \sim 1.5$ as well as lower redshifts, their small-scale clustering must be described by a low-r_0 stable model.

The strong QSO clustering observed by Shanks and Boyle (1994) at $r \sim 10$ h^{-1}Mpc scales would then result from a changeover from stable to comoving evolution at larger physical separations, which at redshifts of $z = 1.5$ would increase the clustering measured in the comoving region ($r \sim 10$ h^{-1}Mpc) by a factor of $(2.5)^{1.2} \simeq 3$ relative to the stable model prediction for the same r_0. If the high-redshift QSOs which dominate deep X-ray selected samples are no more clustered on small scales than galaxies, our ACF upper limits would be unable to constrain f_{QSO} any more strongly than f_{gal}, and with the strong luminosity evolution of QSOs would allow any value of f_{QSO} up to 100%.

However, the arguments for QSO and galaxy clustering being similar depend on the assumption that $z \sim 1.5$ QSOs are no different in their typical clustering properties from the QSOs and Seyferts seen at lower redshifts. Although the radio-quiet QSOs investigated by Ellingson, Yee and Green (1991) appeared to randomly sample the galaxy distribution, the radio-loud QSOs appeared to be preferentially found in environments of high galaxy density, and also appeared to undergo more rapid luminosity evolution from $z \sim 0.3$ to $z \sim 0.6$ than other QSOs. This might suggest that at low redshifts the QSOs visible would be mainly those with $r_0 \sim 6.6$ h^{-1}Mpc (i.e. clustering similar to or only slightly stronger than that of galaxies), but at high redshifts QSO populations with stronger clustering would brighten to a greater extent and increasingly dominate flux-limited samples.

In this way an environmentally dependent luminosity evolution could produce an effective clustering evolution for QSOs even if the clustering remained stable within each separate population. If this effect, rather than a changeover to comoving clustering at $r \sim 10$ h^{-1}Mpc, accounts for the strong clustering of high redshift QSOs measured by Shanks and Boyle (1994), the QSO clustering at $z \sim 1.5$ would be described by the $r_0 \sim 11$ h^{-1}Mpc stable clustering model, and would be much stronger than that of galaxies at $r \sim 1$ h^{-1}Mpc as well as on larger scales. Our constraint of $f_{QSO} \leq 30\%$ from the ACF upper limits would then still apply.

It may be possible to distiguish between these interpretations of the QSO clustering measurements through investigating the form of the faint galaxy $\omega(\theta)$, out to large ($\theta \sim 30$ arcmin) separations corresponding to $r = 10$ h^{-1}Mpc at high redshifts. If the clustering of both QSOs and galaxies changes from a stable model at $r = 1$ h^{-1}Mpc to a comoving model at $r = 10$ h^{-1}Mpc, the power-law index of $\xi(r)$ over this range of r must flatten significantly with redshift, from $\gamma = 1.8$ at $z = 0$ to $\gamma = 1.32$ at $z = 1.5$.

Infante (1990) found some indication of a flattening in the slope of $\omega(\theta)$ from $\omega(\theta) \propto \theta^{-0.75\pm0.04}$ at a $J = 23$ limit to $\omega(\theta) \propto \theta^{-0.67\pm0.04}$ at a $J = 24$ limit. Neuschaefer (1992) claims that the galaxy $\omega(\theta)$ as calculated from his CCD survey may show a rather

greater flattening in slope, even at relatively small separations of $1 \leq \theta \leq 4$ arcmin, from $\omega(\theta) \propto \theta^{-0.8}$ at $B \sim 22$ to to $\omega(\theta) \propto \theta^{-0.4}$ at $B \sim 25$, with these observations being well-fitted by a model where the $\xi(r)$ index evolves as $\gamma = 1.79(1+z)^{-0.4}$. These observations appear to support the Shanks and Boyle (1994) comoving interpretation, as the proposed flattening of $\xi(r)$, giving $\gamma = 1.32$ at $z = 1.15$, is in good agreement with that required to explain the strong clustering of QSOs seen on larger scales if the small scale clustering is given by the $r_0 = 6.6$ h^{-1}Mpc stable model.

However, as the statistical errors on the $\omega(\theta)$ slopes estimated by both Infante (1990) and Neuschaefer (1992) are almost as large as the estimated changes, and sensitivity gradients may introduce systematic errors in the large scale $\omega(\theta)$ towards the faintest limits of any survey, it is not yet clear whether the claimed flattening is a genuine effect, particularly as other observers have obtained different results at comparable depths. For example, JSF found that $\omega(\theta) \propto \theta^{-0.8}$ for galaxies on AAT plates, with no evidence for any flattening in the slope of $\omega(\theta)$ to limits of $B \sim 24$, and Couch, Jercevic and Boyle (1994), measuring the slope of $\omega(\theta)$ at $0.18 \leq \theta \leq 12$ arcmin on large-format CCD images, found that $\omega(\theta) \propto \theta^{-0.70 \pm 0.05}$ with no evidence for any systematic change in the value of the power-law index with apparent magnitude limit to $VR = 23.5$.

Unfortunately, in the deepest surveys yet carried out (Tyson 1988, MSFJ and Metcalfe et al. 1994), where effects produced by high-redshift galaxies would be strongest, the CCD frames cover areas too small to allow changes in the slope of $\omega(\theta)$ to be accurately measured. We would require deep ($B \sim 26$) surveys with large-format CCDs of extremely uniform sensitivity to further investigate claims for a flattening of $\omega(\theta)$.

At this point we can conclude that, whereas faint galaxies are already known to be sufficiently weakly clustered on small scales to produce any fraction of the the XRB, some doubt remains about whether this is the case for QSOs. It is clear that much more data is needed on the clustering properties of both QSOs and galaxies at high redshifts before measurements of the fluctuations in the X-ray background can be used to constrain unambiguously the relative values of f_{gal} and $f_{\rm QSO}$. Unless the clustering of high-redshift QSOs on small scales is found to be no stronger than that given by a stable model scaling from $r_0 \sim 5$ h^{-1}Mpc at $z = 0$, the lack of signal in the ACF appears to favour galaxies at $0 \leq z \leq 3$ and/or truly diffuse emission as the origin of most of the unresolved XRB. We now consider other ways in which upper limits may be set on $f_{\rm QSO}$ and on a diffuse component, before attempting to set a lower limit on f_{gal} thorough a direct galaxy/XRB cross-correlation in the next chapter.

6.8 Other Constraints on the Origin of the XRB

The P(D) analysis of Georgantopoulos at al. (1993) found a high pixel-to-pixel variance on the QSF field images of the XRB, which indicated that the total number counts of X-ray sources increased relatively steeply, with $\gamma \sim 1.2$, faintward of the QSF field detection limits of $S \sim 10^{-14}$ ergs cm^{-2}s^{-1}.

However, at $S \sim 10^{-14}$ ergs cm^{-2}s^{-1}, QSOs can be seen out to redshifts $z \sim 3$, close to their maximum redshift and/or the effective z_{max} resulting from the reduction in volume element at high redshifts (see Section 4.5), so that beyond this flux limit the QSO number counts would be expected to flatten to a slope following the faint end of their luminosity function. Boyle et al. (1993) and Boyle et al. (1994) fitted various parameters describing the form and evolution of the QSO luminosity function to the observed X-ray number counts and the redshift distributions of X-ray selected QSOs. With the luminosity functions and rates of evolution given by these models, the QSO counts would flatten to $\gamma \simeq 0.5$, corresponding to the estimated faint-end

slope of $\alpha \simeq -1.5$, at a flux of $S \sim 10^{-14}$ ergs cm^{-2}s^{-1}, and the QSO number counts extrapolated to much fainter fluxes would account for 34–53 % of the total 1–2 keV background.

An X-ray source number count slope as steep as the $\gamma \simeq 1.2$ inferred from the P(D) analysis could only be produced entirely by QSOs if their X-ray luminosity function at high redshifts possessed a much steeper faint-end slope (i.e. $\alpha \simeq -2.2$) than the Boyle et al. (1994) estimate, requiring a strongly luminosity-dependent evolution.

With the inclusion of results from the very deep GSGP4 ROSAT image, we can extend the QSO number counts to $S \sim 10^{-14.5}$ ergs cm^{-2}s^{-1} to verify whether the slope flattens as predicted or continues to increase as rapidly as $\gamma \sim 1.2$ (see Section 5.7). It was found that the number counts of 4σ-detected QSOs appeared to flatten exactly as predicted by the Boyle et al. (1994) models, suggesting that the fraction of the total XRB flux produced by QSOs is also in the range these models predict, i.e. 34–54%. Furthermore, about half the total X-ray flux from QSOs predicted by the Boyle et al. (1994) models has already been seen in the form of the 4σ detected QSOs. After the subtraction of the detected QSOs from these models, the predicted QSO fraction in the unresolved $\sim 65\%$ of the XRB is somewhat smaller (see Section 7.8), so that the Boyle et al. (1994) models and our QSO number counts actually suggest $f_{\rm QSO} \sim 30\%$.

The ACF upper limits would require the remaining $\sim 70\%$ of the XRB to be produced by very weakly clustered, discrete sources and/or a component of truly diffuse emission from very hot gas ($T \sim 10^7$–$10^8 K$). However, as noted in Section 1.9, COBE results (Wright et al. 1993) appear to exclude the possibility that a uniform intergalactic medium hot enough to fit the XRB spectrum to high energies could be of sufficient density to produce more than $\sim 1\%$ of the XRB. Cooler gas within and surrounding galaxy groups might produce a sufficient fraction of the XRB at soft energies to dilute the small-scale ACF to some extent, but any form of X-ray emission sufficiently extended to dilute the ACF at $\theta \sim 2$ arcmin would also reduce the pixel-to pixel variance measured on even smaller scales ($\theta \sim 30$ arcsec), by adding a Poissonian component to its P(D) distribution. Hence, the fact that the pixel-to-pixel variance on the QSF fields exceeds that predicted for QSOs alone favours a 'second population' of discrete X-ray sources (with small angular diameters not significantly exceeding the point spread function of $\theta \sim 30$ arcsec), rather than any form of extended emission, as the origin of the non-QSO component of the unresolved XRB.

If the 'second population' sources are intrinsically less luminous than QSOs, we would expect their counts to continue rising with a steep Euclidean ($\gamma = 1.5$) slope beyond the point where the QSO counts flatten to $\gamma \sim 0.5$. Georgantopoulos et al. (1993) found that if the 'second population' were assumed to have $\gamma = 1.5$, the source counts inferred from their P(D) analysis gave an estimate of its count normalization corresponding to $N(\log S > -14.4) = 27.87 \pm 7.96$ deg^{-2}. This is in very good agreement with the surface density of 27.18 ± 10.35 deg^{-2} galaxies with $B \leq 23$ we find to be correlated with log $S > -14.4$ sources (Section 5.7).

On our GSGP4 image we obtain a very similar pixel-to-pixel variance ($\langle N \rangle \omega(0)$) to that on QSF3 (Table 6.1), indicating a similar normalization for the 'second population'. On our SGP2 image the pixel-to-pixel variance was somewhat lower, possibly suggesting some 'contamination' by diffuse emission not seen on the other two images. However, the second population of discrete sources inferred from the P(D) distribution on the other fields must be present on SGP2 also, as our ACF results indicate the distribution of faint X-ray sources on the sky to be very uniform.

Hence the correlation between galaxies and X-ray sources detected in Chapter 5

is exactly that expected if galaxies comprise the 'second population' of discrete X-ray sources, and favours the hypothesis that galaxies produce the non-QSO $\sim 50\%$ or more of the XRB. However, we need to support the argument for a high value of f_{gal} by detecting directly a much larger galaxy contribution within the unresolved background. We shall attempt this in the following chapter by cross-correlating the $B \leq 23$ galaxies used in the source/galaxy cross-correlation of Chapter 5 with the images of the unresolved XRB used in the ACF analysis of this chapter.

6.9 Summary and Conclusions

(i) The autocorrelation function of the 0.5–2.0 keV background was calculated from two $\sim$ 30 ksec and one $\sim$ 50 ksec ROSAT PSPC images, with all sources above the 4σ detection threshold on each image excluded (leaving $\sim 65\%$ of the total flux). The resulting ACF showed some signal at $\theta \leq 40$ arcsec, within the range of angular separations corresponding to the instrumental point spread function, indicating that some faint, discrete sources were still present below the flux threshold for individual source detection. At larger separations the ACF was consistent with zero within the statistical errors, and fitting $\theta^{-0.8}$ power-laws (with errors estimated as described in Section 6.4) gave a 2σ upper limit on the ACF amplitude of $\omega(\theta) \leq 1.4 \times 10^{-3}(\mathrm{deg})^{-0.8}$.

(ii) This upper limit on the XRB ACF amplitude is similar to, or slightly below, the $\omega(\theta)$ amplitude of the $B \leq 23$ galaxies on AAT plates of the same fields as the ROSAT images. Fainter ($B > 24$), blue galaxies are much less clustered on the sky, with $\omega(\theta) \sim 4 \times 10^{-4}(\mathrm{deg})^{-0.8}$, which is well within our upper limits on the XRB fluctuations. Our ACF upper limits suggest that these fainter galaxies could produce much of the XRB flux.

When the flux-weighted nature of the ACF is taken into account, we find that an XRB produced entirely by non-evolving, normally clustered galaxies would contain much larger fluctuations than we observe. However, galaxies undergoing strong X-ray luminosity out to high redshifts would produce much smaller fluctuations in the XRB. Evolution similar to that of QSOs was found to be more than adequate to reduce the ACF amplitude predicted for galaxies to a value within our observational upper limits.

Hence our results remain consistent with the hypothesis that normally clustered galaxies, distributed out to $z \sim 4$ produce most of the unresolved XRB, if the mean X-ray luminosities of galaxies increase significantly with redshift.

(iii) The ACF upper limit is lower than the clustering amplitude expected for a source population consisting entirely of QSOs, if the strong QSO clustering (corresponding to $r_0 = 11$ h^{-1}Mpc for a stable model) measured by Shanks and Boyle (1994) on $r \sim 10$ h^{-1}Mpc scales can be extrapolated to the smaller separations of $r \sim 1$ h^{-1}Mpc where our ACF upper limits constrain the source clustering. If this is the case, our 2σ upper limits on the ACF would set an upper limit of $\sim 30\%$ on the QSO contribution to the unresolved 0.5–2.0 keV background.

However, if the clustering of QSOs follows a comoving model at $r \sim 10$ h^{-1}Mpc, but a stable model at $r \sim 1$ h^{-1}Mpc, the small-scale clustering of $z_{mean} \sim 1.5$ QSOs would be weaker by a factor ~ 3 than measurements on larger scales would suggest, and the upper limits on f_{QSO} from the ACF upper limits would be greatly relaxed.

It may be possible to investigate this possibility by measuring the slope of the galaxy $\omega(\theta)$ at faint ($B \sim 25$) limits. A changeover to comoving clustering in the $1 \leq r \leq 10$ h^{-1}Mpc range would cause the slopes of $\xi(r)$ and $\omega(\theta)$ for QSOs and galaxies to flatten significantly at high redshifts, giving approximately $\omega(\theta) \propto \theta^{-0.4}$ for very faint galaxies,

but it is not yet clear whether or not such a flattening of $\omega(\theta)$ is actually observed. Until further data are obtained on the clustering properties of both galaxies and QSOs at high redshifts, it remains uncertain whether or not the ACF upper limits can be used to set an upper limit on the QSO fraction.

(iv) More definite evidence that the QSO contribution to the XRB is no greater than $\sim 50\%$ is provided by the flattening of the X-ray number counts of QSOs (Section 5.7). The Boyle et al. (1994) models of QSO evolution predicted the QSO counts to flatten to $\gamma \sim 0.5$ at $S \sim 10^{-14}$ ergs s^{-1}, where QSOs are seen out to their high redshift limit. With the deeper GSGP4 data we are able to confirm that the predicted flattening in the QSO counts does occur, suggesting that the QSO luminosity function and rate of evolution in the Boyle et al. (1994) models are approximately correct, and therefore that the total X-ray flux from QSOs is also in the range predicted by these models, only $\sim 30\%$ of the unresolved XRB.

The P(D) analysis of Georgantopoulos et al. (1993) on the unresolved XRB on the 2 QSF fields indicated an excess in the pixel-to-pixel variance above the predictions for QSOs alone, indicating that the number counts of all discrete X-ray sources increase as $\gamma \simeq 1.2$ faintward of the detection limit, where the QSO count slope flattens to $\gamma \sim 0.5$. Although diffuse emission from extended (over $\theta \sim 2$ arcmin scales or larger) hot gas could help to explain the lack of signal in the ACF, it would also reduce the pixel-to-pixel variance relative to the QSO prediction, in contradiction with observations. The P(D) results suggest that the non-QSO component of the unresolved XRB consists of a 'second population' of discrete sources, with a number count slope remaining steep ($\gamma \sim 1.5$) at $S < 10^{14}$ ergs $cm^{-2}s^{-1}$. The normalization of the 'second population' number counts estimated by Georgantopoulos et al. (1993) is in very good agreement with the numbers of galaxies we find to be correlated with unidentified X-ray sources.

Hence the QSO number counts suggest that QSOs comprise only $\sim 30\%$ of the unresolved component of the XRB, while the P(D) analysis results, in combination with the galaxy detections of the previous chapter, suggest that galaxies produce most of the remaining $\sim 70\%$. These proportions would be consistent with the ACF upper limits whether QSO clustering is similar to galaxy clustering or as strong as the $r_0 \sim 11$ h^{-1}Mpc stable model.

Chapter 7

The Cross-Correlation of Galaxies with the X-Ray Background

7.1 Introduction

In this chapter we investigate the cross-correlation between galaxies in the magnitude range $18.0 \leq B \leq 23.0$ and the unresolved 0.5–2.0 keV background, on 3 ROSAT fields totalling 1.05 deg^2.

We have already found at least $\sim 10\%$ of the X-ray sources detected individually on these fields to be associated with $B \leq 23$ galaxies, giving a surface density of galaxies with X-ray fluxes above the source detection limit ($S \simeq 10^{-14.4}$ ergs cm^{-2}s^{-1}) of ~ 30 deg^{-2}. As discussed in Section 5.7, galaxies are expected to comprise an increasingly large fraction of the X-ray source counts at even fainter fluxes, where their log N–log S relation is likely to remain approximately Euclidean to at least $S \sim 10^{-16}$ ergs cm^{-2}s^{-1}, whereas QSO number counts are predicted and observed to flatten significantly at $S \sim 10^{-14}$ ergs cm^{-2}s^{-1}. Extrapolating the galaxy counts in the ROSAT band with a Euclidean slope from $S = 10^{-14.4}$ ergs cm^{-2}s^{-1} to $S = 10^{-16}$ ergs cm^{-2}s^{-1} gives a surface density approaching that of $B \leq 23$ galaxies ($\sim 10^4$ deg^{-2}), and accounts for at least 10% of the XRB flux.

Therefore, although the X-ray luminosities of the detected galaxies are unusually high, we would expect the remaining $18 \leq B \leq 23$ galaxies, with lower X-ray luminosities but a much higher surface density, to produce in total a somewhat larger X-ray flux. Most of these galaxies will have X-ray fluxes far too small to be detected individually (e.g. a flux $S = 10^{-16}$ ergs cm^{-2}s^{-1} will only be $\sim 0.1\sigma$ above the background on these images), but when the X-ray emission of several thousand such galaxies is summed in the calculation of a galaxy/XRB cross-correlation, the result is likely to be statistically significant.

Giacconi and Zamorani (1987) estimated that 'normal' galaxies produce at least 13% of the 2 keV background, by assuming a mean $f_\nu(2\text{ keV})/f_\nu(\text{B})$ ratio of $10^{-6.6}$ (derived from *Einstein* observations of local galaxies), and extrapolating to the very faint limit of $B = 27.5$ using the counts of Tyson (1988). However, as we find that some galaxies even at $B < 21$ have X-ray/optical flux ratios higher by factors of ~ 100 than the mean ratio assumed by Giacconi and Zamorani (1987), the total X-ray emission from faint galaxies is likely to exceed their estimate.

Griffiths and Padovani (1990, hereafter GP) then estimated that IRAS and starburst galaxies alone, seen out to high redshifts, would produce $\sim$ 20–30% of the 0.5–3.0 keV XRB, assuming the relation between X-ray and far infra-red (60μm) luminosity seen for galaxies locally and a 'moderate' rate of X-ray evolution estimated from the observed increase of 60μm luminosities with redshift. We consider this model in more detail, and compare its predictions with our cross-correlation results, in Sections 7.8, 7.9 and 7.10.

The cross-correlation between galaxies and the XRB was investigated directly by Lahav et al. (1993), in a very similar analysis to that presented here, but covering a larger area of sky to a lesser depth ($z \leq 0.06$) and with lower resolution. The numbers of galaxies in the catalogues used by Lahav et al. (1993) were counted in cells, giving N_g for each cell, where the XRB intensity within each cell, as mapped by the *Ginga* and HEAO-1 satellites, is I_X. The cross-correlation at zero separation is then the covariance

of these two values divided by the product of their respective mean values i.e.

$$W_{gx}(0) = \frac{\langle (N_g - \langle N_g \rangle)(I_X - \langle I_X \rangle) \rangle}{\langle N_g \rangle \langle I_X \rangle}$$

These authors found a positive and significant (3σ) W_{gx}, and after applying a correction for the effect of galaxy clustering (see Section 7.3), estimated that their galaxies produced a volume X-ray emissivity

$$\rho(2\text{–}10 \text{ keV}) \sim (1.5 \pm 0.5) \times 10^{39} \text{ h ergs s}^{-1}\text{Mpc}^{-3}.$$

By extrapolating this X-ray emissivity out to $z \sim 5$, Lahav et al. (1993) estimated that galaxies would in total account for $\sim 30\%$ of the 2–10 keV XRB with no X-ray luminosity evolution, and larger fractions if the emissivity was any higher at earlier epochs. Miyaji et al. (1994) performed a similar cross-correlation using IRAS galaxies, and estimated a slightly lower emissivity. If these results are genuine and apply similarly at softer energies, at the greater depths of our AAT plate data we should find ~ 2000 of the 14540 photons in the 0.5–2.0 keV unresolved background on our 3 fields to be associated with the AAT galaxies, giving a cross-correlation of high statistical significance ($> 5\sigma$) and enabling us to estimate reasonably accurately the mean X-ray/optical flux ratio and X-ray volume emissivity of these galaxies.

If a sufficiently strong signal is detected it may be possible to investigate the X-ray emission of passive and star-forming galaxies separately, by dividing the GSGP4 galaxies by $B-R$ colour and performing a separate cross-correlation analysis for the red and blue subsamples. Furthermore, with the high resolution of ROSAT data it may be possible to investigate the form of $W_{gx}(\theta)$ at non-zero angular separations, and therefore determine whether extended emission from galaxy groups and clusters is a significant component of the total X-ray flux from galaxies.

We shall also compare our cross-correlation with that of Lahav et al. (1993), taking into account the different energy bands, as this may provide some information about the evolution of the X-ray emissivity of galaxies between the epochs corresponding to the mean redshifts of the two galaxy samples ($z_{mean} \sim 0.35$ for our $B \leq 23$ AAT dataset, on the basis of redshift surveys at this magnitude limit – e.g. Colless et al. 1990, and $z_{mean} \simeq 0.03$ for the much shallower catalogue used by Lahav et al. 1993).

7.2 Calculating the Cross-correlation

In calculating W_{gx} we use the $18.0 \leq B \leq 23.0$ galaxies found on the three AAT plates described in Section 5.2.3, together with the 0.5–2.0 keV ROSAT images of the same areas – the GSGP4, SGP2 and QSF3 fields. X-ray sources detected above 4σ were excluded, as described in Section 6.2, giving the holed images shown on Figures 6.4, 6.5 and 6.6. As in our calculation of the background ACF, this analysis used only the ROSAT pixels and galaxies within 16 arcmin radii of the ROSAT image centres.

Cross-correlation functions were calculated separately for each of the 3 fields. As in the source/galaxy cross-correlation of Chapter 6, the AAT galaxy positions were converted to pixel co-ordinates on the corresponding ROSAT images. The cross-correlation as a function of angular separation, $W_{gx}(\theta)$, is given by

$$W_{gx}(\theta_n) = \frac{\sum N_{gx}(\theta_n)}{\sum N_{gp}(\theta_n)\langle N_X \rangle} - 1$$

where $\langle N_X \rangle$ is the mean number of photons per pixel for the whole image area, $\sum N_{gx}(\theta_n)$ is the number of photons counted in annular bin n centred on a galaxy, summed for

all galaxies in the sample, $\sum N_{gp}(\theta_n)$ is the number of ROSAT pixels in annular bin n, summed for all galaxies, and the annular bins of angular separation are defined as $10^{0.2(n-1)} \leq \theta_n < 10^{0.2n}$ pixels as in the previous chapter.

Errors were estimated by dividing each galaxy dataset randomly into 10 subsets and calculating $W_{gx}(\theta)$ separately for each. The subset-to-subset dispersion in $W_{gx}(\theta)$ at each value of θ was then divided by $\sqrt{10}$ to give the error bars for the $W_{gx}(\theta)$ of all galaxies in the field.

7.3 Cross-correlation Results

Figure 7.1 shows the galaxy/XRB cross-correlation function for the 2461 $18.0 \leq B \leq 23.0$ galaxies found within the 16 arcmin radius circular area on the GSGP4 field. A positive and significant cross-correlation is seen, with an amplitude of $W_{gx}(0) = 0.10$ indicating each galaxy to be producing on average an enhancement of the XRB intensity of $\sim 10\%$, spread over the point-spread function area of ~ 1 arcmin^2. As the surface density of $18.0 \leq B \leq 23.0$ galaxies is ~ 2 arcmin^{-2} their total contribution to the XRB, discussed in detail in Section 7.4 below, may be closer to $\sim 20\%$.

On the GSGP4 field, a total of 4025 photons were detected at $\theta \leq 15$ arcsec from a galaxy, compared to 3651 expected by chance, which is 5.9 sigma on the basis on Poisson statistics. The true errors will be slightly larger than Poisson, as the presence of discrete unresolved sources in the XRB will produce an effective clustering of the photons on small scales. When errors are estimated by dividing the galaxy sample, as described in Section 7.2 above, the significance of the cross-correlation at $\theta \leq 15$ arcsec is $\sim 4.7\sigma$. To check that the radial sensitivity gradient in the ROSAT data was not producing a spurious signal, the galaxy/XRB cross-correlation function was calculated for only the central 12 arcmin radius central area of the GSGP4 field. This cross-correlation function is also shown on Figure 7.1. It is clear that excluding the outer annulus between off-axis angles of 12 and 16 arcmin has no significant effect on the form or amplitude of the galaxy/XRB cross-correlation function, which is reduced in significance (to 3.5σ) only to the extent expected from the $\sim 40\%$ reduction in area.

Figures 7.2 and 7.3 show $W_{gx}(\theta)$ for the 1551 $18.0 \leq B \leq 23.0$ galaxies on SGP2 and the 2337 on QSF3. These are somewhat lower in amplitude and significance (approx. 3.5σ and 2.0σ respectively) than the GSGP4 cross-correlation. Again we find that, as in the cross-correlation of the detected sources with galaxies (Chapter 5), it is the deeper GSGP4 image which gives the strongest result.

Figure 7.4 shows an overall galaxy/XRB cross-correlation function obtained by summing the galaxy-photon pairs $N_{gx}(\theta_n)$ over all three fields and separately summing the $N_{px}(\theta_n)\langle N_X \rangle$ terms. This gave a combined $W_{gx}(\theta)$ in which each galaxy-photon pair, rather than each field, has the same weighting. The longer exposure of GSGP4 means that this field will contribute a larger proportion of the signal in this combined $W_{gx}(\theta)$ than the other two. Although the addition of the weaker QSF3 and SGP2 cross-correlations functions to that seen on GSGP4 reduced $W_{gx}(0)$ to 0.062, the overall significance of our detection of a correlation between $18.0 \leq B \leq 23.0$ galaxies and the XRB remains high ($\sim 4\sigma$ in the $\theta \leq 15$ arcsec interval alone).

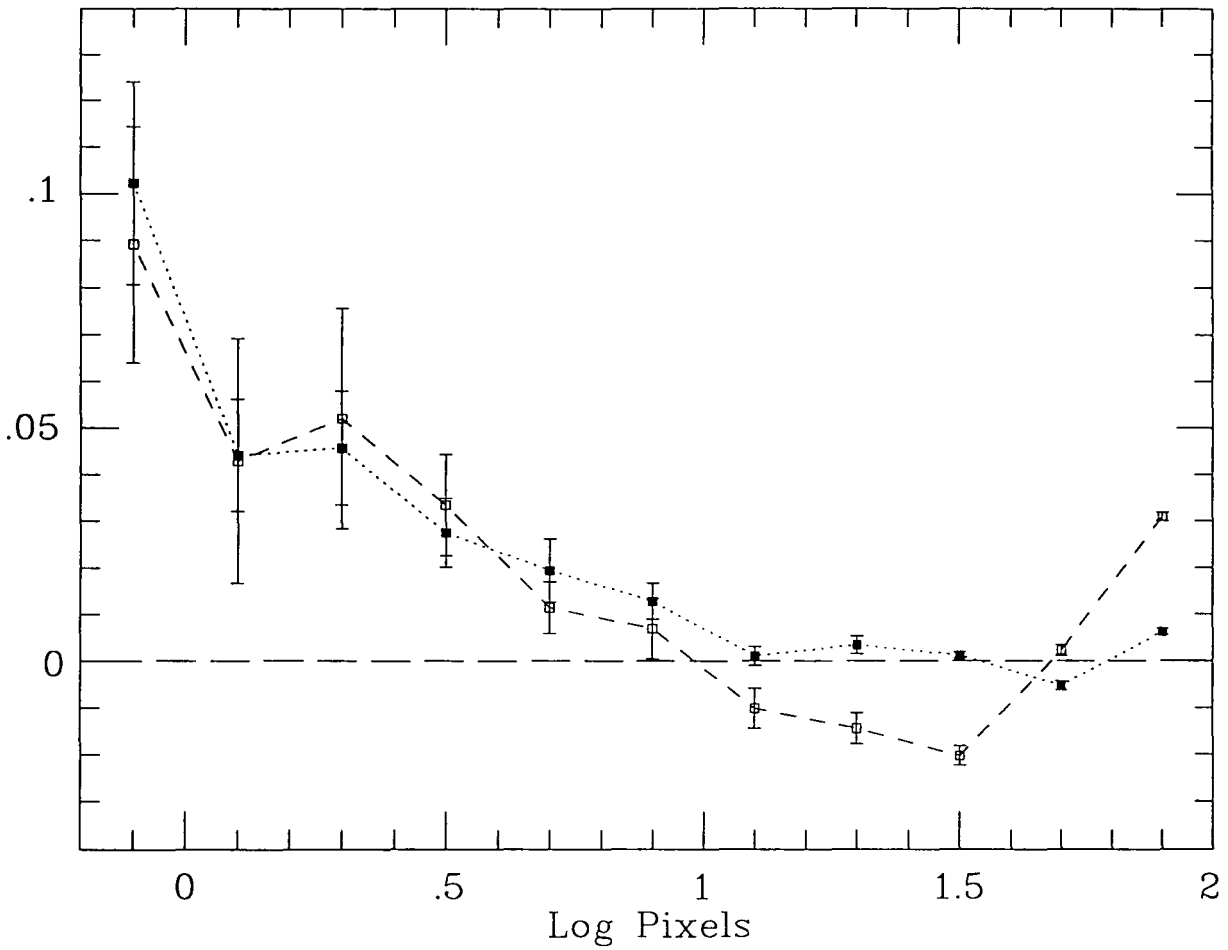

Figure 7.1 Cross-correlation of the $18.0 \leq B \leq 23.0$ galaxies on the GSGP4 field with the unresolved 0.5–2.0 keV X-ray background on the same area, as a function of the logarithm of angular separation in units of ROSAT pixels (15 arcsec). The filled squares (with dotted lines) show the cross-correlation function calculated using the full 16 arcmin radius central area of GSGP4, while the open squares (with dashed lines) show the cross-correlation function calculated using only the central 12 arcmin radius central area of this field (see Section 7.3).

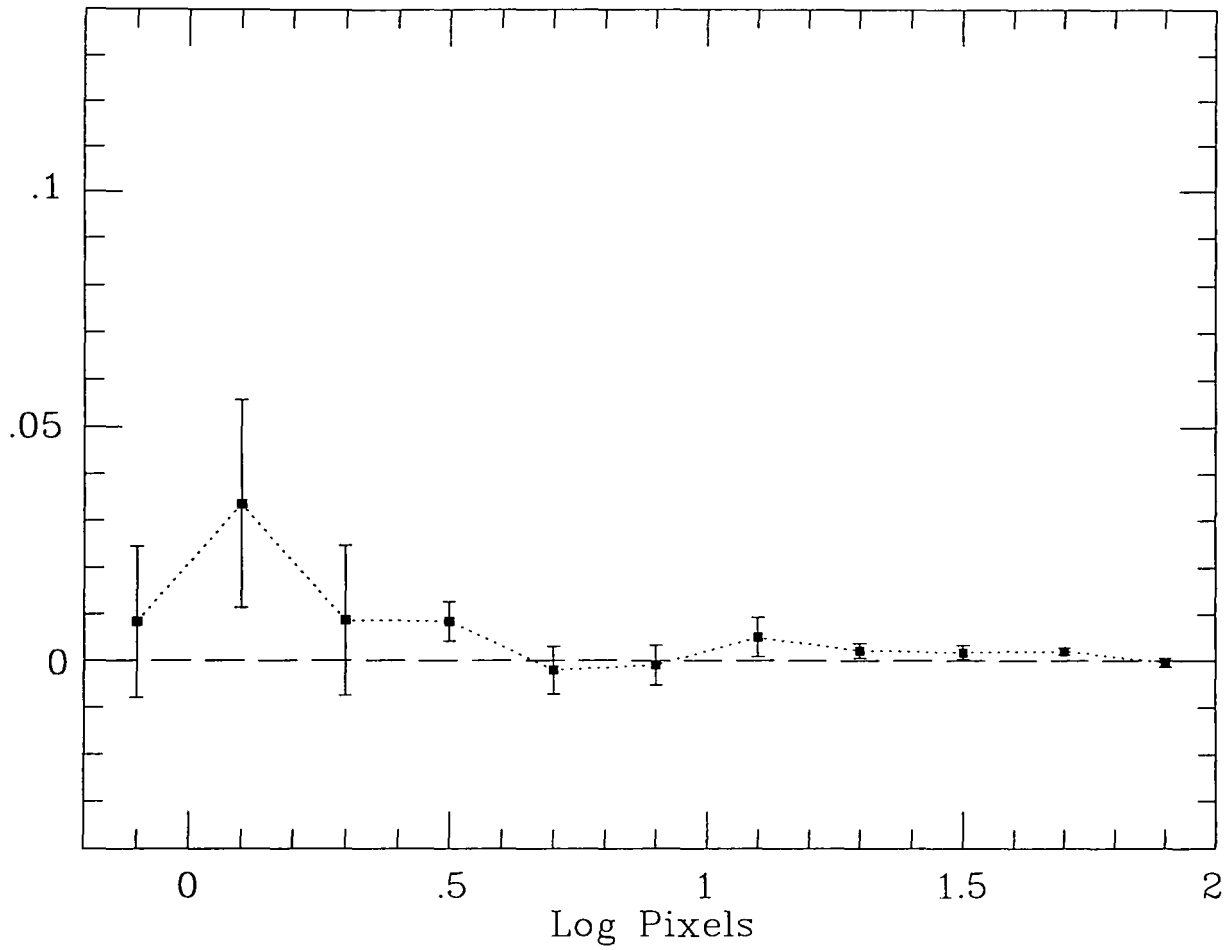

Figure 7.2 Cross-correlation of the $18.0 \leq B \leq 23.0$ galaxies on the SGP2 field with the unresolved 0.5–2.0 keV X-ray background on the same area, as a function of the logarithm of angular separation in units of ROSAT pixels (15 arcsec).

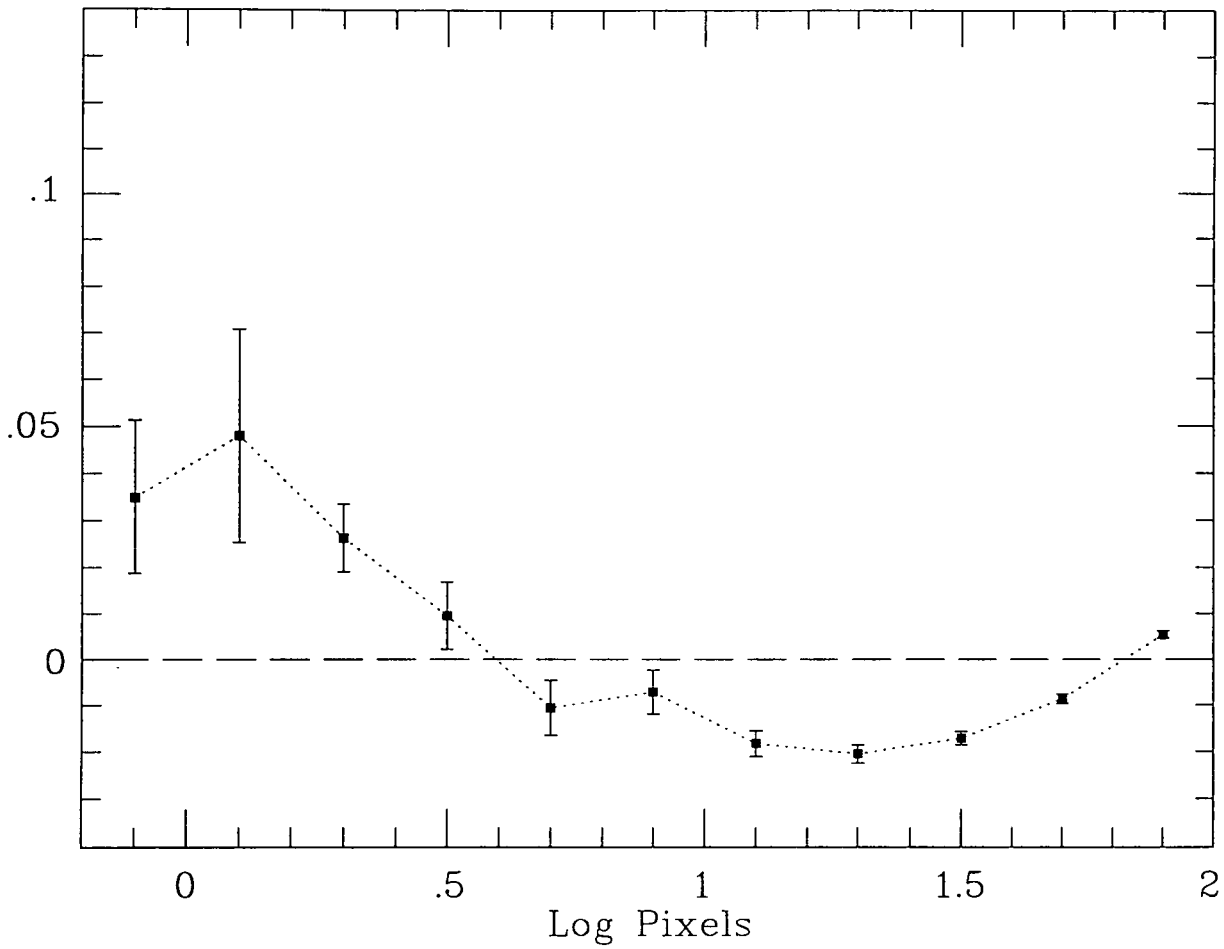

Figure 7.3 Cross-correlation of the $18.0 \leq B \leq 23.0$ galaxies on the QSF3 field with the unresolved 0.5–2.0 keV X-ray background on the same area, as a function of the logarithm of angular separation in units of ROSAT pixels (15 arcsec).

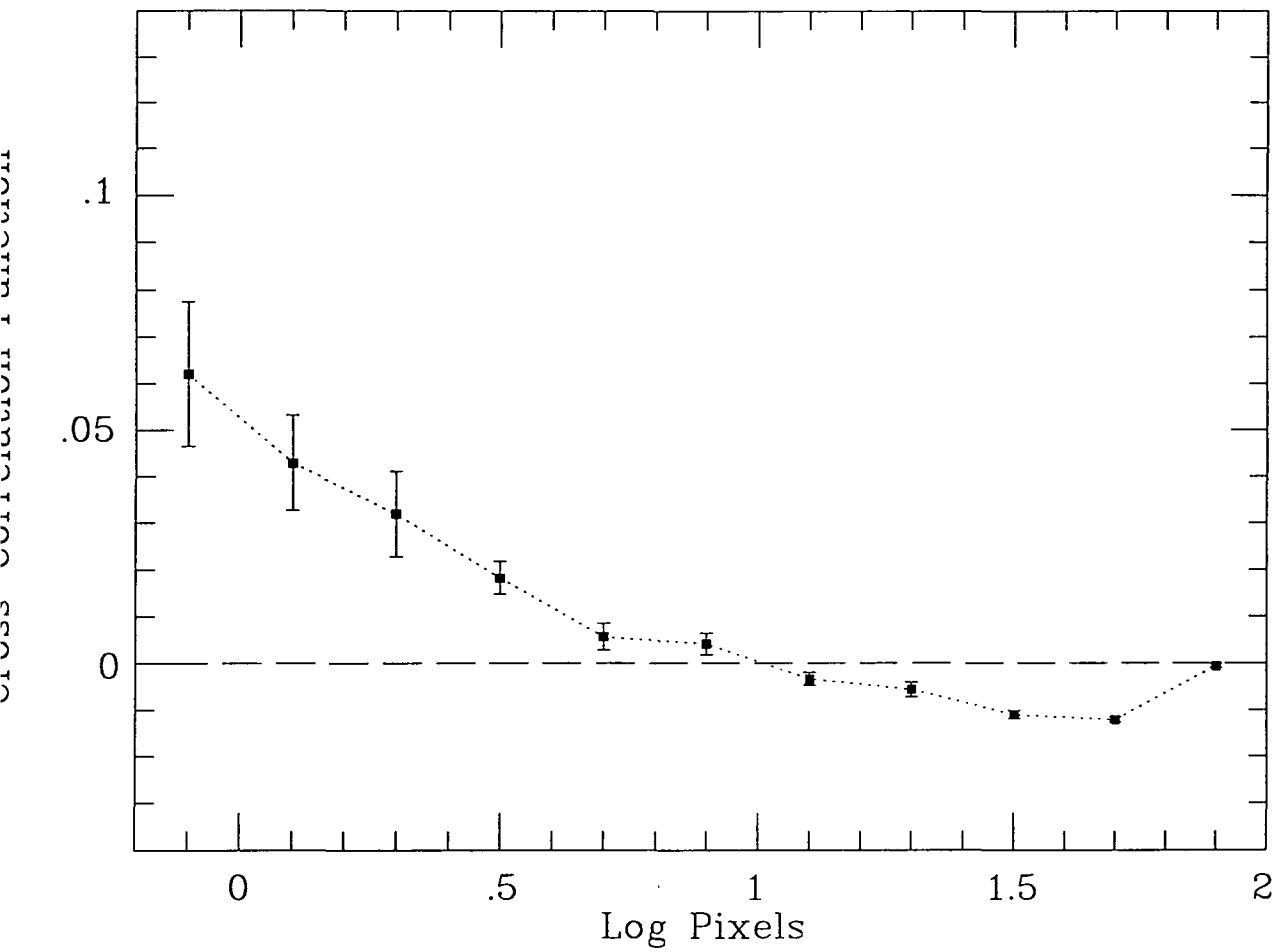

Figure 7.4 Cross-correlation of $18.0 \leq B \leq 23.0$ galaxies with the unresolved 0.5–2.0 keV X-ray background for our 3 AAT plate areas combined, weighting the results from each field by the number of galaxy-photon pairs (see Section 7.3).

7.4 The XRB Contribution of $18.0 \leq B \leq 23.0$ Galaxies

A significant correlation between the galaxies on these AAT plates and the unresolved X-ray background is seen in the first four bins of angular separation (θ_0 to θ_3) on Figures 7.1, 7.2, 7.3 and 7.4, i.e. at angular separations in the range $0 \leq \theta \leq 1$ arcminute.

The number of X-ray photons associated with the galaxies could be estimated by summing

$$\sum_{n=0}^{n=3} N_{gx}(\theta_n) - \langle N_X \rangle \sum_{n=0}^{n=3} N_{gp}(\theta_n)$$

i.e. the number of pairs of galaxies and X-ray photons at $\theta < 1$ arcmin over that expected if these were entirely uncorrelated.

For our three fields this gives:

GSGP4: 2187.0 ± 322.4 photons

SGP2: 281.2 ± 134.4 photons

QSF3: 640.4 ± 178.6 photons.

However, if these galaxies are clustered at $\theta < 1$ arcmin scales this will be an overestimate, as each galaxy will have been cross-correlated with the X-ray emission of its cluster neighbours as well as its own. This effect is also discussed (and corrected for) in the analyses of Lahav et al. (1993) and Miyaji et al. (1994), where clustering was estimated to increase the measured cross-correlation by large factors of ~ 2–4.

Consider an image area divided into a large number of cells N_c, with the mean number of galaxies per cell being $\langle N_g \rangle$ and the mean number of X-ray photons per cell being $\langle N_X \rangle$.

We can estimate the mean X-ray flux per galaxy, f, by fitting a line

$$(N_X - \langle N_X \rangle) = f(N_g - \langle N_g \rangle)$$

to the data by a least-squares method – ie. by minimizing χ^2 where

$$\chi^2 = \sum [f(N_g - \langle N_g \rangle) - (N_X - \langle N_X \rangle)]^2$$

and the summation is over all N_c cells in the image. Differentiating,

$$\frac{d\chi^2}{df} = 2 \sum [f(N_g - \langle N_g \rangle) - (N_X - \langle N_X \rangle)](N_g - \langle N_g \rangle)$$

The χ^2 will be at a minimum for $\frac{d\chi^2}{df} = 0$ giving

$$f \sum (N_g - \langle N_g \rangle)^2 = \sum (N_X - \langle N_X \rangle)(N_g - \langle N_g \rangle)$$

which is equivalent to

$$f = \frac{covariance(N_X, N_g)}{variance(N_g)}$$

We can also express the covariance as

$$covariance(N_X, N_g) = \langle N_X \rangle \langle N_g \rangle \int_{cell} \int_{cell} W_{gx}(\theta) \delta\Omega_1 \delta\Omega_2$$

where the cross-correlation function $W_{gx}(\theta)$ – the angle θ being the separation between the integration elements $\delta\Omega_1$ and $\delta\Omega_2$ – is doubly integrated over the cell area.

The excess of galaxy-photon pairs within θ of a galaxy above that expected in the absence of a correlation,

$$N'_{gx}(\theta) = \sum N_{gx}(\theta) - \langle N_X \rangle \sum N_{gp}(\theta)$$

is equivalent to

$$N'_{gx}(\theta) = \langle N_X \rangle \langle N_g \rangle \int_{area} \int_{\theta} W_{gx}(\theta) \delta\Omega_1 \delta\Omega_2$$

where the $\delta\Omega_2$ integration covers the entire image area (ie. all the galaxies) but $\delta\Omega_1$ is only integrated out to a radius θ from the position of the $\delta\Omega_2$ element (ie. counting the photons within a radius θ of each of these galaxies).

Hence if each cell has a radius θ and there are N_c cells in the total area,

$$N'_{gx}(\theta) = N_c \times covariance(N_X, N_g)$$

Considering the variance of N_g, which relates to the galaxy clustering,

$$var(N_g) = \langle N_g \rangle + \langle N_g \rangle^2 \int_{cell} \int_{cell} \omega_g(\theta) \delta\Omega_1 \delta\Omega_2$$

where $\omega_g(\theta)$ is the autocorrelation function of the galaxies.

The excess number of galaxy-galaxy pairs at separations $\leq \theta$ above that expected for a random distribution, $N'_{gg}(\theta)$, relates to $\omega(\theta)$ of the galaxies as

$$N'_{gg}(\theta) = \langle N_g \rangle^2 \int_{area} \int_{\theta} \omega_g(\theta) \delta\Omega_1 \delta\Omega_2$$

again where $\delta\Omega_2$ integration covers the entire image area but $\delta\Omega_1$ is only integrated out to a radius θ from the position of the $\delta\Omega_2$ element. Hence

$$N'_{gg}(\theta) = N_c \langle N_g \rangle^2 \int_{cell} \int_{cell} \omega_g(\theta) \delta\Omega_1 \delta\Omega_2$$

and

$$var(N_g) = \langle N_g \rangle + N_c^{-1} N'_{gg}$$

As each cell contains on average $\langle N_g \rangle$ galaxies, the total X-ray photon contribution from all galaxies in the area will be given by

$$N_c f \langle N_g \rangle = \frac{\langle N_g \rangle N_c \times covariance(N_X, N_g)}{var(N_g)} = \frac{\langle N_g \rangle N'_{gx}(\theta)}{\langle N_g \rangle + N_c^{-1} N'_{gg}(\theta)}$$

If G_{tot} is the total number of galaxies in the entire image, given by $G_{tot} = N_c \langle N_g \rangle$, this can also be written as

$$N_c f \langle N_g \rangle = G_{tot} f = \frac{N'_{gx}(\theta)}{1 + G_{tot}^{-1} N'_{gg}(\theta)}$$

We have already calculated $\omega(\theta)$ for the same $18.0 \leq B \leq 23.0$ galaxies as used here, in Section 6.6. The galaxy-galaxy pair excess N'_{gg} at $\theta < 1$ arcmin, counted in the process of calculating $\omega(\theta)$, was 874 for the galaxies on GSGP4, 217 on SGP2, and 229 on QSF3.

Our estimates (given earlier in this section) of the total numbers of X-ray photons in each image produced by $18 \leq B \leq 23$ galaxies can then be corrected for the clustering of these galaxies simply by dividing by the $(1 + G_{tot}^{-1} N'_{gg}(\theta))$ term, which is 1.355 for GSGP4, 1.140 on SGP2 and 1.098 on QSF3. The effects of clustering are evidently much smaller in our analysis than in the cross-correlations of Lahav et al. (1993) and Miyaji et al. (1994), presumably as a result of the greater depth (and therefore the lower $\omega(\theta)$ amplitude) of our galaxy dataset and the smaller resolution elements of our X-ray images.

Considering the three fields separately, we obtain estimates of the numbers of X-ray photons on each image produced by the $18 \leq B \leq 23$ galaxies of:

GSGP4: 1613.9 ± 237.9 photons

SGP2: 246.7 ± 117.9 photons

QSF3: 583.3 ± 162.7 photons.

The 16 arcmin radius central areas of each image, with pixels containing detected sources excluded, contain 6215 photons on GSGP4, 4450 on SGP2 and 3875 on QSF3. Combining the results from the three fields, and weighting each photon rather than each field equally, gives a clustering-corrected estimate of the $18.0 \leq B \leq 23.0$ galaxy contribution to the unresolved X-ray background of:

$$\begin{aligned}(1613.9 \pm 237.9 + 246.7 \pm 117.9 + 583.3 \pm 162.7)/(6215 + 4450 + 3875) \\ = (2443.9 \pm 311.4)/14540 \\ = 16.8 \pm 2.1\%\end{aligned}$$

Miyaji et al. (1994) also consider and apply corrections for the effects of the cross-correlation between galaxies and AGN, in addition to the effects of galaxy clustering. In our analysis, our estimate of the number of X-ray photons asociated with each galaxy, f, will actually include both the photons produced by the galaxy itself (f_g) and the photons produced by any sources which may be correlated with the galaxies but not included in the galaxy catalogue. These sources will consist primarily of the AGN with fluxes too low to be individually detected above 4σ and therefore excluded from the X-ray data, which lie within the same volume of space (i.e. $z \leq 0.6$) as the AAT galaxies.

If each of these AGN produces on average a flux f_A, and the total number of galaxy-AGN pairs within a radius θ above the number expected by chance is N'_{gA}, then

$$f \simeq f_g + N'_{gA} G_{tot}^{-1} f_A$$

If low redshift AGN are assumed to randomly sample the galaxy distribution,

$$N'_{gA} \simeq \frac{N_A}{N_g} N'_{gg}$$

where $\frac{N_A}{N_g}$ is the number ratio of AGN to galaxies. This gives an AGN correction

$$f - f_g \simeq f_A \frac{N_A}{N_g} N'_{gg} G_{tot}^{-1}$$

which for the whole image becomes

$$G_{tot}(f - f_g) \simeq f_A A_{tot} N'_{gg} G_{tot}^{-1}$$

where A_{tot} is the total number of $z < 0.6$ AGN in a ROSAT image, and $f_A A_{tot}$ is therefore the total photon contribution of these AGN.

When the flux from 4σ-detected QSOs is subtracted from the Boyle et al. (1994) models of QSO evolution (see Section 7.9), the remaining unresolved QSOs would produce no more than $\sim 30\%$ of the unresolved XRB, and only $\sim 5\%$ of the XRB would be produced by the AGN at $z < 0.6$. To estimate very approximately the overestimation of the contribution of AAT galaxies to the XRB, we can multiply this percentage by the $N'_{gg} G_{tot}^{-1}$ term, which varies from 0.098–0.355 between our images, giving an AGN correction of only 0.49–1.78%.

We conclude that, whereas the galaxy-AGN cross-correlation may have made a significant contribution in the shallower Miyaji et al. (1994) analysis, it produces a very small effect here, less than our 1σ error bar, and more than an order of magnitude less than the XRB contribution from the AAT galaxies themselves. As the AGN correction is more difficult to estimate accurately than the larger corrections caused by the directly observable clustering of the AAT galaxies with each other, we therefore, having shown the contribution of correlated AGN to our results to be very small, ignore the effect of AGN in this analysis.

7.5 Colour Dependence of the Cross-correlation

For GSGP4 we also have red magnitudes from another AAT plate (see Section 5.2.3). The cross-correlation analysis for this field was repeated with the galaxies divided into red ($B - R \geq 1.5$) and blue ($B - R < 1.5$) subsets.

Figures 7.5 and 7.6 show the XRB cross-correlation functions of the 1942 blue and the 519 red galaxies. The amplitudes are similar at $\theta \leq 25$ arcsec, in agreement with the findings of Chapter 5 that the X-ray sources showed similar correlations with both red and blue galaxies.

Summing

$$\sum_{n=0}^{n=3} N_{gx}(\theta_n) - \langle N_X \rangle \sum_{n=0}^{n=3} N_{gp}(\theta_n)$$

out to $\theta = 1$ arcmin for the red and blue galaxy cross-correlations with the XRB gives estimates of the X-ray photon contributions –

From the bluer galaxies: 1362.2 ± 349.4 photons

From the red galaxies: 824.8 ± 168.8 photons.

These estimates correspond to 1.59 photons per red galaxy but only 0.70 photons per blue galaxy, the difference being due entirely to the fact that the red galaxy $W_{gx}(\theta)$ shows more signal at larger separations ($40 \leq \theta < 60$ arcsec). However, corrections for the clustering of the galaxies must still be applied. If the difference between the cross-correlation of red and blue galaxies with the XRB at larger separations is significant, it may indicate that

(i) the redder X-ray luminous galaxies are more strongly clustered, and/or

(ii) some of the X-ray emission associated with the red galaxies is produced by extended sources (such as hot gas within the gravitational wells of rich clusters).

To investigate this further, the galaxy $\omega(\theta)$ was calculated (as described in Section 6.6) for the galaxies within the GSGP4 area, divided into red ($B - R \geq 1.50$) and blue ($B - R < 1.5$) subsamples.

The red galaxies were indeed found to be much more clustered, with a $\omega(\theta)$ amplitude of $(94.6 \pm 16.8) \times 10^{-4}(\mathrm{deg})^{-0.8}$ compared to $(30.0 \pm 5.5) \times 10^{-4}(\mathrm{deg})^{-0.8}$ for the bluer galaxies. The red and blue galaxy $\omega(\theta)$ are shown in Figure 7.7, together with a cross-correlation between the red and blue galaxies, which appears consistent with zero. On our CCD dataset at a deeper ($B_{ccd} \leq 24.5$) limit, we also found that redder galaxies possess a higher $\omega(\theta)$ amplitude than bluer galaxies, with little cross-correlation between the two (Section 3.4). In both cases the colour dependence could involve stronger intrinsic clustering for early-type galaxies, and/or a less broad redshift distribution for the red subsamples.

The excess of galaxy pairs at $\theta < 1$ arcmin (above that expected for a random distribution), N'_{gg}, is 788.7 for the blue galaxies and 256.3 for the red galaxies. Applying the clustering correction described above then gives estimates of the numbers of photons contributed by each subset of

968.8 ± 248.5 for the $B - R < 1.5$ galaxies (0.50 photons galaxy^{-1})

552.2 ± 113.0 for the $B - R \geq 1.5$ galaxies (1.06 photons galaxy^{-1}).

Hence even after correcting for the stronger clustering of the redder galaxies, each red galaxy was found to produce on average approximately twice the number of X-ray photons as each of the bluer galaxies in the same B magnitude range. The difference between $W_{gx}(40 \leq \theta < 60$ arcsec) for the two colour subsets may then not be due entirely to the stronger clustering of the red galaxies.

Galaxies in our sample as red as $B - R \geq 1.5$ will mainly be E/S0 types at $z \sim 0.2$–0.5, and being ellipticals are more likely to be within the central regions of rich clusters than the bluer galaxies. According to Fabbiano (1989), most early and late type galaxies tend to have similar mean L_X/L_B ratios, but giant ellipticals in the central regions of clusters produce X-ray emission in excess of that expected from the L_X/L_B ratio typical of other galaxies. This excess emission is produced by the hot gas trapped within the gravitational well of the cluster as a whole, so the X-ray luminous region may extend far beyond the visible radius of the giant elliptical at its centre. This may explain why our red and blue galaxies appear to have similar X-ray fluxes associated with each galaxy at small separations ($\theta < 40$ arcsec), within the ROSAT point-spread function, whereas the red galaxies show an excess cross-correlation with the XRB above that seen for blue galaxies at slightly larger separations ($40 \leq \theta \leq 60$ arcsec), comparable to the angular diameter on the ROSAT image of the bright GSGP4X:32 source, identified as a rich galaxy cluster (see Section 5.6.3).

The more extended form of the cross-correlation of red galaxies with the XRB can therefore be explained if some of these galaxies lie within groups or clusters containing very hot X-ray emitting gas, although as these clusters are not detected individually they must be of lesser X-ray luminosity than GSGP4X:32.

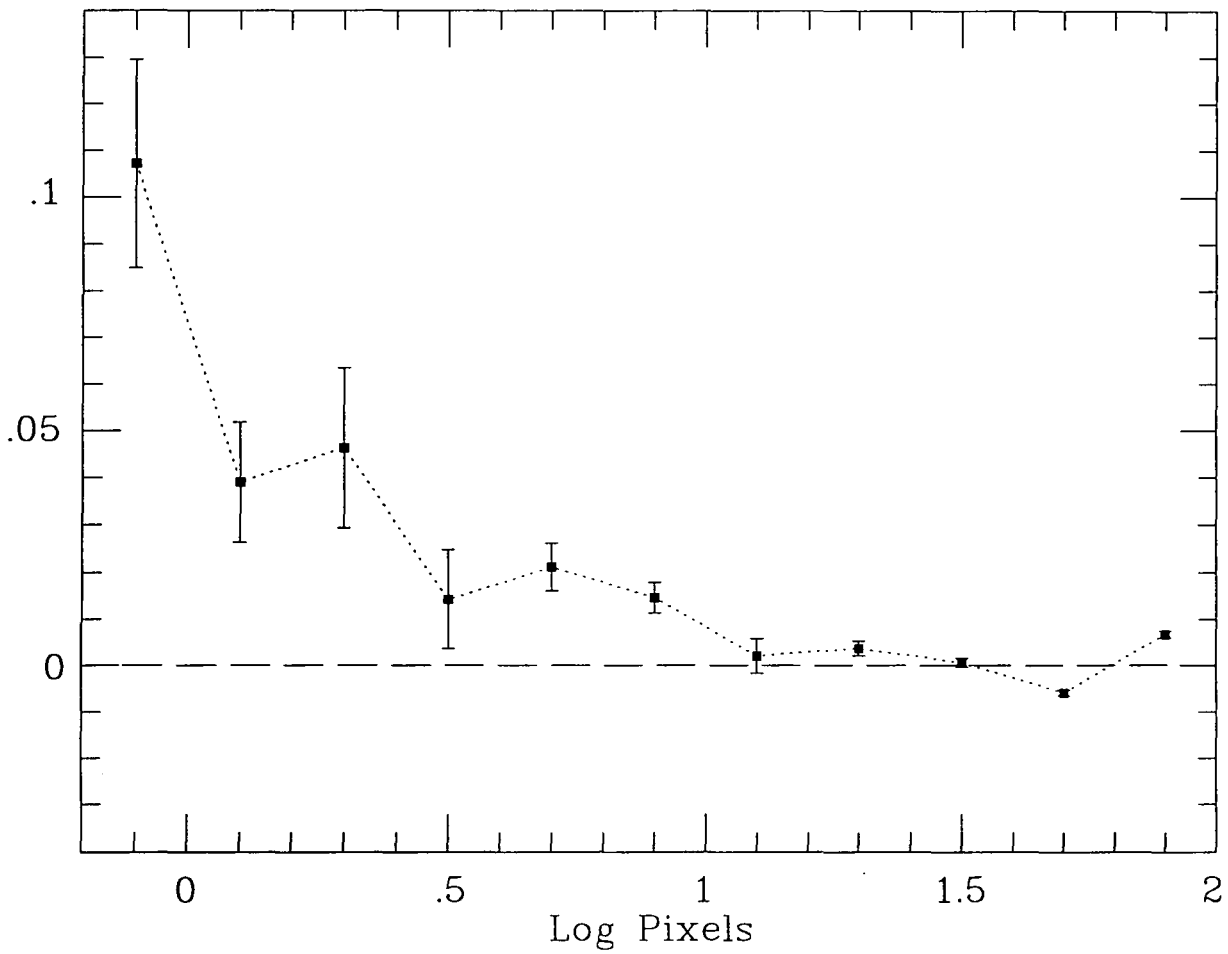

Figure 7.5 Cross-correlation of the $18.0 \leq B \leq 23.0$ galaxies with blue ($B - R < 1.50$) colours on the GSGP4 field with the unresolved 0.5–2.0 keV X-ray background on the same area.

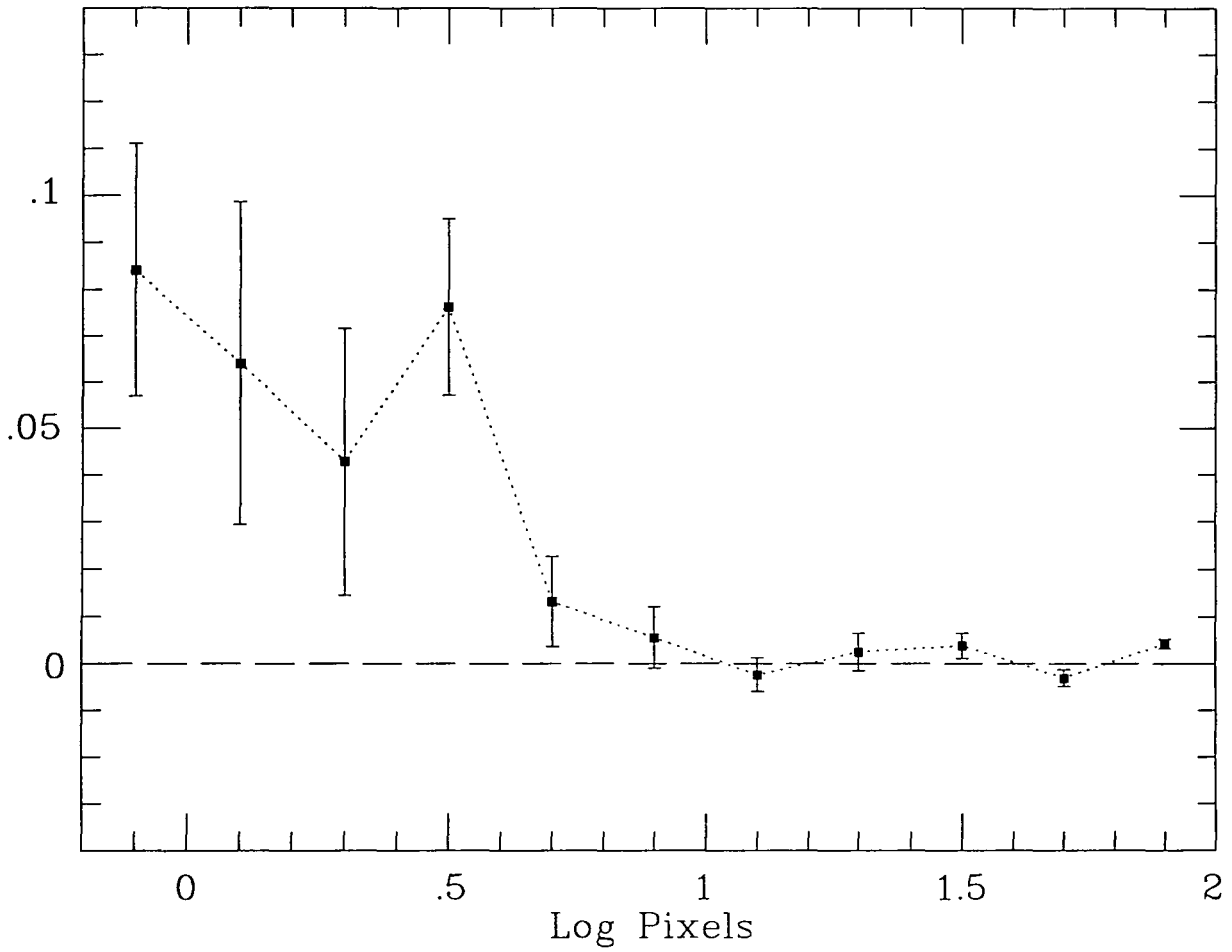

Figure 7.6 Cross-correlation of the $18.0 \leq B \leq 23.0$ galaxies with red ($B - R \geq 1.50$) colours on the GSGP4 field with the unresolved 0.5–2.0 keV X-ray background on the same area.

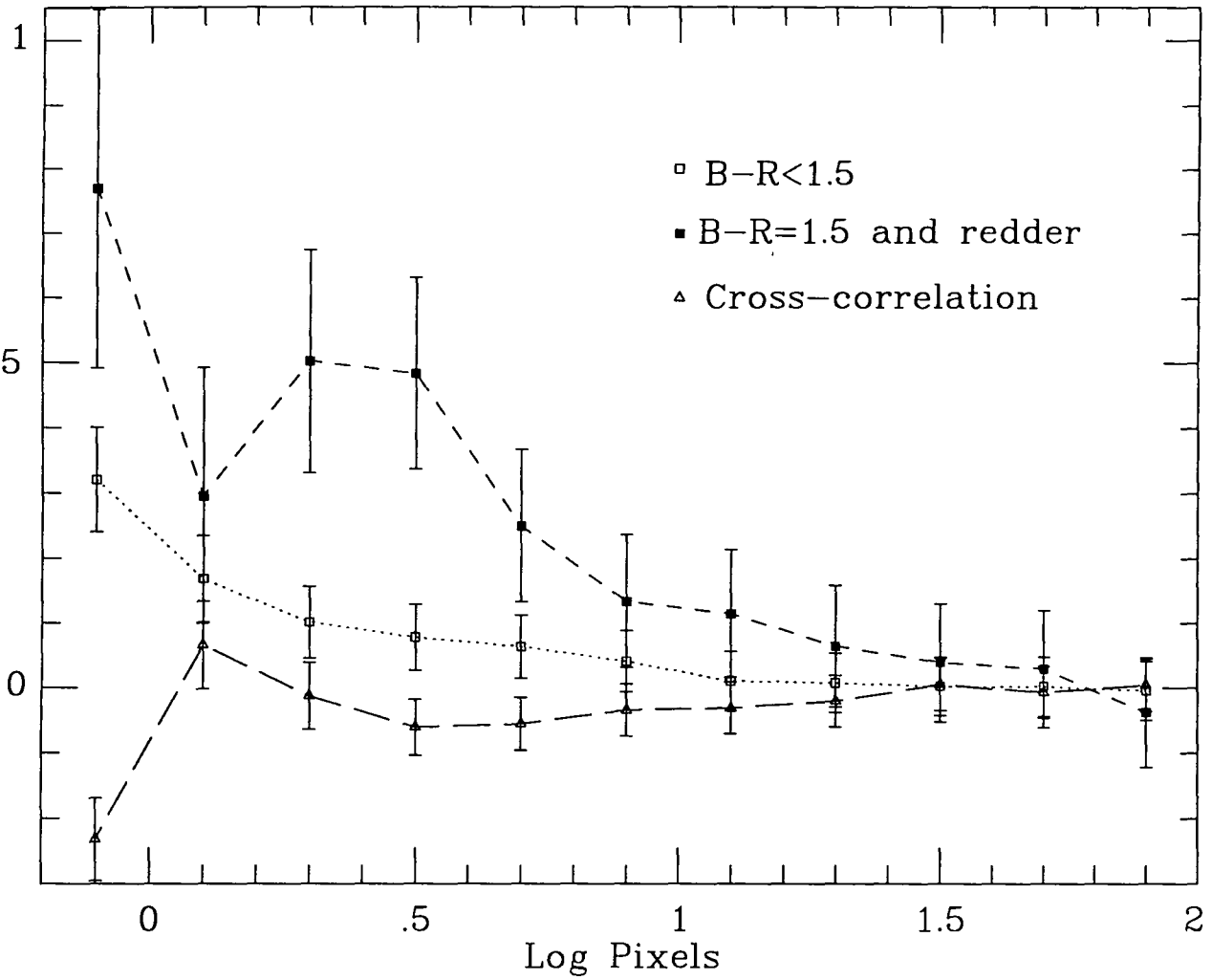

Figure 7.7 The angular correlation function, $\omega(\theta)$ of two colour-divided subsets of the $18.0 \leq B \leq 23.0$ galaxies on the AAT plate of the GSGP4 area. The graph shows $\omega(\theta)$ for red ($B - R \geq 1.50$) and blue ($B - R < 1.5$) galaxies, and the cross-correlation between the red and blue galaxies, as a function of the logarithm of angular separation in units of ROSAT pixels (15 arcsec), with errors estimated using the formula from Section 6.4.

7.6 The X-ray/Blue-band Flux Ratio

The 0.5–2.0 keV flux corresponding to one photon detected during the exposure time for each field is, in units of 10^{-15} ergs cm^{-2}s^{-1}photon^{-1}, 0.243 on GSGP4, 0.436 on QSF3 and 0.482 on SGP2.

Using the mean number of photons per pixel for the holed images, as listed in Table 6.1, the intensity of the unresolved background can then be estimated as, in units of 10^{-12} ergs cm^{-2}s^{-1}deg^{-2}, 7.77 for GSGP4, 10.40 for SGP2 and 8.19 for QSF3.

On each of the 3 AAT fields a term $10^{0.4(18.0-B)}$, where B is the blue magnitude, was summed for all $18 \leq B \leq 23$ galaxies within the 16 arcmin radius central area, to give their total B-band flux in units of $B = 18.0$ galaxies. This was found to be 90.00 on GSGP4, 60.77 on SGP2 and 72.43 on QSF3.

If the estimated number of XRB photons produced by the galaxies, after correction for clustering, is N_X, the X-ray flux per photon is S_p and the blue-band flux of the same galaxies is f_B, a mean X-ray/B-band flux ratio can be estimated for the galaxies on each field as $S_p N_X / f_B$. For the 3 fields separately this gives, in units of 10^{-15} ergs cm^{-2}s^{-1} per $B = 18.0$ galaxy,

GSGP4: 4.36 ± 0.64

SGP2: 1.96 ± 0.94

QSF3: 3.51 ± 0.98

The result for SGP2 is not as low in comparison to the other two as was the case for its galaxy contribution as a proportion of the XRB – this field has a high unresolved background (with less of the total flux resolved into sources) but a low galaxy count compared to the others. Taking the mean of the above ratios gives $(3.24 \pm 0.50) \times 10^{-15}$ ergs cm^{-2}s^{-1} per $B = 18.0$ galaxy, but we can instead calculate a ratio for which each X-ray photon has equal weighting as

$$\frac{\sum N_X}{\sum (S_p^{-1} f_B)}$$

where the summation is over the 3 fields, and this gives:

$S(0.5\text{–}2.0 \text{ keV}) = (3.69 \pm 0.47) \times 10^{-15}$ ergs cm^{-2}s^{-1} per $B = 18.0$ galaxy.

For a galaxy of absolute blue magnitude $M_B = -21.0$, this ratio corresponds to an X-ray luminosity

$L_X(0.5\text{–}2.0 \text{ keV}) = (3.69 \pm 0.47) \times 10^{-15} \times 10^{0.4 \times 39} \times 10^{40.08}$ ergs s^{-1}

the $10^{40.08}$ term being $4\pi r^2$, where $r = 10$ pc in units of cm, giving

$L_X(0.5\text{–}2.0 \text{ keV}) = (1.77 \pm 0.22) \times 10^{41}$ ergs s^{-1} per $M_B = -21.0$ galaxy.

This X-ray luminosity is much higher than, for example, the estimates given by Fabbiano (1989) of $L_X \sim 10^{39.5}$ ergs s^{-1} for our Galaxy and for M31, but is less than the $L_X \sim 10^{42}$ ergs s^{-1} luminosities of many of the galaxies detected as individual X-ray sources on these ROSAT images (Table 5.6).

We can also express our result as a monochromatic flux ratio. If the X-ray SED can be approximated by a $f_\nu \propto \nu^{-1}$ power law, the monochromatic 2 keV flux corresponds to the 0.5–2.0 keV flux as

$f_\nu(2 \text{ keV}) = 1.492 \times 10^{-18} S(0.5\text{–}2.0 \text{ keV})$.

Hence for a $B = 18.0$ galaxy, with the mean X-ray/B-band flux ratio estimated above,

$f_\nu(2\ \mathrm{keV}) \simeq 3.69 \times 10^{-15} \times 1.492 \times 10^{-18} = 10^{-32.26}$ ergs cm^{-2}s^{-1}Hz^{-1}.

As $\log f_\nu(B) \simeq -0.4(b_J + 48.65)$, for the B_J magnitude system used on these AAT plates a $B = 18.0$ galaxy produces a monochromatic blue flux

$f_\nu(B) \simeq 10^{-26.66}$ ergs cm^{-2}s^{-1}Hz^{-1}.

and therefore we estimate a mean flux ratio for galaxies

$$f_\nu(2\ \mathrm{keV})/f_\nu(B) = 10^{-5.60}.$$

If the X-ray SED of these galaxies has a flatter slope of $f_\nu \propto \nu^{-0.3}$, typical of the MXRBs which may dominate the X-ray emission from starbursting galaxies, then

$f_\nu(2\ \mathrm{keV}) = 2.331 \times 10^{-18}\ S(0.5\text{–}2.0\ \mathrm{keV})$

and with the same X-ray/B-band flux ratio, a $B = 18.0$ galaxy would produce a monochromatic 2 keV flux

$f_\nu(2\ \mathrm{keV}) \simeq 3.69 \times 10^{-15} \times 2.331 \times 10^{-18} = 10^{-32.07}$ ergs cm^{-2}s^{-1}Hz^{-1},

giving for the flatter SED a mean flux ratio

$$f_\nu(2\ \mathrm{keV})/f_\nu(B) = 10^{-5.41}.$$

Our estimate of the mean flux ratio is about an order of magnitude higher than the typical value for normal galaxies of $f_\nu(2\ \mathrm{keV})/f_\nu(B) = 10^{-6.6}$, as given by Giacconi and Zamorani (1987), and would give an X-ray flux per $B = 18.0$ galaxy slightly higher than the 5σ detection threshold on the GSGP4 image. If this ratio applied to all nearby galaxies, we would therefore expect most of the 13 galaxies with $B < 18.0$ found within the 20 arcmin radius circular area of the GSGP4 photographic plate to be detected on the ROSAT image. However, as we only detected one of these galaxies (GSGP4X:109, at $z = 0.098$) in our source/galaxy cross-correlation of Chapter 5, it seems more likely that most galaxies on the photographic plates have 'normal' flux ratios of $f_\nu(2\ \mathrm{keV})/f_\nu(B) \sim 10^{-6.6}$, and that our observed galaxy/XRB cross-correlation is dominated by a small fraction of galaxies at the high end of the distribution of L_X/L_B.

The source/galaxy cross-correlation of Chapter 5 indicated $\sim 1\%$ of galaxies to have very high flux ratios of $f_\nu(2\ \mathrm{keV})/f_\nu(B) \sim 10^{-5}$–$10^{-4}$, leading to the suggestion in Section 5.6.3 that $\log(L_X/L_B)$ for galaxies may possess a Gaussian distribution with a very wide dispersion of $\sigma \sim 0.8$. For a Gaussian distribution of the logarithm of the flux ratio, the ratio of total X-ray flux received from galaxies to the total B-band flux will be higher than the ratio of the galaxies at the mode of the distribution by a factor of

$$\int_{-\infty}^{+\infty} 10^x \exp(-0.5(x/\sigma)^2)dx \Big/ \int_{-\infty}^{+\infty} \exp(-0.5(x/\sigma)^2)dx$$

giving $10^{0.74}$ for $\sigma = 0.8$. Hence the same dispersion suggested by the numbers of discrete sources found to be correlated with galaxies can also account for the difference between the mean flux ratio we estimated from the galaxy/XRB cross-correlation and the typical ratio of normal galaxies.

Lahav et al. (1993) find their cross-correlation amplitude to correspond to a similar mean X-ray luminosity per $L \sim L^*$ galaxy of $L_X(2\text{–}10\ \mathrm{kev}) \sim 10^{41}$ ergs s^{-1} (for $H_0 = 50$ km s^{-1}Mpc^{-1}). These authors suggested that the strength of their cross-correlation could be explained if, for example, a fraction $\sim 10\%$ of optically bright galaxies have even higher X-ray luminosities, $L_X \sim 10^{42}$ ergs s^{-1}, so that a small fraction of galaxies with high L_X/L_B ratios would dominate their observed cross-correlation. This is essentially the same explanation as suggested here, on the basis of our individual detections of galaxies with $L_X \sim 10^{42}$ ergs s^{-1}. These detections appear to confirm the hypothesis that a wide dispersion in L_X/L_B ratios accounts for the high amplitude of the galaxy/XRB cross-correlation.

7.7 Extrapolating to Fainter Galaxies

To estimate the contribution to the XRB from galaxies fainter than $B = 23.0$, we assume for now that these will possess the same mean ratio of observed 0.5–2.0 keV and blue-band fluxes as was estimated above for $18.0 \leq B \leq 23.0$ galaxies.

On the deep INT CCD frame of Metcalfe et al. (1994), the total B-band flux from the 2028 galaxies in the range $23.0 \leq B_{ccd} \leq 27.5$ was equivalent to 1.749 $B_{ccd} = 18.0$ galaxies. For the mean colours at this depth $b_J \simeq B_{ccd} - 0.09$, and the area is $4.927 \times 10^{-3}\mathrm{deg}^2$, so this corresponds to 385.6 $B_J = 18.0$ galaxies deg^{-2}.

Assuming the same X-ray/B-band flux ratio for these fainter galaxies as was estimated above for $18 \leq B \leq 23$ galaxies, the $23.0 \leq B_{ccd} \leq 27.5$ galaxies would produce a mean 0.5–2.0 keV intensity of 1.42×10^{-12} ergs $\mathrm{cm}^{-2}\mathrm{s}^{-1}\mathrm{deg}^{-2}$.

Using the estimate of photons counted per unit flux ratios for the each of these 3 images as given in Section 7.6, this intensity would correspond to 1135.3 XRB photons on the 16 arcmin radius circular area on the GSGP4 image, 607.6 on SGP2 and 672.0 on QSF3. Hence these $23.0 \leq B_{ccd} \leq 27.5$ galaxies would be expected to contribute

$$(1135.3 + 607.2 + 672.0)/(6215 + 3875 + 4450) = 16.61\%$$

of the unresolved XRB.

This is approximately the same fraction as $18 \leq B \leq 23$ galaxies, and gives a total $18 \leq B \leq 27.5$ galaxy contribution of 33.42%. At these depths we are likely to be observing galaxies on the faint-end slope of the luminosity function at all redshifts up to the maximum redshift (see Chapter 4). For luminosity functions flatter than $\alpha = -2$, the flux contribution per magnitude interval of galaxies on the faint-end slope will decrease on going faintward, so even if galaxy counts continue to increase at $B \geq 27.5$ the total flux from faint galaxies converges to a maximum. Our Bruzual pure luminosity evolution model, computed with $q_0 = 0.05$ and $z_{max} = 4$, predicts an intensity from $23.0 \leq B_{ccd} \leq 27.5$ galaxies equivalent to 367.0 $B_{ccd} = 18.0$ galaxies deg^{-2}, or 398.7 $b_J = 18.0$ galaxies deg^{-2}, very close to the observed value. For galaxies at all fainter magnitudes ($B_{ccd} > 27.5$) the same model predicts a total blue-band intensity only 12.8% of this value (ie. 47.0 $B_{ccd} = 18.0$ galaxies deg^{-2}). Using this model at $B \geq 27.5$, and assuming the same X-ray/B-band flux ratio to apply at these even fainter limits, we estimate a total contribution from $B \geq 18.0$ galaxies to the unresolved 0.5–2.0 keV background of

$$16.81 + (1.128 \times 16.61) = 35.5\% \pm 4.5\%$$

This estimate depends on the assumption that L_X and L_B evolve similarly with redshift, and also that the k-corrections caused by the fact that we are observing shorter wavelength regions of the spectra at the higher redshifts of the CCD sample can be neglected, or at least assumed to be the same for X-ray and blue-band observations. At higher redshifts, where the observed B-band will correspond to $\lambda \sim 2000$Å in the rest-frame, the first assumption may be reasonable for blue, star-forming galaxies. If the total X-ray emission is dominated by emission from MXRBs associated with star-formation, the evolution of L_X may be similar to the 2000Å luminosity evolution, as both would depend on the numbers of very massive stars. However at low redshifts, the observed blue-band flux will correspond to the rest-frame luminosity at longer ($\lambda \sim 4000$Å) wavelengths, where it will be less sensitive to the SFR. Hence an increase in the SFR between $z = 0$ and $z \sim 1$ might increase the observed X-ray flux more than the observed B-band flux, and therefore the mean observed $f_\nu(2\ \mathrm{keV})/f_\nu(B)$ ratio might increase somewhat when high-redshift galaxies appear faintward of $B = 23$.

The second assumption requires that the mean spectral index α (where $f_\nu \propto \nu^{-\alpha}$) is the same in both $1000 \leq \lambda \leq 4000$Å and 0.5–8 keV regions of the rest-frame spectra of the galaxies. This may be a good approximation for very blue galaxies with $0 \leq \alpha \leq 1$ in both spectral regions. However, for early-type red galaxies, the B-band k-correction increases steeply with redshift to $\sim 2.5^m$ at $z \sim 1$, whereas the X-ray SED is close to $f_\nu \propto \nu^{-1}$ at these relatively soft energies, giving a zero X-ray k-correction. Hence the ratio $f_\nu(4\text{ keV})/f_\nu(2\text{ keV})$ in the rest-frame is likely to exceed the ratio $f_\nu(2000\text{Å})/f_\nu(B)$, by a factor as large as an order of magnitude, and therefore the observed $f_\nu(2\text{ keV})/f_\nu(B)$ ratios for red galaxies would increase from $z = 0$ to $z \sim 1$.

We conclude that the mean observed $f_\nu(2\text{ keV})/f_\nu(B)$ ratio, for both red and blue galaxies, is likely to increase with redshift to some extent, and would therefore be higher for $B > 23$ galaxies than those in our AAT dataset. Hence we can regard the above estimate of f_{gal} given by extrapolation to faint magnitudes as a probable lower limit, and – considering also the upper limits on f_{gal} set by the proportion of the unresolved XRB already accounted for by QSOs – estimate at this point that $35\% \leq f_{gal} \leq 70\%$.

7.8 The X-ray Emissivity of Galaxies and its Rate of Evolution

Our cross-correlation results can be used to estimate the mean X-ray luminosity per unit volume of the galaxies in our sample. Firstly, we estimate the blue-band luminosity density of galaxies by integrating

$$\int \Phi(M_B) 10^{-0.4(M_B+21.0)} dM_B$$

where M_B is the absolute blue magnitude and $\Phi(M_B)$ the luminosity function of galaxies. The luminosity functions of each of the types of galaxy in our model (from E/S0 to Irr), with the Schechter function parameters of each as listed in Table 1.1, were summed at each value of M_B to give a 'total' $\Phi(M_B)$. The luminosity functions were assumed to cut-off seven magnitudes faintward of M^*, but as (for faint-end slopes much flatter than $\alpha = -2$) the total luminosity density (as opposed to the number density) is dominated by $L \sim L^*$ galaxies, the result is insensitive to the position of this lower limit. The above integration gave a B-band luminosity density of 2.975×10^{-3} in units of $M_B = -21.0$ galaxies per cubic Mpc of comoving volume (for $H_0 = 50$ km s^{-1}Mpc^{-1}).

Our cross-correlation analysis produced an estimate of the mean X-ray luminosity per $M_B = -21.0$ galaxy of $L_X(0.5\text{–}2.0\text{ keV}) = (1.77 \pm 0.22) \times 10^{41}$ ergs s^{-1}, so galaxies producing the above B-band luminosity density would give an X-ray volume emissivity,

$$\rho(0.5\text{–}2.0\text{ keV}) = (5.27 \pm 0.65) \times 10^{38} \text{ ergs s}^{-1}\text{Mpc}^{-3}.$$

This is of the same order as the Lahav et al. (1993) estimate of

$$\rho(2\text{–}10\text{ keV}) = (7.5 \pm 2.5) \times 10^{38} \text{ ergs s}^{-1}\text{Mpc}^{-3}.$$

(for $H_0 = 50$ km s^{-1}Mpc^{-1}), which was obtained by cross-correlating optically-detected and IRAS galaxies at $z \leq 0.06$ with the XRB. To compare the Lahav et al. (1993) estimate with ours, the difference in the mean redshifts of the galaxy samples ($z_{mean} \sim 0.03$ and $z_{mean} \sim 0.35$ respectively) and in the X-ray energy bands, must be taken into account. The Lahav et al. result would correspond to $\rho(2.06\text{–}10.3\text{ keV})_{z=0.03}$, whereas our estimate of the X-ray emissivity from galaxies corresponds approximately to $\rho(0.675\text{–}2.70\text{ kev})_{z=0.35}$ in the rest frame of the galaxies. If we assume the two cross-correlation results to be produced by the same type of source, the comparison of the two results may provide some information about their spectral index and rate of evolution. For sources

with an SED of $f_\nu \propto \nu^{-\alpha}$, the emissivities would be in the ratio

$$L_X(z=0.03)\int_{2.06}^{10.3}\nu^{-\alpha}d\nu / L_X(z=0.35)\int_{0.675}^{2.70}\nu^{-\alpha}d\nu$$

If there is no evolution in L_X, the ratio of the two integrals is 1.16 for a steep $\alpha = 1$ spectrum (typical of AGN), increasing to 2.78 for the flatter spectral index of $\alpha = 0.3$ typical of MXRBs in the range $\sim$ 1–10 keV. As the spectral index of the XRB as a whole is relatively flat ($\alpha \sim 0.4$) at 2–10 keV energies, the $\alpha = 0.3$ index may be more appropriate if we are attempting to explain the entire non-QSO component of the XRB.

Griffiths and Padovani (1990) proposed a model for the X-ray luminosity evolution of galaxies in which the total X-ray emission of galaxies, being associated primarily with star-formation, possesses a spectral index of $\alpha = 0.3$ and increases exponentially with look-back time $T(z)$, ie.

$$L_X \propto \exp(T(z)/\tau)$$

where τ is the exponential timescale expressed in units of the Hubble time, H_0^{-1}. GP derived an estimate of τ for the summed X-ray emission of all types of star-forming galaxy by combining the rate of far infra-red (60μm) luminosity evolution estimated for IRAS galaxies with the observed correlation between L_X and $L_{60\mu m}$. This correlation is best fitted by a line of slope $L_X \propto (L_{60\mu m})^{0.7}$ and is thought to be similar for IRAS, starburst and normal galaxies. In this way, GP estimated a timescale of $\tau = 0.4$ as being appropriate for the X-ray luminosity evolution of star-forming galaxies, and described this model as 'moderate' evolution, as it is somewhat less strong than the 'extreme' X-ray (and optical) luminosity evolution of QSOs (see Section 7.9 following).

With $\tau = 0.4$ evolution, L_X increases by a factor of exp((0.26-0.03)/0.40))=1.78 from $z = 0.03$ to $z = 0.35$. If we assume our cross-correlation to be caused by galaxies with a spectral index $\alpha = 0.3$ and X-ray luminosity evolution described by $\tau = 0.4$, an extrapolation of our estimated emissivity back to $z = 0.03$, taking into account the effect of evolution and the $\alpha = 0.3$ k-correction, would predict the low-redshift counterparts of these galaxies to produce an emissivity of

$$\begin{aligned}\rho(\text{2–10 keV}) &= (1.78)^{-1} \times 2.78 \times (5.27 \pm 0.65) \times 10^{38} \text{ ergs s}^{-1}\text{Mpc}^{-3} \\ &= (8.23 \pm 1.02) \times 10^{38} \text{ ergs s}^{-1}\text{Mpc}^{-3},\end{aligned}$$

which is very close to the Lahav et al. (1993) estimate. However, it is probable that part of the cross-correlation detected by Lahav et al. would have been produced by AGN within the IRAS galaxy catalogue. The higher redshift counterparts of most of these AGN would have been excluded from our cross-correlation analysis, through the removal of detected sources from the X-ray data and the star-galaxy separation carried out on the optical dataset, but the lower angular resolution of the X-ray data used by Lahav et al. allowed only the very brightest individual sources to be excluded from the analysis. We were able to exclude all sources down to a much fainter flux limit, which in itself would have removed about half of the total QSO emission, and we showed in Section 7.4 above than the AGN correlated with galaxies could account for only a few % of our estimated emissivity, so it is reasonable to assume that the AGN contamination within our analysis will be much smaller.

To estimate an upper limit on the possible effect of AGN contamination on the Lahav et al. results, we calculate the total X-ray emissivity of AGN at $z = 0$ using the Boyle et al. (1994) models of the luminosity function and evolution of QSOs. In the best-fitting Boyle et al. (1994) model for a low-q_0 Universe (model U), QSOs produce

$$\rho(\text{0.5–2.0 keV}) = 1.22 \times 10^{38} \text{ ergs s}^{-1}\text{Mpc}^{-3}$$

locally, which for a $f_\nu \propto \nu^{-1}$ SED corresponds to

$$\rho(2\text{–}10 \text{ keV}) = 1.41 \times 10^{38} \text{ ergs s}^{-1}\text{Mpc}^{-3}.$$

In a $q_0 = 0.5$ Universe, the best-fitting model (model V) possessed a somewhat higher local QSO emissivity of

$$\rho(0.5\text{–}2.0 \text{ keV}) = 3.29 \times 10^{38} \text{ ergs s}^{-1}\text{Mpc}^{-3}$$

which for a $f_\nu \propto \nu^{-1}$ SED corresponds to

$$\rho(2\text{–}10 \text{ keV}) = 3.81 \times 10^{38} \text{ ergs s}^{-1}\text{Mpc}^{-3},$$

(although when the QSO emission is integrated out to $z \sim 4$ the difference in emissivities is largely cancelled out by the difference in volume elements, so the two models give similar predictions for the total QSO flux contribution).

Miyaji et al. (1994) quoted an intermediate estimate for the local AGN emissivity, derived using more detailed forms of the SED for Seyfert 1 and 2 AGN, of

$$\rho(2\text{–}10 \text{ keV}) = 2.0 \times 10^{38} \text{ ergs s}^{-1}\text{Mpc}^{-3},$$

Hence even if we assume the Lahav et al.(1993) result to include the X-ray emission from all AGN at $z \leq 0.06$, in addition to the emission from galaxies, subtraction of the local AGN emissivity from the Lahav et al. estimate leaves a significant emissivity of

$$\rho(2\text{–}10 \text{ keV}) \simeq 5 \times 10^{38} \text{ ergs s}^{-1}\text{Mpc}^{-3}$$

This seems reasonably consistent with the emissivity expected from the low-redshift counterparts of the galaxies producing our AAT/ROSAT cross-correlation, if these evolve as in the GP model.

However, when Miyaji et al. (1994) cross-correlated $z \leq 0.06$ IRAS galaxies with the XRB, they estimated a somewhat lower emissivity of

$$\rho(2\text{–}10 \text{ keV}) = 4.3 \times 10^{38} \text{ ergs s}^{-1}\text{Mpc}^{-3}$$

of which the non-AGN component was estimated to be no more than

$$\rho(2\text{–}10 \text{ keV}) \simeq 2.0 \times 10^{38} \text{ ergs s}^{-1}\text{Mpc}^{-3}$$

This lower value would only be consistent with our estimated emissivity for AAT galaxies if

(i) the X-ray luminosity evolution out to $z \sim 0.35$ is even more rapid than $\tau \sim 0.4$

and/or

(ii) the spectral index of low-redshift X-ray luminous galaxies is quite steep – with $\alpha = 1$ the low-redshift counterparts of our AAT galaxies would produce only

$$\rho(2\text{–}10 \text{ keV}) = (3.43 \pm 0.43) \times 10^{38} \text{ ergs s}^{-1}\text{Mpc}^{-3}$$

in the higher energy band used by Miyaji et al.

and/or

(iii) a significant component of our cross-correlation was produced by galaxies with high X-ray and optical luminosities, but low luminosities at 60μm, i.e. non-star-forming, passive galaxies. These might be seen on AAT plates and in the optical data used in part of the Lahav et al. analysis, but under-represented in the 60μm-selected sample used by Miyaji et al., resulting in a lower estimate of ρ_0 when only IRAS galaxies are used.

Using our estimate of ρ_0, and a range of plausible values for α and the rate of evolution, we now attempt to improve on the estimate made in Section 7.7 of the XRB contribution of all galaxies out to high redshifts.

7.9 The XRB Contribution from Galaxies out to High Redshifts

The total intensity from sources out to z_{max} is given by

$$I(z \leq z_{max}) = \rho_0 \int_0^{z_{max}} (1+z)^{1-\alpha}(L(z)/L(0))(d_L(z))^{-2}(\frac{dV_{com}}{dz})dz$$

where ρ_0 is the emissivity at $z = 0$ per unit comoving volume element, α the spectral index, $(L(z)/L(0))$ the luminosity evolution, $d_L(z)$ the luminosity distance in Mpc, $\frac{dV_{com}}{dz}$ the comoving volume element.

Figures 7.8 and 7.9 show predictions of the 0.5–2.0 keV intensity produced by galaxies, as a function of z_{max}, for $q_0 = 0.5$ and $q_0 = 0.05$ respectively. For spectral indices of both $\alpha = 0.3$ and $\alpha = 1$, which bracket the likely range of spectral energy distributions of X-ray emitting galaxies, three models of the evolution of L_X are plotted:

(i) No evolution of L_X.

(ii) Exponential brightening with look-back time $T(z)$; $L_X \propto \exp(T(z)/\tau)$, with a timescale $\tau = 0.4\ H_0^{-1}$ (the GP model). The look-back times appropriate to the two choices of q_0 were used – consequently the $q_0 = 0.5$ model has less evolution at higher redshift where the look-back time is less than for $q_0 = 0.05$.

(iii) X-ray luminosity evolution identical to that of QSOs, as estimated by Boyle et al. (1994) from the most recent ROSAT data. The models plotted here are the best-fitting Boyle et al. (1994) models, which differ slightly for the two values of q_0:

For $q = 0.5$, $L_X(z) \propto (1+z)^{3.25}$ at $z \leq 1.60$, and L_X remains constant at $z > 1.60$ (model V).

For $q_0 = 0.05$, $L_X(z) \propto (1+z)^{3.34}$ at $z \leq 1.79$ and L_X remains constant at $z > 1.79$ (model U).

For a given rate of evolution, the flatter spectrum produces a higher observed emissivity at high redshifts, as a spectral index $\alpha < 1$ introduces a k-correction brightening with redshift, whereas the $f_\nu \propto \nu^{-1}$ SED gives a zero k-correction.

If the X-ray emission from these galaxies is dominated by X-ray binaries rather than hot gas at the temperatures typical of ellipticals ($kT \sim 1$ keV), their spectral index will be closer to $\alpha = 0.3$ than $\alpha = 1$. Georgantopoulos et al. (1994) found that the spectrum of the unresolved XRB on the five ROSAT images used in this thesis, with detected sources removed, was somewhat flatter ($\alpha_{mean} \simeq 0.33$) than that of the detected QSOs ($\alpha_{mean} \simeq 1.2$). Although the errors on α are large due to the limited spectral resolution of the ROSAT PSPC, this result would seem to suggest that $\alpha \sim 0.3$ is a better approximation to the X-ray SED of the whole galaxy component, and therefore that the higher of our two estimates of f_{gal} for each model is the more appropriate one.

A low q_0 will also increase the X-ray flux from galaxies at $z > 1$, simply as a result of the larger volume element at high redshifts.

The graphs also show the intensity of the unresolved background on GSGP4, estimated as

$$I(0.5\text{–}2.0\text{ keV}) = 7.77 \times 10^{-12}\text{ ergs cm}^{-2}\text{s}^{-1}\text{deg}^{-2}.$$

For each model, our cross-correlation results were used to normalize the emissivity at $z = 0.35$, so that the evolving models begin with a lower ρ_0 at $z = 0$. As a result of this, galaxies out to $z \sim 1$ produce similar fractions of the unresolved XRB ($\sim 32\%$ for $q_0 = 0.5$, and $\sim 38\%$ for $q_0 = 0.05$) whether or not evolution is included.

If there is no evolution of L_X with redshift, most of the galaxy contribution is produced at $z < 1$, and including higher redshift galaxies out to $z \sim 4$ only increases

f_{gal} by a further $\sim$ 10%. However, in Chapter 6, we set upper limits on the ACF amplitude of the unresolved XRB of $\omega(\theta) \leq 1.4 \times 10^{-3}(\mathrm{deg})^{-0.8}$. As the only sources known to be as weakly clustered on the sky as this are the faint ($B > 24$) blue galaxies, distributed out to high redshifts, our ACF upper limits would suggest that $1 \leq z \leq 3$ galaxies produce more of the XRB than non-evolving models predict.

Furthermore, on the basis of our cross-correlation amplitude and that of Lahav et al. (1993), non-evolving galaxies would produce only $\sim$ 30% of the XRB, but the fraction of the XRB which must be accounted for by sources other than QSOs, on the basis of the flattening of QSO number counts, and possibly the upper limits on the ACF also, is closer to $\sim$ 70%.

In the Boyle et al. (1994) QSO model for $q_0 = 0.05$ (model U), the QSOs out to $z = 4$ would produce a total intensity in this passband (assuming a $f_\nu \propto \nu^{-1}$ SED) of 4.02×10^{-12} ergs cm^{-2}s^{-1}deg^{-2}, while in the best-fitting model for $q_0 = 0.5$ (model V), QSOs out to $z = 4$ would produce a slightly lower total intensity of 3.41×10^{-12} ergs cm^{-2}s^{-1}deg^{-2}. The 127 QSOs already identified by spectroscopy within the resolved component (see Section 5.6.2) produce a total flux 2.83×10^{-12} ergs cm^{-2}s^{-1} from an area of 1.75 deg^2, so the detected QSO intensity is 1.62×10^{-12} ergs cm^{-2}s^{-1}deg^{-2}. Subtracting this from the Boyle et al. models leaves a QSO intensity within the unresolved XRB of 2.40×10^{-12} ergs cm^{-2}s^{-1}deg^{-2} ($f_{\mathrm{QSO}} = 31\%$) for $q_0 = 0.05$ and 1.79×10^{-12} ergs cm^{-2}s^{-1}deg^{-2} ($f_{\mathrm{QSO}} = 23\%$) for $q_0 = 0.5$. To account for the remainder of the XRB, galaxies from $z = 0$ out to their maximum redshift must produce $f_{gal} = 69\%$ (i.e. 5.36×10^{-12} ergs cm^{-2}s^{-1}deg^{-2}) for the $q_0 = 0.05$ model and $f_{gal} = 77\%$ (i.e. 5.98×10^{-12} ergs cm^{-2}s^{-1}deg^{-2}) in the $q_0 = 0.5$ model.

When $\tau = 0.4$ evolution is introduced, the predicted f_{gal} from galaxies out to $z = 4$ is increased to 44–53% for $q_0 = 0.5$ and 62–82% for $q_0 = 0.05$, for spectral indices in the $0.3 \leq \alpha \leq 1.0$ range. The increased intensity in comparison to non-evolving models is produced by galaxies at $z > 1$. It is clear that high redshift galaxies produce a much larger fraction of the XRB if the X-ray luminosity of galaxies undergoes even 'moderate' evolution, as is also shown in the graphs of GP and Lahav et al. (1993).

The QSO-type luminosity evolution models in the low-redshift limit approximate to $L_X \propto 1 + 3.34z$ (model U) and $L_X \propto 1 + 3.25z$ (model V), which is only a little stronger than the $\tau = 0.4$ model low-redshift approximation of $L_X \propto 1 + 2.5z$. However from $z \sim 1$ out to $z = 1.79$ (model U), or $z = 1.60$ (model V), the QSO evolution is much faster than $\tau = 0.4$, and closer to a $\tau = 0.2$ exponential timescale. Hence when $z > 1$ galaxies are included, the QSO-like evolution models predict a much higher total X-ray fluxes from galaxies than does $\tau = 0.4$ evolution.

When integrated out to $z = 4$ the QSO-like evolution predicts $f_{gal} = 79$–112% if $q_0 = 0.5$ and $f_{gal} = 125$–191% for $q_0 = 0.05$. Hence if the low-redshift X-ray emissivity of galaxies is as high as our cross-correlation results suggest, a model in which the X-ray luminosity evolution of galaxies is as rapid as that of QSOs would predict a total X-ray flux from galaxies which exceeds the entire unresolved XRB intensity, at least in a low q_0 Universe. Even if $q_0 = 0.5$ the flux from galaxies evolving as rapidly as QSOs would exceed the total unresolved XRB intensity at high redshifts unless their spectral index is very steep or the maximum redshift of galaxies is less than $z \sim 3$. This might argue against the hypothesis that the galaxy/XRB cross-correlation detected here is caused primarily by AGN 'hidden' within apparently normal galaxies, and favour non-AGN mechanisms with a more moderate evolution at high redshifts.

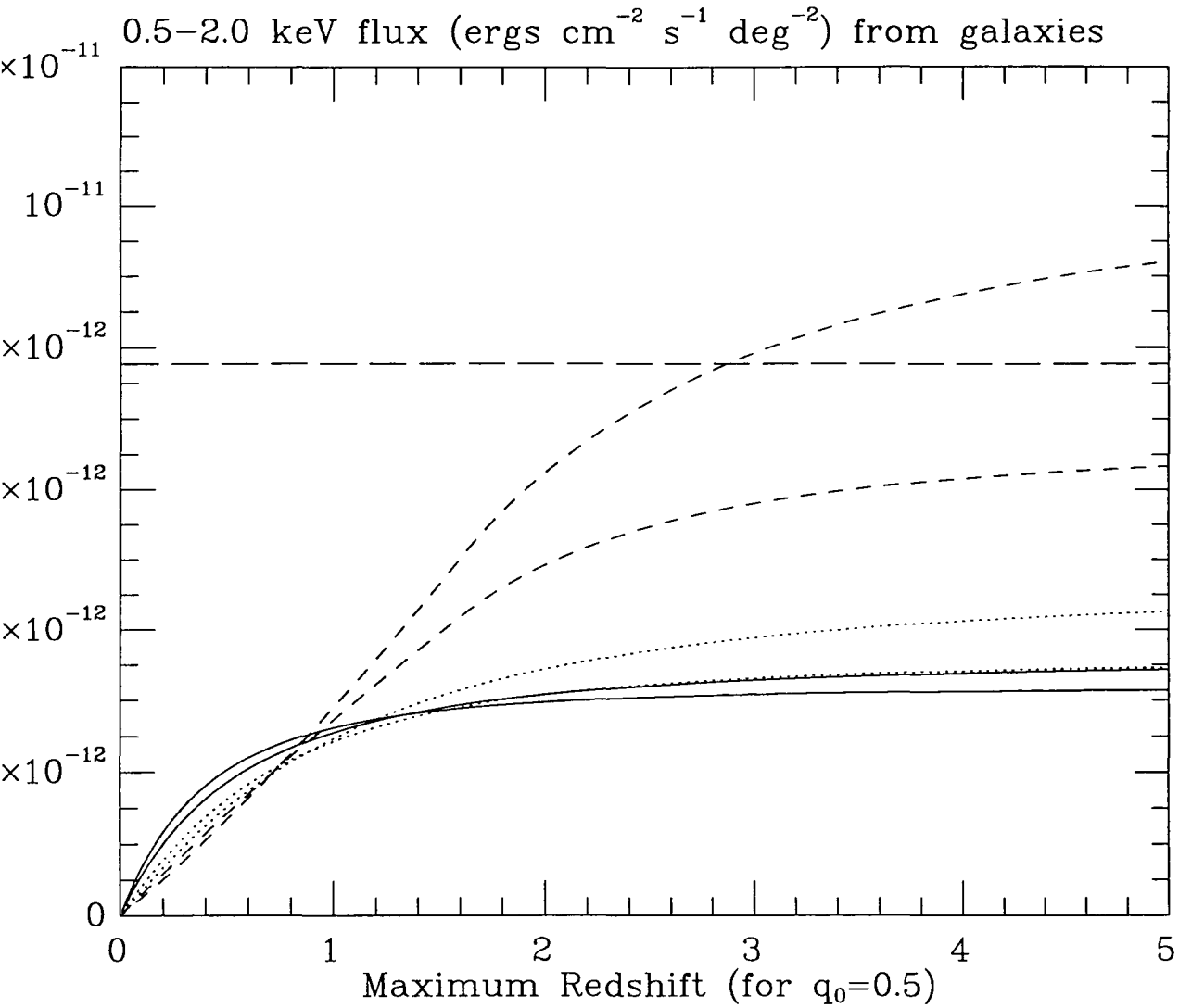

Figure 7.8 Total 0.5–2.0 keV intensity produced by galaxies out to a maximum redshift z_{max}, in a $q_0 = 0.5$ Universe, for three models of their X-ray luminosity evolution. The models are (i) no evolution (solid lines), (ii) X-ray luminosity evolution as in the $\tau = 0.4$ model of GP (dotted lines), and (iii) X-ray luminosity evolution equal to that given by the Boyle et al. (1994) V model for QSOs (short-dashed lines). The upper and lower predictions for each evolutionary model correspond to spectral indices for the galaxies of $\alpha = 0.3$ and $\alpha = 1$, the $\alpha = 0.3$ models giving the higher fluxes at higher redshifts. The three models are normalized (at $z = 0.35$) to the X-ray emissivity estimated from our cross-correlation of AAT galaxies with the XRB, and the long-dashed line shows the *total* intensity of the unresolved XRB on the GSGP4 image.

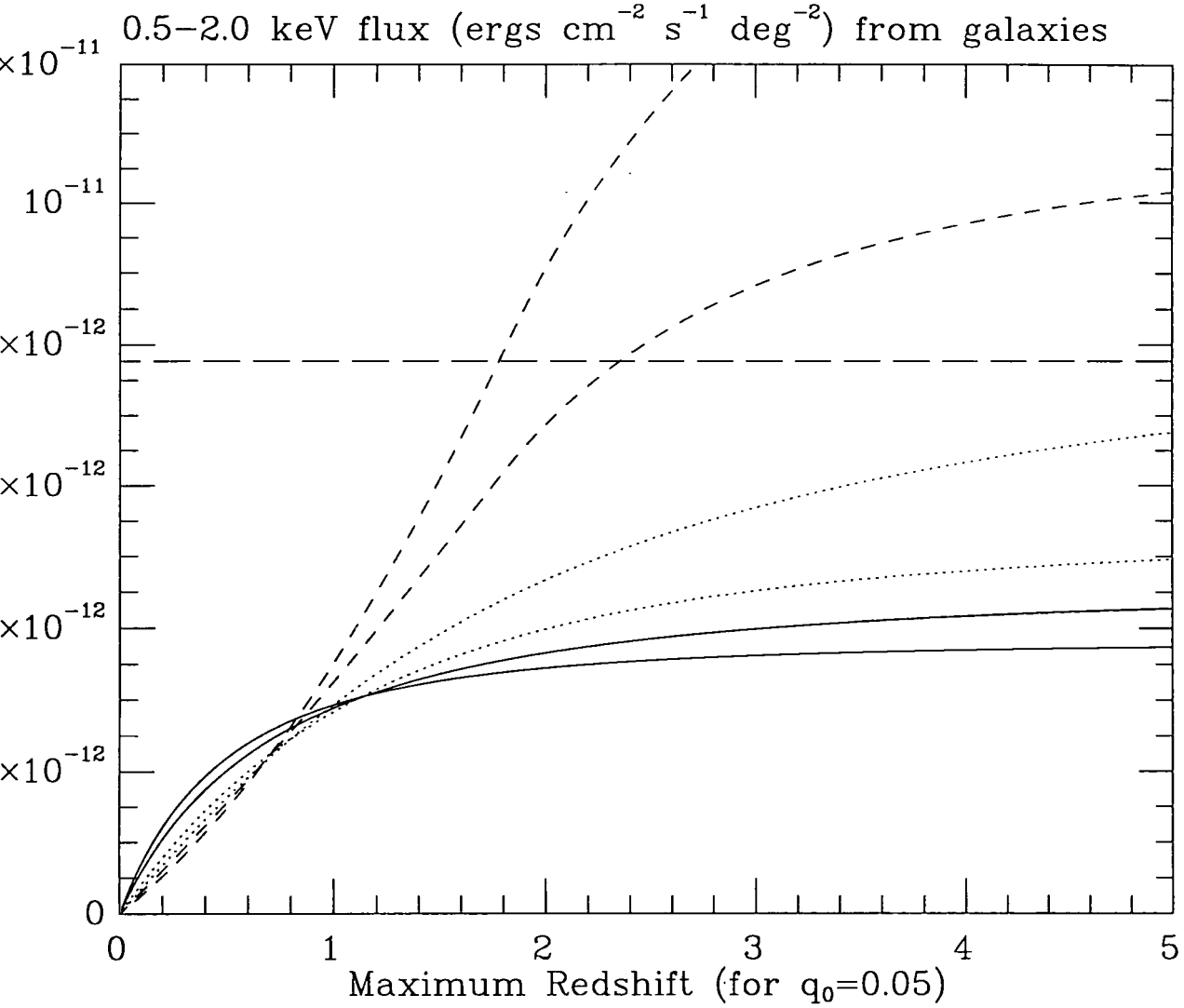

Figure 7.9 Total 0.5–2.0 keV intensity produced by galaxies out to a maximum redshift z_{max}, in a $q_0 = 0.05$ Universe, for three models of their X-ray luminosity evolution. The models are (i) no evolution (solid lines), (ii) X-ray luminosity evolution as in the $\tau = 0.4$ model of GP (dotted lines), and (iii) X-ray luminosity evolution equal to that given by the Boyle et al. (1994) U model for QSOs (short-dashed lines). The upper and lower predictions for each evolutionary model correspond to spectral indices for the galaxies of $\alpha = 0.3$ and $\alpha = 1$, the $\alpha = 0.3$ models giving the higher fluxes at higher redshifts. The three models are normalized (at $z = 0.35$) to the X-ray emissivity estimated from our cross-correlation of AAT galaxies with the XRB, and the long-dashed line shows the *total* intensity of the unresolved XRB on the GSGP4 image.

With our estimated X-ray emissivity ρ, and $3 \leq z_{max} \leq 5$ for galaxies, the rate of X-ray luminosity evolution required for galaxies to produce the entire non-QSO component of the XRB is, in a low q_0 universe, exactly that given by the $\tau = 0.4$ evolution model of GP. If $q_0 = 0.5$ we may require the X-ray luminosity evolution of galaxies to be slightly faster than $\tau = 0.4$, to give $f_{gal} \sim 70\%$, but still slower than that of QSOs.

Treyer et al. (1992) found a model in which the XRB was produced mainly by rapidly evolving star-forming galaxies to be consistent with both the spectral energy distribution of the XRB and the upper limits on its ACF. However, these authors used a much lower value of the local X-ray volume emissivity ($\rho_0 \sim 10^{37}$ ergs s^{-1}Mpc^{-3}) than that estimated here, and consequently required extremely rapid evolution ($\tau \sim 0.1$) for star-forming galaxies to produce the bulk of the XRB. The results of our cross-correlation analysis suggest a much higher local value of ρ_0, requiring only $\tau \sim 0.4$ evolution for galaxies to produce all of the background not already accounted for by QSOs.

Treyer et al. also considered a 'local model' with a very high emissivity at $z = 0$ ($\rho_0 \sim 10^{39}$ ergs s^{-1}Mpc^{-3}), requiring no evolution to produce the entire 3 keV XRB, but this would be excluded by the ACF upper limits. We found in Section 6.6 that the XRB could not be produced by non-evolving sources clustered as normal galaxies, as they would produce much larger fluctuations than are observed, whereas an XRB produced by galaxies evolving like QSOs would have a much lower ACF amplitude, within the observed upper limits. Using the methods described in Section 6.6, we can now investigate whether the slower rates of evolution we estimate to be required to give $f_{gal} \simeq 70\%$ are still consistent with our ACF upper limits of $\omega_{ACF}(\theta) < 1.4 \times 10^{-3}(\mathrm{deg})^{-0.8}$.

Normally clustered galaxies, distributed out to $z = 4$, evolving as in the $\tau = 0.4$ model with $\alpha = 0.3$ would produce an ACF amplitude of $\omega_{ACF}(\theta) = 6.08 \times 10^{-4}(\mathrm{deg})^{-0.8}$ if $q_0 = 0.05$. In a $q_0 = 0.5$ Universe, we require evolutionary rates intermediate between $\tau = 0.4$ evolution with $\alpha = 0.3$ and and and QSO-like evolution with $\alpha = 1$ to give $f_{gal} \simeq 70\%$, which would give ACF amplitudes in the range $\omega_{ACF}(\theta) = (7.21\text{–}13.56) \times 10^{-4}(\mathrm{deg})^{-0.8}$. It is clear that, whereas the Treyer et al. model with low ρ_0 and very rapid evolution is excluded by our cross-correlation results which indicate a higher ρ_0, and the opposite extreme of a very high ρ_0 with no evolution is ruled out by the ACF upper limits, an intermediate model with $\rho_0 \sim 5 \times 10^{38}$ ergs s^{-1}Mpc^{-3} and $\tau \sim 0.4$ would be consistent with both sets of results.

The rate of X-ray luminosity evolution which we estimate to be that required to give $f_{gal} \sim 70\%$ does not appear to be unphysically rapid, being somewhat less than the 'extreme' rate of X-ray luminosity evolution of QSOs, and quite similar to the strong luminosity evolution already observed for galaxies in the passbands most sensitive to star-formation. The $\tau = 0.4$ rate of L_X evolution in GP's model was originally derived from the observed $L_{60\mu\mathrm{m}}$ evolution of IRAS galaxies, which is related primarily to an increase in their SFR with redshift. Furthermore, the exponential timescale for the evolution of the SFR in late-type (e.g. Sc) galaxies, as determined by comparing their spectra with the spectral evolution models of Bruzual and Charlot (1993), is also typically $\sim 0.4 H_0^{-1}$. Both these comparisons suggest that the evolution of the mean L_X of galaxies closely follows that of their star-formation rates.

However, we find that at the depths of our AAT sample, galaxies without ongoing star-formation produce a similar total X-ray emissivity to star-forming galaxies. A $\tau \sim 0.4$ rate of evolution for the summed X-ray emission from all types of galaxy might then suggest that the X-ray emission from hot gas in the early-type galaxies increases similarly with redshift – although if the total X-ray emission from galaxies becomes increasingly dominated at higher redshifts by the MXRBs in star-forming galaxies, the

evolution of the SFR alone might be sufficient to account for the increase of the mean L_X. Much deeper surveys will be needed to separately investigate the X-ray luminosity evolution of different galaxy types, as we discuss further in Section 8.9.

7.10 The X-ray Luminosity Function of Galaxies

Although our results appear to favour the $\tau = 0.4$ model of moderate X-ray evolution for galaxies, as proposed by GP, our estimate of f_{gal} is higher than the 20–30% predicted by these authors using a $\tau = 0.4$ evolution model and a low q_0. The difference obviously lies in the values of ρ_0 used to normalize the models.

GP assumed a local X-ray emissivity of

$$\rho_0(0.5\text{–}3.0 \text{ keV}) = 7.7 \times 10^{37} \text{ ergs s}^{-1}\text{Mpc}^{-3}$$

(for $H_0 = 50$ km s^{-1}Mpc^{-1}), obtained by integrating over an X-ray luminosity function derived using the IRAS galaxy 60μm luminosity function and the measured correlation between L_X and $L_{60\mu\text{m}}$. Their value of ρ_0 was described as a lower limit, as it only included emission from galaxies with $L_X(0.5\text{–}3.0 \text{ keV}) \geq 10^{39.4}$ ergs s^{-1}.

For a spectral index $\alpha = 0.3$, $\rho(0.5\text{–}2.0 \text{ keV}) = 0.65\rho(0.5\text{–}3.0 \text{ keV})$, so GP's emissivity corresponds in the ROSAT band to

$$\rho_0(0.5\text{–}2.0 \text{ keV}) \simeq 5.0 \times 10^{37} \text{ ergs s}^{-1}.$$

At $z = 0.35$, the $\tau = 0.4$ evolution and the k-correction would increase this to

$$\rho(0.5\text{–}2.0 \text{ keV}) \simeq 1.2 \times 10^{38} \text{ ergs s}^{-1},$$

which is still lower than our value by a factor of ~ 4. Consequently, GP required very rapid QSO-like ($\tau \sim 0.2$) X-ray luminosity evolution for galaxies with their lower local emissivity to account for $> 50\%$ of the 0.5–3.0 keV background, whereas we find $\tau \sim 0.4$ evolution to be adequate.

One possible explanation for this difference would appear to be that GP underestimated ρ_0 greatly by not including the emission from the low-luminosity galaxies, ie. those with $L_X(0.5\text{–}3.0 \text{ keV}) < 10^{39.4}$ ergs s^{-1}. The X-ray luminosity function (LF) derived by GP,

$$\Phi(L) \propto L^{-2.3} \text{ for } 10^{39.4} \leq L_X < 10^{40.7}$$
$$\Phi(L) \propto L^{-4.4} \text{ for } L_X \geq 10^{40.7}$$

is extremely steep even at their faint-end cut-off. Indeed the total emissivity diverges if the $\alpha = -2.3$ slope continues faintward. GP found that extending their faint-end slope to a luminosity a factor of 3 smaller increased ρ_0 (and hence their estimate of f_{gal}) by 60%. A faintward extension by a factor of ~ 30 to $L_X = 10^{37.9}$ ergs s^{-1} would be sufficient to give the high value of ρ_0 estimated from our cross-correlation analysis. However, it is unlikely that the X-ray LF remains divergently steep at luminosities as low as this, as for galaxies with normal L_X/L_B ratios, the faint-end cut-off used by GP corresponds to $M_B \simeq -19$, where the optical luminosity functions will have flattened to faint-end slopes with α in the region of -1.0 to -1.5.

The X-ray LF derived by GP is steeper by a factor of $(0.7)^{-1}$ than the IRAS galaxy far infra-red luminosity function as a result of the non-linear relation $L_X \propto (L_{60\mu m})^{0.7}$. In contrast, fitting a relation $L_X \propto (L_B)^\epsilon$ gives a linear correspondence $\epsilon = 1.0$, at least for spiral galaxies and $L \leq L^*$ ellipticals (Fabbiano 1989), which suggests that the X-ray and blue-band LFs should have similar faint-end slopes. At $L_X(0.5\text{–}3.0 \text{ keV}) \leq 10^{39.4}$ ergs s^{-1}, the X-ray LF must be dominated by galaxies on the faint end slope of the optical LF, and so it would be more reasonable to extend the GP X-ray LF faintward of this luminosity with, for example, $\alpha = -1.5$ (ie. the optical faint-end slope for the

bluest galaxies), which increases the total emissivity ρ_0 by only $\sim 10\%$ when summed from $L_X = 10^{39.4}$ to $L_X = 0$.

At presently attainable flux limits, the detected source counts probe only the bright-end of the X-ray LF of galaxies (i.e. $L_X > 10^{41.5}$ ergs s^{-1}, see Table 5.7). GP predict an approximately Euclidean ($\gamma = 1.5$) slope for the X-ray number counts of galaxies, continuing to at least $S \simeq 10^{-16}$ ergs cm^{-2}s^{-1}, but with a number count normalization lower by a factor of more than ~ 10 than that estimated from our correlation between detected sources and galaxies (Section 5.7). This is even greater than the difference between the total emissivity ρ_0 used by GP and the higher value derived from our galaxy/XRB cross-correlation, so that the underprediction of the X-ray emission from galaxies is greater for the bright-end of GP's X-ray LF than for the integrated X-ray luminosity of their LF as a whole. Hence the relatively low X-ray emissivity from galaxies in GP's model, and therefore their failure to account for more than $\sim 25\%$ of the XRB with a moderate rate of evolution, appears to be primarily the result of including too few galaxies with very high X-ray luminosities, rather than their failure to include the emission from very low-luminosity ($L_X < 10^{39.4}$ ergs s^{-1}) galaxies.

Figure 7.10 shows the X-ray LF derived by GP, normalized at $\log \Phi(10^{40.7}) = -43.235$ L^{-1}Mpc^{-3} so as to give the total luminosity density (summed for all $L_X > 10^{39.4}$ ergs s^{-1} galaxies) of $\rho_0 = 7.7 \times 10^{37}$ ergs s^{-1}Mpc^{-3} used by these authors. The graph also shows an X-ray LF derived from the blue-band LF of all galaxy types, by assuming a linear relation $f_\nu(2\text{ keV})/f_\nu(B) = 10^{-6.6}$ with no dispersion in the flux ratios of the galaxies. For a flux ratio $f_\nu(2\text{ keV})/f_\nu(B) = 10^{-6.6}$, a galaxy with absolute magnitude $M_B = -21.0$ and spectral index $\alpha = 0.3$ will have $L_X(0.5\text{–}3.0\text{ keV}) = 1.72 \times 10^{40}$ ergs s^{-1}.

From a comparison of these luminosity functions, it is clear that the X-ray LF must flatten to a non-divergent (ie. $\alpha > -2$) slope at $L_X < 10^{39.5}$, to avoid exceeding the total number density of galaxies at these lower luminosities.

Over the range $10^{39.5} \leq L_X \leq 10^{41.5}$ the optical-derived and IRAS-derived X-ray LFs give very similar densities of galaxies. At $L_X > 10^{41.5}$, the optical-derived LF predicts a much lower density of galaxies than does the IRAS-derived LF, and falls away rapidly towards zero. This results from the different form of the bright ends of the respective luminosity functions (exponential cut-off and power-law decrease). However, the numbers of $L_X > 10^{41.5}$ galaxies in the 'IRAS-derived' X-ray LF are still insufficient to explain the numbers detected in our source/galaxy cross-correlation analysis (Chapter 5). On the basis of these detections we suggested that a large dispersion $\sigma \sim 0.8$ existed in the logarithms of the L_X/L_B ratios of galaxies, and the mean flux ratio of $f_\nu(2\text{ keV})/f_\nu(B) \simeq 10^{-5.6}$ derived from the amplitude of the galaxy/XRB cross-correlation suggests a similar dispersion.

If the X-ray luminosity of galaxies evolves as $\tau \sim 0.4$, increasing by a factor ~ 2 between $z = 0$ and the depth of our AAT sample, the required dispersion would be reduced slightly to $\sigma \sim 0.7$. To investigate further the effect of such a dispersion, we derive a third X-ray luminosity function, Φ'_B, from the optical luminosity function using the same linear $\log L_X$-$\log L_B$ relation as was used for Φ_B, but with a $\sigma = 0.7$ dispersion in the $\log L_X$ of the galaxies of a given $\log L_B$.

This function was calculated by means of a convolution of the optical-derived LF Φ_B with a Gaussian distribution with $\sigma = 0.7$, i.e. by integrating

$$\Phi'_B(\log L_X) = \int \Phi_B(\log L_X)\exp(-0.5(\log L_X - \log L'_X)/0.70)^2 d(\log L'_X)$$

at each value of log L_X, and normalizing by dividing by

$$\int \exp(-0.5(x/0.70)^2)dx = 0.70\sqrt{2\pi}$$

Figure 7.10 also shows the luminosity function Φ'_B, and by comparison with Φ_B it is clear that the introduction of our estimated dispersion into the log L_X-log L_B relation greatly increases the predicted number density of very X-ray luminous (L_X(0.5–3.0 keV) > $10^{41.5}$ ergs s^{-1}) galaxies.

We then derived integral number counts of galaxies as a function of X-ray flux limit for each of the three modelled forms of the X-ray luminosity function shown here. The models assumed $z_{max} = 4.0$, $q_0 = 0.05$, a spectral index $\alpha_x = 0.3$, and luminosity evolution as $\tau = 0.4$. The three X-ray number count models are shown in Figure 7.11, together with the 'observed' galaxy count of 27.2 ± 10.4 deg^{-2} at a flux limit of S(0.5–3.0 keV) = $10^{-14.2}$ ergs cm^{-2}s^{-1} (i.e. S(0.5–2.0 keV) = $10^{-14.4}$ ergs cm^{-2}s^{-1}) estimated from the source/galaxy cross-correlation analysis of Section 5.7.

Only the $\sigma = 0.7$ model predicts a sufficiently high number count at this limit, of 23.55 deg^{-2}, to be consistent with our results. The IRAS-derived LF predicts a galaxy number count of only 1.01 deg^{-2} and the $\sigma = 0$ optical-derived LF the even lower count of 0.69 deg^{-2}. The $\sigma = 0.7$, IRAS-derived and $\sigma = 0$ optical-derived LFs predict mean redshifts for galaxies detected at this flux limit of 0.309, 0.025 and 0.023 respectively. Only for the $\sigma = 0.7$ model is this in reasonable agreement with spectroscopic observations of ROSAT-detected galaxies (giving $z_{mean} = 0.22$ for the galaxies listed in Table 5.6, which would perhaps increase to $z_{mean} \sim 0.3$ if all the $21 \leq B \leq 23$ galaxies correlated with sources were included).

We find that an X-ray LF derived from the optical LF of galaxies with no dispersion in the log L_X–log L_B relation underpredicts ρ by a factor of ~ 5 and the X-ray counts of galaxies by a factor ~ 40, even with $\tau = 0.4$ evolution of L_X. We verify that the dispersion required in the log (L_X/L_B) ratio to fit the ROSAT observations is indeed $\sigma \simeq 0.7$.

The GP X-ray LF, derived from the 60μm LF with no dispersion, underpredicts ρ by a slightly smaller factor ~ 4 and the counts by a factor of ~ 30. Hence the dispersion required in the log L_X–log $L_{60\mu m}$ relation to fit the ROSAT observations would be slightly smaller (perhaps $\sigma \sim 0.6$) than that required for log (L_X/L_B). The scatter in GP's plot of log L_X against log $L_{60\mu m}$ for IRAS and starburst/interacting galaxies is quite large and appears consistent with this value, suggesting that if Griffiths and Padovani had included the observed dispersion in the log L_X – log $L_{60\mu m}$ relation in deriving an X-ray LF, their modelled galaxy counts may have been high enough to agree with the ROSAT observations.

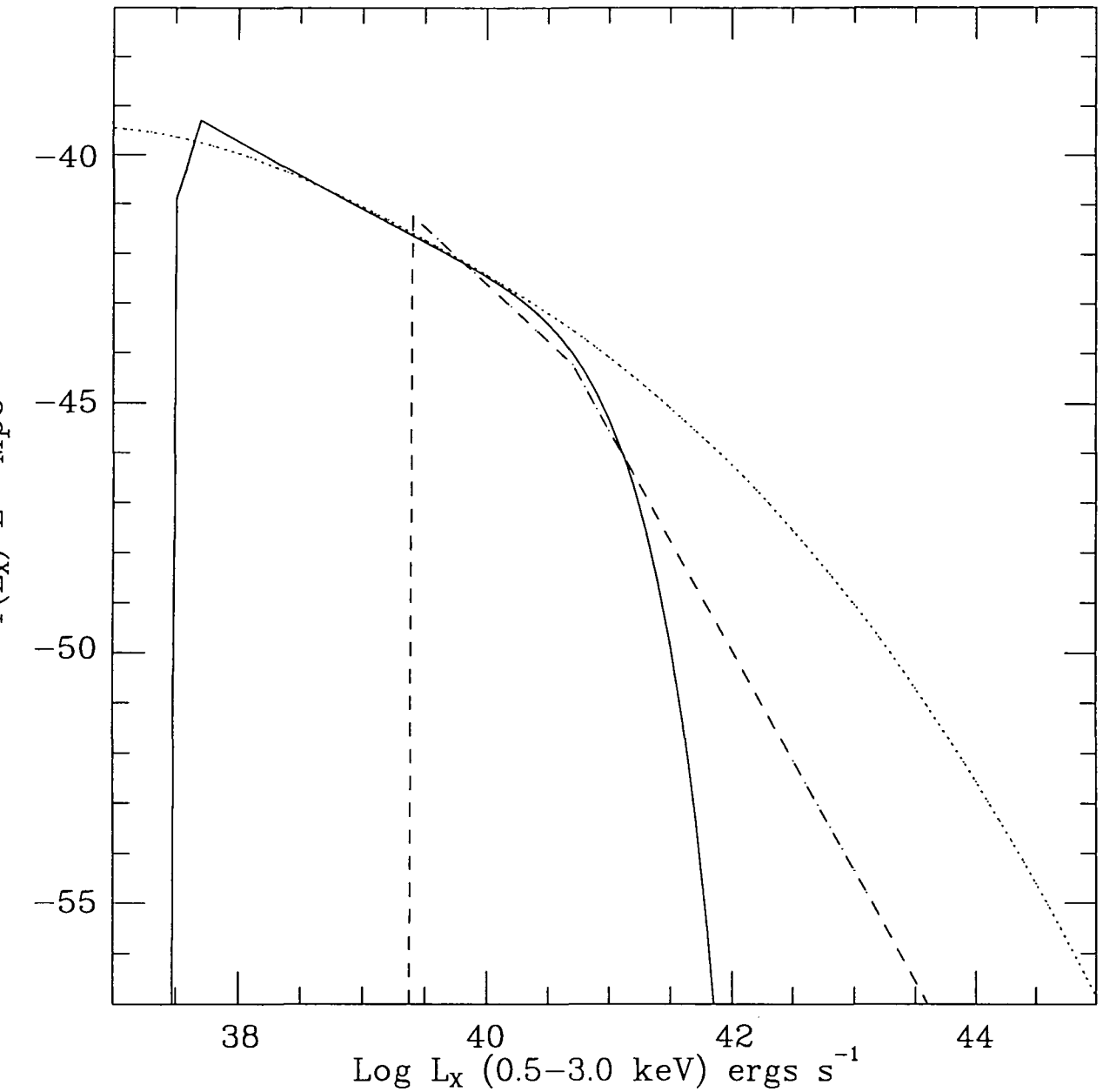

Figure 7.10 X-ray luminosity functions of galaxies, derived from the blue-band luminosity function by assuming a L_X/L_B ratio corresponding to $f_\nu(2\text{ keV})/f_\nu(B) = 10^{-6.6}$, with no dispersion in L_X/L_B ratios (solid line), and with a dispersion of $\sigma = 0.7$ in log (L_X/L_B) (dotted line), and the X-ray luminosity function derived by GP from the 60μm luminosity function of IRAS galaxies (dashed line).

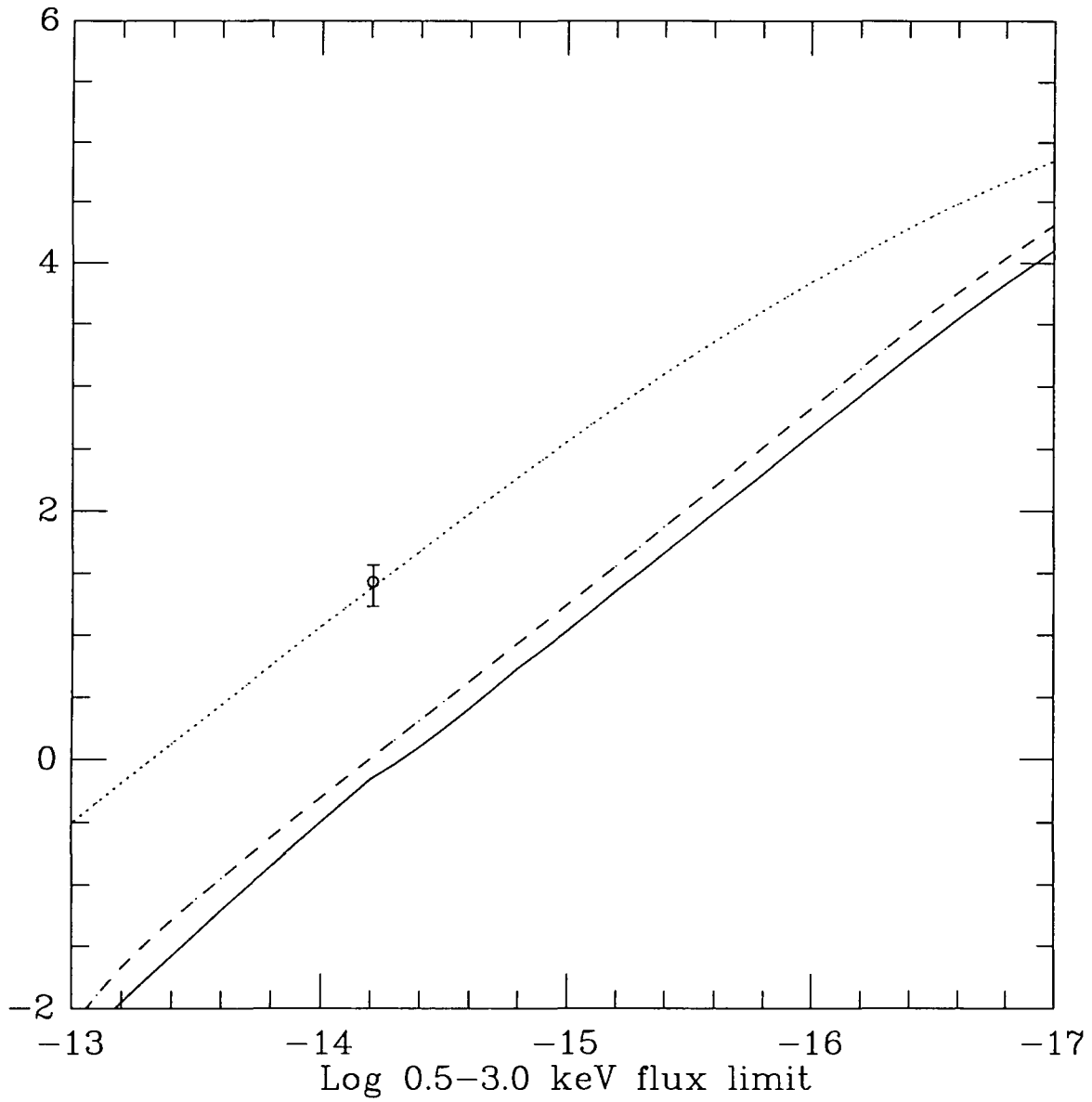

Figure 7.11 Integral X-ray number counts of galaxies, in galaxies deg^{-2}, as a function of the logarithm of the 0.5–3.0 keV flux limit, calculated from the three models of the X-ray luminosity function of galaxies shown in Figure 7.10. The graph shows the counts given by an X-ray luminosity function derived from the blue-band LF assuming no dispersion in log (L_X/L_B) (solid line), the X-ray LF derived from the same optical LF with a $\sigma = 0.7$ dispersion in log (L_X/L_B) (dotted line), and the X-ray LF derived by GP from the IRAS LF (dashed line). All three models plotted are computed for a $q_0 = 0.05$ geometry, and assume an X-ray spectral index of $\alpha = 0.3$ and X-ray luminosity evolution as $\tau = 0.4$ for all galaxies, differing only in the assumed X-ray luminosity functions.

The plotted point is our X-ray galaxy number count of 27.2 ± 10.4 deg^{-2}, which was estimated in Section 5.7 from the cross-correlation between $B \leq 23.0$ galaxies and unidentified X-ray sources brightward of a flux limit of S(0.5–2.0 keV) = $10^{-14.4}$ ergs cm^{-1}s^{-1}, assumed here to correspond to S(0.5–3.0 keV) = $10^{-14.2}$ ergs cm^{-1}s^{-1}.

7.11 Discussion: Parameters Influencing L_X/L_B

It is clear that a model in which a wide dispersion of $\sigma \sim 0.7$ in the log (L_X/L_B) ratios of galaxies greatly increases both the numbers of very X-ray luminous galaxies, and the X-ray volume emissivity produced by galaxies as a whole, can explain very well both the individual detections of faint galaxies on ROSAT images and the strength of the galaxy/XRB cross-correlation.

The reason for such a high dispersion in L_X/L_B ratios remains uncertain at present, and we now consider possible physical causes. Our estimate of the dispersion of L_X/L_B ratios for galaxies is somewhat higher than the dispersion estimated by Georgantopoulos (1991) for AGN, expressed as $\sigma = 0.12$ in the power-law index α_{ox}, which corresponds to a dispersion in log L_X/L_B of $\sigma \simeq 0.3$, for the factor of $\sim 10^{2.5}$ difference in wavelength between the ROSAT and blue bands. However, *Einstein* observations of a wide variety of galaxies have already provided evidence that galaxies vary in L_X/L_B to a greater extent than this.

A high dispersion in the L_X/L_B ratios of galaxies may be related to the fact that star-formation rates (per unit mass) obviously vary greatly between galaxies, and that the formation of massive stars may increase L_X to a greater extent than L_B if it leads to the formation of large numbers of very luminous X-ray binaries. The variation in star-formation rates amongst galaxies at a given blue-band luminosity would then produce a wide dispersion in L_X/L_B. However, it is unlikely that starbursting alone can explain all the results discussed here, for the reasons discussed below.

Firstly, normal and starburst galaxies have been found to follow the $L_X \propto (L_{60\mu\mathrm{m}})^{0.7}$ relation with the same constant of proportionality, and so L_X and $(L_{60\mu\mathrm{m}})^{0.7}$ must be equally sensitive to starburst activity. Variation in the star-formation rates could account for the fact that the IRAS-derived LF follows a power-law at the bright end, rather than an exponential cut-off, by producing a wide dispersion in the $L_{60\mu\mathrm{m}}/L_B$ ratios. However, as GP's IRAS-derived X-ray LF still greatly underpredicts the X-ray number counts, the true X-ray LF of galaxies must be even more extended at its bright end than the IRAS LF, requiring a a wide dispersion in the $L_X/(L_{60\mu\mathrm{m}})^{0.7}$ ratio. The difference between our estimate of the X-ray emissivity of AAT galaxies and the lower estimate of Miyaji et al. (1994) for IRAS galaxies also suggests that significant numbers of galaxies possess a high L_X but a low 60μm luminosity.

Hence the X-ray properties of galaxies must depend on at least one additional parameter, which must be independent of the SFR if it is to increase L_X without increasing $(L_{60\mu m})^{0.7}$ by the same ratio. One obvious choice might be the chemical composition of the galaxies. X-ray emission from star-forming regions has been found to be inversely correlated with metallicity, as is illustrated by GP – the metallicity of the Large Magellanic Cloud, for example, is lower than that of our own Galaxy by a factor ~ 10 and the X-ray luminosity per type O star is more than an order of magnitude higher. For star-forming galaxies, the effect of metallicity on L_X may then be sufficiently strong to produce the required $\sigma \sim 0.6$ dispersion in the log L_X–log $L_{60\mu m}$ relation. The even larger dispersion in the L_X/L_B ratios of star-forming galaxies might then result from the combined effects on X-ray luminosity of differences in metallicity and differences in star-formation rates.

Secondly, our X-ray detected galaxies possessed a wide range of $B-R$ colours and 3727Å equivalent widths, typical of a randomly selected galaxy sample in this magnitude range. The X-ray selected sample included some 'passive' galaxies with no indication of ongoing star formation. The galaxy/XRB cross-correlation was also similar for red and blue galaxies. Although large k-corrections at $z \sim 0.3$–0.5 could have shifted the colours

of a few spiral galaxies into the $B-R \geq 1.5$ subsample, some dependence on $B-R$ colour would still be expected if the high X-ray luminosities of some galaxies were associated entirely with star-formation activity. It therefore appears that early-type galaxies, with little or no ongoing star-formation, produce an X-ray luminosity density comparable to that produced by star-forming galaxies, at least at moderate ($z < 0.5$) redshifts.

Furthermore, there is already observational evidence that the dispersion in log (L_X/L_B) ratios for early-type galaxies is similar to our estimate of $\sigma \sim 0.7$ for galaxies in general. For example, as described by Kim et al. (1992), one sample of 37 early-type galaxies observed with *Einstein* was found to have a mean log (L_X/L_B) ratio of 30.5 – where L_X is measured in ergs s^{-1} in the 0.8–3.5 keV passband, and L_B given in units of solar luminosities – corresponding to a mean $\log(f_\nu(2\text{ keV})/f_\nu(B)) \simeq -6.0$, with a dispersion in log (L_X/L_B) within the sample of $\sigma = 0.6$. The highest L_X/L_B ratio of these 37 galaxies exceeded the mean ratio of the sample by a factor of 41, so it would seem reasonable that a $\sim 1\%$ fraction of galaxies might exceed the mean L_X/L_B ratio by factors of ~ 100, as our cross-correlation results of Chapter 5 would suggest. Furthermore, the galaxies in the Kim et al. (1992) sample with higher L_X/L_B ratios tended to have softer C32 colours, where C32 is defined as the ratio of L_X(1.4–3.5 keV) to L_X(0.8–1.4 keV), so that for observations in the softer ROSAT band (0.5–2.0 keV) the dispersion in L_X/L_B would be even higher than that of $\sigma = 0.6$ seen at 0.8–3.5 keV.

As these *Einstein* observations obtained a similar mean L_X/L_B ratio and a similar wide dispersion in log (L_X/L_B) from a sample limited to early-type galaxies as our cross-correlation results suggest for galaxies in general, it is clear that our results cannot be attributed entirely to star-formation processes. Quite different mechanisms must be involved in producing a similar dispersion in L_X/L_B ratios for the early-type galaxies.

Some of the variation in L_X/L_B between early-type galaxies must result from the non-linear relation $L_X \propto (L_B)^{1.5-2.0}$, which has been observed for the most luminous ellipticals (Fabbiano 1989, Sarazin 1990). This would introduce a dependence of L_X/L_B on L_B, rather than a scatter in L_X at each value of L_B. The fact that our X-ray detected early-type galaxies (see Section 5.6.2) tended to be those with high optical luminosities ($M_B \sim -22$), while our X-ray detected late-type galaxies appeared to possess the same distribution of L_B as an optically-selected sample, may reflect this non-linear relation. As discussed by Sarazin (1990), a relation of the form $L_X \propto (L_B)^{1.5-2.0}$ might be expected if the X-ray emission of the largest ellipticals is dominated by thermal bremsstrahlung from hot gas. The main sources of energy for heating the gas, which originates through mass loss from stars, are the orbital motions of the gas-losing stars and gravitational infall of the gas. For both these mechanisms, the heating rate per unit mass of gas is proportional to the σ_*^2, the square of the velocity dispersion of the stars (or, equivalently, the depth of the gravitational potential well of the galaxy). This relates to blue luminosity as $\sigma_*^2 \propto (L_B)^{0.5-1.0}$, so if we assume the mass of hot gas in the galaxy as a whole is proportional to its optical luminosity, we obtain a relation $L_X \propto (L_B\sigma_*^2) \propto (L_B)^{1.5-2.0}$. When Sarazin (1990) fitted power-laws to the log L_X–log L_B relation of 81 early-type galaxies observed using *Einstein*, a very steep relation $L_X \propto L_B^{2.27\pm0.24}$ was estimated, whereas when fitting to log L_X–log $(L_B\sigma_*^2)$ for a slightly smaller sample of 57, the observed relation became $L_X \propto (L_B\sigma_*^2)^{1.19\pm0.13}$, consistent with the linear relation predicted by the hot gas model.

However, in both these cases a high dispersion of $\sigma(\log L_X) = 0.51$ was still observed about the fitted relations, suggesting that at least one further parameter, in addition to σ_*^2, influences the L_X/L_B ratio of early-type galaxies. This additional parameter is unlikely to be metallicity for early-type galaxies. In contrast to the strong inverse relation between MXRB emission and metallicity in late-type galaxies, Sarazin (1990)

found a slight positive correlation between L_X and magnesium abundance in early-type galaxies, although this was weak and of marginal ($\sim 2\sigma$) significance. This effect could result from the fact that in a low-density, hot gaseous medium, the presence of metals would produce emission lines at keV energies rather than absorption, or might simply be the result of a dependence of metallicity on mass. However, the effect of metallicity on L_X for early-type galaxies appears to be much smaller than the observed dispersion in L_X/L_B.

The globular clusters found in very large numbers around some giant ellipticals might also be involved in producing the high X-ray luminosities of some early-type galaxies, as the very high density of stars and stellar remnants in the central regions of globulars favours the formation of low-mass X-ray binaries. A wide range in the numbers of globulars associated with each galaxy (relative to the total stellar mass) would produce a wide dispersion in the ratio of the numbers of low mass X-ray binaries to the numbers of stars, and would therefore contribute to the dispersion in L_X/L_B. However, the low X-ray temperatures of individual ellipticals ($kT \sim 1$ keV) compared to those of binary sources ($kT \geq 5$ keV), and the presence of emission lines in the X-ray spectra of ellipticals, suggests that diffuse hot gas accounts for more of their X-ray emission than any population of accreting binaries (see e.g. Sarazin 1988). If this is the case, the contribution of globular clusters to the L_X/L_B dispersion of early-type galaxies would probably be of less significance than differences between galaxies in the mass and/or temperature (i.e. velocity dispersion) of the X-ray emitting gas.

Sarazin (1990) suggested that, as $L_X/(L_B\sigma_*^2)$ would be proportional to the ratio of the mass of hot gas to the mass of stars, the $\sigma \sim 0.5$ dispersion in log L_X at a given $L_B\sigma_*^2$ may result from differences in the evolutionary history of the ellipticals. Some galaxies may have undergone ram pressure stripping within dense regions, removing most of the hot gas lost from stars, and thus reducing the $L_X/(L_B\sigma_*^2)$ ratio, whereas other giant ellipticals may have been able to retain much larger amounts of this very hot gas, resulting in much higher X-ray luminosities at the present day.

The true explanation of the dispersion in L_X/L_B of galaxies, and therefore our cross-correlation results, may be very complicated. Variations in the star-formation rates, chemical composition, velocity dispersions and ram pressure stripping histories of the galaxies may be involved, to varying degrees in different types of galaxy. There may be other parameters influencing the X-ray properties of galaxies which we have not considered here. Further investigation of the cross-correlations of early and late-type galaxies with the XRB are required, ideally using new instruments with sensitivity to harder (2–10 keV) X-rays and high spectral resolution (e.g. the new ASCA satellite). Observations of X-ray detected galaxies with high spectral resolution (to determine spectral indices, gas temperatures, emission line widths, etc.), and the cross-correlation of galaxies with the unresolved XRB imaged in a number of different energy bands, may then enable us to establish the relative importance of the various possible X-ray emission mechanisms (e.g. massive binaries, low mass binaries, 'hidden' AGN, hot gas in galaxies and the even hotter gas in clusters) in producing the cross-correlation results discussed in this thesis.

7.12 Summary and Conclusions

(i) A significant cross-correlation was detected between $18.0 \leq B \leq 23.0$ galaxies and the 0.5–2.0 keV X-ray background on three 0.35 deg^2 areas of sky. The strength of the cross-correlation indicated these galaxies to be the origin of a fraction of the unresolved component of the 0.5–2.0 keV background estimated as $16.81 \pm 2.14\%$. The ratio of the total X-ray flux to the total blue-band flux from these galaxies was estimated as $S(0.5\text{–}2.0 \text{ keV}) = (3.69 \pm 0.47) \times 10^{-15}$ ergs cm^{-2}s^{-1} per $B = 18.0$ galaxy. In terms of luminosities this is $L_X(0.5\text{–}2.0 \text{ keV}) = (1.77 \pm 0.22) \times 10^{41}$ ergs s^{-1} for a galaxy of absolute blue magnitude $M_B = -21.0$.

(ii) Extrapolating this flux ratio to fainter magnitude limits ($B \sim 27.5$) using galaxy counts from deep CCD surveys gave an estimate of $f_{gal} = 35\%$ for the total fraction of the unresolved 0.5–2.0 keV background produced by galaxies. This can probably be regarded as a lower limit, as the ratio of observed X-ray to blue-band fluxes is likely to increase at higher redshifts (see Section 7.7).

(iii) Red and blue galaxies in our sample show the same (within 1σ) cross-correlation with the XRB at small separations (≤ 25 arcsec) within the ROSAT point-spread function, suggesting that the mean X-ray luminosities of early-type and star-forming galaxies are similar. However, for the red ($B-R \geq 1.5$) galaxies there is more signal in the cross-correlation at $40 \leq \theta \leq 60$ arcsec separations, which may indicate that some early-type galaxies lie within extended X-ray sources, i.e. galaxy groups and clusters.

(iv) The amplitude of the cross-correlation between galaxies and the XRB gave an estimate of the X-ray luminosity density of the galaxies in our sample of

$\rho(0.5\text{–}2.0 \text{ keV}) = 5.27 \pm 0.65 \times 10^{38}$ ergs s^{-1}Mpc^{-3} (for $H_0 = 50$ km s^{-1}Mpc^{-1}).

This result would indicate that $z < 1$ galaxies produce a fraction $f_{gal} \sim 30\%$ of the unresolved XRB.

The contribution from galaxies at higher redshifts depends on their X-ray luminosity evolution, and is only a further $\sim 10\%$ if there is no increase in their mean L_X with redshift. However, the upper limits on the autocorrelation function of the XRB (Chapter 6) require that the X-ray sources, if clustered as normal galaixes, must increase significantly in luminosity with redshift. If, as suggested by Griffiths and Padovani (1990), the X-ray luminosity of galaxies increases with look-back time following an exponential timescale $\sim 0.4H_0^{-1}$, this would increase our estimate of f_{gal} to $\sim 70\%$, with about half of this flux being produced by galaxies at $1 \leq z \leq 4$.

The QSO counts of Section 5.7, and possibly the ACF upper limits discussed in Chapter 6, suggest that QSOs produce only $\sim 30\%$ of the unresolved XRB, so the $\tau = 0.4$ evolution appears to be exactly that required for galaxies to produce the remainder. If galaxies are the main source of the unresolved XRB, we find that this rate of evolution would be consistent with the upper limits on the ACF. However, a more rapid X-ray luminosity evolution for galaxies, equal to that observed for QSOs, may predict a galaxy contribution exceeding the entire XRB intensity.

Hence our observations appear to favour the $\tau = 0.4$ model of GP as a good description of the X-ray luminosity evolution of galaxies.

(v) The total X-ray luminosity density of galaxies, as estimated here from the galaxy/XRB cross-correlation, and the X-ray number counts of galaxies (see Chapter 5) are both much higher than would be expected from the L_X/L_B ratios of most galaxies seen locally. Deriving an X-ray luminosity function for galaxies from either their optical luminosity function or the 60μm IRAS galaxy luminosity function greatly underpredicts

the numbers of high–L_X galaxies detected by ROSAT, unless we include a wide dispersion of $\sigma \sim 0.7$ in the log L_X–log L_B relation, and a slightly smaller dispersion in the log L_X–log $L_{60\mu m}$ relation, in addition to the $\tau = 0.4$ evolution of L_X suggested above. These dispersions would greatly increase the numbers of galaxies with very high X-ray luminosities ($L_X \sim 10^{42}$ ergs s^{-1}) which we detect as individual sources, and would also increase the total X-ray volume emissivity of galaxies by factors of ~ 5, accounting for the high amplitude of our galaxy/XRB cross-correlation function and that of Lahav et al. (1993).

Uncertainty remains about the cause of the inferred $\sigma \sim 0.7$ dispersion in log L_X/L_B. In spiral galaxies, it may be the result of variations in metallicity between the galaxies (low metallicity has been found to correlate with high X-ray emission) in addition to the enhancement of the X-ray luminosity of those galaxies undergoing starburst activity. In early-type galaxies without active star-formation, variation in the velocity dispersion and in the proportion of the hot gas lost from stars remaining in the galaxy may be involved in producing a very similar dispersion in L_X/L_B ratios.

Chapter 8

Conclusions and Future Prospects

8.1 Summary of Main Conclusions

In the course of the investigations into the clustering, evolution and X-ray properties of galaxies described in this thesis a number of interesting results have been obtained, but owing to the limited size of the available datasets, some of these are at present only suggestive rather than conclusive.

Our strongest results are that:

(i) The $\omega(\theta)$ amplitude of galaxies at $B \geq 23.5$ is much lower than would be predicted by a model without a significant increase in the luminosity of $L \sim L^*$ galaxies at $z > 1$, and/or a reduction in the strength of the intrinsic galaxy clustering relative to a stable model at earlier epochs.

(ii) There is a significant cross-correlation between $B \leq 21$ galaxies and X-ray sources, indicating that $\sim$ 1% of such galaxies ($\sim$ 12 in a $\sim$ 1 deg^2 area) are sufficiently X-ray luminous to be detected above 0.5–2.0 keV flux limits of $S \simeq 10^{-14.4}$ ergs s^{-1}. The X-ray detected galaxies possess high X-ray luminosities of $L_X \sim 10^{42}$ ergs s^{-1}, and L_X/L_B ratios higher by factors of order of $\sim$ 100 than the majority of galaxies seen locally.

(iii) There is a significant cross-correlation between $18 \leq B \leq 23$ galaxies and the unresolved X-ray background, indicating that galaxies in this magnitude range produce in total $\sim$ 17% of the XRB flux at 0.5–2.0 keV energies. If the X-ray luminosity of galaxies increases with look-back time approximately as in the $\tau \sim 0.4H_0^{-1}$ model of GP, faint galaxies would produce in total about 70% of the unresolved XRB and account for its entire non-QSO component.

Our investigations have also suggested, at somewhat lower levels of significance, that:

(i) The scaling of the galaxy $\omega(\theta)$ amplitude levels out at $25 \leq B \leq 27$, at an amplitude of $\omega(\theta) \simeq 4 \times 10^{-4}(\mathrm{deg})^{-0.8}$, suggesting that galaxies are seen out to their maximum redshifts at these limits. The $\omega(\theta)$ amplitude measured at $B_{ccd} = 25.0$ and fainter limits would be consistent with a maximum redshift of $3 \leq z_{max} \leq 4$ for galaxies, stable clustering and $0 \leq q_0 \leq 0.5$.

(ii) Pure Luminosity Evolution models, with a low value of q_0 and a normalization consistent with that obtained from the K-band counts, fit the blue-band galaxy number counts well to $B \sim 26$, and the $\omega(\theta)$ scaling at all magnitude limits. However, the the differential number counts of galaxies at even fainter magnitudes ($B \geq 26$) appear to be steeper ($\frac{d(logN)}{dm} \sim 0.3$) than even low-$q_0$ PLE models would predict.

(iii) Bluer ($B - R \leq 1.5$) galaxies appear weakly clustered on the sky in comparison to redder galaxies at the same blue magnitude limit, and the cross-correlation between red and blue galaxies is much weaker than the autocorrelation of the red galaxies. This is seen at limits of both $B = 23$ (on an AAT plate) and $B_{ccd} = 24.5$ (on our CCD survey).

(iv) The autocorrelation function of the unresolved X-ray background shows no detectable signal on arcminute scales, and we can set a 2σ upper limits on its amplitude

of $\omega(\theta) \leq 1.4 \times 10^{-3}(\mathrm{deg})^{-0.8}$. This would allow the XRB to be produced by normal galaxies, if these increase in X-ray luminosity with redshift at least as rapidly as $\tau \simeq 0.4$, so as to give a large contribution from galaxies at $z > 1$. However, the ACF upper limits would allow no more than $\sim$ 30% of the unresolved 0.5–2.0 keV background to be produced by QSOs, if high redshift QSOs are as clustered on $r \sim 1$ h^{-1}Mpc scales as the Shanks and Boyle (1994) measurements indicate on large scales (ie. the power-law index of $\xi(r)$ remains as steep as $\gamma = -1.8$ at high redshifts).

(v) In the 0.5–2.0 keV band, number counts of galaxies are lower than those of QSOs by a factor ~ 7 at $S \geq 10^{-14}$ ergs $\mathrm{cm}^{-2}\mathrm{s}^{-1}$. However, faintward of this limit the QSO count slope flattens significantly, as predicted by the models of Boyle et al. (1994), suggesting that QSOs produce only $\sim$ 30% of the unresolved XRB. The number counts of galaxies continue rising with a Euclidean slope to fainter limits, suggesting that galaxies may overtake the QSO number counts at $S \sim 10^{-15}$ ergs $\mathrm{cm}^{-2}\mathrm{s}^{-1}$, and if the galaxy counts remain steep to even fainter limits, may account for the remaining $\sim$ 70% of the XRB.

(vi) A high-redshift ($z = 0.56$) rich galaxy cluster was detected on one ROSAT image, but was found to possess an X-ray luminosity only $\sim$ 30% of that expected for a similar cluster at the present day.

We now consider some of these results further, and suggest ways in which the conclusions can be better verified and the investigations extended.

8.2 Galaxy Counts and Clustering at $23 \leq B \leq 25$

8.2.1 Interpretation of the Low $\omega(\theta)$ Amplitude

The low $\omega(\theta)$ amplitude of $B \sim 24$ galaxies in comparison to non-evolving predictions, first reported by Koo and Szalay (1984), is now a well-established result, having been observed in many photographic and CCD surveys of faint galaxies. The investigations described in Chapters 2, 3 and 4 of this thesis, together with the $\omega(\theta)$ results of Efstathiou et al. (1991), have verified that low $\omega(\theta)$ amplitudes continue to be obtained at even fainter limits ($B \sim 25$), where the discrepancy with non-evolving models is even larger (a factor of ~ 4).

Our observation that the clustering of the redder galaxies at $B \leq 24.5$ is consistent with non-evolving models would appear to exclude the very rapid ($\epsilon \sim 3$) rate of clustering evolution which would be needed to explain the $\omega(\theta)$ scaling with a non-evolving $N(z)$ and similar clustering for all types of galaxy. We found that the BEG merging model might still be marginally consistent with our $\omega(\theta)$ amplitudes if clustering evolution occurs as rapidly as $\epsilon = 1.2$, as the Melott (1992) models of the growth of clustering might predict if the index of the initial power spectrum of fluctuations is as negative as $n = -2$. However, according to the Roukema and Yoshii (1993) models of clustering evolution, if galaxy merging is a significant process in causing density evolution then it will also slow the growth of clustering, giving $\epsilon = -0.4 \pm 0.3$ whether the power spectrum is $n = 0$ or as negative as $n = -2$. Our $\omega(\theta)$ results would then strongly exclude the BEG merging model, quite apart from the difficulty of reconciling the rapid recent merging of $L \sim L^*$ galaxies in this model with the disk/spiral-dominated morphologies of the majority of present-day large galaxies. Hence it does not appear that physical merging alone could cause a very low (non-evolving) median redshift for the excess blue galaxies at $B \sim 24$.

A large excess of blue galaxies at $z \sim 0.4$ may instead consist of a vanishing population of starbursting dwarf galaxies, but this can only be reconciled with our $\omega(\theta)$ results if the blue starburst galaxies are intrinsically very weakly clustered in comparison to, and uncorrelated with, other galaxies at the same redshifts. If the excess blue galaxies at $B \sim 24$ lie entirely within a no-evolution $N(z)$, then even if they possess a zero strength of clustering, the $\omega(\theta)$ scaling would require most or all of these excess galaxies to have effectively disappeared at the typical redshifts of $B \sim 22$ surveys, where the $\omega(\theta)$ amplitude is much higher. It would be difficult for any physical model of galaxy evolution to account for this. The extreme brightening of blue dwarf galaxies ($\sim 3.5^m$) between $z = 0$ and $z \sim 0.4$ which would be needed for low redshift dwarf galaxies to produce the entire number count excess at $B \sim 24$ would only be possible if these galaxies formed their entire stellar populations at $z \sim 0.4$ epochs. Even then, for these galaxies to fade sufficiently since $z \sim 0.4$ to fit within the present day luminosity function, or merge into ellipticals without making present-day elliptical colours too blue, an extremely top-heavy IMF would be required for their stellar populations.

The interpretation of faint galaxy observations might be aided by much more detailed investigations of local galaxies, providing information about, for example, the distribution of the ages of their stellar populations and therefore a 'fossil record' of their star-formation histories. On the basis of investigations of local group dwarf galaxies, van den Bergh (1994) recently claimed that star-formation in the more isolated dwarf galaxies appears to have begun at an early epoch of ~ 15 Gyr ago and continued at a fairly constant rate to the present day (see Section 8.3.3). Blue dwarf galaxies formed at high redshifts, with constant SFRs, would brighten too slowly with redshift to account for the entire number count excess at $B \sim 24$, so that, even if intrinsically very weakly clustered, they could not explain the low $\omega(\theta)$ amplitude. The van den Bergh investigations, as they suggest a high $z_{formation}$ for even the smallest ($L \sim 0.0001L^*$) dwarf galaxies as well as $L \sim L^*$ giants, would appear to support our interpretation of both the number count excess and the low $\omega(\theta)$ amplitude at $B \sim 24$ as being caused by the initial starbursting of *large* galaxies at *high* redshifts.

However, an entirely unambiguous determination of the the relative importance of L^* and ϕ^* evolution may only be possible when true spectroscopic redshifts can be obtained for *all* galaxies at these magnitudes. For galaxies at $z > 1$, this will require detection of the OII[3727Å] and OIII[5007Å] emission lines at infra-red (10000Å $\leq \lambda \leq$ 20000Å) wavelengths, where the sky background is much brighter than at blue wavelengths. It may therefore be necessary to place very large ($\sim$ 10m aperture) telescopes in orbit or on the moon, before $\sim 100\%$ completeness can be reached in spectroscopic redshift surveys at sufficiently faint limits ($B \sim 25$) to distinguish between the various evolutionary models.

8.2.2 Additional Constraints from Ultraviolet Observations

In the absence of complete spectroscopy, investigations into the nature of the excess blue galaxies at $B \sim 24$ can be continued with further broad-band imaging and correlation analysis, including the extension of observations into other wavelengths. For example, extending very deep CCD imaging to the U-band at $\lambda \simeq 3500$Å, may greatly facilitate investigations of the dependence of clustering on the type of galaxy. Star-forming galaxies will be blue in $U - B$ at all redshifts up to $z \sim 3$, so the use of this colour will better distinguish between these and the 'passive' early-type population, independently of redshift, than is possible with $B - R$ colours alone.

The addition of UV observations at even shorter ($\lambda \sim 2000$Å) wavelengths would be even more useful. The Lyman limit cut-off will be shifted through $\lambda \sim 2000$Å at

$z \simeq 1$, so that high redshift galaxies will not be seen in this passsband, whereas star-forming galaxies at $z < 1$ will be quite blue in their $m_{2000} - U$ colour, as well as in $U - B$ and $B - R$. Furthermore, if the number count excess is dominated by low-redshift 'disappearing dwarf' galaxies, the top-heavy IMFs which may be required for such galaxies to fade sufficiently rapidly would result in extremely blue $m_{2000} - U$ colours compared to normal galaxies. Sufficiently deep imaging in a $\lambda \sim 2000$Å passband could in itself distinguish such galaxies from a high redshift blue population.

Number counts in a $\lambda = 2000$Å passband have recently been obtained by Armand and Milliard (1994), but, at present, only to relatively shallow depths corresponding approximately to $B \sim 19$ for galaxies of blue colours. The relatively high UV number counts obtained suggested a high local ϕ^* with a mix of galaxy types rich in late-type galaxies, as used in the models of MSFJ and in this thesis. This might support the claim of MSFJ that the $B \leq 21.5$ spectroscopic results of BES were still consistent with a PLE model.

Furthermore, the bluer galaxies in the Armand and Milliard (1994) sample possessed UV colours of $m_{2000} - B \simeq -1.5$, typical of normal Sdm/Irr galaxies seen locally and corresponding to an approximately $f_\nu \propto \nu^{-1}$ SED, rather than the extremely blue colours of $m_{2000} - B \simeq -2.5$ which correspond to a truly flat spectrum of $f_\nu \propto \nu^0$. As the $m_{2000} - B$ colour would be particularly sensitive to the proportion of extremely massive stars, the observed distribution of this colour might argue against the presence of significant numbers of galaxies with 'top-heavy' IMFs, at least at low redshifts. However, this survey would need to be extended by a further 5 magnitudes to reach $B \sim 24$ blue galaxies and therefore constrain the redshifts and/or IMFs of individual members of the excess faint blue galaxy population.

Measurements of the unresolved $\lambda \sim 2000$Å background (Pagel 1993) might also be used to set constraints on any starburst processes at redshifts less than $z \sim 1$, especially if these produce stellar populations with a top-heavy IMF. At present, only upper limits have been obtained, but these are much higher at $\lambda \sim 3000$Å than at $\lambda \sim 2000$Å, and so would allow much more star formation at $z > 1$ than at lower redshifts. If actual measurements of the spectrum of the UV background confirm the drop in the intensity between $\lambda \sim 3000$Å and $\lambda \sim 2000$Å suggested by the upper limits, this would, by indicating the presence of a very large population of star-forming galaxies at $z \sim 2$, support the 'Bruzual-type' coeval PLE models.

As flat spectrum objects will produce about half of their total energy output in the ultraviolet, it should eventually be possible to extend $\lambda \sim 2000$Å galaxy counts to the same limits as have been reached in the blue band with comparable telescope apertures and exposure times, although this will require satellite observatories, as $\lambda < 3300$Å wavelengths are strongly absorbed by the ozone layer. A deep CCD survey with thousands of faint galaxies imaged in U, B and $\lambda \sim 2000$Å to at least $B \sim 25$, $U \sim 25$, and $m_{2000} \sim 25$, could be divided into passive galaxies (red in $U - B$), low redshift starburst galaxies (blue in $U - B$, blue in $m_{2000} - U$), and $z > 1$ star-forming galaxies (blue in $U - B$, red in $m_{2000} - U$).

Because of the additional constraints on the redshift of star-forming galaxies provided by 2000Å observations, such a multi-band survey would not merely indicate the relative numbers of low-redshift and high-redshift galaxies within the 'excess' blue galaxy population, but would also, through the $\omega(\theta)$ analysis of the colour-divided subsets, allow us to compare the *intrinsic* clustering properties of passive $z < 1$ galaxies with those of both their high-redshift progenitors (indicating the rate of clustering evolution of $L \sim L^*$ galaxies out to high redshift) and those of dwarf starburst or late-type galaxies

at $z < 1$ (indicating the type-dependence of galaxy clustering). Furthermore, the cross-correlation of $z < 1$ star-forming galaxies with passive galaxies may provide information about the dependence of star-formation history on the galaxy environment, by indicating the relative numbers of dwarf galaxies undergoing starbursts induced by mergers and interactions with larger galaxies relative to the numbers undergoing star-formation in isolation.

8.3 Galaxy Counts and Clustering at $B \geq 25$

8.3.1 Summary and Interpretation

Analysis of our very deep ($B \simeq 27$) CCD image, in comparison with the counts and clustering results from the Tyson (1988) survey, gave two important results concerning galaxies at $B \geq 25$:

(i) At $B \simeq 25$, the scaling of $\omega(\theta)$ appears to level out at a minimum amplitude of $\omega(\theta) \simeq 4 \times 10^{-4}(\mathrm{deg})^{-0.8}$, suggesting that galaxies are seen out to a maximum redshift at this limit, with the low amplitude suggseting that this maximum redshift is at least $z \simeq 3$. The luminosity of large ($L \sim L^*$) galaxies must therefore brighten sufficiently on going back in time to $2 \leq z \leq 4$ epochs to enable these 'primordial' galaxies to be seen at $B = 25$ magnitudes. This requires that star-formation rates were generally much higher at $z \geq 2$, as in Bruzual's μ models, and that most $L \sim L^*$ galaxies have *not* merged with other large galaxies since $z \sim 2$ epochs.

(ii) At $B > 26$ the galaxy number count increases with a gradient $\frac{d(logN)}{dm} \sim 0.3$, steeper than would be expected if a maximum redshift has been reached and the differential number count is simply looking down the faint-end slope of a luminosity function similar in shape to that of galaxies seen locally (i.e. with $\alpha \simeq -1.25$). This would suggest that the faint-end slope of the luminosity function steepens to $\alpha \simeq -1.75$ at $z > 1$.

These two results are as would be expected for a combination of Bruzual-type luminosity evolution and the '$\phi^* - \alpha$' mass-dependent merging process proposed by GRV. However, both these results are at present of somewhat marginal ($\sim 2\sigma$) significance, on account of the small areas covered by present surveys at these very faint limits, where very long (> 10 hour) exposure times are necessary on each field, even with the largest telescopes. The evidence for a steepening of α with redshift is therefore suggestive rather than conclusive at present, in comparison to the much stronger evidence from the low $\omega(\theta)$ amplitudes at $B \sim 24$–25 that the luminosity L^* does evolve significantly.

8.3.2 Future Observations

Measurement of the number count slope at $B > 25$ with improved statistics, and verification of the possible levelling out of the $\omega(\theta)$ scaling, are obviously both very important, as significant constraints could then be placed on the nature and extent of galaxy evolution at high redshifts. The use of large-format CCDs would improve the analysis both by providing larger faint-galaxy samples ($> 10^4$ galaxies) and by minimizing the integral constraint correction – for the purposes of analysing the galaxy clustering, a single large image is preferable to many small images with the same total area. Furthermore, the use of larger fields would enable the measurement of $\omega(\theta)$ out to large angles of $\theta \sim 20$ arcmin, indicating whether there is any flattening in its slope for high redshift galaxies, and therefore whether there is a changeover from stable to comoving clustering evolution at large physical separations (see Section 6.7).

If the $\omega(\theta)$ amplitude becomes constant at $B > 25$ while number counts continue to rise, the signal-to-noise in the $\omega(\theta)$ amplitude will actually improve at the faintest limits. Hence the best way to verify these results would be through CCD surveys which both cover larger areas *and* reach even fainter (ie. $B > 27$) magnitude limits. Using the 4.2 m William Herschel Telescope, Metcalfe et al. (1994) obtained galaxy number counts to limits $\sim 0.5^m$ fainter than the INT data used in this thesis, although only for a much smaller area at the time of writing. It seems probable that with the latest generation of large ground-based optical telescopes, such as the 10m Keck Telescope, the combination of even larger apertures with image sharpening through in-built active optics will enable number counts and $\omega(\theta)$ amplitudes to be obtained reliably to limits faintward of $B \sim 28.5$ and galaxy surface densities exceeding $10^6 \mathrm{deg}^{-2}$.

A large-format CCD survey at these depths could not merely verify whether a levelling out of the $\omega(\theta)$ scaling does occur, but would be able to determine both the slope of the number counts and the asymptotic minimum $\omega(\theta)$ amplitude quite accurately. The number count slope could then be used to estimate the evolution of the faint-end slope (discussed further in Section 8.3.3) and the minimum $\omega(\theta)$ amplitude could be used to set constraints on q_0 (Section 8.3.4).

8.3.3 Evolution of the Faint-end Slope

It has recently been claimed that a steepening of α, in addition to a brightening of L^*, is seen in the Glazebrook et al. (1993) redshift survey if it is divided into $0 \leq z < 0.3$ and $0.3 \leq z \leq 1$ intervals. The significance of this result remains poor at present, but is is interesting that the results of this survey appear to be at least as consistent with a mixture of L^* and α evolution, which we found to be favoured by our number count and $\omega(\theta)$ results, as with the original BEG interpretation of pure ϕ^* evolution. However, an accurate determination from spectroscopy of the change in α at high redshifts is obviously more difficult than an estimation of the L^* evolution – at present we appear to be limited, even more so than is the case for the measurement of the high redshift proportion at $B \sim 24$, to the use of number count and $\omega(\theta)$ data.

A steepening of the blue-band luminosity function with redshift, if we assume for now that this is genuinely observed in our number counts, could be the result of a number of possible physical processes. For example, a steepening of the luminosity function of galaxies may reflect a steepening of their mass function, due to a mass dependent merging process in which dwarf galaxies frequently accrete onto larger galaxies, whereas mergers between giant galaxies are rare events. Recent physical models of galaxy merging processes (e.g. Cole et al. 1994) suggest that merging could produce an evolution of α in agreement with that inferred from our data.

A change in the α of a blue or UV selected sample could also result from differences in the star-formation histories of galaxies of different mass. For example, as suggested by Babul and Rees (1992), dwarf galaxies may lose their entire gas content in their initial starbursts, preventing further star-formation and causing very rapid fading, whereas the stronger gravity of $L \sim L^*$ galaxies may oppose the pressure exerted by supernova winds sufficiently to retain most of the hydrogen. The gas content of $L \sim L^*$ galaxies would then undergo a more gradual exponential decline through gas being formed into stars, resulting in a slower luminosity evolution, as in the Bruzual PLE models.

However, the observations of local group dwarf galaxies described by van den Bergh (1994) suggest that even the smallest isolated dwarf galaxies may contain stars with a very wide range of ages (0–15 Gyr), indicating that they formed at early epochs but were able to continue forming new stars until the present day. This suggests that

'isolated' blue dwarf galaxies tend to be 'normal' late-type galaxies, formed $\sim$ 15 Gyr ago and undergoing luminosity evolution described approximately by a constant-SFR model such as the 'Irr' model of Bruzual, rather than more recently formed galaxies undergoing initial starbursts of short duration, as in the Babul and Rees (1992) model.

The Cole et al. (1994) models of galaxy formation predict evolution of this type for low-mass (circular velocity $V_C < 100$ km s^{-1}) galaxies. In this model, supernovae do not remove all the gas from dwarf galaxies, but instead reheat the gas to the extent that only a small fraction remains in the cool phase and is available for star formation. This has the effect of increasing the SFR evolution timescale from $\tau_{SFR} \sim 2$ Gyr to $\tau_{SFR} \geq 20$ Gyr, leading to spectral evolution approximated by a constant-SFR model. Blue dwarf galaxies undergoing evolution of this type would brighten only very slowly with redshift. Such galaxies could become somewhat more dominant in blue-selected samples at moderate redshifts as a result of their near-zero k-corrections, and, as the LF measured for blue galaxies is relatively steep ($\alpha \simeq -1.5$), cause some steepening with redshift of α as determined from blue-limited samples. However, as we have already included a population of constant-SFR galaxies with $\alpha \simeq -1.5$ in our Bruzual PLE model, this effect would seem insufficient to explain the steep counts at $B > 25$.

On the other hand, van den Bergh found that dwarf galaxies very close to giant galaxies (within $\sim$ 100 kpc in the case of our own Galaxy) generally ceased forming stars very soon after an early ($\sim$ 15 Gyr ago) initial starburst, becoming dwarf spheroidals with red colours and a near-zero gas content at the present day. This environmental dependence would suggest that the main mechanism involved in removing the gas content of dwarf galaxies, and halting star-formation, is ram pressure stripping from the halo of nearby giant galaxies, rather than supernova winds from the initial starbursts of the dwarf galaxies themselves. In the models of Lacey et al. (1992), supernova-driven mass loss from dwarf galaxies produced a significant flattening of α between $z \sim 2$ and $z = 0$, without affecting the L^* luminosity, and we would expect mass loss from ram-pressure stripping to produce a similar effect on the luminosity function. Even closer to $L \sim L^*$ galaxies, van den Bergh found a lack of dwarf galaxies, suggesting that dwarfs forming in these regions might have merged into the larger galaxies.

Both luminosity dependent luminosity evolution (ram-pressure stripping and/or self-destruction of dwarfs) and luminosity dependent number evolution (merging of dwarfs into giant galaxies) may then have played a part in causing a reduction in the number of dwarf galaxies since early epochs, depending on the proximity of the dwarfs to $L \sim L^*$ galaxies. The cross-correlation of $B \sim 25$ blue galaxies (ie. $L \sim L^*$ galaxies starbursting at high redshift) with the even fainter $B \sim 27.5$ blue galaxies (ie. $L \sim 0.1L^*$ galaxies starbursting at high redshift) on a very deep CCD image might help to determine whether there is any influence of environment on the evolution of dwarf galaxies, and high resolution imaging of faint blue galaxies, for example with the HST, might provide some indication of the proportion undergoing mergers.

An alternative explanation for the steep number counts at $B > 25$ may be suggested by recent claims (e.g. Driver et al. 1994) that the local luminosity function of blue galaxies may possess a faint-end slope as steep as $\alpha = -1.8$. By combining such a steep local LF with strong L^* evolution, the $\omega(\theta)$ scaling and the steep number counts at $B > 25$ might both be fitted by a PLE model, although this model would overpredict the number of low redshift dwarfs in the redshift surveys of BES and Glazebrook et al. (1993).

It would clearly be easier for dwarf galaxies with a low surface brightness (in the blue band) to be missed in the $B < 24$ surveys (where they would lie at low redshifts), but

detected at higher redshifts in the number counts at $B \sim 27$, if their surface brightness is much higher at the rest-frame wavelengths of $\lambda \sim 2000$Å which are shifted into the observed blue band at $z > 1$. As described by MSFJ, the LF of late-type galaxies with blue $B - R$ colours has already been measured to be significantly steeper ($\alpha \simeq -1.5$) than that of the early-type galaxies with the reddest $B-R$ colours (for which $\alpha \simeq -0.7$). If this trend extends further, there may be a population of extremely blue (in $m_{2000} - B$ as well as $B - R$ colours) galaxies, with a local luminosity function as steep as $\alpha \simeq -1.8$, which might dominate a 2000Å-selected sample to a much greater extent than at blue or longer wavelengths. In a blue-limited sample, an observed steepening of α with redshift might then result from the negative k-corrections of the $\alpha \simeq -1.8$ population, rather than from any form of merging or luminosity-dependent luminosity evolution.

However, the $\lambda \sim 2000$Å selected sample of Armand and Milliard (1994) found few local galaxies with $m_{2000} - B$ colours bluer than the $f_\nu \propto \nu^{-1}$ SED of normal Sdm galaxies, and so might argue against such a hypothesis. Further observations of nearby galaxies at $\lambda \sim 2000$Å are clearly needed, including galaxies with a low surface brightness, to determine the form of the local UV luminosity function for comparison with blue-band observations of galaxies at the high redshifts where the same region of the rest-frame spectrum is observed.

Additional information about the processes causing the steep blue-band number counts may be provided by the K-band counts at comparable depths (ie. reaching the maximum redshift). As discussed in Section 1.5, the K-band luminosity of a galaxy reflects its total stellar mass, regardless of whether this exists as red dwarfs or blue giants, and so is insensitive to star formation processes. Hence the form of the K-band luminosity function will be very similar to that of the mass function, and the slope of the K-band number counts at very faint limits will indicate the faint-end slope of the mass function.

If the number counts continue to rise as steeply at faint limits in the K-band as in the blue-band (i.e. with $\frac{d(logN)}{dm} \sim 0.3$), this would indicate that the mass function steepens with redshift as much as the blue-band luminosity function, and would therefore favour '$\phi^* - \alpha$' physical merging models over luminosity-dependent luminosity evolution as the main explanation of the steep number count gradient.

On the other hand, if K-band number counts level out as much as PLE models, with no steepening of α, would predict (i.e. to $\frac{d(logN)}{dm} \sim 0.1$), this would suggest that the steepening of α in the blue-band is caused by differences in star-formation histories between dwarf and giant galaxies rather than any merging process. If there is no evolution at all of the rest-frame α, and the steep blue-band number counts simply result from a steeper α for an ultraviolet-selected galaxy sample, we would expect counts in the K-band, which at high redshifts corresponds to the rest-frame I-band or R-band, to flatten at faint limits to the gradient corresponding to the faint-end slope of red-selected local galaxies. This faint-end slope is no steeper than $\alpha \simeq -1.25$, again giving a differential K-band count slope of only $\frac{d(logN)}{dm} \sim 0.1$.

A turn-over in the K-band counts from $\frac{d(logN)}{dm} \simeq 0.67$ to $\frac{d(logN)}{dm} \simeq 0.26$ has already been observed (Gardner, Cowie and Wainscoat 1993), which appears closer to the merging prediction, but with present data the K-band counts also remain consistent with low-q_0 PLE models. The K-band counts plotted in Chapter 1 of this thesis would need to be extended at least another magnitude fainter, to $K \geq 23.5$, to distinguish between the $\frac{d(logN)}{dm} \simeq 0.3$ slope seen in the blue band, and the $\frac{d(logN)}{dm} \simeq 0.1$ slope given by a PLE model at faint limits.

With the new 10m Keck telescope, designed for both optical and K-band observations, it should be possible to obtain accurate number counts to at least $B = 28.5$ and $K = 24$, sufficient to verify at a statistically significantly level whether the number count slopes in either or both passbands are steeper than low-q_0 PLE model predictions, and therefore determine whether the blue-band luminosity function and the mass function evolve in the same way.

8.3.4 Possible Constraints on q_0 from Number Counts and $\omega(\theta)$

The high number counts and low $\omega(\theta)$ amplitudes obtained from our data and that of Tyson (1988) would tend to favour the large volume elements and angular diameter distances of either a negatively curved, low density Universe with zero cosmological constant (ie. $\Omega \sim 0.1$–0.2, $q_0 \sim 0.05$–0.1) or, alternatively, a flat Universe with a 'moderate' cosmological constant (e.g. $\Omega \sim 0.3$, $\Lambda \sim 0.7$), which might be more consistent with the inflationary model (see e.g. Peebles 1984, Koo 1990).

Even with the relatively high normalization of our number count models, which the K-band counts confirm as being appropriate, PLE models require a very low q_0 to fit the number counts at $B > 25$. These high number counts may still be consistent with $q_0 = 0.5$ if very strong evolution of α and/or ϕ^* of the galaxy luminosity function has occurred, in addition to L^* evolution. However, when we combined the L^* evolution given by our Bruzual models with a '$\phi^* - \alpha$' merging process, which conserved the comoving luminosity density, a low q_0 was still required to fit the counts. In a $q_0 = 0.5$ Universe, the comoving blue-band luminosity density of galaxies would therefore have to increase with redshift to a much greater extent than in Bruzual's models, regardless of any merging processes which may also occur.

In view of the uncertainties about the evolution of α and ϕ^*, to which number counts at faint limits are sensitive but the $\omega(\theta)$ amplitude is not, correlation analysis of deep galaxy data will continue to be more useful than number counts alone. The minimum value reached by the $\omega(\theta)$ amplitude at faint limits will depend only on the value of the maximum redshift, the angular diameter distance of high-redshift galaxies (and therefore q_0), and the rate of evolution of clustering. However, if the redshift cut-off is at least $z \sim 3$ for blue-band observations and clustering is approximately stable, our $\omega(\theta)$ results remain consistent with any value of Ω from 0 to 1. To obtain meaningful constraints on q_0, we would require both improved statistics on the $\omega(\theta)$ amplitude at $B \geq 25$ and more definite constraints on the maximum redshift and the rate of clustering evolution.

Extending very deep number counts into other wavelengths, from U to K, would enable the position and nature of the maximum redshift cut-off to be investigated. Any starbursting galaxies at $3 \leq z \leq 4$ will be blue in $B - R$ but red in $U - B$, or not visible at all in the U band, as a result of the Lyman cut-off. At $4 < z < 6$ the Lyman cut-off would be shifted to a wavelength between B and R, so any galaxies at these redshifts would become red in $B - R$, but remain blue in $R - K$ if they are undergoing active star-formation.

As discussed in Section 8.2.2, through the $\omega(\theta)$ analysis of large colour-divided subsets it may be possible to determine accurately the rate of evolution of clustering. When these other parameters are constrained, the $\omega(\theta)$ amplitude of $B \geq 25$ galaxies (measured from a larger CCD survey) could then be used to estimate directly the angular diameter distance of high-redshift galaxies, and therefore q_0.

8.4 Further Investigation of X-Ray Sources

8.4.1 X-Ray Luminous Galaxies

We have found that $\sim$ 1% of galaxies seen at $z \sim 0.25$ possess very high X-ray luminosities of $L_X \sim 10^{42}$ ergs s^{-1}, suggesting that there is a high dispersion of $\sigma \sim 0.7$ in the log (L_X/L_B) ratios of galaxies. Explaining these results will require further observations of high-L_X galaxies, including those detected on these ROSAT images, to determine the relative importance of the various possible mechanisms of X-ray emission.

As described by, for example, Kim, Fabbiano and Trinchieri (1992), and Pellegrini and Fabbiano (1994), it is already possible, using the low resolution X-ray spectral data from *Einstein* and ROSAT, to estimate the relative proportions of the thermal and accreting binary components of the X-ray emission of some galaxies. The new ASCA satellite, providing similar angular resolution to the ROSAT PSPC with a larger effective area, will be much more effective in this as a result of its much higher spectral resolution and its sensitivity to harder X-ray energies (2–10 keV).

Measurement of the 'flat-spectrum' component of the X-ray emission from galaxies, caused by MXRBs rather than hot gas, would indicate the numbers of MXRBs formed in starbursts. This might help to determine whether galaxies differ in the high-mass ends of their Initial Mass Functions (as would $\lambda \sim 2000$Å observations). It has been also suggested by, for example, Griffiths and Padovani (1990), that X-ray emission from star-forming regions could be enhanced by conditions of low metallicity. Measuring the MXRB component of the X-ray luminosity of a sample of star-forming galaxies, in combination with far infra-red and UV ($\lambda \sim 2000$Å) observations to determine the numbers of very massive stars and optical spectroscopy to estimate the metallicity, will enable the effects of metallicity and star-formation rate on the MXRB emission to be disentangled.

As the low mass X-ray binaries tend to form in globular clusters, the strength of this component of X-ray emission might enable the numbers of globular clusters associated with galaxies to be estimated, even at distances too great for individual globulars to be seen. This would provide information about the dependence of the number of globular clusters on the morphological type, mass and environment of galaxies.

Furthermore, it will be possible with ASCA to measure the temperature of the hot X-ray emitting gas much more accurately than with *Einstein* or ROSAT, determining its velocity dispersion and distinguishing between the gas in individual ellipticals (with $kT \sim 1.5$ keV) and the hotter gas in rich clusters (with $kT \sim 7$ keV).

A combination of X-ray spectroscopy and multi-wavelength observations – including optical spectroscopy, radio, sub-mm (e.g. with the James Clerk Maxwell Telescope), ultraviolet and far-infra-red observations – of X-ray detected galaxies could be used to study the relationship between X-ray emission and the star-formation rate, chemical composition and cluster environment of galaxies, and identify other possible parameters which may influence the L_X/L_B ratio.

8.4.2 X-Ray Observations of Clusters

We found that a rich Coma-type galaxy cluster at $z = 0.56$ produced an X-ray flux an order of magnitude above the 4σ threshold on ROSAT images of the depth used in our survey. Using ROSAT or ASCA it should therefore be possible to detect many other rich clusters on X-ray images, and identify these with their optical counterparts, out to redshifts of at least $z \sim 1$. It will then be possible to estimate the rate of their X-ray luminosity evolution.

Our comparison of the X-ray luminosity of GSGP4X:32 with that of the Coma cluster suggested that rich clusters possessed lower X-ray luminosities at earlier epochs. Bower et al. (1994) describe recent ROSAT observations of 14 other high-redshift ($z_{mean} = 0.42$) clusters, which appear to confirm this trend. Castander et al. (1994) describe recent ROSAT observations of 5 clusters at even higher redshifts ($0.7 \leq z \leq 0.9$), for which they measure relatively low X-ray luminosities of $L \leq 10^{44}$ ergs s^{-1}. Their luminosity function indicates that either the comoving number density or the X-ray luminosity of rich clusters must be lower by a factor of at least $\sim 10^{-0.5}$ at $z \simeq 0.8$ relative to the present day. Our measurements of the X-ray luminosity of GSGP4X:32 would obviously be consistent with this rate of negative evolution.

Using ASCA it will also be possible to measure accurately the temperature of the X-ray emitting gas in high-redshift clusters, and the equivalent widths of emission lines in the X-ray spectra. This will provide information about the nature and cause of the luminosity evolution.

The X-ray temperature of a gravitationally bound cloud of hot gas is proportional to the square of its velocity dispersion, which depends on the depth of the potential well. X-ray temperatures of clusters could therefore provide information about the evolution of their physical structure – galaxy merging within the cluster would deepen the potential wells and increase the X-ray temperature and luminosity, as would the transfer of hot gas from the small gravitational wells of individual galaxies to the centre of the cluster's much larger gravitational well. An increase of the X-ray luminosity of rich clusters between $z \sim 1$ and $z = 0$ would indicate that these heating/merging processes have generally been dominant over cooling processes during the last 10 Gyr. As the cooling time of the hot gas in a rich cluster is typically H_0^{-1} or longer, their X-ray luminosities may not reach a peak and start to decline until some Gyr into the future.

Equivalent widths of emission lines may provide information about the ionization state and chemical evolution of the cluster gas, and therefore its origin. The detection of emission lines, in particular the very strong Fe line at 7 keV, would also help to determine the redshift of a cluster, if this is difficult from optical data, e.g. if the optical image is contaminated by foreground objects, or is simply too faint for significant features to be found in the optical spectrum (which unlike the X-ray spectrum would probably not contain strong emission lines if the cluster galaxies are early-type).

Furthermore, the use of X-ray observations to identify very massive clusters at $0.3 \leq z \leq 1$, and accurately determine their centres of mass, will enable studies of the gravitational lensing of faint galaxies seen close to the cluster positions. The proportion of the faint galaxies near each cluster which show indications of lensing could be used to estimate the relative numbers of these galaxies which lie at redshifts higher or lower than the cluster itself (see e.g. Tyson 1990), providing information about the galaxy $N(z)$ at very faint ($24 \leq B \leq 27$) magnitudes.

8.5 Faint Galaxy Clustering and the X-ray Background

One of the most important results presented in this thesis, and also one of the most statistically significant ($\sim 5\sigma$), is the detection and measurement of a cross-correlation between the unresolved X-ray background, as observed on deep ROSAT PSPC images, and $18 \leq B \leq 23$ galaxies on AAT photographic plates. The $18 \leq B \leq 23$ galaxies appeared to produce $16.8 \pm 2.1\%$ of the unresolved component of the 0.5–2.0 keV background, with a similar strength of cross-correlation being seen for the redder and bluer galaxies in the sample.

The nature of the X-ray emission associated with these galaxies might be investigated further by cross-correlating similar galaxy samples with the XRB imaged, using the new ASCA satellite, in a number of different energy bands between 0.5 keV and 10 keV. It would be useful to again divide the galaxy sample by colour into passive and star-forming galaxies. If, as discussed in Section 7.11, the X-ray emission from late-type galaxies is dominated by MXRBs and that from ellipticals by thermal emission, we might expect the bluer galaxies to be more correlated with the 2–10 keV background than with the XRB at softer (0.5–2.0 keV) energies, while the reverse would be true for the red galaxies.

In combination with the detection of a cross-correlation between $18 \leq B \leq 23$ galaxies and the XRB, the fact that a similarly weak clustering amplitude ($\omega(\theta) < 10^{-3}(\mathrm{deg})^{-0.8}$) was obtained for both the fainter ($B > 24$) blue galaxies and the unresolved XRB supports the hypothesis that faint blue galaxies do produce a large component of the XRB. However, it will only be possible to verify this directly by cross-correlating these fainter galaxies with the XRB, and the resolution of the ROSAT PSPC (FWHM $\sim$ 25 arcsec), and that of ASCA, may be insufficient for such an analysis – at least 5 galaxies at $B \sim 25$ would be found in each X-ray resolution element. The use of, for example, the ROSAT high resolution imager (FWHM $\sim$ 5 arcsec), with sufficiently long exposure times ($> 10^5$ s), would reduce this confusion problem.

The cross-correlation between galaxies in a deep CCD survey with a high-resolution X-ray image of the same area would enable the contribution of these fainter galaxies to the X-ray background to be measured directly, thus distinguishing between diffuse emission (which would show no correlation with the faint galaxy sample) and the weakly clustered faint blue galaxies as the cause of the uniformity of the XRB, and enabling the rate of X-ray luminosity evolution of galaxies to be estimated.

Soltan and Hasinger (1994), combining results from a large number of ROSAT images, recently claim to have detected a significant signal in the ACF of the unresolved XRB. For a $\theta^{-0.8}$ power-law, their result corresponds to an ACF amplitude of only $\omega_{ACF}(\theta) = (4.5 \pm 1.6) \times 10^{-4}(\mathrm{deg})^{-0.8}$, which is consistent with the upper limits obtained from our smaller dataset. More importantly, the Soltan and Hasinger estimate is very similar to both the $\omega(\theta)$ amplitude we measure for faint blue galaxies, and the ACF amplitude predicted by models in which galaxies with X-ray luminosity evolution of at least $\tau \sim 0.4$ produce most of the unresolved XRB (see Section 7.9).

The narrower point-spread function of a deep HRI image would allow the ACF to be measured at smaller separations, where the signal from any clustering of the unresolved discrete sources will be stronger. In this way, higher resolution imaging should further improve the constraints on the clustering of X-ray sources.

8.6 Extending X-Ray Observations of Galaxies to High Redshifts

To investigate directly the X-ray luminosity evolution of individual galaxies would require us to reach extremely faint detection limits of $S \sim 10^{-15}$–10^{-16} ergs cm^{-2}s^{-1}, with ~ 1 arcsec angular resolution. Such observations would require much higher spatial resolution and larger effective areas than are attainable using ASCA or any of the ROSAT instruments, and must await the availability of the AXAF observatory in the late 1990s. Much larger numbers of galaxies could then be detected in X-rays, out to at least $z \sim 1$ and possibly $z \sim 3$, enabling the galaxy X-ray luminosity function to be studied as a function of redshift, and allowing the X-ray properties of individual galaxies, as well as those of large clusters, to be studied at much earlier evolutionary stages. It may also be possible to obtain redshifts for some high-redshift galaxies from X-ray observations alone, by detecting the Fe emission line at 7 keV, which can be extremely strong (equivalent width ~ 1 keV) in some sources.

We might expect to see a strong increase of the hard X-ray emission from MXRBs with redshift, similar to the luminosity evolution already seen at ultraviolet and far infrared wavelengths, as the luminosity in all these passbands would reflect the numbers of very massive stars. The emission from low mass X-ray binaries might show only a slight increase with redshift, similar to the K-band evolution, if it simply relates to the total number of stars of any mass in a galaxy. However, if merging processes cause globular clusters to be formed, we might observe stronger evolutionary trends for this component of the X-ray emission in some galaxies.

The luminosity and temperature of the thermal component of X-ray emission, together with observations of emission lines, will provide information about the velocity dispersion and chemical composition of the hot gas in individual giant ellipticals as well as in rich clusters. While X-ray emission associated with star-formation would definitely be expected to increase with redshift, and the X-ray emission from hot gas in clusters appears to decrease on going out to $z \sim 0.5$, it may be less obvious how the X-ray luminosity of early-type galaxies would evolve. The X-ray temperature of the hot gas in ellipticals would increase (by a factor of $\sim 2^{0.5-1.0}$ if $\sigma_*^2 \propto (L_B)^{0.5-1.0}$) if two similar galaxies merged, but the cooling times would be much shorter (ie. less than H_0^{-1}) than for the much more massive clusters. If a significant fraction of the heating of the gas in ellipticals is caused by supernovae, the total rate of heat input would be lower at present than during the initial starbursts. Furthermore, the mass of the X-ray emitting gas in individual galaxies, if they lie within clusters, would gradually be reduced by ram pressure stripping.

These considerations suggest that the X-ray luminosity of the hot gas in ellipticals would probably have been higher at $z \sim 1$ epochs (see e.g. Sarazin 1990) than at the present day, except perhaps for galaxies which have recently undergone a great deal of merging. Through observations of X-ray luminosities and temperatures it may be possible to set constraints on the importance of merging in the evolution of large galaxies.

The spectrum of the XRB with resolved sources removed bears more resemblance to the hard, power-law spectrum of MXRB emission than to the softer ($kT \sim 1$ keV) X-ray emission from hot gas in early-type galaxies. This suggests that, even if star-forming and early-type galaxies contribute similarly to the total X-ray emissivity of galaxies at the present-day, the MXRB component is likely to increase with look-back time to a greater extent. At $z > 2$ the star-formation rates in early-type galaxies would be very high, so the X-ray emission from MXRBs would increase by a much greater extent, and might dominate the total X-ray emission even for the largest ellipticals with the highest

gas temperatures. High-redshift elliptical galaxies would then become 'blue' in their X-ray colours as well as their optical colours (so could be described as a 'flat-spectrum' population in both passbands), and could account for the hard, power-law ($f_\nu \propto \nu^{-0.4}$) SED of the unresolved XRB as well as the lack of signal in its ACF.

The cross-correlation of faint blue galaxies with the XRB, imaged at high resolutions in a number of X-ray passbands, would verify whether these galaxies produce the non-QSO component of the XRB and can explain its uniformity and the form of its SED. However, the combination of high-resolution X-ray and optical observations of individual galaxies may eventually, as described above, provide much more information, determining the dependence of the X-ray luminosity evolution and the evolution of the star-formation rate on the morphological types of galaxies, their environment at the time of formation, and their subsequent interactions with other galaxies and the intergalactic or intra-cluster medium.

8.7 Afterword

Whether we visualize an expanding and evolving universe or simply a limitless array of quantum states through which our stream of consciousness moves outwards from the 'Big Bang' to regions of higher entropy, it is clear that we now find ourselves in a universe full of various types of stars, which are clumped into galaxies, which are themselves clustered together. Both our optical and X-ray observations indicate that we are in the midst of a transition between a universe full of blue galaxies and one of red galaxies. The blue galaxies contain dense gas clouds and undergo rapid star-formation, and consequently their stellar populations include hot, massive stars and massive X-ray binaries. The red galaxies consist of only red dwarf stars and less massive red giant stars, and tend to be found within centrally condensed clusters containing very hot, diffuse, X-ray luminous gas.

Locally we see a mixture of these types of source, while at high redshifts the blue galaxies predominate. We find that large galaxies appear to have formed at early ($z \geq 3$) epochs, over a much shorter timescale than the age of our Universe, and that the conversion of gas into stars within galaxies has followed more or less intermediate evolutionary timescales (~ 0.1–$1 H_0^{-1}$), varying greatly between individual galaxies. The inferred timescales suggest that the Universe is now in a fairly late stage of its star-formation history, having already formed ~ 70–90% of the stars which will ever be formed.

In the distant future ($\sim 10^{12}$ years hence) only condensed clusters and red dwarf stars will remain as significant sources of X-ray and optical emission. Further on, even these will cool and cease to be luminous, and the Universe will enter a black-hole dominated epoch. From the gradual decline of the hot blue stellar population we infer from our observations, we may obtain the picture of a luminous universe fading inevitably towards darkness. Yet, if each black hole connects to the 'white hole' at the beginning of another universe, in which the process of galaxy formation can begin anew, then – even in an open universe – galaxy evolution forms only part of Nature's endless cycle of creation and destruction.

Appendix 1

Limber's Formula

In this thesis, we make extensive use of Limber's formula, which relates the projected clustering of sources on the two-dimensional sky plane (described by the angular correlation function $\omega(\theta)$) to the clustering of sources in three-dimensional space (described by the two-point correlation function $\xi(r)$), by means of an integration over the source redshift distribution $N(z)$.

In this appendix, we describe the form and derivation of Limber's formula, as given previously by, for example, Phillips et al. (1978) and Peebles (1980).

First consider two solid angle elements, $\delta\Omega_1$ and $\delta\Omega_2$, separated on the sky by angle θ. If the mean surface density of the galaxies in a survey is N, and their angular correlation function is $\omega(\theta)$, the probability $\delta P(\theta)$ of finding a galaxy in $\delta\Omega_1$ and another in $\delta\Omega_2$, will be given by

$$\delta P(\theta) = N^2(1 + (\omega(\theta))\delta\Omega_1\delta\Omega_2$$

Now consider the two volume elements, $\delta\Omega_1\delta z_1$ and $\delta\Omega_2\delta z_2$, which lie on the lines of sight to $\delta\Omega_1$ and $\delta\Omega_2$, at redshifts z_1 and z_2 respectively. The separation of these two volume elements in proper distance is r, and the mean of the two redshifts, $\frac{1}{2}(z_1 + z_2)$, is z. If the galaxies in the survey possess a redshift distribution $N(z)$, and a two-point correlation function $\xi(r, z)$, the probability $\delta P(r, z)$ of finding a galaxy in $\delta\Omega_1\delta z_1$ and another in $\delta\Omega_2\delta z_2$, will be

$$\delta P(r, z) = N(z_1)N(z_2)(1 + (\xi(r, z))\delta\Omega_1\delta z_1\delta\Omega_2\delta z_2$$

The surface density N is given by summing $N(z)$ in all the volume elements along the line of sight to the solid angle $\delta\Omega$,

$$N = \int_0^\infty N(z)dz$$

Similarly, the galaxy-galaxy pair probability $\delta P(\theta)$ will be equal to the double integration of $\delta P(r, z)$ over z_1 and z_2, covering all possible separations of the two volume elements,

$$\delta P(\theta) = \int_0^\infty \int_0^\infty \frac{\delta P(r, z)}{\delta z_1 \delta z_2} dz_1 dz_2$$

Substituting for $\delta P(\theta)$ and $\delta P(r, z)$ then gives

$$N^2[1 + \omega(\theta)] = \int_0^\infty \int_0^\infty N(z_1)N(z_2)[1 + \xi(r, z)]dz_1 dz_2$$

If we consider only the volume elements for which $z_1 - z_2$ is small compared to the mean redshift z (i.e. assume clustering is only significant on scales which are small compared to the survey depth), we can approximate both $N(z_1)$ and $N(z_2)$ by $N(z)$. We can then subtract N^2 from both sides of the equation, leaving

$$N^2\omega(\theta) = \int_0^\infty \int_0^\infty [N(z)]^2\xi(r, z)dz_1 dz_2$$

Defining $y = z_1 - z_2$, and changing variables from (z_1, z_2) to (y, z),

$$\omega(\theta) = N^{-2} \int_0^\infty \int_{-\infty}^\infty [N(z)]^2 \xi(r, z) dy dz$$

The radial component of the separation r is $y\frac{dr(z)}{dz}$, where $\frac{dr(z)}{dz}$ is the derivative of proper distance with respect to redshift, and the transverse component of r, assuming the small-angle approximation, is $\theta d_A(z)$, where $d_A(z)$ is the angular diameter distance. With

$$r^2 = y^2(\frac{dr(z)}{dz})^2 + \theta^2(d_A(z))^2$$

Limber's formula then becomes

$$\omega(\theta) = N^{-2} \int_0^\infty \int_{-\infty}^\infty [N(z)]^2 \xi([y^2(\frac{dr(z)}{dz})^2 + \theta^2(d_A(z))^2]^{0.5}, z)] dy dz$$

We now assume for $\xi(r, z)$ the power-law form

$$\xi(r, z) = (\frac{r_0}{r})^\gamma (1 + z)^{-(3+\epsilon)}$$

where the strength of clustering is parameterized by the correlation length r_0 (the separation at which the probabilty of finding another galaxy is twice that expected from a random distribution). The power-law index is γ, assumed to remain constant, and ϵ expresses the rate of clustering evolution with redshift, relative to a stable model for which $\epsilon = 0$ (see Section 3.2).

Limber's formula would then give an angular correlation function of the form

$$\omega(\theta) = A\theta^{1-\gamma}$$

with a dimensionless amplitude at one radian separation of A, given by the integration over the redshift distribution,

$$A = C r_0^\gamma N^{-2} \int_0^\infty [N(z)]^2 (d_A(z))^{1-\gamma} (\frac{dr(z)}{dz})^{-1} (1 + z)^{-(3+\epsilon)} dz$$

where C is calculated from the power-law index as

$$C = \sqrt{\pi} \frac{\Gamma[(\gamma - 1)/2]}{\Gamma(\gamma/2)}$$

giving $C = 3.679$ for $\gamma = 1.8$. The use of the Limber's formula integration to investigate the galaxy redshift distribution is discussed in Section 1.7, and its use to interpret the autocorrelation function of the X-ray background is discussed in Section 6.6.

References

Abramopoulos, F. and Ku, W.H., 1983. *Astrophys. J.*, **271**, 442.

Aragón-Salamanca, A., Ellis, R.S., Couch, W.J., Carter, D., 1993. *Mon. Not. R. astr. Soc.*, **262**, 764.

Armand, C. and Milliard, B., 1994. *Astron. Astrophys.*, **282**, 1.

Babul, A. and Rees, M.J., 1992, *Mon. Not. R. astr. Soc.*, **255**, 498.

van den Bergh, S., 1994. *Astrophys. J.*, **428**, 617.

Bower, R.G, Bohringer, H., Briel, U.G., Ellis, R.S, Castander, F.J. and Couch, W.J., 1994. *Mon. Not. R. astr. Soc.*, **268**, 345.

Boyle, B.J., Fong, R., Shanks. T. and Peterson, B.A., 1990. *Mon. Not. R. astr. Soc.*, **243**, 1.

Boyle, B.J., Griffiths, R.E., Shanks, T., Stewart, G.C. and Georgantopoulos, I, 1993. *Mon. Not. R. astr. Soc.*, **260**, 49.

Boyle, B.J., Shanks, T., Georgantopoulos, I, Stewart, G.C. and Griffiths, R.E., 1994. Preprint submitted to *Mon. Not. R. astr. Soc.*.

Broadhurst, T.J., Ellis, R.S. and Glazebrook, K., 1992. *Nature*, **355**, 55. (BEG)

Broadhurst, T.J., Ellis, R.S. and Shanks, T., 1988. *Mon. Not. R. astr. Soc.*, **235**, 827. (BES)

Bruzual, G., 1981. *Ph.D. thesis*, University of California, Berkeley.

Bruzual, G. and Charlot, S, 1993. *Astrophys. J.*, **405**, 538.

Carlberg., R.G. and Charlot, S., 1992. *Astrophys. J.*, **397**, 5.

Carlberg., R.G. and Couchman, H.M.P., 1989. *Astrophys. J.*, **340**, 47.

Carrera, F.J., Barcons, X., Butcher, J.A., Fabian, A.C., Stewart, G.C., Warwick, R.S., Hayashida, K. and Kii, T., 1991. *Mon. Not. R. astr. Soc.*, **249**, 698.

Castander., F.J., Ellis, R.S., Frenk, C.S., Dressler, A. and Gunn, J.E., 1994. *Astrophys. J.*, **424**, L29.

Cole., S., Aragón-Salamanca, A., Frenk, C.S., Navarro, J.F. and Zepf, J.E., 1994. Preprint.

Colless, M., Ellis, R.S., Taylor, T. and Hook, R.N., 1990. *Mon. Not. R. astr. Soc.*, **244**, 408.

Couch, W.J., Jercevic, J.S. and Boyle, B.J, 1993. *Mon. Not. R. astr. Soc.*, **260**, 241.

Couch, W.J., Shanks, T., and Pence, W.D., 1985. *Mon. Not. R. astr. Soc.*, **213**, 215.

Cowie, L.L., Songaila, A. and Hu, E.M., 1991. *Nature*, **354**, 460.

Dalcanton, J.J., 1993. *Astrophys. J.*, **415**, L87.

Davis, M., Efstathiou, G., Frenk, C.S. and White, S.D.M., 1985. *Astrophys. J.*, **292**, 371.

Driver, S.P., Phillipps, S., Davies, J.I, Morgan, I., Disney, M.J., 1994. *Mon. Not. R. astr. Soc.*, **266**, 155.

Efstathiou, G., Bernstein, G., Katz, N., Tyson, J.A. and Guhathakurta, P., 1991. *Astrophys. J.*, **380**, L47.

Ellingson, E., Yee, H.K.C. and Green, R.F., 1991. *Astrophys. J.*, **371**, 49.

Fabbiano, G., 1989. *Ann. Rev. Astr. Ap.*, **27**, 87.

Fukujita, M., Takahara, F., Yamashita, K. and Yoshii, Y., 1990. *Astrophys. J.*, **361**, L1.

Gardner, J.P., Cowie, L.L., and Wainscoat, R.J., 1993. *Astrophys. J.*, **361**, L1.

Georgantopoulos, I., 1991. *PhD Thesis*, University of Durham.

Georgantopoulos, I., Stewart, G.C., Shanks, T., Griffiths, R.E. and Boyle, B.J., 1993. *Mon. Not. R. astr. Soc.*, **262**, 619.

Georgantopoulos, I., Stewart, G.C., Shanks, T., Boyle, B.J., and Griffiths, R.E., 1994. Preprint submitted to *Mon. Not. R. astr. Soc.*.

Giacconi, R. and Zamorani, G., 1987. *Astrophys. J.*, **313**, 20.

Glazebrook, K., 1991. *Ph.D. thesis*, University of Edinburgh.

Glazebrook, K., Ellis, R., Colless, M., Broadhurst, T., Allington-Smith., J., Tanvir, N.R. and Taylor, K., 1993.

Griffiths, R.E., Georgantopoulos, I., Boyle, B.J., Stewart, G.C. and Shanks, T., 1993, in preparation.

Griffiths, R.E. and Padovani, P., 1990. *Astrophys. J.*, **360**, 483.

Griffiths, R.E., Tuohy, I.R., Brissenden, R.J. and Ward, M.J., 1992. *Mon. Not. R. astr. Soc.*, **255**, 545.

Groth, E.J. and Peebles, P.J.E., 1977. *Astrophys. J.*, **217**, 385. (GP77)

Guhathakurta, P., 1989. *Ph.D. thesis*, University of Princeton.

Guiderdoni, B. and Rocca-Volmerange, B., 1990. *The Quest for the Fundamental Constants in Cosmology*, eds. J. Andouze and J. Tran Thanh Van, Editions Frontières, France, p. 149.

Guiderdoni, B. and Rocca-Volmerange, B., 1991. *Astron. Astrophys.*, **252**, 435. (GRV)

Hamilton, T.T. and Helfand, D.J., 1987. *Astrophys. J.*, **318**, 93.

Infante, L., 1990. *Ph.D. thesis*, University of Victoria.

Jones, L.R., Fong, R., Shanks, T., Ellis, R.S. and Peterson, B.A., 1991. *Mon. Not. R. astr. Soc.*, **249**, 481.

Jones, L.R., Shanks, T. and Fong, R., 1987. *High Redshift and Primeval Galaxies*, eds. J. Bergeron, D. Kunth, B. Rocca-Volmerange and J. Tran Thanh Van Editions Frontières, France, p. 29. (JSF)

Kim, D.W., Fabbiano, G. and Trinchieri, G., 1992. *Astrophys. J.*, **393**, 134.

Koo, D.A., 1990. *The Evolution of the Universe of Galaxies*, ed. R.G. Kron, ASP Conf. Series No. 10, p. 268.

Koo, D.A. and Szalay, A., 1984. *Astrophys. J.*, **282**, 390.

Lacey, C., Guiderdoni, B., Rocca-Volmerange, B. and Silk, J., 1993. *Astrophys. J.*, **402**, 15.

Lahav, O., Fabian, A.C., Barcons, X., Boldt. E., Butcher. J., Carrera. F.J., Jahoda, K., Miyaji. T., Stewart, G.C. and Warwick, R.S., 1993. *Nature*, **364**, 693.

Larson, R.B., 1990. *Publications of the Astronomical Society of the Pacific*, **102**, 709.

Lilly, S.J., Cowie, L.L. and Gardner, J.P., 1991. *Astrophys. J.*, **369**, 79.

Metcalfe, N., Shanks, T., Fong, R. and Jones, L.R., 1991. *Mon. Not. R. astr. Soc.*, **249**, 498. (MSFJ)

Metcalfe, N., Shanks, T., Fong, R. and Roche, N., 1994. Preprint submitted to *Mon. Not. R. astr. Soc.*.

Miyaji, T., Lahav, O., Jahoda, K. and Boldt, E., 1994. *Astrophys. J.*, in press.

Mo, H.J, Jing, Y.P. and Börner, G., 1993. *Astrophys. J.*, **392**, 452.

Mobasher, B, Ellis, R.S., and Sharples, R.M., 1986. *Mon. Not. R. astr. Soc.*, **223**, 11.

Neuschaefer, L.W., 1992. *Ph.D. thesis*, Arizona State University.

Pagel, B.E.J., 1993. NORDITA Preprint.

Peebles, P.J.E., 1980. *The Large-Scale Structure of the Universe*, Princeton University Press.

Peebles, P.J.E., 1984. *Astrophys. J.*, **284**, 439.

Pellegrini, S. and Fabbiano, G., 1994. *Astrophys. J.*, **429**, 105.

Phillipps, S., Fong, R., Ellis, R.S., Fall, S.M. and MacGillivray, H.T., 1978. *Mon. Not. R. astr. Soc.*, **182**, 673.

Rocca-Volmerange, B. and Guiderdoni, B., 1990. *Mon. Not. R. astr. Soc.*, **247**, 166.

Roukema, B.F. and Yoshii, Y., 1993. *Astrophys. J.*, **418**, L1.

Sarazin, C.L., 1988. *X-ray Emission from Clusters of Galaxies*, Cambridge University Press.

Sarazin, C.L., 1990. *The Interstellar Medium in Galaxies*, 201, eds. H.A. Thronson and J.M. Thrull, Kluwer Academic Publishers.

Shanks, T., 1979. *Ph.D. thesis*, University of Durham.

Shanks, T., 1989. *The Galactic and Extragalactic Background Radiation*, 269, eds. S. Bowyer and C. Leinert, IAU.

Shanks, T. and Boyle, B.J., 1994. Preprint.

Shanks, T., Fong, R., Ellis, R.S. and MacGillivray H.T., 1980. *Mon. Not. R. astr. Soc.*, **192**, 209.

Shanks, T., Georgantopoulos, I., Stewart, G.C., Pounds, K.A., Boyle, B.J. and Griffiths, R.E., 1991. *Nature*, **353**, 315.

Shanks, T., Hale-Sutton, D., Fong, R., and Metcalfe, N., 1989. *Mon. Not. R. astr. Soc.*, **237**, 589.

Stevenson, P.R.F., Shanks, T., Fong, R. and MacGillivray, H.T., 1985. *Mon. Not. R. astr. Soc.*, **213**, 953.

Tóth, G. and Ostriker, J.P., 1992. *Astrophys. J.*, **389**, 5.

Treyer, M.A., Mouchet, M., Blanchard, A., and Silk, J., 1992. *Astron. Astrophys.*, **264**, 11.

Tyson, J.A., 1988. *Astron. J.*, **96**, 1.

Tyson, J.A., 1991. *Relativistic Astrophysics, Cosmology and Fundamental Physics*, 164, eds. J.D. Barrow, L. Mestel, and P.A. Thomas, New York Academy of Sciences.

White, S.D.M. and Frenk, C.S. 1991. *Astrophys. J.*, **379**, 52.

Wright, E.L., Mather, J.C., Fixsen, D.J., Kogut, A., Shafer, R.A., Bennett, C.L., Boggess, N.W., Cheng, E.S., Silverberg, R.F., Smoot, G.F. and Weiss, R, 1993. Preprint.